Hygrothermal Propertied of Building Materials at Different Temperatures and Relative Humidities

Youness Yousefi

A Thesis

In

The Graduate Program of Building Engineering / Building Science

The School of Construction and the Environment

Presented in Partial Fulfillment of the Requirements for the Degree of

Master of Applied Science

At the

British Columbia Institute of Technology

Burnaby, British Columbia, Canada

August 2019

BRITISH COLUMBIA
INSTITUTE OF TECHNOLOGY

Building Science Graduate Program
School of Construction
and the Environment
3700 Willingdon Avenue
Burnaby, British Columbia
Canada V5G 3H2

bcit.ca

This is to certify that the thesis prepared

By: YOUNESS YOUSEFI Student Number: A00905279

Entitled: HYGROTHERMAL PROPERTIES OF BUILDING MATERIALS AT DIFFERENT TEMPERATURES AND RELATIVE HUMIDITIES

And submitted in partial fulfillment of the requirement for the degree of:

Master of Applied Science in Building Engineering/Building Science

Complies with the regulations of the Institute and meets the accepted standards with respect to originality and quality.

Signed by the final Examining Committee:

Rodrigo Mora, Chair

Leslie Peer, Examiner, external to program

Ali Fallahi, Examiner, program

Fitsum Tariku, Supervisor

Approved by:

Graduate Program Director

Abstract

Hygrothermal Properties of Building Materials at Different Temperatures and Relative Humidities

Youness Yousefi

British Columbia Institute of Technology (BCIT)

Recently, due to the rise of public awareness of energy saving issues, energy modeling and building simulation are increasingly becoming inevitable. Designers, engineers and even clients prefer to examine different models of energy performance of building through computer-based simulation tools at early stages of design in order to achieve higher energy efficiency in buildings. However, the building industry is constantly developing and moving towards a similar approach with building envelopes. Recent unprecedented advances in technologies and materials, coupled with elevated expectations of performance for both the envelope and the building, have emphasized a true need for the use of hygrothermal analysis techniques.

All simulation engines utilize different libraries in their database including material properties, assemblies, windows, HVAC systems, climate and occupancy profiles. Fundamental knowledge of hygrothermal characteristics of building materials is required to profoundly analyze and interpret the output of building energy simulations, and to select suitable materials for buildings. The significance of up to date hygrothermal properties of building materials are more highlighted where the reliability of these models depends on the quality of their inputs which includes thermal properties, moisture storage and transport properties of building materials. Given the fact that building envelopes globally are exposed to various extreme climate conditions, therefore a comprehensive set of material properties under different conditions will enhance reliability of the results from building energy modeling.

This research project investigated and measured a set of hygrothermal characteristics of several building materials commonly used across the North America. This study examined the behavior of building materials under various climate conditions other than what is proposed by the standards. Improving available standard test methods by using state-of-the-art equipment, enabled me to measure thermal conductivity, sorption isotherms, water vapor permeability and water absorption coefficient of tested materials under nine different combinations of temperatures from

3°C to 45°C and relative humidities from 50% to 90%. The results clearly present dependency of material properties on varying temperature and relative humidity. For example, thermal conductivity, vapor permeability and water absorption coefficients of all tested materials increased with respect to temperature, while the sorption isotherms of all materials decreased when temperature rose. The obtained results from this research can be utilized in Heat, Air and Moisture (HAM) modeling to improve effective and realistic analysis hygrothermal and energy performance of whole buildings.

Acknowledgement

It is a great honor to acknowledge my deepest gratitude to my thesis supervisor, Dr. Fitsum Tariku who introduced me to building physics. He generously gave me the freedom and support to explore my experimental research. I would also like to extend my special thanks to my teachers Dr. Rodrigo Mora (BCIT), Dr. Leslie Peer (RJC), Bo Li (BCIT) and Dave Ricketts (RDH) for sharing their knowledge of building science and building materials. Many thanks to Douglas Horn and Wendy Simpson, the staff from BCIT Building Science Centre of Excellence who shared their valuable time and knowledge during my experiments. I would also like to express my appreciation to my dear friend, Hossein Mirzaghafour for his priceless help in the long days of running the experiments.

I would also like to sincerely thank my wife Tahereh Rashnavadi for her support and being my biggest fan and my daughters Diana and Anahid for their endless love. I would like to extend my thank to my family for their great help and support during this research.

Table of Contents

List of Tables

List of Figures

1 Introduction

Today with the emergence of powerful personal computers, hygrothermal simulation models have become powerful tools for building scientists, building physicists and building practitioners. These models require a set of very reliable inputs to yield meaningful results. Some of these inputs include thermal properties, moisture storage and transport properties of the building materials (Kumaran, 2006). Presently, the most used properties are extracted from an International Energy Agency Annex (Kumaran, 1996b) and ASHRAE report (Kumaran, 2002).

During the past decades, several research organizations have been systematically determining the hygrothermal properties of building materials. However, building materials are continuously evolving due to the evolution and variation of the manufacturing processes among different manufacturers of the same product. Therefore, it is desirable to determine the changes in building materials' properties at least once in a decade. This will ensure that the hygrothermal models are using valid database and functional dependencies for the properties of each material.

Building scientists agree that there is not enough description for material identification in the literature (Karagiozis et al., 2001). It is rare to find all information about manufacture, location, environmental condition, and detailed measurement data in a single published literature (Wu, 2007). Hygrothermal properties of materials are often stated without making references or giving an insufficient information about the material source, manufacturing process, test conditions, origin of the raw materials, etc. Usually, the available data is not complete in many aspects and calculated coefficients and dissipated information are not adequate to be used in simulation programs.

Furthermore, constant developments in manufacturing processes may cause substantial variations in material properties due to the new technologies and composition in producing new building materials. Therefore, it is expected that new materials would have different characteristics compared to those which have been documented in the existent literature.

1.1 Thesis Arrangement

In section 2, a literature review on material properties, their fundamentals and temperature dependencies under different conditions is presented. This section also reviews different published and well-developed experimental methods and international standard test procedures to determine

the materials properties. Section 3 is describing the problem statement and current issues in the field of building science pertaining the material properties which followed by section 4 in which, the current research significances and goals are articulated through an appropriate approach. This section ends with the research methodology. Brief descriptions related to each tested material of this project are provided in section 5. In section 6, the discussion is presented regarding the experimental procedure including: facilities, materials sample preparation and different proposed test conditions according to the pertaining standard test method. Section 7 presents the tabulated empirical results accompanied with discussion for each measured property. Finally, the conclusion of this research project is presented in section 8.

2 Literature Review

The literature review has been conducted on three major areas:

- Moisture transport theories and mechanisms
- Property measurement methods of building materials
- Temperature dependency of material properties

Since the presence of moisture in buildings is critical thus, understanding the properties of materials with regards to the moisture transport mechanisms in building envelope is important. The literature review is intended to investigate the current knowledge of physical properties as well as the challenges in moisture storage and transport theory in building materials under different combinations of temperature and relative humidity. This knowledge is fundamental to understand the complex interaction of heat, air, and moisture transport in the built environment.

Besides dry density and porosity as basic characteristics, the set of material properties that currently are used for hygrothermal analysis in computer simulation models are as following:

1. Thermal conductivity.
2. Specific heat capacity.
3. Sorption isotherms.
4. Water vapor permeability.
5. Water absorption coefficient.

2.1 Basic Material Properties

2.1.1 Density

Bulk density (or density in a mass) is the weight of the material including the solid, intergranular air space and water in unit volume. Dry density of a building material is considered as the mass of the solid per unit volume of the dry material. The samples must be dried until constant mass change is reached within 0.1% during three successive daily weighings (ASTM-C1498−04a, 2011). The samples volume is calculated based on the average of three measurements of each dimension. However, for practical purposes, the term "dry material" does not necessarily comply absolutely dry material (Kumaran, 2001b). In order to experimentally determine the density of different classes of the building materials such as cementitious, wooden, or plastic, different temperatures

can be applied according to the pertinent standard conditions. For example, for wood and gypsum this may refer to drying at 105˚C and 40˚C, respectively.

2.1.2 **Porosity**

The apparent porosity of a porous medium is defined as a percentage the ratio of the open pores volume to the total volume of a representative sample of the medium (ASTM-C20-00, 2015). The mass of the water inside the open pores of a specimen can be obtained by subtracting the dry weight, D [kg] from the saturated weight, W [kg] of the water-saturated material sample. Therefore, the volume of the open pores V_{Pores} [m^3] can be calculated by using equation (2.1):

$$V_{Pores} = \frac{W-D}{\rho_w} \qquad (2.1)$$

Where ρ_w [kg/m^3] is the density of water. It is assumed that the density of water at room temperature is 997 [kg/m^3]. Then, the porosity of the specimen ε [%] can be obtained by dividing the volume of the open pores by the exterior volume V_e [m^3] of the specimen:

$$\varepsilon = \frac{V_{Pores}}{V_e} \times 100 \qquad (2.2)$$

Open pores are accessible for water vapor.

2.2 Thermal Properties

Thermal properties of materials explain the behavior of material during heat transfer. The thermal properties include the heat capacity and the thermal conductivity of materials.

2.2.1 **Specific heat capacity**

Specific heat capacity of a material is defined as the heat (energy) required to increase the temperature of unit mass of the material by 1 K.

The mass in the above definition refers to the dry mass. If the material is wet, the specific heat capacity c is to be calculated as:

$$c = c_0 + 4187.\ (w/w_{sat}) \qquad (2.3)$$

where c_0 is specific heat capacity, w is moisture content and ρ_0 is density of the material. The above relation assumes that the specific heat capacity of water is constant and equal to 4187 [J/kg. K].

2.2.2 **Thermal conductivity**

Thermal conductivity characterizes the heat transport property of materials. Understanding of a material's thermal conductivity is critical for home insulation using broad range of building materials and insulation.

Majority of thermal insulation materials are highly porous and contain of a solid matrix with small cavities within the cells, pores or interstices that form more than 90% of the entire volume (ASHRAE, 2017). These voids comprise air or some other harmless gases such as CO_2 due to their better insulating and radiation absorbing qualities. The insulation may take the form with open or closed cells, loose fill with nodules, granules, powders or fibers, and fibers with binder.

Heat transfer through insulation materials occurs through three primary mechanisms, separately or in combination: conduction, convection, and radiation (Peavy, 1996; Budaiwi et al., 2002; Berardi and Naldi, 2017).

Conduction is the flow of heat by direct molecular contact. It is the most important heat transport mode for solids, sometimes important for liquids, and only occasionally important for gasses. In thermal insulating materials, the factors that mainly influence the heat conduction are the raw material, the density of the material, the microstructure of the solid matrix, the moisture content, the temperature, and the gas. Convection is the transfer of heat by the movement or flow of molecules (liquid or gas) with a change in their heat content. This is an important heat transfer mode between fluids and solids or within fluids. Finally, radiation is the transfer of heat by electromagnetic waves through a gas or vacuum. Heat transfer by this last mode requires a line of sight connection between the involved surfaces. Radiation can be diffuse, specular or non-gray between the surfaces of the pores or gaps as well as the destructing and dispersing of transmitted radiation through a void in matrix material (Budaiwi et al., 2002). Since, the radiation properties vary with wave length, the radiation component can be expected to change considerably with the increase in temperature difference (Peavy, 1996). This phenomenon is one of the factors which causes the thermal conductivity in low density materials to be more sensitive to temperature difference.

A specific combination and the interactions among the three modes of heat transfer determine the overall effectiveness of heat transfer through a porous material and are represented by its "apparent

thermal conductivity" (ASHRAE, 2017). This term is used to represent the lack of a "pure conduction" mode of heat transfer in porous materials (Berardi and Naldi, 2017).

Considering the substances type, the apparent thermal conductivity is based on several factors at the microscopic level including cell size, diameter and arrangement of fibers or particles, transparency to thermal radiation, type and pressure of the gas, bonding materials, etc.

At the macroscopic level, the apparent thermal conductivity mainly depends on five factors: density, porosity, moisture content, mean temperature difference, and age (Budaiwi et al., 2002; Domínguez-Muñoz et al., 2010; Yener et al., 2018). The influence of natural convection has been shown to be negligible under normal operating conditions (Papadopoulos, 2005). In a practical definition of thermal conductivity of a dry building material, all three modes of heat transfer are included. In wet materials, the density of heat flux will be increased by adding the heat transferred by moisture through the capillaries and the enthalpy associated with phase changes (Černý and Pavlík, 2007).

The thermal conductivity of a material at a point is defined as the ratio between the density of heat flow rate and the magnitude of the thermal gradient at that point in the direction of the flow. The definition for thermal conductivity stems from Fourier's law of heat conduction based on continuum concept (Kumaran, 2001b; Hens, 2017; Yener et al., 2018). In study of heat conduction, where only macroscopic information is of interest, the molecular structure of the substance is ignored and it is considered to be continuous medium or continuum (Yener et al., 2018):

$$q_c = -k \,.\nabla T \qquad (2.4)$$

Where q_c [W/m^2] is the density of heat transfer, k [W/ (m.K)] is the thermal conductivity and T [K] is the temperature. This is driven from the Fourier's law of heat conduction. By considering a solid flat plate with a thickness of L and very large other two dimensions and the surface area of A exposed to different temperatures at both surfaces, then according to the second law of thermodynamics, heat will flow through the plate from the higher temperature surface to the lower one. The equation that governs the rate of heat flow is:

$$q \sim A \frac{T_h - T_l}{L} \qquad (2.5)$$

According to the first law of thermodynamics, under the steady state conditions, the flow of the heat will be constant (Yener et al., 2018). The relation can be written as:

$$q = k\,A\frac{\Delta T}{L} \qquad (2.6)$$

Where the positive proportionality constant *k* is called the thermal conductivity of the material of the plate.

Considering the fact that heat transfer is dependent to the temperature and moisture, therefore, the thermal conductivity (k) can be defined as a function of temperature and moisture content and calculated as (Delgado et al., 2013):

$$k = k_d + C_T\left(T - T_{ref}\right) + C_w.w \qquad (2.7)$$

where k_d [W/ (m. K)] is the thermal conductivity of the building material under dry conditions and C_T and C_w are temperature and moisture modification coefficients, respectively.

Furthermore, Domínguez-Muñoz et al. (2010) delineated the general relationship between conductivity and density as following:

(a) at low densities, conductivity increases as density decreases due to the effect of radiant exchange inside the pores,

(b) at high densities, conductivity increases with density as porosity decreases.

(c) the lowest thermal conductivity occurred at densities between 30 and 60 kg/m^3.

The relationship between average conductivity and density can be modelled with a simple polynomial function. The conductive part of the total thermal conductivity is the sum of the conductivity of air (constant) and solid matrix (increases with density) and can be expressed as

$$k_{cond} = a + b\rho \qquad (2.8)$$

The radiative portion of the thermal conductivity is a reciprocal function of density, because as density increases, the more solid components blocking radiant exchange are found in the internal structure of the material:

$$k_{rad} = \frac{c}{\rho} \qquad (2.9)$$

The total conductivity can be expressed as the sum of (2.8) and (2.9) which is usually called the inverse relationship (Anderson et al., 1999):

$$k = a + b\rho + \frac{c}{\rho} \qquad (2.10)$$

However, it worth to mention that some materials such as extruded polystyrene, polyurethane and phenolic foam show no relationship between conductivity and density in the considered range of densities (Domínguez-Muñoz et al., 2010).

In addition to temperature and density, the thermal conductivity of a material depends on the moisture content of the material. Measuring thermal conductivity also requires knowledge about the pore fraction and distribution and some other properties of solid particles such as density. Moreover, in case of exposure to moisture some other material properties such as hygric properties as well as pore structure must be taken into account. According to Ochs et al. (2008) the effective thermal resistance of insulation materials are inversely related to the increase in temperature and moisture content. For instance, in high temperatures (more than 60˚C), the actual thermal losses of insulation are 30-50% higher than the design value even with small water content of less than 5%. Tye and Spinney (1979) who studied the impact of moderate moisture on thermal performance in wall constructions with cellulose insulation found a decrease of the thermal resistance by 15% when the moisture content increased only by 10%. Studying insulation materials, Hansen et al. (2001) measured thermal conductivity of cellulose fiber, flax, sheep's wool, perlite, rock fiber, and glass fiber. Their empirical results revealed that the thermal conductivity for all the materials, was relatively constant at most humidity levels and then increased significantly when the mean relative humidity was above 70% RHs.

2.2.3 **Measurement Methods**

When we study thermal performance and energy efficiency of an insulation material, the most important property to consider is the *k* value known as thermal conductivity. A summary of available measurement methods for thermal conductivity of building materials is represented in the following diagram.

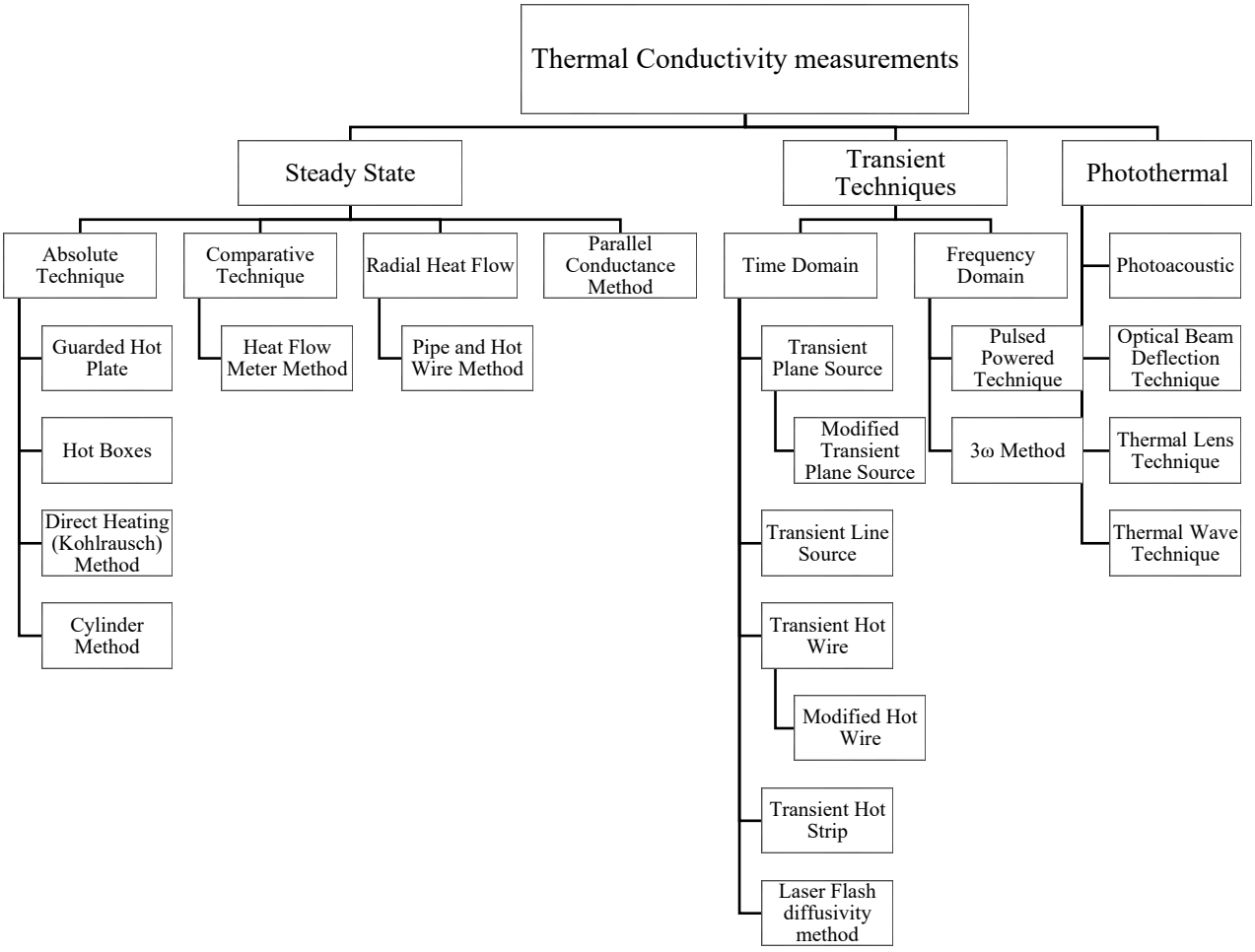

Figure 2-1. Different measurement methods of thermal conductivity (Czichos et al., 2006).

There are two main types of techniques to measure thermal conductivity, steady-state techniques (Asdrubali et al., 2010; Salmon and Tye, 2010), and transient techniques (Bouguerra et al., 2001; He, 2005). The most commonly used equipment for steady state method is the guarded hot plate (GHP) apparatus (ASTM-C177, 2013) or the heat flow meter (HFM) apparatus (ASTM-C518, 2010). Currently, heat flow meter apparatus is known as a very good instrument for evaluating the thermal performance of thermal insulation materials, shown in Figure 2-1 . An important factor pertaining the use of this method is heat flow meter calibration, especially of the whole apparatus (McElroy and Tye, 1980). The schematic of the heat flow meter device is shown in Figure 2-2 . Each plate has a built-in heat flow sensor. The plates are maintained at different constant temperatures by electric resistance heating and a circulating thermostated fluid in a counter-flow

pattern pumped by water baths. During the test, three quantities are measured from each plate including:

- Output, E (mV), from the heat flow sensor
- Temperature, Tp (°C) from the exterior surface of the plate and
- Temperature, T (°C) from the inner surface of the plate

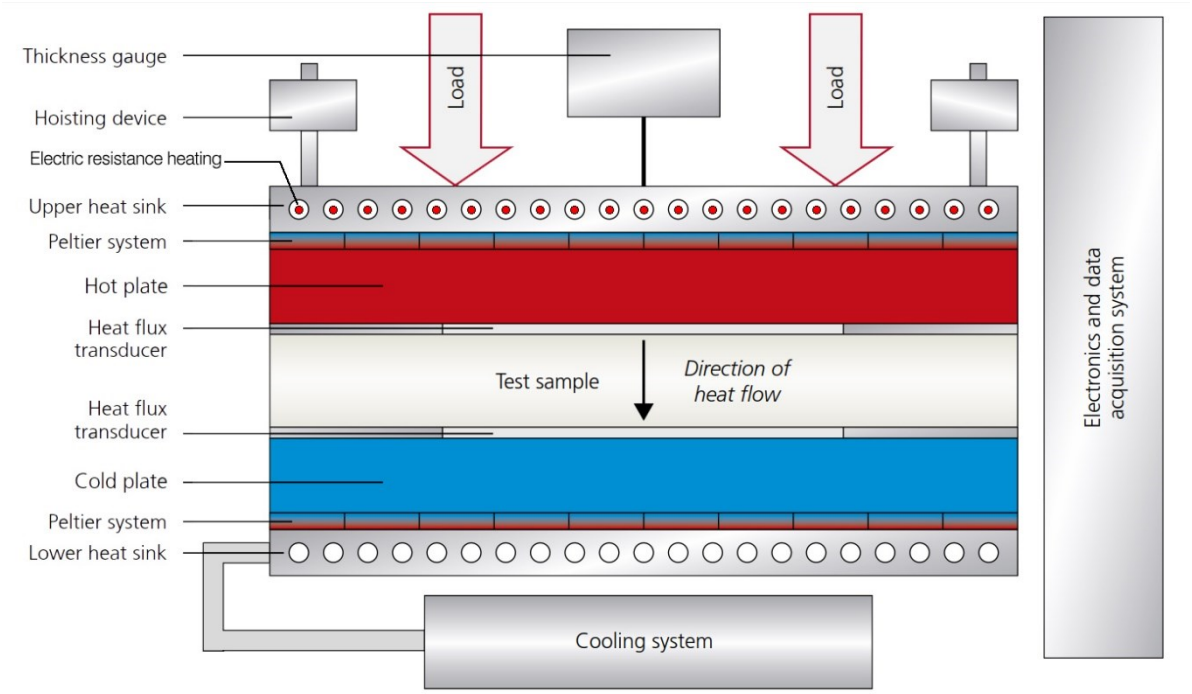

Figure 2-2. Schematic design of the NETZSCH HFM 436/3/1 Lambda (plate temperatures between 0˚C and 100˚C) (Netzsch, 2018)

The accuracy of an HFM test relies on the construction of the apparatus and the testing procedure, both factors must be considered in selecting a range of test conditions. Since the accuracy of an HFM depends on several factors pertinent to the structure of the apparatus: for example, flatness and parallelism of the hot and cold plates (a description of these factors are presented in ASTM-C518 (2010)). An external computer system with specialized software controls the measuring apparatus, records and analyzes the data, and prints the results.

Since the heat flow meter apparatus is a comparative or secondary method of measurement, it requires to be calibrated to specimens of known thermal transmission properties which were tested using an absolute measurement method such as the guarded-hot-plate apparatus (Scott and Bell,

1994). To minimize errors, the apparatus should be calibrated with the Calibrated Transfer Specimen (CTS) or Standard Reference Material (SRM) to measure the response of the heat flow transducer at different temperatures. According to Bomberg and Solvason (1983) who have compared various calibration techniques, using transfer standards is the preferred technique for calibrating the HFM apparatus. The thermal insulation program at the National Institute of Standards and Technology (NIST) provides both aforementioned groups of reference materials which are used by standard test methods for the purposes of checking guarded-hot-plate apparatus, calibration of heat flow meter apparatus and checking or calibrating hot-box apparatus if required (Zarr, 2008). CTS also known as transfer specimen is an insulation specimen with an established mean R-value and an approximated uncertainty of its thermal resistance provided to the customer individually. SRM is a Certified Reference Material (CRM) from a batch of homogeneous material which their instabilities and thermal transmission have been characteristics (Hust, 1985). In contrast to a NIST CTS which its thermal resistance value is directly measured in a NIST guarded-hot-plate, the thermal conductivity of insulation SRMs is characterized statistically as a function of bulk density, mean temperature and ambient pressure, if necessary (Zarr, 2008; Zarr et al., 2014). Consequently, the measured thermal conductivities for a thermal insulation SRMs are associated with greater uncertainties. Started from 1958, the National Bureau of Standards (NBS) has developed series of thermal insulation SRMs: fibrous-glass board, 1450 (and ensuing lots 1450a, 1450b, 1450c and 1450d); fibrous-glass blanket, 1451 and 1452; and fumed-silica board, 1449 and 1459 (which is dimensionally smaller unit). Accordingly, NIST issued expanded polystyrene board 1453 which is utilized in calibration procedure for testing windows in a hot box (Zarr et al., 2014). Periodically, NIST has provided reports on SRMs which describes the historical background of the SRM 1450 series, along with the assessment of industry requirements, material characterization, thermal conductivity measurements, regression analysis, certified values of thermal resistance, and analysis of uncertainties for a specific SRM. The thermal characterization of SRM 1450c, high density fibrous glass board with a bulk density ranged from 150 kg/m^3 to 165 kg/m^3, has been accomplished over the range of mean temperatures from 280 K to 340 K at NIST laboratory facilities by Zarr (1997). He developed a model that described the thermal conductivity over the range of those parameters:

$$\lambda(\rho, T) = a_0 + a_1 \times \rho + a_2 \times T_m \qquad (2.11)$$

Where λ(ρ,T) is the thermal conductivity as a linear function of density ρ(kg/m^3) and temperature (mean temperature T_m, (°C)) and a_0, a_1, a_2 are the regression coefficients. Based on the results of the curve fit analysis, they determined the regression coefficients as follow:

$a_0 = -7.7663 \times 10^{-3}$ (W/m.K),

$a_1 = 5.6153 \times 10^{-5}$ (W.m^2/K.kg), and

$a_2 = 1.0859 \times 10^{-4}$ (W/m.K^2).

Zarr (1997) explained that the predicted values of thermal conductivity for SRM 1450c are within 2 % of the North American results of an international round robin and agreed to within 1 % to 7 % of predicted values for previous material lots of SRM 1450 series.

A number of transient measurement methods that have been developed include the transient hot wire (Backstrom, 1982; Glatzmaier and Ramirez, 1985), transient line source (Cull, 1974), transient hot strip and transient plane source techniques (Gustafsson et al., 1979; Gustafsson, 1991; Al-Ajlan, 2006). The thermal properties of isotropic and homogeneous materials have been successfully measured with these methods.

Salmon and Tye (2010) compared steady-state and transient methods by measuring the thermal conductivity of thin (6-7 mm) specimens of brick materials through utilizing guarded heat flow meter apparatus and the plane source technique as single strip or bridge for those methods, respectively.

Normally, this thickness range is not suitable for precise measurements on such types of solid material using a standard guarded hot plate or heat flow meter apparatus. However, considering the inhomogeneity, anisotropy of the material and the measurement uncertainties, the results for the guarded heat flow meter method and the transient methods are within ±3% of the mean guarded hot plate values which can be acceptable.

It is expected that the measured thermal conductivity values would be influenced by several factors such as operating temperature, laboratory conditions, material preparation and workmanship. Zarr and Filliben (2002) investigated the variability in the results of thermal conductivity of two insulation reference materials including resin-bonded glass fiberboard and expanded polystyrene board using guarded hot plate apparatus. The investigation conducted internationally between

laboratories from Canada, France, Japan, United Kingdom and the United States. They compared the results based on the effects of factors such as laboratory and material through five replicate measurements at 297.15 K (24˚C). The final results indicated some differences in thermal conductivities from laboratory to laboratory and material-to-material where the latter one was greater.

Hay et al. (2013) compared the results of thermal conductivity of mineral wool and expanded polystyrene at temperatures 10˚C, 23˚C, and 40˚C from seven laboratories internationally using the guarded hot plates method (GHP). They circulated the same material sets around laboratories except one laboratory. In addition, they performed a repeated thermal conductivity measurement at 23˚C to determine and eliminate inconsistent data and increase the validity of the results. After analyzing the replicated measurements, results from two laboratories were removed due to data anomaly. Therefore, at the other laboratories the standard deviation (SD) for repeatability and reproducibility of the GHP were predicted to be less than 0.1 % and 1.2 %, respectively.

2.2.4 **Temperature Dependency**

Thermal insulating materials are quite different from other solids in that they are generally heterogeneous, anisotropic and contain gaseous additions whereby heat transfer modes other than conduction are quite evident. For most thermal insulations, the thermal conductivity increases with increase in temperature due to an effect of radiation. Thermal conductivity as a function of temperature is an empirical relationship based on experimental data. Therefore, it is essential that a useful range of temperature suitable to the material should be employed in order to determine the function, $k(t)$ (Peavy, 1996). In an appropriate temperature range, it is important to perform tests at enough mean temperatures, T_m. Furthermore, it may become necessary to carry out additional experiments at diverse temperature differences, preferably at the selected mean temperatures. This is important since extrapolation to other temperature differences outside of the experimental parameters is not always possible and is considered to be hypothetical.

The thermal conductivity values that are published or documented by the material manufacturers are usually obtained under laboratory standard conditions where temperature and moisture conditions are controlled to allow a comparative evaluation of thermal performance (Budaiwi et al., 2002). However, insulation materials used in building envelopes are exposed to different temperatures and moisture levels depending on the local environmental conditions where the

buildings are built. In some places, for instance, the temperature of the roofs and walls may reach over 80˚C in summer and below 0˚C in winter. Therefore, it is important to take those conditions into consideration when analysing the thermal performance of an insulation material as their real thermal performance may noticeably differ from that predicted under standard conditions. The influence of operating temperature on the thermal conductivity performance of insulation materials has been the subject of several studies.

Bomberg studied the thermal conductivity of mineral fiber insulation through a numerical and experimental method considering three factors of thickness, density and mean temperature. They presented an equation for thermal conductivity combining varing proportions of three basic heat transfer mechanisms in fibrous insulations including conduction, convection and radiation. They found a good agreement between their predicted values and the experimental results from National Research Council Canada (NRC) and other literature. Their analysis revealed that the thermal conductivity in mineral fiber insulation increased with rising temperature and thickness while decreased with increasing density.

Aldrich and Bond (1985) theoretically and experimentally investigated the thermal performance of extruded polystyrene and polyurethane foams (polyisocyanurate) at different mean temperatures below zero where they are used for subfreezing applications such as refrigerators. They developed a numerical computer model to simulate the thermal conductivity against the temperature profile across the insulation. The model was verified by using k-values for extuded polystyrene and polyurethane insulations obtained from the ASHRAE (1985). Accordingly, by using guarded hot plate method, each insulation samples was tested at four operating conditions. The cold side was maintained at approximately -30˚F for all tests. In correlation with the computer model, the warm side temperatures were set to approximately +25˚F, +65˚F, +75˚F and +100˚F. Consequently, the temperature differences (ΔT) were 55˚F, 95˚F, 105˚F and 130˚F, as typical seasonal fluctuations throughout a year. Their experimental results revealed an increase in k-values with elevating operating temperature in both tested insulations. The results for extruded polystyrene showed a good correlation with the predicted results. However, unlike the computed R-values at for polyisocyanurate insulation which were increasing with temperature, the measured thermal resistance decreased with rising temperature.

Peavy (1996) theoretically attempted to propose a numerical method for determination of thermal conductivity of porous materials at different operating temperature. He outlined the higher variation of thermal conductivity with temperature is associated with lower density insulating materials.

In an international investigation, Zarr and Filliben (2002) compared the results of thermal conductivity of two insulation reference materials including resin-bonded glass fiberboard and expanded polystyrene board. They studied the impact of different factors including temperature by performing five single-point measurements at 280 K, 290 K, 300 K, 310 K and 320 K. According to their measured k values from different laboratories, in general the temperature elevation increased the thermal conductivity, whereas there was a discrepancy in results among all laboratories for temperatures below 297.15 K.

Similarly, Hay et al. (2013) internationally compared the results of thermal conductivity of same samples of mineral wool (MW) and expanded polystyrene (EPS) at temperatures 10˚C, 23˚C, and 40˚C from seven laboratories. The results indicated an upward trend in thermal conductivity by temperature in five laboratories in which the same materials were been used. The maximum differences between these 5 laboratories for MW and EPS were 1.8 % and 2.5 %, respectively.

Abdou and Budaiwi studied the thermal performance of 32 different locally manufactured insulation materials from seven categories namely, fiberglass, wood wool, rock wool, mineral wool, polyethylene, polyurethane and polystyrene (Budaiwi et al., 2002; Abdou and Budaiwi, 2005). The samples were collected from different manufacturers with variable densities and physical and thermal characteristics. The insulation materials were tested as a compartment of a wall assembly at five different mean temperatures including 4, 10, 24, 38, and 43˚C, based on ASTM C 1058-92 (ASTM 1991a) ISO 8301 protocols. According to their research, the thermal conductivities of all insulation materials were increased upon increasing the operation temperature. However, the thermal conductivity of polyethylene and polystyrene insulations represented maximum and minimum increases, with a rate of 0.000384 W/m.C per ˚C and 0.0001 W/m.C per ˚C, respectively. In addition, they highlighted a correlation between the higher density of the insulation materials and lower variation in thermal conductivities and vice versa.

Using different test method, Al-Ajlan (2006) also investigated temperature dependency of thermal conductivity of a few insulation materials at different mean temperatures of 22˚C, 35˚C, 50˚C and

65˚C. He used the transient plane source (TPS) technique, which also called the hot disk (HD) method. According to his observations, the thermal conductivity increased when temperature elevated and decreased where the density increased. For instance, by increasing the temperature from 22˚C to 35˚C (the most common range of local temperature change), the conductivity of polyurethane with the average density of 30.5 [kg/m^3] increased by approximately 19% while that of polystyrene with the average density of 30.3 [kg/m^3] increased by an average value of only about 7%. However, the impact of temperature was observed to be higher than density.

In addition to temperature, Ochs et al. (2008) investigated the impact of moisture on effective thermal conductivity of porous insulation materials made of different granules using guarded heating plate device according to DIN 52612 and ASTM C177. They performed the tests on eleven different bulk porous insulation materials from four categories (expanded glass granules, expanded perlite, expanded clay, foam glass gravel) at different temperatures from 20˚C to 80˚C for a water content between 0 and free saturation water content. For modeling the thermal conductivity of porous materials, they used temperature dependent parameters such as: the vapor diffusion coefficient and the saturation vapor pressure. In order to model the presence of moisture, the authors calculated effective thermal conductivity of liquid water and water saturated air separately.

The results indicated a significant increase in effective thermal conductivity of materials at higher temperature (more than 60˚C) even with small water content of less than 5%. Since manufactures results are measured at 10˚C based on DIN specifications so the authors anticipated a higher thermal conductivity of insulations in real life performance to be 4 to 10 times higher. They concluded that variation in thermal conductivity is associated with the pore fraction, distribution, structure, density and even hygric properties in case of moisture exposure.

In a study, Zhang et al. (2008) numerically and experimentally investigated the thermal conductivity, specific heat and the transmittance spectra of high-alumina fibrous insulation under a range of mean temperature from 27°C to as high as 700°C. The presence of the radiation heat transfer through highly porous materials, poses complications in determining the effective thermal conductivity. They modeled a two-flux approximation in order to simulate the radiative heat transferring through the fibrous insulation. Based on the specific heat capacity and Rosseland mean extinction which they measured experimentally, a numerical heat transfer was modeled to predict the effective thermal conductivity. According the obtained results of the study, the thermal

conductivity and specific heat of the tested material rose with increasing the temperature. However, they observed a difference of approximately 13.5 % between the numerical and experimental values for effective thermal conductivity.

Studying the thermal performance of stone wool, Karamanos et al. (2008) explained the effective thermal conductivity of fibrous insulations as a combination of heat radiation through the fibers and heat conduction through the fibers body and the air between the fibers. By analyzing the numerical equation for each heat transfer mechanism, he investigated their participation in the total thermal conductivity. It was observed that by increasing temperature, the impact of radiation increased while the impact of conduction decreased. Similarly, Daryabeigi et al. (2011) investigated the thermal performance of five high-porosity unbonded (loose) fibrous insulations as a combination of radiation and conduction heat transfer through the material structure. They highlighted that the solid conduction has the lowest impact on heat transfer in highly porous fibrous insulation. In contrast, the radiation and gas conduction are considered as the primary components affecting the heat transfer which both increase with temperature. However, the radiation decreases with increasing the density of insulation. Furthermore, their measurements and predicted results for effective thermal conductivity at different ranges of extreme low and high temperatures revealed a highly nonlinear function of temperature.

Yüksel et al. (2010) investigated the thermal conductivity of multi-layered glass wool reinforced with layers of reflective aluminum foil or with low reflective materials such as nylon sheet or white paper. They carried out the experiments with samples of binary (two layers), ternary (three layers) and quadruple (four layers) glass wools at temperatures 25˚C and 40˚C with temperature differences of 5˚C, 10˚C and 15˚C. The results showed a slight increase of thermal conductivity with rising temperature in the insulations without aluminum foil layers while in the insulations with aluminum foil the increase was significant. Additionally, the amount of increase was observed to be associated with the number of the foil layers. Furthermore, according to their results, the thermal conductivities with lower temperature difference had larger increases with rising mean temperature.

Later in a similar study with the same approach, Yüksel et al. (2012) studied the effective thermal conductivity in binary and ternary glass wools insulation at lower temperature range from 0°C to 25°C in comparison with low density EPS layered insulation. Similar to their previous study, a

low fluctuation in thermal conductivity was observed with increasing temperature in both glass wools and EPS insulations. Based on the experiment results, the effective thermal conductivities in both cases increased rapidly with temperature while large changes were noted at temperature difference of 5°C.

Abdou and Budaiwi (2013) conducted a research on variation of the thermal conductivities of three fibrous insulations: fiberglass, rock wool and mineral wool with different moisture contents at mean temperatures of 14°C, 24°C and 34°C. Concluded from the experimental results, they pointed out an increase in thermal conductivity with increasing temperature while the samples with higher moisture content represented higher values. Furthermore, they observed less impact of operating temperature on the changes of thermal conductivity in the insulations with higher density at all different moisture content levels.

Similarly, Vololonirina et al. (2014) investigated the impacts of temperature, density, moisture content and fiber orientation on the thermal conductivity of three common wood-based building materials (wood-fiber insulation, oriented strand board and spruce solid wood according to standard NF EN 12664. The thermal conductivity measurements were conducted at temperatures: 10˚C, 25˚C and 40˚C with different moisture contents as a result of exposure to the following climatic conditions: dry, mid-state and wet with relative humidities of 7%, 50% and 90%, respectively.

Their measurements revealed that the thermal conductivity of the materials increased linearly with the rise of temperature and moisture content in both dry and wet states. The higher values of thermal conductivity were noted to be correlated with materials with higher moisture content and density. Additionally, they observed an inconsistency in thermal behavior of the woods' samples with different fiber orientation relative to the heat flux direction which they stated that can be associated with the anisotropy nature of the wood. The effects of fiber direction were outlined as an increment factor of 2 for wood fiber, 2.2 for OSB and 2.8 for solid wood.

Koru (2016) studied the temperature dependency of the thermal conductivity along with the impact of the density in closed-cell insulation materials. He measured the conductivity values for Expanded polystyrene (EPS), extruded polystyrene (XPS), expanded nitrile rubber (ENR), polyurethane (PUR), polyethylene (PE) and ethylene vinyl acetate (EVA) at fourteen different mean temperatures from −10˚C to +55˚C with 5˚C steps and ΔT of 20˚C. The measurements were

carried out using heat floe meter apparatus and according to ASTM C518, EN 12664, EN 12667 and ISO 8301 standards. Their results represented an increase in thermal conductivity with rising temperature and decrease with increasing density in tested materials. Furthermore, the thermal conductivity increased faster with temperature in materials with lower densities. He concluded that in materials with low-density values, the volume of air in the structure increases which intensifies the kinetic energy levels of the molecules. This leads to an escalation in thermal conductivity values.

Berardi et al. (2018) experimentally investigated the temperature dependency of four insulation materials including fiberglass, rockwool, polyisocyanurate (PIR), and extruded polystyrene (XPS). Thermal conductivity of the insulations was measured at mean temperatures ranging from -10˚C to +50˚C with increasing steps of 10˚C. Their empirical results represented a linear temperature dependency of thermal conductivity for inorganic materials made of fibers such as rockwool or fiberglass, showing lower thermal conductivities at lower temperatures. However, for foamed insulation materials like polyisocyanurate a nonlinear behavior was observed, with higher conductivity values for colder temperatures. They explained that at lower temperatures the blowing agent within the polyisocyanurate microstructure starts condensing, resulting the rise of conductivity. This effect has recently been extensively discussed by (Berardi and Naldi, 2017).

The full list of the literature reviewed along with the factors influencing the thermal conductivity are tabulated in Table 2-1.

Table 2-1. Published Literature in Temperature Dependency of Thermal Conductivity.

Paper	Theoretical	Experimental	Properties	Mean Temperature	Materials	Remarks
Bomberg and Klarsfeld (1983)	•	•	Thermal Conductivity	23.9°C - 40.7°C,	Dry Mineral Fiber	The thermal conductivity in mineral fiber insulation increased with rising temperature and thickness while decreased with increasing density.
Aldrich and Bond (1985)	•	•	Thermal performance	The cold plate was maintained at -34.45°C an d hot plate temperature increased in steps. Mean temperature: -19.16°C, -8°C, -5.27°C and +1.67°C ΔT: 12.78°C, 35°C, 40.55°C and 54.45°C	Extruded polystyrene and Polyisocyanur ate	The experimental results showed an increase in k-values with elevating operating temperature in both tested insulations. The test results for polyisocyanurate did not agree with the predicted values.
Wijeysundera et al. (1989)	•	•	Heat Flux, Water Vapor Diffusion	0°C -58°C	Fiberglass Slab	The thermal conductivity of slabs increased with temperature and temperature difference even with the presence of condensation of water vapor in the material.
Peavy (1996)	•		Thermal Conductivity	N/A	N/A	The temperature dependent function to calculate thermal conductivity is an empirical relationship and is reliable only

						based on experimental results. Extrapolation beyond the experimental parameters is hypothetical.
Smith (1997)	•	•	Thermal Conductivity	10°C, 24°C and a third arbitrary mean temperature between 0°C and 40°C	Dry Fiberglass Insulation Board	The thermal conductivity increased with increasing the mean temperature.
Dorthe Wildenschild et al. (1998)		•	Thermal Conductivity	20°C – 90°C	Topopah Spring Tuff with a water content of 0.030 (cm^3/cm^3)	The thermal conductivity decreased with increasing temperature.
Budaiwi et al. (2002)		•	Thermal Conductivity	4°C, 10°C, 24°C, 38°C and 43°C	Fiberglass, Wood Wool, Mineral Wool, Rock Wool, Polyethylene, Polyurethane, and Polystyrene	The thermal conductivity increased with increasing temperature.
Spinnler et al. (2004)	•	•	Thermal Conductivity	0°C – 1000°C	Multilayer Thermal Insulation consist of: Fibrous and Microporous materials	The theoretical and experimental results indicated a rising in thermal conductivity with increasing temperature.

					separated by multi screens.	
Zhao et al. (2004)	•	•	Thermal Conductivity	227°C – 527°C	open-celled steel alloy foam (FeCrAlY foam)	Measurements were carried out under vacuum and atmospheric conditions. The thermal conductivity showed a direct relationship with temperature, pore size and relative density.
Abdou and Budaiwi (2005)		•	Thermal Conductivity	4°C, 10°C, 24°C, 38°C and 43°C	Fiberglass, Wood Wool, Mineral Wool, Rock Wool, Polyethylene, Polyurethane, and Polystyrene	The thermal conductivity represented a direct and inverse relationship with temperature and density of the material.
Al-Ajlan (2006)	•	•	Thermal Conductivity	22°C, 35°C, 50°C and 65°C	molded Polystyrene, Extruded Polystyrene, Injected Polystyrene, Polyurethane Board, Glass Fiber, Rock Wool, And Loose Fill Perlite	The thermal conductivity increased relatively large with increasing temperature and decreased relatively small with increasing the density.
Zhang et al. (2008)	•	•	Thermal Conductivity, Specific Heat and the Transmittance Spectra	27°C – 700°C	High-Alumina Fibrous Insulation: Includes	The thermal conductivity and specific heat capacity increased with increasing temperature.

					alumina and silica.	
Karamanos et al. (2008)	•	•	Thermal Conductivity, Water absorption	25°C – 1000°C	Stone Wool	The thermal conductivity increased with increasing temperature.
Ochs et al. (2008)	•	•	Thermal Conductivity	20°C – 80°C	Expanded glass, Expanded clay, Expanded perlite, Foam glass	The effective thermal conductivity of the insulations with a small moisture content increased significantly with increasing temperature particularly at higher temperatures than 60°C.
(Yüksel et al., 2010)	•	•	Thermal Conductivity	25°C and 40°C ΔT: 5°C, 10°C and 15°C	Binary, Ternary and Quadruple Glass Wools Reinforced with Aluminum Foil or nylon and white paper	The results showed a slight increase of thermal conductivity with rising temperature in the insulations without aluminum foil layers while in the insulations with aluminum foil the increase was significant. The thermal conductivities with lower temperature difference had larger increases with rising mean temperature.
(Yüksel et al., 2012)	•	•	Thermal Conductivity	0°C, 5°C, 10°C, 15°C, 20°C and 25°C. ΔT: 5°C, 10°C and 15°C	Binary, Ternary Glass Wools, Ternary Expanded Polystyrene Foams all reinforced with layers of Aluminum	The effective thermal conductivities in both insulations increased rapidly with temperature while large changes were noted at temperature difference of 5°C.

					Foil or nylon and white paper	
Abdou and Budaiwi (2013)		•	Thermal Conductivity	14°C, 24°C, 34°C ΔT: 15°C	Fiberglass, Rock wool, Mineral wool (with different Moisture content level)	An increase in thermal conductivity was noted with increasing temperature while the samples with higher moisture content represented higher values
(Vololonirina et al., 2014)		•	Thermal Conductivity, Vapor Permeability, Sorption/Desorption Isotherm	10°C, 25°C, 40°C	Wood-Fiber Insulation, OSB, Solid Wood	The thermal conductivity of the materials increased linearly with the rise of temperature and moisture content. The higher values of thermal conductivity were noted to be correlated with materials with higher moisture content and density.
(Koru, 2016)		•	Thermal Conductivity	From -10°C to 50°C with 5°C intervals ΔT = 20˚C	Expanded polystyrene, extruded polystyrene, expanded nitrile rubber, polyurethane, polyethylene and ethylene vinyl acetate	The thermal conductivity increased and decreased with rising temperature and the density of tested materials, respectively.

2.3 Moisture Storage Functions

Similar to heat flow, the moisture transfer through a material is characterized by its moisture storage and moisture transfer properties. Moisture capacity is one of the important properties of materials which indicate their ability to hold moisture at different levels of relative humidity. The sorption isotherm is a key input data in moisture transport models, and it can also be used to evaluate properties of the microstructure.

Moisture storage data, in general, represents the hygroscopic and the over hygroscopic moisture content range. Different procedures and measurement technologies are applied in both moisture regions. The moisture content in porous bodies may vary between the dry state and a fully saturated state when the open pores are completely filled with water.

2.3.1 Adsorption Isotherm

When a gas or vapor as the adsorbate is brought in contact with a solid as the adsorbent, a certain amount of gas is taken up by the solid. The International Union of Pure and Applied Chemistry (IUPAC) described this general phenomenon as a term "physisorption", and its quality depends on the pores structure and the quality of their surfaces (Sing, 1985). The molecules that are deducted from the gas are either inside of the solid or attached to its outside surface and they are referred as absorption and adsorption, respectively. However, these two phenomenon occur simultaneously, therefore, the entire uptake of the gas or vapor is considered as the term sorption (Brunauer, 1943).

The phenomenon of adsorption has been discovered almost more than two centuries ago. The first description pertaining the uptake of gas by charcoal was provided by C.W. Scheele in 1773 and Abbe F. Fontana in 1777 (Brunauer, 1943). Later at the beginning of the nineteen century, De Saussure (1814) conducted the earliest systematic investigation on adsorption by measuring the adsorption of a variety of gases on several substances. The aforementioned names and dates are only representing the early pioneers and milestones in studying adsorption and exploring the history of adsorption is not the interest of this literature review. Brunauer and Emmett (1937) determined the adsorption isotherms of several gases on 30 different substrates based on the Van der Waals adsorption isotherms. Later they introduced five classification types of adsorption isotherms of gases on various solid surfaces (Brunauer et al., 1938). Expanding Brunauer's classification, Sing (1985) classified physisorption isotherms into six types with relation to the

pore size as shown in Figure 2-3. This classification considers adsorption at subcritical temperatures.

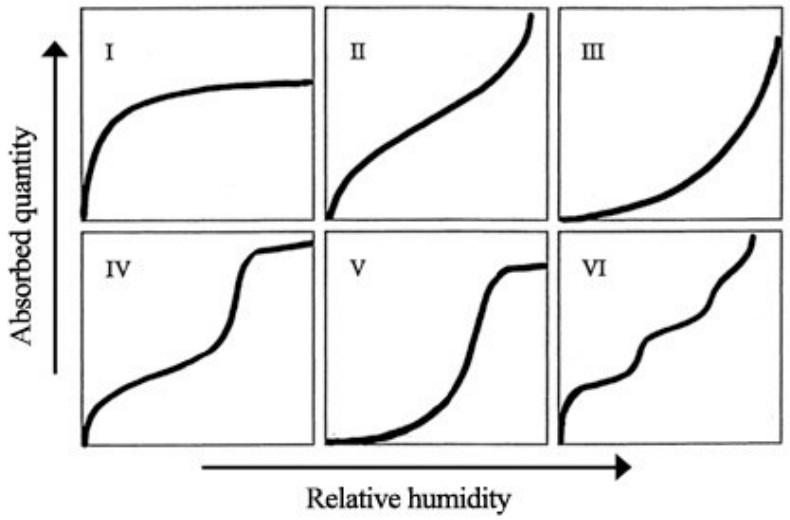

Figure 2-3. The IUPAC Classification of Physisorption Isotherms (Sing, 1985).

Type I isotherms characterize microporous solids with rather small external surfaces. The reversible types II isotherm describes a macroporous or even non-porous solid with strong adsorbate adsorbent interactions in which monolayer and multilayer adsorption occurs. Type III indicates adsorption on macroporous adsorbents with weak adsorbate adsorbent interactions. Types IV and V represent adsorption isotherms with hysteresis for the materials which contain mesoporosity and has a great adsorption energy. Finally, type VI which is not included within Brunauer's classification has temperature dependent steps and represents either materials with multiple pore sizes or phase change of multilayer adsorption. Although, this classification covers large number of adsorption systems, Donohue and Aranovich (1999) later suggested the new classifications which cover incomplete wetting systems as they pointed out that the IUPAC classification is limited to condensable vapors.

The ability to absorb water vapor is an important property of many technical materials and products. When porous materials are exposed to a certain environmental condition, they will absorb or desorb water molecules to stabilize their inner moisture content with the moisture level in the surrounding air and reach to a state called equilibrium moisture content (EMC). For a given environmental condition, building materials are different in the measured EMC and the time to

attain it, which depend on their physical and chemical characteristics at micro level and the nature of the process: adsorption or desorption. For instance, according to Kumaran (2002) at 23°C and 71.5 % RH a specimen of cellulose fiber insulation adsorbed 0.096 kg kg^{-1} and a specimen of low-density glass fiber insulation adsorbed only 0.0034 kg kg^{-1} of water vapor while clay brick could reach to the EMC of 0.047 kg kg^{-1} at 21°C and 90 % RH (Kumaran et al., 2004). In the research carried out by (Schwartz, 1988; Schwartz et al., 1989), they pointed out that in the insulation materials with cellular plastics structure such as polyurethane (PUR), extruded polystyrene (XPS), the boundary conditions including temperature will impact the moisture content accumulation and it distribution within the material.

Reaching EMC is a slow process, it may takes several days or weeks (Kumaran et al., 2006). The sorption isotherm expresses the moisture storage of a material in the hygroscopic range. Their values are determined by measuring the EMC in material samples when stabilize with the condition of the surrounding air in an ascending step of relative humidity and constant temperature (Delgado et al., 2013). Therefore, the sorption isotherm curve is a graphical representation of the relationship between the EMC and the relative humidity for the material which is exposed to steady-state conditions of relative humidity (RH) and temperature (T) (ASTM-C1498−04a, 2011). According to Hill et al. (2009), a typical sorption isotherm curve has three parts representing different process of water molecules accumulation in material pores pertinent to different ranges of relative humidity, Figure 2-4. At lower relative humidity range between 0 and 15% (Collet et al. (2011) specified this range between 5-35%), monomolecular layer of water molecules is formed on the walls inside the pores. At the relative humidity range between 15-70%, water molecules are adsorbed in multi-molecular layers. From the curve associated with these region, it is possible to determine the inner surface using the Brunauer–Emmett–Teller (BET) isotherm model (Brunauer et al., 1938). At the relative humidity ranges above 70% capillary condensation occurs. However, in building physics, the sorption isotherm region below 95% relative humidity is generally referred as hygroscopic region (Krus, 1996; ASTM-C1498−04a, 2011; Wang et al., 2014). Kumaran (2001b) and Peuhkuri (2003a) extended the hygroscopic region to 98% relative humidity and defined the corresponding EMC as a Critical Moisture Content as shown in Figure 2-4.

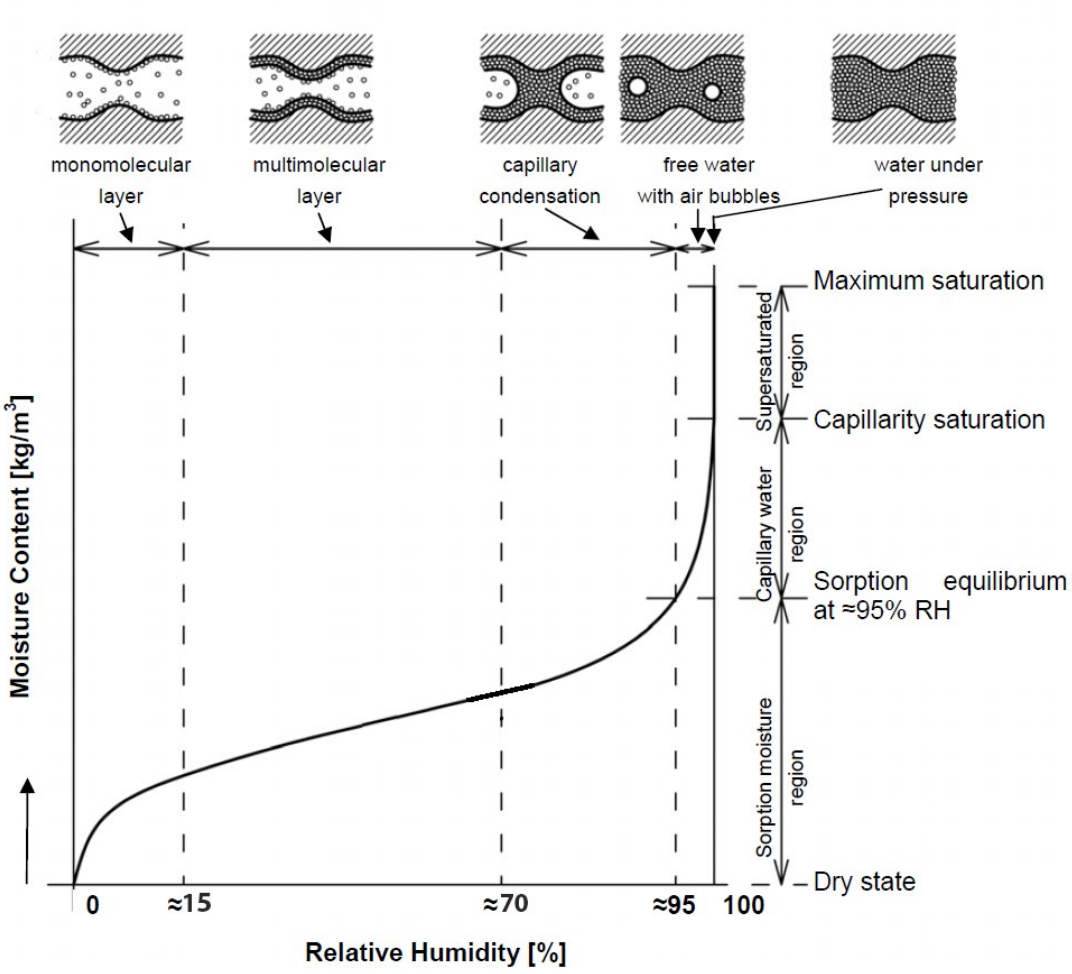

Figure 2-4. A typical curve of sorption Isotherm of a porous building material (Hansen, 1986)

The maximum free moisture uptake beyond the critical moisture content is referred as capillary moisture content. Even by exposing to the relative humidities higher than 95% up to 100% materials still assumed not to be fully saturated. Krus (1996) explained that under normal conditions and without external forces the entrapped air bubbles prevent open pore spaces in the porous materials to be fully occupied by water. In order to attain the maximum saturation moisture content, the porous materials should be fully drenched by immersion in the de-aerated water for several days and the corresponding EMC is called vacuum saturation moisture content (Kumaran et al., 2006). For hygroscopic porous building materials sorption isotherms have two different curves adsorption and desorption. Desorption is a process in which water is released from materials. Therefore, the desorption isotherm is obtained by measuring EMC in material samples in different climatic conditions in a descending step of RH. Desorption process ideally starts from

the condition of full water saturation of the material which is not necessarily the same as the adsorption curve. The difference between sorption and desorption isotherm is called hysteresis effect and it is widely explained as the result of differing wetting characteristics for adsorption and desorption or other phenomena attributed to the pore size and pore space geometry (Krus, 1996). Therefore, building materials with different internal structures express different shape of desorption curves.

Moisture content can be expressed by weight, u (kg/kg):

$$u = \frac{m_w - m_d}{m_d} \qquad (2.12)$$

Or by volume, w [kg/m^3]:

$$w = \frac{m_w - m_d}{\mathrm{V}} = \rho_d \,.\, u \qquad (2.13)$$

or by the ratio of moisture volume and dry material volume: ψ [m^3 /m^3] (Kumaran, 1996a):

$$\psi = \frac{(m_w - m_d)/\rho_w}{m_d} \qquad (2.14)$$

m_w [kg] is the mass of the test specimen, m_d [kg] is the mass of dry specimen, V [m^3] is the volume of the specimen, ρ_d [kg/m^3] is dry density of the material and ρ_w [kg/m^3] is the density of water. Equation (2.15) represents an example of a function that is commonly used for fitting sorption test data (Delgado et al., 2013):

$$u = u_h.(1 - \ln \phi / A_1)^{-1/n} \qquad (2.15)$$

Numerous efforts have been accomplished, theoretically and experimentally, to accurately calculate values for sorption isotherm for different types of materials. It has been proven among the relevant literature that calculation accurate values particularly at relative humidities higher than 90 % has been challenging.

Simpson (1973) explored nine different numerical sorption models including Hailwood and Horrobin (1946) model, in order to examine their accuracy in terms of relationship between equilibrium moisture content and relative humidity using nonlinear regression technique. Verifying with the Wood Handbook (USDA, 1955) for EMCs dependent on temperature and

relative humidity[1], he concluded that the two-hydrated forms of the Hailwood-Horrobin theory and the King (1960) theory of multilayer adsorption were the most accurate models as the average and greatest deviations of the values calculated for the former were 0.1% and 0.5% and for latter were 0.1% and 0.8% moisture content, respectively.

Pavlík et al. (2012) numerically analyzed their experimental results based on the isotherms equations derived from literature as Brunauer–Emmett–Teller (BET) (Brunauer et al., 1938), Brunauer–Skalny–Bodor (BSB) (Brunauer et al., 1969) , Brunauer–Deming–Deming–Teller (BDDT) (Brunauer et al., 1940), and Frenkel–Halsey–Hill (FHH) (Halsey, 1948; Hill, 1951) considering both mono and multi-layer vapor adsorption. Their analysis revealed that the experimental results for the RHs lower and higher than 50 % fit into BSB and FHH isotherms, respectively. Additionally, they improved a semi-empirical equation with a good correlation with whole range of RHs which they stated that can be used for characterizing the water vapor adsorption in building materials. They concluded that BDDT demonstrated the lowest accuracy among the others.

Wang et al. (2014) investigated and described sorption isotherms, capillary suction and equilibrium moisture content of the red pine particularly under high relative humidities above 95% using conventional sorption measurement and the pressure plate methods. The measurements indicated no inconsistency in results around 95% RH between two methods. However, a discontinuity was found with other EMC data using pressure plate techniques for instance at high RH levels close to 100%. Similar to many of physical and mechanical properties of wood, its sorption behavior is highly dependent on the structure of the cell walls. Heat and chemical treatments are among the factors that have considerable impacts on wood structure and properties. Thygesen et al. (2010) investigated the desorption isotherms of untreated and modified wood at very high levels of relative humidities from 91.9% to 99.9%. They compared an untreated, cetylated, and furfurylated samples of Norway spruce sapwood using three different methods of creating constant RH levels including: saturated salt solutions, climate chambers, and the pressure plate technique. According to their results, the high range of relative humidities did not affect the desorption curve in untreated and acetylated wood samples. However, the results indicated a

[1] The EMC data start at the temperature of 30°F (-1.12°C) and increase in 5°F (2.78°C) increments up to 130°F (54.45°C), and then in 10°F (5.56°C) increments up to 210°F (98.89°C) (Simpson, 1971).

systematical influence only on relaxation curves for the furfurylated samples at freezing temperature of -20°C established by using low field time domain NMR. Additionally, based on the theoretical results of moisture content by means of the Kelvin and Laplace equations considering idealized microstructural geometries, a very small impact of capillary condensation on the EMC was observed at 99.9% RH for the equilibrium moisture content below 0.35%. In contrary to what is found in literature, the results indicated no significant influence of capillary condensation in sorption process of wood below fiber saturation.

Many definitions have been established regarding the way water molecules bound to the wood cell due to the presence of humidity. Wood cells contain capillary water as a liquid in their Lumina or cavities and bound water joined to the wood polymer (within the wood cell wall) which also they are called free water and hygroscopic water, respectively (Siau, 1984; Thygesen et al., 2010; Wang et al., 2014). Eitelberger and Hofstetter (2011) believed that there is also water vapor inside Lumina below the fiber saturation point. Kelly and Hart (1970) carried out experiments on the rates of water vapor sorption by cell walls of yellow poplar and white oak at 40°C and different relative humidities. By analyzing the obtained results and comparing them to Fick's law driven diffusion values, they observed that the rates were far below their expectation for Fickian diffusion of bound water. Desorption occurred quicker than adsorption, particularly at relative humidities above 54%. They concluded that heat transfer to the specimen was the major cause of decreasing the rate of moisture change in desorption.

The ability of storing moisture in insulation materials is of great importance in determining their effective thermal resistance (Hokoi and Kumaran, 1993; Ochs et al., 2008; Jerman and Černý, 2012; Lakatos and Kalmár, 2012). Therefore, insulation materials has been studied along with other building materials to characterize their hygrothermal properties (Vololonirina et al., 2014). A set of sorption/desorption measurements of insulation materials can be found in Burch and Desjarlais (1995). Gnip et al. (2006) experimentally determined the sorption isotherms of glass fiber, mineral wool, EPS boards and ecowool[2] under a relative humidity range from 0 to 97% and at temperature of 20°C. Based on the results, they explained that the equilibrium moisture content in fiber glass and mineral wool depends on binder content in the products and density while EMC in EPS boards is largely depends on the density with an inverse relation. They additionally, stated

[2] Light downy cellulose wool is ground chipboard or paper waste with chemical additives.

that fiber glass generally absorbs more moisture than mineral wool. For instance, according to their results, it was noted that at 90% RH the mean value for equilibrium moisture content of fiber glass board with density of 79.6 kg/m^3 was approximately 15% volume which was 4.3-9.7 times higher than the mean values obtained for mineral wool with density of 49.5-117 kg/m^3. However, ecowool loose-fill insulation showed a significant moisture absorbed amount at RH higher than 80% which demonstrated its hygroscopic characteristics due to the capillary mechanism of sorption. Lakatos and Kalmár (2013a) conducted a study on the water sorption properties of EPS boards with different densities of 14, 17.5, 23.7 and 27.5 kg/m^3 and gray EPS (EPS mixed with graphite with the density of 13.62 kg/m^3 under a range of relative humidities from 25% to 90% at 20°C. The obtained results illustrated that for higher RH moisture content has an inverse exponential relation with the density while at lower RH this dependency was found nearly linear.

Latif et al. (2014) characterized adsorption-desorption isotherm along with other hygric properties of five types of hemp insulation materials available in the UK market. They analyzed the experimental adsorption results based on the Guggenheim Andersen and de Boer (GAB) isotherm (Timmermann, 2003) as an improvement version of the multilayer sorption model of Brunauer, Emmett and Teller (BET). The experimental results reflected a varying adsorption and MC in tested samples where the standard deviation for adsorption capacity in high-density insulation samples was less compared to the low-density samples. They explained the difference between results to be due to the dependency on components and fiber saturation.

2.3.2 **Measurement Methods**

There are two complementary Standard test methods that can be used to measure adsorption/ desorption isotherms of porous materials: ASTM-C1498−04a (2011); (EN.ISO.12571, 2013) and ASTM-C1699 (2009). ASTM-C1498−04a (2011) and ISO 12571 standards are based on measurements of EMC of a material at a set of environmental conditions with constant temperature and varying relative humidity between 30% and 98% to determine the hygroscopic sorption isotherms. The desired environmental conditions can be obtained by using climatic chambers or sealed container with saturated salt solutions. The test method in ASTM-C1699 (2009) is used for determining over hygroscopic sorption isotherms, which is also referred as moisture retention curve, of a material using pressure plate testing technique. These test procedures are recommended to be performed at constant room temperature of 23˚C and 22±1˚C by C1498 and C1699,

respectively. The measurement of moisture storage within the hygroscopic moisture content range is widely done by exposing a material specimen to a defined relative humidity, waiting until equilibrium (constant mass) is reached and gravimetrically determining the corresponding moisture content. There are different methods and devices in published literature for measuring the sorption isotherm, such as the climate box (conventional desiccators) with saturated aqueous salt solutions (Brocken, 1998). To adjust a defined relative humidity inside a desiccator, saturated aqueous salt solutions are used. A broad combination sets of temperature and relative humidity of saturated salt solutions can be found in Wexler and Hasegawa (1954) and Arai et al. (1976). A fan inside the desiccator creates uniform humidity conditions. To keep the temperature constant, either a water bath for the desiccators, or a temperature-controlled room can be used. The material specimens are placed into the desiccator and left there for a certain time, normally two to four weeks, until equilibrium is reached. Since these test methods are time consuming, sorption/desorption isotherms are often derived for the moisture storage of materials based on a few points determined at different relative humidity level.

Sorption isotherms are generally measured with steady-state and transient methods. The available test methods for measuring sorption isotherm are summarized in Figure 2-5.

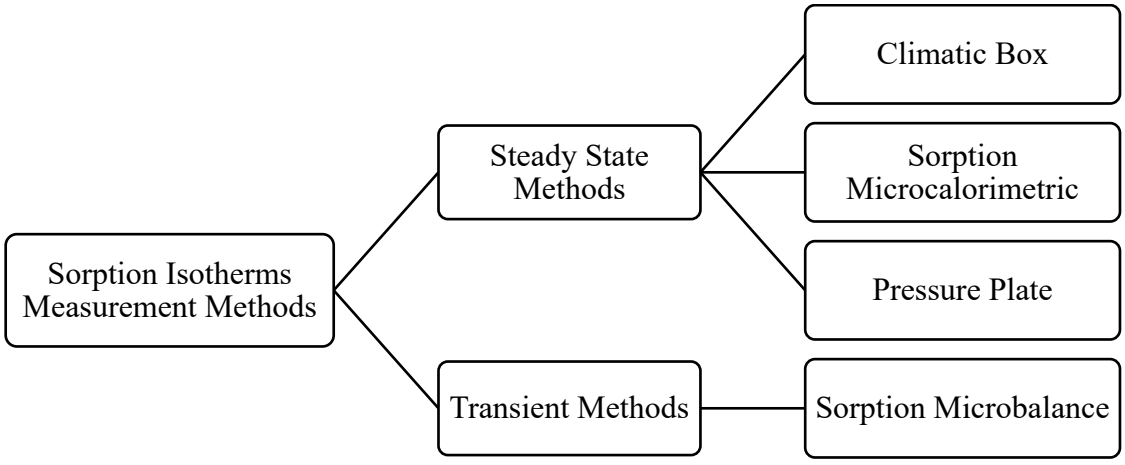

Figure 2-5. Different measurement methods of sorption isotherms.

There are some attempts in published literature to develop special apparatus in order to obtain sorption isotherms. For instance, Wadsö (1993a) proposed and built an apparatus for measuring and studying sorption in which three ranges of humidity from 33% to 84% could successfully be maintained at the constant temperature of 23˚C. The instrument included a main wind tunnel at the

upper part which could accommodate up to 117 material samples, containers with saturated salt solutions at the lower part and a balance (weighing setup). Each sample was attached to a steel frame, so they could be lifted and moved to the top of the balance by using an electromagnet for weighing process without touching or removing from the conditioned space. The disadvantage of his device was the relatively slow process of changing the RH. Using the new device, he examined the water vapor sorption of spruce samples with two thicknesses of 4 and 8 mm at two relative humidity sets varied between 54 to 75% and 75 to 84% and constant temperature of 23˚C. He later examined the validity of his experimental sorption results by comparing them with the results from Fick's law (Wadsö, 1993b). His results showed that the absorption only in lower range of relative humidity was in a good agreement with Fick's law.

The method of sorption microbalance system was investigated by Johannesson and Janz (2002). In this method the sample is weighed by a sensitive microbalance while it is being exposed to a programmed increasing relative humidity. The instrument was placed in a temperature-controlled incubator and the desired relative humidity was obtained by mixing dry and saturated nitrogen with mass flow regulators. The velocity of the air passing the sample was typically 5 mm/s. According to their study, the microbalance measured changes in sample mass even lower than one in ten million and therefore it showed a good precision in the measurement of vapor sorption phenomena, particularly in the small samples.

Sorption microcalorimetric is another method which was used by (Adan, 1994; Wadsö and Wadsö, 1996; Wadsö and Wadsö, 1997; Brocken, 1998). This method includes a double heat conduction microcalorimeter in twin arrangement. A central part which is a calorimeter vessel with two chambers connected by a thin tube. In one calorimetric chamber the vapor evaporated; in a second calorimetric chamber the vapor was absorbed by a small dry sample of cotton wool. The water vapor formed in the vaporization chamber is allowed to diffuse to the sample through a thin tube. The vessel was placed in a built double micro-calorimeter that separately measured the thermal power produced in the sorption and vaporization vessels. Then, the sorption isotherm was calculated using the measured thermal power from the vaporization chamber. Applying their method, it was possible to derive sorption enthalpies and the kinetics of sorption too.

Another method is pressure plate apparatus which has been investigated by Richards (1948). In this test method, a certain air pressure will be maintained in the apparatus until EMC is attained.

The air pressure correlates with suction/capillary pressure through capillary theory, which is relational to relative humidity according to Kelvin's equation. Thus, at the end the test method provides relationship between relative humidity and EMC at higher moisture content level (95-100%).

Johannesson and Janz (2002) explored the microcalorimetric method and compared it with three other different methods including: Climate Box Method, Pressure Plate Method, Sorption Microbalance Method. They performed those four sorption isotherm measurement methods on sandstone and porous glass specimens. Although the four techniques are different in nature, they found a satisfactory correlation between the obtained results.

Furthermore, they concluded that, the sorption microbalance revealed hysteresis in sorption, which was not detectable with the simple method of using climate boxes. The pressure plate extractor device had more precision than the other two methods for measuring moisture contents at very high relative humidities, as high values could not be obtained either in climate boxes or in the sorption microbalance instrument. However, they highlighted that using the pressure plate extractor was probably rather time-consuming compared to the other methods, since equilibrium must be reached by normal absorption rather than being drained. Another limitation of the pressure plate technique was that only materials with pore sizes larger than approximately 14 nm can be examined. For example, they stated that the results for porous glass which obtained from sorption microbalance and the calorimetric method, was acceptable. However, at medium relative humidities, the sorption microbalance measured slightly higher water content than the calorimetric method. In an another attempt Pavlík et al. (2012) experimentally and theoretically investigated the water vapor sorption of several porous building materials including autoclaved aerated concrete, lightened ceramic brick, micronal DS 5008X, lime plaster and ceramic brick zopa using DVS-advantage (Dynamic Vapor Sorption) instrument (Surface Measurement Systems Ltd.) at different ranges of temperature and RHs. The apparatus contains two measurement hanging pans (sample and reference holders) suspended from a microbalance with an accuracy of 0.1-1.0μg. The pans are located inside the linked double chamber with the ability of precisely maintaining the range of temperature from 5-60˚C and RH from 0-98% with the accuracy of ±0.2˚C and ±0.5% RH, respectively. The instrument gravimetrically measures vapor gain and loss of material samples in a transient method. It works based on the change of mass per minute (dm/dt) while running

through several ascending or descending steps of T and RH. By setting a fixed value of d*m*/d*t* for each step of relative humidity as a criterion, the DVS program determine the equilibrium moisture content of the samples once the rate of mass change goes below the aforementioned value and the chamber proceed to the next pre-defined segment of relative humidity level (Hill et al., 2010; Pavlík et al., 2012).

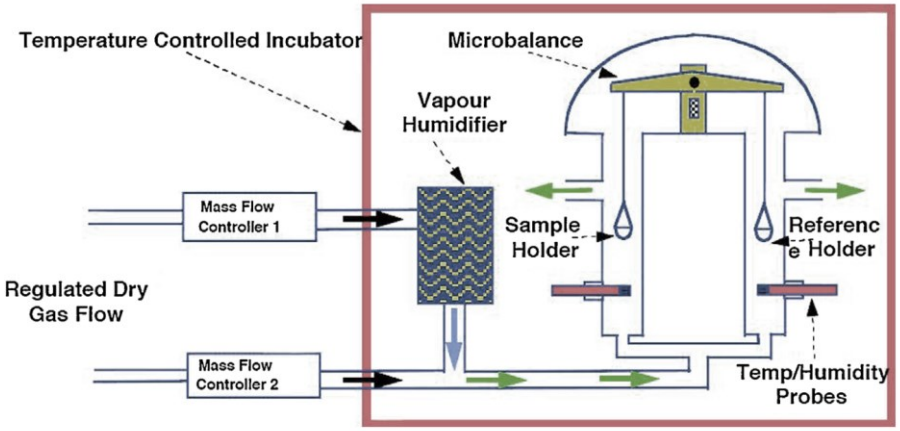

Figure 2-6. Schematic depicting the working principals of DVS-Advantage (dynamic vapor sorption instrument)(Cagnon et al., 2014)

de Burgh and Foster (2017) designed and made two apparatus including sixteen separate chambers for conducting water vapor sorption experiment at different temperatures. Each apparatus included eight fully insulated and air sealed chambers with regulated temperature and relative humidity, Figure 2-7.

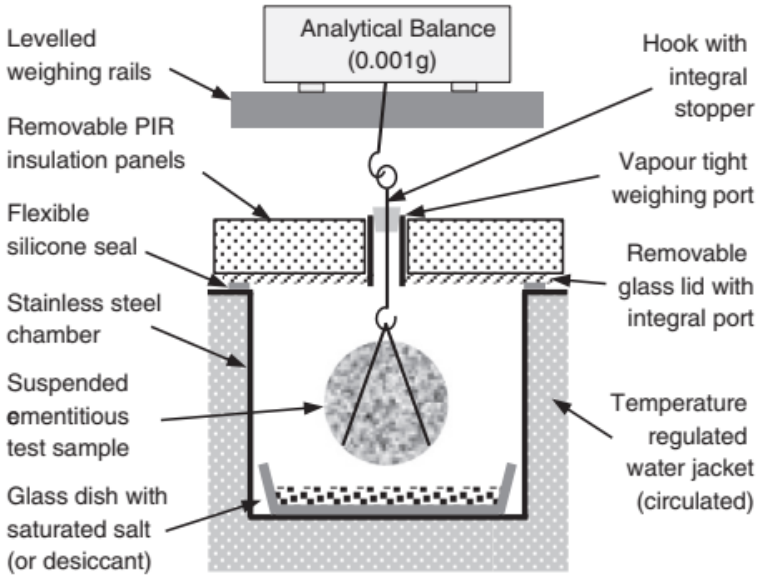

Figure 2-7. Schematic section view of each test chamber (de Burgh and Foster, 2017).

The temperature of chambers could be provided within the ranges of 10˚C to 85˚C by heating and 5˚C to 50˚C by heating/refrigerating through circulating temperature regulated water around and below them. The relative humidities in chambers were regulated by different salt solutions or conditioned 4A molecular sieve for low relative humidities. A small fan in each chamber pointed away from the test specimen, provided a constant airflow. Inside each chamber, a specimen was suspended from a stainless steel hook and hanger through a small hole in a glass lid on the top surface. The glass lid enabled the operator to inspect the chamber without interfering its condition. The glass was covered by a 60 mm thick removable block of foam insulation. A rail with stops was provided above chambers to allow weighing samples individually by attaching the hooker to a balance without removing them from the chambers. The authors successfully tested the sorption isotherms of cementitious materials over temperatures of 23˚C to 80˚C. Their results and findings are described in the section 2.3.3.

Determining the sorption isotherms in cementitious materials is a long time process due to its micropore structure. Therefore, there are some attempts in literature in applying transient methods to decrease the time of measuring sorption isotherms in concrete. Tada and Watanabe (2005) introduced an improvement of a dynamic method for determining the sorption isotherm of very small samples of cement paste and autoclaved aerated concretes in order to shorten the time to reach equilibrium and avoiding of the carbonation of the cement based specimens. Test was carried

out by measuring the water adsorption rate in the specimen with a very short intervals of a minute while it was exposed to different relative humidity levels from 5% to 95% at 20°C. Then an analytical diffusion equation was fitted to the results which led to the quick calculation of the EMC at 12h and 8h for cement pastes and autoclaved aerated concretes, respectively at each relative humidity. Accordingly, fitting the obtained results to the values of steady-state (conventional) methods from previous literature expressed a good agreement. For instance, the correlation coefficients of the curve fitting in each equation and for all curves, were greater than 0.994. Later in the similar attempt Anderberg and Wadsö (2008) studied and described a method to determine the sorption isotherms and moisture diffusion property of two cementitious products simultaneously. The experiment was conducted to measure the desorption of sample with the same process as Tada and Watanabe (2005) at the relative humidity levels from 97% to 10% in order to prevent some difficulties of the conventional methods for such properties as they are time consuming and need large amount of laboratory work. However, contrary to Tada and Watanabe (2005) the step changes of relative humidities were made where the equilibrium was reached to about 70% to 90% of its final value thus they extrapolated the final EMC by applying their suggested simulation method. The values for sorption/desorption isotherm and diffusivity for cementitious samples were obtained in about 10 days with maximum errors of less than 10 % which was assumed to be due to non-complete steps and external mass transfer during weighing.

Cagnon et al. (2014) studied the hygrothermal properties of five types of fired and unfired bricks from southern of France. They performed sorption-desorption isotherms with two test methods of saturated salt solutions and dynamic vapor sorption (DVS) method. The results of transient method highlighted the need for more research in dynamic vapor sorption methods since according to the steady state method, samples were observed to be very fast in response to the changes of relative humidity.

2.3.3 **Temperature Dependency**

The American and European measurement standards (ASTM-C1498−04a, 2011; EN.ISO.12571, 2013) for determining sorption isotherm recommend measurement at test temperature of 23˚C and 23.5-27.5˚C, respectively. In reality, however, building envelope components are exposed to a wide temperature range from +50˚C to -50˚C all around the world. Therefore, the standards measurement temperature adopted is not representative of the exposure conditions of construction

materials in practice. Generally, it is known through several literatures that sorption isotherms for porous materials are temperature dependent (Brunauer, 1943; Chahal, 1965; Tveit, 1966; Tobiasson et al., 1987; Hokoi and Kumaran, 1993; Maroulis et al., 2005; Schneider and Goss, 2011; Brue et al., 2012). Brunauer (1943) defined the process of adsorption as exothermic function which releases heat, so based on Le Chatelier principle, at equilibrium state, the amount of adsorbed water vapor should decrease by increasing temperature.

The mathematical models have been always associated with the experimental methods for determining the sorption isotherm to conform the measured data. According to the literature, more than 200 different equations have been developed to fit the moisture sorption isotherms (Staudt et al., 2013b), describing the relationships between EMC, relative humidity (RH), and temperature (T). Most of them have been developed for soil science (Ferrand and Sulayman, 1996), agriculture (Klute, 1986) and food (Maroulis et al., 1988) then some have been applied successfully to building materials such as wood (Simpson, 1971).

Simpson (1971) introduced an improvement on Hailwood and Horrobin (1946) model in order to predict the equilibrium moisture content for wood at a given temperature and relative humidity. This model considers adsorbed water by the cell wall in two states: water dissolved with polymer (multilayer water) and hydrated water combined with a unit of polymer (monolayer water). Hailwood-Horrobin model is based on two chemical equilibriums within the cell wall at the presence of three components: polymer, hydrated polymer, and the dissolved water. First equilibrium is between the hydrated and dissolved water and second equilibrium is between dissolved water and water vapor in the surrounding atmosphere. The EMC values for each temperature and relative humidity were verified with the data from the Wood Handbook of U.S. Forest Product Laboratory (USDA, 1955), and found that the average and maximum deviation between calculated and actual values were 0.13% and 0.9%, respectively.

Avramidis (1989) applied nonlinear curve fitting to evaluate four models of sorption isotherm as a function of relative humidity and temperature derived from Henderson, Day and Nelson (1965), Zuritz et al. (1979), and Chung and Pfost (1967). He performed this method by fitting the functions to a set of sorption data from USDA wood handbook at a temperature range from 21.1°C to 71.1°C. According to his analysis which were based on Root Mean Square Error (RMSE) and Residual Sum of Squares (RSS), Zuritz model represented the best fit among the others with the average

and maximum deviation of 0.13% and 0.53% at 21°C respectively and the lowest RSS of 4.27. Studying desorption of two high performance concretes, Brue et al. (2012) pointed out that all isotherms for both concretes at all temperatures were well described by Kelvin-Laplace's capillary law as well as Brunauer Skalny–Bodor (BSB) model (Brunauer et al., 1969).

Promis et al. (2019) compared four temperature dependent sorption models: Poyet, Milly, Staudt and modified GAB, in order to assess their precision in modeling the sorption isotherm while considering the influence of temperature and hysteresis. The Poyet model is based on isosteric heat of sorption (Poyet and Charles, 2009). The Milly model is based on thermodynamic properties of water (Milly, 1980). The Staudt model as an extension to GAB equation is also based on isosteric heat of sorption and relies on temperature dependency of the energetic coefficient C with an Arrhenius expression (Staudt et al., 2013a). The physically modified GAB relies on the monolayer and multilayer enthalpies of sorption (Maroulis et al., 1988; Goula et al., 2008; Vishwakarma et al., 2011; Zhang et al., 2015). The sorption isotherm of bio-based hemp and straw concretes were experimentally measured at temperatures of 10°C and 23°C to evaluate their theoretical analysis. According to their comparison between the test results and the predictive values, the Poyet and Milly models presented overestimate (or underestimate) but consistent results while the values from Staudt model showed more difference with the experimental results. The modified GAB model results appeared to be in the most correlation with the experimental sorption values.

Parallel to theoretical developments in sorption isotherm phenomena, numerous experimental measurements at varied environmental conditions have been carried out on different materials. Some of the first experimental measurements are conducted in soil science and agriculture (Wilkinson and Klute, 1962; Romero et al., 2001; Bachmann et al., 2002; Della Vecchia et al., 2011). For instance, Moore (1940) experimentally studied the influence of temperature (in the range of 0°C to 45°C) on some properties of three types of moistened soil including: pressure potential, retention and infiltration rate. The results demonstrated that the fluctuation of pressure potential with temperature was small at the higher soil moisture contents and increased by reduction of moisture content in soil. The moisture retaining capacity of the soil decreased approximately by 10% as the temperature increased from 10°C to 45°C. Furthermore, infiltration was affected proportionally by temperature with a mild upward trend up to 35°C after which the curve increased sharply up to a peak at 35°C and followed by a plunge up to 45°C. Based on the

maximum and minimum peaks in the results curves the author concluded that temperature might not be the major factor of influencing the soil moisture properties. Accordingly, he described that some other properties such as viscosity, surface tension, and expansion of liquids and gases may be impacted first by temperature. Therefore, he stated the combination of those impacts with the shape and size of the soil pores through a dynamic mechanism which are influenced by temperature, caused the alterations in properties of moistened soils.

Chahal (1964) investigated the trapped air at temperatures 4°C and 44°C on pressure potential due to the changes in energy status of water in porous media. He theoretically suggested larger temperature coefficients for pressure potential and fine-textured soils because, the former described the volume change of trapped air with temperature and the latter described larger volumes of entrapped air in them rather than coarse-textured soils. Based on his results, the relationship between desorption curve and the volume of trapped air in the system should be considered in any theoretical model of impact of trapped air.

Later in another study from this author, the effects of temperature and trapped air on matric suction of the soil was investigated (Chahal, 1965). According to his theoretic analysis and results, even at the same pressure setting, temperature affected the sorption and desorption curves. For instance, desorption isotherm and the moisture content in the soil at a given matric suction decreased when the temperature increased.

Schneider and Goss (2011) studied the temperature dependency of water retention curve for nine European soils under the relative humidity below 90% and temperature range between 5°C and 40°C. They stated that water retention curve is considerably depended on temperature as the absolute value of the adsorption enthalpy of water increased with decrease of water content. Therefore, they improved an average equation for calculating the adsorption enthalpy of water in the dry region down to 30% RH and in the temperature range between 5°C and 40°C.

After introducing of the water movement theory of soil physics, it found its way through the research in the field of building materials (Philip and De Vries, 1957). Tveit (1966) measured moisture sorption of 48 materials at 14 different combinations of temperatures and relative humidities within the range of 5-45˚C and 10-97%, respectively. He outlined temperature as a major driving force for the moisture movement which also influences sorption characteristics of the both organic and inorganic building materials. Based on his experimental results, it was stated

that the effect of temperature on the sorption for the organic materials is higher than the inorganic materials while the impact was small on the sorption isotherm of brick. However, he pointed out the exceptions that the effects of temperature on cellular concrete and wood was identical.

Tobiasson et al. (1987) investigated the accumulated moisture content in Expanded Polystyrene (EPS), Extruded Polystyrene (XPS) and Urethane roof insulation under the temperature gradient through a long time laboratory experiment. They set up a wetting apparatus in which a sample of insulation was secured horizontally between a cold environment with 4°C and 75% RH at the top and warm climatic condition with 29°C and 100% RH at the bottom to simulate a severe condition on the roofs. All sides of specimens were sealed by two coats of vapor barrier coating in order to eliminate drying during the test. According to their results after 400 days the moisture content in Urethane and EPS exceeded 30 percent by the volume while moisture content in XPS after 1800 days of exposure was less than 10 percent.

Concrete as structure or envelope in buildings are exposed to different climate conditions therefore determining its hygrothermal properties under different temperatures is of interest through concrete studies. Xi et al. (1994) investigated several factors which influence moisture diffusion in cementitious materials through an improvement on the numerical model that has been proposed by Bažant and Najjar (1972). They formulated diffusion equation with two coefficient of moisture capacity and diffusivity. A good agreement was found between the predicted and the experimental adsorption isotherms of cement paste. However, they explained that temperature causes the thermal expansion and contraction of the adsorbed layer. Therefore, since the volumetric changes of water at the room temperature is very small, the effect of temperature on sorption isotherm of cementitious materials is negligible. For the higher temperatures particularly, the temperature above 100°C a complicated model needed in which thermodynamic properties of water is taken into account along with the factors: cement ratio, age, and type of cement.

Maroulis et al. (2005) experimentally and theoretically studies the sorption isotherms of two bricks, four sandstones, and six plasters at different temperatures 15°C, 25°C and 35°C. Results showed an inverse relationship between temperature and sorption isotherms. Their results demonstrated a moisture content less than 1% for bricks and sandstones which had a good agreement with the results obtained by Kumaran et al. (2004). However, the moisture content for plasters was observed higher from 0.67% to 12%. They explained that this difference was related

to microstructure and specific surface area of the building materials. Accordingly, an estimated data of water activity driven from a modified Oswin model (Tsami et al., 1998) was satisfactorily fitted to experimental results.

Eitelberger et al. (2011) explained that temperature changes can be a driving force along with pressure differences in sorption since the EMC can be defined as a function of water vapor concentration in air and temperature (Eitelberger and Hofstetter, 2011). The sorption/desorption in wood occur by phase change from water vapor to bond water and vice versa. The molar enthalpies of water vapor in the lumens and bound water in the cell walls are different (Skaar, 1988). Therefore, they stated that the variations of moisture content in wood are never isothermal due to the changes in internal energy upon the phase change in water.

Trabelsi et al. (2012) studied the influence of temperature gradient on sorption isotherm of a brick and calcium silicate under isothermal and non-isothermal conditions both numerically and theoretically. Based on their experimental results, moisture content at lower temperature was higher. They concluded that by decreasing the temperature, condensation will occur in pores within material structure which lead to more moisture accumulation. On the other hand, Jerman and Černý (2012) explained that at higher temperatures, the transport of water molecules is faster. Therefore, the amount of adsorbed water decreases as the bonds can be released more easily.

Brue et al. (2012) experimentally studied temperature dependency of the desorption isotherm of two high performance concretes at three different temperature levels: 20°C, 50°C and 80°C. Analyzing the results, they concluded that concrete with finer pores had a greater water desorption and despite its high porosity (compare to the other type of concrete in the study), its first desorption isotherm was more influenced by temperature.

Utilizing the dynamic vapor sorption (DVS) method, Wu et al. (2014) studied the impact of temperature on the sorption isotherms and pore structure of two types of hardened cement pastes. For comparison purpose, they used the material MCM-41 as a model in which pore structure is stable during the studied temperatures of 25°C, 33°C and 40°C. The experimental results revealed a small difference between the sorption isotherms at different temperatures with no impact on desorption isotherms. They concluded that the differences were primarily triggered by the changes in water thermodynamic properties under different temperatures. Furthermore, no difference

between the first and second sorption-desorption cycles represented no changes in pore structure of the hardened cement pastes.

de Burgh and Foster (2017) investigated the variations sorption isotherms of a hardened cement paste and a concrete over the temperature range of 23°C to 80°C. The experiments were carried out in two set of eight climatic chambers custom made for sorption isotherms tests under different temperatures. Agreed with other literature results, they highlighted a decrease in moisture content in tested material samples upon increasing temperature. Analyzing their measured results represented that increasing the temperature shifted the starting point of pronounced changes in moisture contents towards higher relative humidities. For example, at temperature 23°C the noticeable increase in moisture content started at about 45 % RH while at temperatures of 40°C, 60°C and 80°C, the similar change begun around 55 %, 70 % and 80 % RH, respectively. Furthermore, they concluded that upon rising temperature, the decrease in retained moisture took place faster in desorption than in adsorption.

The full list of the literature reviewed along with the factors influences the water vapor permeability are presented in Table 2-2.

Table 2-2. Characteristics of Published Literature in Temperature Dependency of Sorption/Desorption Isotherms

Paper	Experimental	Theoretical	Properties	Temperature Range	Materials	Remarks
Brunauer (1943)		•	Adsorption Isotherm	Varied	Various	He stated that the amount of adsorbed at equilibrium has to decrease with increasing temperature as the adsorption process is always exothermic.
Moore (1940)	•		Pressure Potential, Retention and Infiltration	0-45˚C	Soil	The combination of properties such as viscosity, surface tension, and expansion of liquids and gases along with the shape and size of the soil pores which are influenced by temperature, caused the alterations in properties of moistened soils.
Chahal (1964)	•	•	Desorption Curve	4°C and 44°C	Soil	The relationship between desorption curve and the volume of trapped air in the system

						was highlighted to be considered in any theoretical model of impact of trapped air.
Chahal (1965)	•	•	Sorption/Desorption Isotherm	5˚C and 55˚C	Soil	The desorption isotherm and the moisture content in the soil at a given matric suction decreased when the temperature increased.
Tveit (1966)	•		Vapor Permeability, Sorption Isotherm	5˚C - 45˚C	Various	It was stated that the effect of temperature on the sorption for the organic materials is higher than the inorganic materials while the impact was small on the sorption isotherm of brick.
Simpson (1971)		•	Sorption Isotherms	NA	NA	Introduced an improvement on Hailwood and Horrobin (1946) model as a function of temperature and relative humidity. Hailwood-Horrobin model is based on two chemical equilibriums within the cell wall. First equilibrium is between the hydrated and dissolved water and second equilibrium is between dissolved water and water vapor in the surrounding atmosphere.
Tobiasson et al. (1987)	•		Sorption Isotherms	Temperature gradient 4˚C – 29˚C	Two EPSs, XPS, Urethane	After 400 days the moisture content in Urethane and EPS exceeded 30 percent by the volume while moisture content in XPS after 1800 days of exposure was less than 10 percent.
Avramidis (1989)		•	Sorption Isotherms	21˚C - 71.1˚C	Wood	Used nonlinear curve fitting to evaluate four models of sorption isotherm as a function of relative humidity and temperature. All isotherms for both concretes at all temperatures were well described by Kelvin-Laplace's capillary law as well as Brunauer Skalny–Bodor (BSB) model. However, the Zuritz model represented the best fit among the others.
Xi et al. (1994)	•	•	Adsorption Isotherms	20.85˚C & 24.85˚C & 34.85˚C	Cementitious Materials	However, they explained that temperature causes the thermal expansion and contraction of the adsorbed layer. Therefore, since the volumetric changes of water at the room temperature is very small, the effect of temperature on sorption isotherm of cementitious materials is negligible.

Maroulis et al. (2005)	•	•	Sorption/Desorption Isotherm	15˚C & 25˚C & 35˚C	Brick, Sandstone, Plaster	The moisture content for plasters was observed higher from 0.67% to 12%. The difference was explained to be related to microstructure and specific surface area of the building materials. The estimated data of water activity driven from a modified Oswin model (Tsami et al., 1998) was satisfactorily fitted to experimental results.
Schneider and Goss (2011)	•	•	Sorption/Desorption Isotherm	5˚C, 20˚C,30˚C and 40˚C	Soil	They stated that water retention curve is considerably depended on temperature as the absolute value of the adsorption enthalpy of water increased with decrease of water content.
Trabelsi et al. (2012)	•	•	Sorption Isotherm	Temperature gradient 10˚C – 23˚C	Calcium silicate and Brick Joens	They concluded that by decreasing the temperature, condensation will occur in pores within material structure which lead to more moisture accumulation.
Brue et al. (2012)	•		Absorption /Desorption isotherms	20˚C- 50˚C- 80˚C	High performance concrete	In concrete with finer pores a greater water desorption was observed despite its high porosity. The first desorption isotherm was more influenced by temperature.
Eitelberger et al. (2011)	•		Sorption Isotherm	NA	NA	They stated that the variations of moisture content in wood are never isothermal due to the changes in internal energy upon the phase change in water
Wu et al. (2014)	•	•	Sorption Isotherms	25˚C, 33˚C and 40˚C	Two types of hardened cement paste	A small difference between the sorption isotherms at different temperatures was reported with no impact on desorption isotherms.
de Burgh and Foster (2017)	•	•	Sorption Isotherms	23˚C, 40˚C, 60˚C and 80˚C	A hardened cement paste and a concrete	Agreed with other literature results, they highlighted a decrease in moisture content in tested material samples upon increasing temperature. Increasing the temperature shifted the starting point of pronounced changes in

						moisture contents towards higher relative humidities. They concluded that upon rising temperature, the decrease in retained moisture took place faster in desorption than in adsorption
Promis et al. (2019)		•	Sorption Isotherms	10°C and 23°C	Bio-based hemp and straw concretes	Compared four temperature dependent sorption models: Poyet, Milly, Staudt and modified GAB. The modified GAB model results appeared to be in the most correlation with the experimental sorption values.

2.4 Moisture Transport Mechanism

Moisture can be migrated in porous material through various mechanisms. Based on the conditions, water can exist in one or more of its three phases, solid (ice), liquid and gas (vapor). When water is present in an hygroscopic material, another phase may exist which composed of adsorbed layer of water molecules on the surface of the solid and is known as bound water (Chevrier, 1996). Large portions of water can be stored in the adsorbed layer phase. For instance, wood can adsorb moisture up to 30 percent on a dry weight basis. Moisture is mainly transported either by diffusion (molecular mass transfer) or convection depending on its driving forces. Diffusive transport is relative to the gradient of the driving force(s) which is determined experimentally as a proportional coefficient (Peuhkuri, 2003a). The convective flux is a product of the vehicle flux, e.g. air, and the transported density of moisture (Hens, 1996). Moisture in a porous material can be transported either as water vapor or as liquid water, or as a combination of these two phases. The solid phase of moisture, ice in not considered as movable (Pedersen, 1990), Figure 2-8.

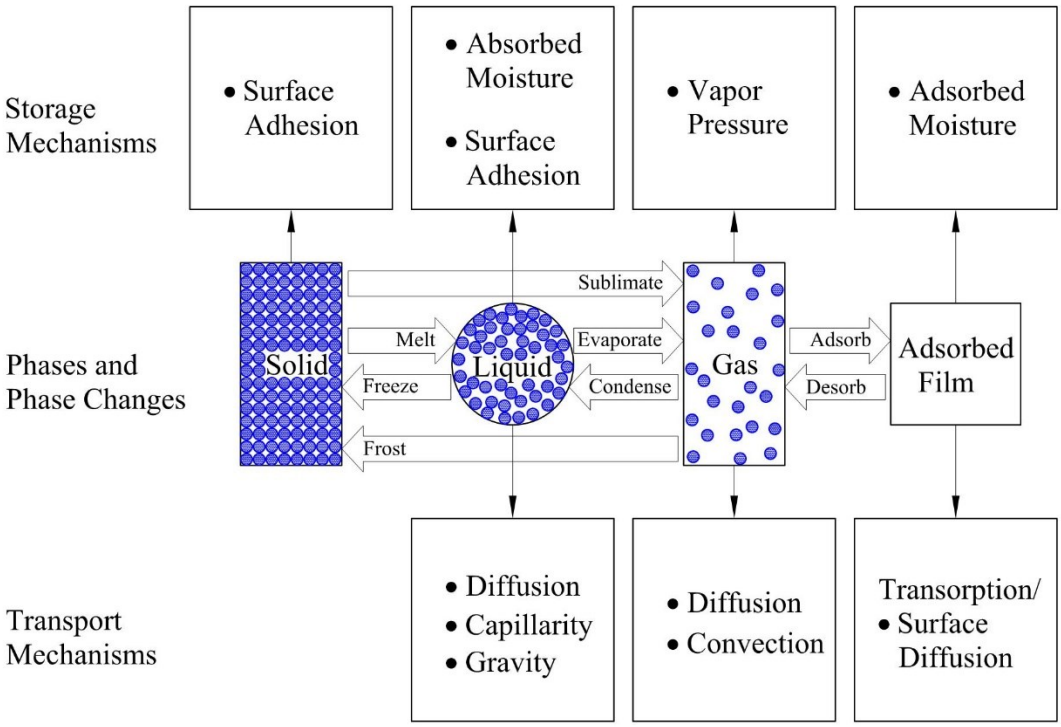

Figure 2-8. Mechanisms of moisture migration (TenWolde, 1989).

A difference in concentration of moisture between two locations is the primary reason for moisture transport. Additionally, difference in temperature, capillary forces, vapor pressure and relative humidity can also be considered as driving forces. Forms of moisture transport commonly mentioned in the literature are shown in Table 2-3 and depend on the pore structure of the material as well as environmental conditions. Convective moisture transfer is not covered here, because all the experiments and analysis in this study are performed with no air pressure difference within the material. Therefore, the possibilities for natural convection are minimized. In addition, Gravitational flow, hydraulic flow, Electrokinesis and osmosis are also ignored. Effusion (Knudsen diffusion) is water vapor diffusion that takes place in very narrow capillaries, where the mean free path of the water vapor molecules is higher than the pore dimensions, ~10^{-8}m (Krus, 1996). The thermodiffusion base on temperature gradients (also called the Soret effect) is negligible in building components (Künzel, 1995). Krus (1996) stated that only about 0.05% of total moisture transport accounts for thermal diffusion due to small temperature gradients across building materials and is different from thermally-controlled portion of vapor diffusion. Gravitational flow is not considered in the horizontal suction experiments as it only starts to impact liquid transport at pore radii greater than 10^{-6} m (Krus, 1996).

Table 2-3. Forms of moisture Transports.

Phase	**Transport mechanisms**	**Driving forces**
Vapor	Water vapor diffusion	Vapor pressure (temperature and total pressure)
	Molecular transport-effusion (Knudsen diffusion)	Vapor pressure and temperature
	Convection	Total pressure gradient
Liquid	Capillary suction	Suction (capillary) pressure
	Surface diffusion	Moisture content or relative humidity
	Thermal diffusion (Soret effect)	Temperature
	Gravity-assisted flow	Gravitation
	Hydraulic flow	Total pressure differentials
	Electrokinesis	Electrical fields
	Osmosis	Ion concentration

2.4.1 **Water Vapor Transport**

In building physics, the transport of water vapor is a transport of gas in the pores of any porous material. The vapor permeability is considered as the ratio between the density of vapor flow rate and the vapor pressure gradient in the direction of the flow (Kumaran, 2001a). The vapor permeability is a strong function of the mean relative humidity of the material.

2.4.1.1 Isothermal Vapor Transport

Theory on moisture transport in porous materials is originally based on Fick's law of diffusion of ions in water (Fick, 1855). Fick's law is generally given for the concentration of the water vapor ρ_v as:

$$g_a = -D_a \frac{\partial \rho_v}{\partial \mathrm{x}} \qquad (2.16)$$

where g_a $[kg/(m^2 s)]$ is the density of vapor transport in air and D_a $[m^2/s]$ the diffusivity of water vapor in still air. This simple law is adopted in building physics to explain the diffusion of water vapor in porous materials. According to Equation 2.16, the driving potential of pure water vapor diffusion is ρ_v. This law is adopted to describe the diffusion of water vapor in porous materials.

The total pressure P [Pa], and especially temperature T also play roles in transport, Equation 2.17 shows this influence (Kumaran, 1996a):

$$D_a = \frac{2.306 \times P_0}{R_v T P_a}\left(\frac{T}{273.15}\right)^{1.81} \qquad (2.17)$$

where P_0 is standard atmospheric pressure (101325 Pa), P_a is the ambient air pressure (Pa), T the temperature (K) and R_v the gas constant of water vapor (461.5 [J/(kg.K)]). When considering water vapor diffusion through a porous material, the water vapor flux density g_v [$kg/(m^2 s)$] can be given as:

$$g_v = -\frac{D_a}{\mu}\frac{\partial \rho_v}{\partial \mathrm{x}} \qquad (2.18)$$

where the vapor diffusion resistance μ (-) is defined as:

$$\mu = \frac{D_a}{\delta_v} \qquad (2.19)$$

where δ_v [kg/Pa.m.s] is the water vapor permeability of the porous material. The diffusion of water vapor in a porous material will therefore be regarded as diffusion in air, but with reductions because of the pore system, and is a function of parameters like porosity and tortuosity. The concentration of water vapor ρ_v and water vapor pressure $\mathcal{P}$ have the following relationship by applying the ideal gas law:

$$\rho_v = \frac{\mathrm{P}}{R_v.T} \qquad (2.20)$$

Equation 2.18 becomes, under isothermal conditions:

$$g_v = -\delta_{\mathrm{P}}\frac{\partial \mathrm{P}_v}{\partial \mathrm{x}} \qquad (2.21)$$

where $\mathcal{P}_v$ is the water pressure (Pa), $\delta_{\mathcal{P}}$ [kg/Pa.m.s] is the water vapor permeability which can be determined as:

$$\delta_{\mathrm{P}} = \frac{\delta_v}{R_v.T} \qquad (2.22)$$

2.4.1.2 Non-Isothermal Vapor Transport

When a material is exposed to a temperature gradient, moisture transport occurs based on (according to Table 2-3) the Knudsen diffusion and thermal diffusion forms of transports. Thermal diffusion is due to the density difference between dry air and vapor molecules, which makes the lighter vapor move from cold to warm, and thus results in migration against the temperature gradient (Pedersen, 1990). The thermal diffusion can be expressed as the non-isothermal vapor flux density $g_{T,v}$ [$kg/(m^2 s)$]

$$g_{T,v} = -D_{T,v} \frac{\partial T}{\partial \mathrm{x}} \qquad (2.23)$$

where $D_{T,v}$ [kg/(K.m.s)] is the non-isothermal vapor diffusion coefficient. The non-isothermal transport equation (Equation 2.24) given by (Philip and De Vries, 1957) is in general considered as the governing equation for water vapor transport under a temperature gradient, where the first part represents vapor diffusion determined by a moisture content gradient and the second part thermal diffusion determined by the thermal gradient:

$$g_v = -D_{w,v} \frac{\partial_w}{\partial \mathrm{x}} - D_{T,v} \frac{\partial T}{\partial \mathrm{x}} \qquad (2.24)$$

where $D_{w,v}$ is the coefficient for moisture content-driven vapor diffusion.

According to Pedersen (1990), by increasing the temperature gradient in a moist material, the permeability will also increase. (Peuhkuri, 2003a) explained that by only increasing temperature, without a gradient, the water vapor permeability will increase, particularly for high relative humidities. The influences of temperature on the permeability for some building materials has been similarly confirmed by Galbraith et al. (2000a). Some literature, however, consider that the influence of temperature on the vapor transfer coefficients is negligible (Delgado et al., 2013).

2.4.2 **Measurement Methods**

All measurement methods of water vapor permeability of building materials can be described by the following diagram.

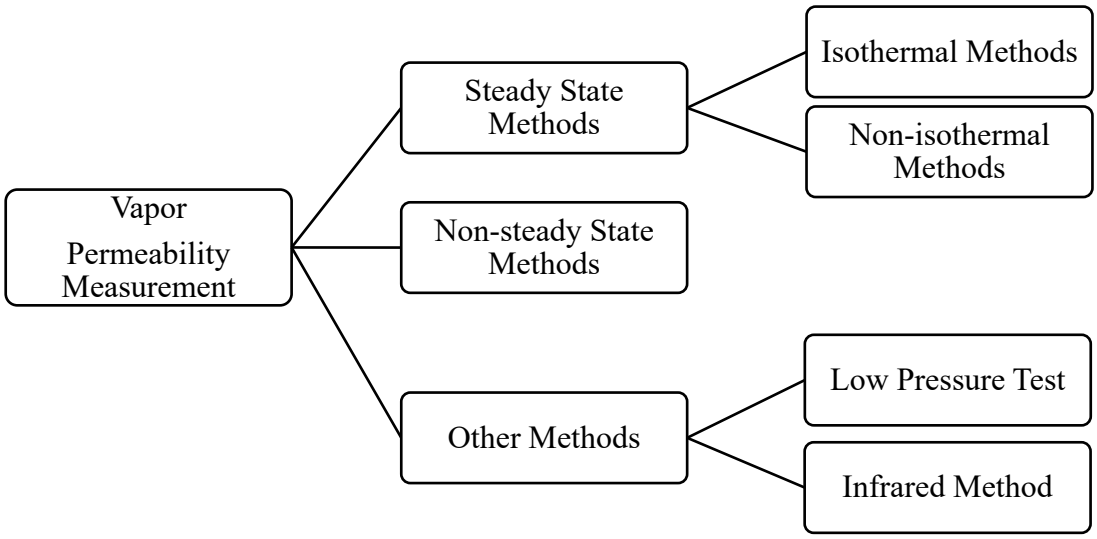

This classification of methods is based on separate efforts to measure diffusion properties of materials with regards to time and accuracy.

2.4.2.1 Steady state methods

Steady state methods are the oldest and the most prevalent methods in the literature. The principle of these methods is to create two constant environmental conditions on both sides of a specimen during the whole time period of the measurement. The results are calculated after water vapor flux reaches constant value. Steady state methods can be further separated in two categories: isothermal and non-isothermal methods.

Steady state isothermal methods run under constant temperature on the both sides of the specimen. Therefore, only a difference in relative humidity on the surfaces of the specimen is a driving force for water vapor transport. The cup methods are the most common steady state isothermal experiments.

2.4.2.1.1 Isothermal Methods: Cup Methods

The cup methods are the simplest and the widely used tests to measure the rate of water vapor transmission of building materials (Joy and Wilson, 1966). The principle of the experimental procedure in these methods have not been changed significantly since 1954 where they were standardized by the American Standard Testing Materials (ASTM) for the first time (Kumaran, 1998b). The principle of steady-state vapor permeability measurements of materials lays on

achieving steady state flow conditions under a constant vapor pressure (potential) gradient. The vapor pressure can be adjusted by controlling the relative humidity and keeping the temperature constant. The relative humidity can either be adjusted by saturated aqueous salt solutions or by a climatic chamber. Then, the cup set with a material specimen of known area and thickness is placed inside a climatic chamber where the relative humidity value is regulated differently from inside the cup. As a result, a vapor pressure gradient will be created between two sides of the material specimen which initiates one-dimensional vapor flux cross the specimen. Depending on the vapor pressure gradient, vapor will enter or leave the cup. If the flow rate through the material is measured, the transport properties can be derived for the corresponding potential gradient. The rate of vapor flow across the specimen is obtained through gravimetric measurements and , once a steady state flow has been reached, the vapor permeability can be derived (Plagge et al., 2007). The measurements are usually done under isothermal conditions.

Recently, a number of technical papers in the literature deal with various technical aspects, limitations, and analyses of the experimental data of these procedures (Lackey et al., 1997; Kumaran, 1998a). However, water vapor permeance is widely measured using cup method which is explained in the standard ASTM E96 (ASTM-E96/E96M, 2013) and ISO 12572 (EN.ISO.12572, 2001). In ASTM standard E96 explains three main recognized different methods as wet-cup (water method), dry-cup (desiccant method) and inverted wet-cup (inverted water method), Figure 2-9.

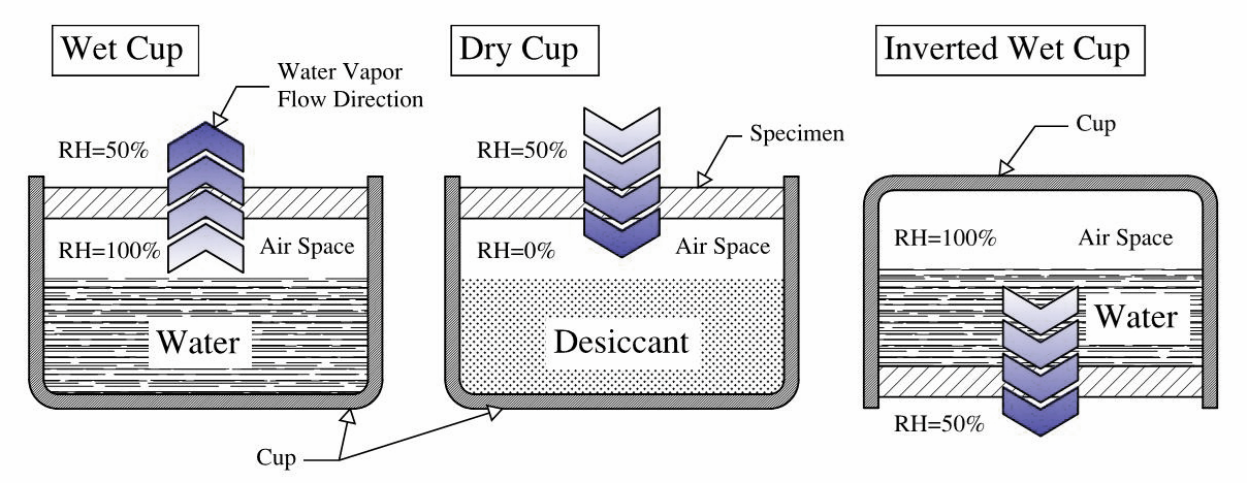

Figure 2-9. Three basic cup methods based on ASTM Standard E96/E96M.

Using these three different test methods, Joy and Wilson (1966) measured the vapor permeability of several weather resistive barriers including different sheathing papers and roofing felts. Their results showed that the highest permeability values were associated with inverted cups methods followed by wet cups and dry cups methods, respectively. The recommended test conditions for different test method are summarized in Table 2-4 according to ASTM E96. Similarly, different conditions for the cup methods are adjusted in European standard EN ISO 12572, Table 2-5.

Table 2-4. Conditions and names for the cup methods according to standard ASTM E 96/E 96M

Procedure	Name of Method	Temperature [˚C]	RH [%] on each surface of specimen	
			Inside Cup	Outside Cup
A	Dry Cup	23	0	50
B	Wet Cup	23	100	50
Bw	Inverted Wet Cup	23	100	50
C	Dry Cup	32.2	0	50
D	Wet Cup	32.2	100	50
E	Dry Cup	37.8	0	90

Table 2-5. Conditions and names for the cup methods according to standard EN ISO 12572

Procedure	Name of Method	Temperature [˚C]	RH [%] on each surface of specimen	
			Dry Condition	Wet Condition
A	Dry Cup	23	0	50
B	-	23	0	80
C	Wet Cup	23	50	93
D	-	38	0	93

Each cup method determines water vapor permeability of a material for specific boundary conditions. For example, dry cup method provides water vapor permeability values for materials at relative humidity ranges lower than 50%. Accordingly, wet cup method gives water vapor permeability values for materials at relative humidity ranges higher than 50%. The relation between the dry and wet cup results for vapor permeability has been illustrated in Figure 2-10 where the area A and C are equal to B and D, respectively (Chang and Hutcheon, 1956).

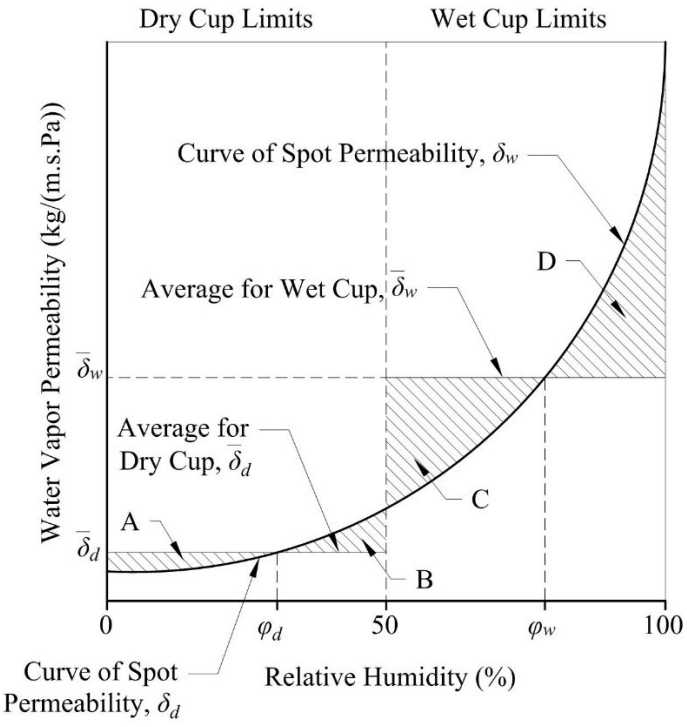

Figure 2-10. The relation between the vapor permeability results from dry cup and wet cup test methods (Chang and Hutcheon, 1956).

Using cup test method, Sonderegger et al. (2011) measured water vapor resistance factor (WVR) as well as diffusion coefficient from both steady state and unsteady state for Norway spruce and European beech. They investigated the impacts of different fiber directions including radial (R), tangential (T) and longitudinal (L) and steps of 15 degrees between the directions. The cup test method was carried out according to EN.ISO.12572 (2001) at two relative humidities of 35% and 65% and constant temperature of 20˚C. The results from cup test methods showed that, for spruce, the trends in WVR between all directions were almost similar. However, for beech, the values of WVR increased considerably from the L to the T than to the R direction. Particularly, at angles 75 and 90 degree. The WVR for both species at wet cup test method increased from above 15 degree while in dry cup test method WVR increased from above 60 degree. They stated that independent of the wood fiber direction, the diffusion coefficient from steady state method was generally twice the diffusion coefficient from unsteady state method. The measurement showed that in all directions, both diffusion coefficient in spruce were up to three times more than beech. while the larger difference was observed for longitudinal direction which was almost 15 times higher than the other directions. In both species, the WVR factor and the diffusion coefficients exponentially

decreased and increased, respectively with increasing moisture content. The changes in water vapor resistance factor was observed to be reversed to the diffusion coefficients.

Following a similar approach, Vololonirina et al. (2014) investigated hygrothermal properties of three wood-based materials considering the impact of pre-conditioning of the specimens. He performed wet and dry cup test method for vapor permeability measurement under one constant climate condition and different thickness of materials. The pointed out that values of water vapor diffusion resistance from dry cup tests was higher than the values from wet cup tests. Furthermore, the results of this study declared that initially dry material samples were more resistant to moisture than material samples which were initially wet.

The ASTM E96 standard prescribes that all tests to be performed at 50% relative humidity, therefore, the results from the wet and dry cup methods provide an average value of the vapor permeability at mean relative humidity of 75% and 25%, respectively. Kumaran (1998a) believed that this information is insufficient for detailed hygrothermal analysis of building materials. The majority of current computer models require more water vapor permeability values at different relative humidities reliable analysis of hygrothermal performance of building components. As a logical extension of the existing procedure described in ASTM E 96, Kumaran (1998a) proposed two series of measurements for dry cup and wet cup methods to be started at relative humidity of approximately 30% for both methods. The series of measurements should be repeated in both methods with increasing the relative humidity with the increments of 10 to 15%. The dry cup tests can stop at 70% relative humidity while the wet cup test should be continued to relative humidity of 100%. Likewise, Scheffler (2007) suggested that in order to achieve reliable measurement results, the relative humidity difference shall be rather small (i.e. 10% to 20% RH).

2.4.2.1.2 Non-isothermal Methods

It is commonly recognized that the environmental test conditions used in any measurement procedure will significantly influence the results obtained. It could, therefore, be expected that results of permeability tests will produce different data in different laboratories. In addition, there could be many other factors related to the details of test procedure and equipment used which could influence the results (Toas, 1989). Consequently, these concerns have been the motivation for several research group to investigate and develop different new test methods for measuring the vapor permeability of building materials.

There are different developed methods other than conventional cup method in literature regarding measuring the permeability of materials. Through these new methods, researchers have attempted to improve the permeability test by applying different temperature and relative humidities on both sides of the specimens in order to investigate the non-isothermal moisture transport and obtain more realistic and accurate results for water vapor transmission and permeance.

Douglas et al. (1992) developed a new experimental setup for measuring the water vapor permeability of building materials. The setup comprised of two separate stainless-steel chambers which connected side by side with individually controlled conditions of temperature and relative humidity. The material sample were placed and sealed vertically on a small orifice on the shared side between the two climate conditions.

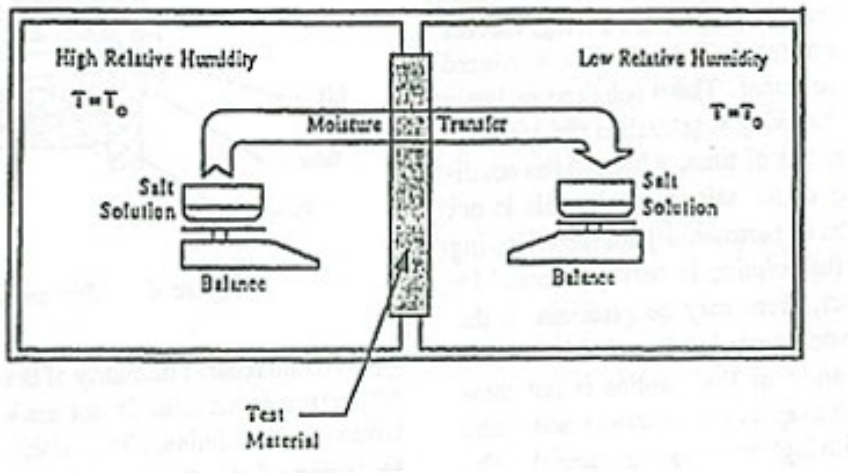

Figure 2-11. Schematic experimental setup (Douglas et al., 1992)

According to their study, the new apparatus enabled them to apply a broad range of temperature and relative humidities on both sides of the materials. They tested the vapor permeability of two different gypsum wallboards (high permeance and low permeance) under the standard environmental condition of 20% and 50% RH at 23˚C to simulate the dry cup testing. Considering the statistical uncertainties, they noted a good agreement, between the preliminary results with the permeance results of the cup methods obtained by the manufacturer and ASHRAE handbook (ASHRAE, 1985).

Galbraith et al. (1998) studied two cases in which they applied moisture flux on small-scale material samples under different temperatures and humidities using a device they developed shown in Figure 2-12 and measured the non-isothermal moisture diffusivity.

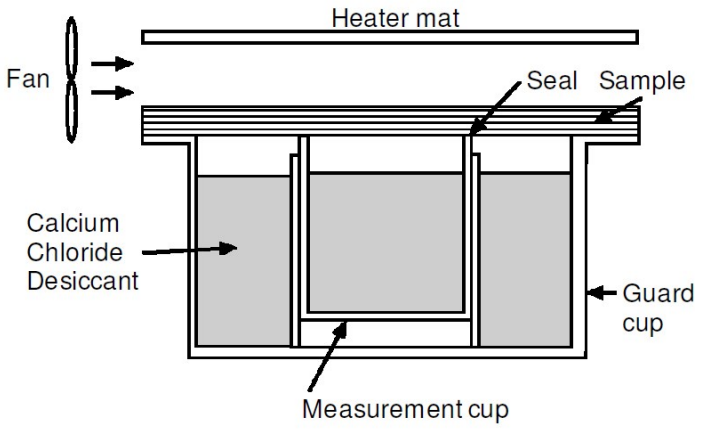

Figure 2-12. Guarded Cup Setup (Galbraith et al., 1998)

The test cup which they referred it as Guarded Cup, includes a circular measurement cup containing two regulators a vapor pressure regulator located inside a larger diameter 'guard' cup with similar regulator. The cups were manufactured from acrylic which is impermeable to water vapor and allows inspection of the sample and vapor pressure regulator during the experiments. They employed guard arrangement shown above in order to minimize sample edge effects. They tested different materials with the following experimental approaches:

1. Isothermal tests to evaluate the dependency of average permeability on temperature and humidity.
2. Non-isothermal tests to evaluate the importance of thermal diffusion flow and the corresponding values of thermal diffusion coefficient.

The isothermal test using particle board and polystyrene within a hot water bath arrangement didn't give measurable thermal diffusion flux.

The non-isothermal test in which they used a radiant heat source to provide the temperature difference, enabled them to obtain data for three test cases with different temperature differences across plasterboard and insulation test samples. In both tests, the small samples were used. But this method of measurement highlighted some difficulties such as:

- The structure of the samples affects the results,
- Due to the edge effects, achieving uniform temperature across the sample is very difficult,
- It is difficult in practice to obtain a range of temperature differences between two surfaces,
- It is not possible to create a wide range of relative humidity and temperature differences.

Schwartz et al. (1989) developed a new method named the 'modified-cup-method' to investigate and measure water vapor transmission property of building materials. They combined both wet and dry cup test method by attaching them onto both sides of the specimen. A schematic diagram of the modified cup is shown in Figure 2-13.

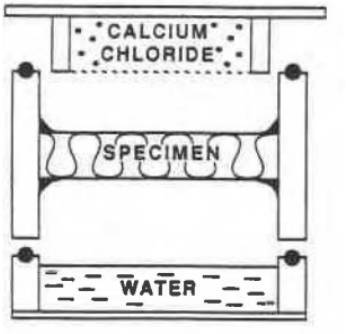

Figure 2-13. Schematic Diagram of Modified Cup Test Assembly (Schwartz, 1988).

A round material sample is sealed with silicone rubber inside the cylindrical container made of plexiglass. This container is placed between two wet and dry cups at the bottom and the top, respectively. The desiccant in the dry cup at the top is separated from the specimen with a layer of a highly permeable material. Two aluminum plates were bolted on both sides holding the test setup in place. The average nominal relative humidity inside the test assembly was assumed to be 50 %. Then the whole setup was placed inside a controlled temperature chamber. Alternatively, the specimen container was sandwiched between a cold plate and water in contact with a hot plate to create a temperature gradient, Figure 2-14.

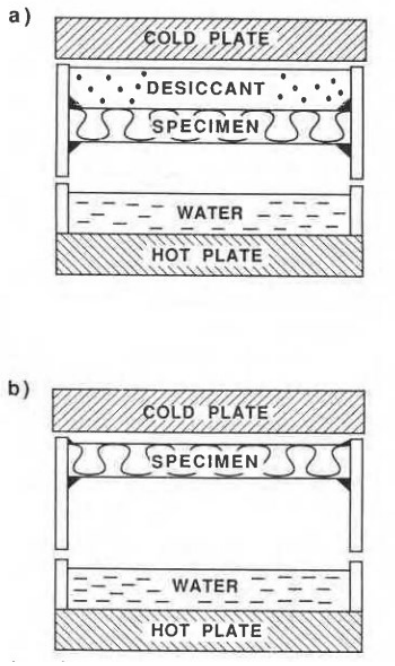

Figure 2-14. Schematic of the temperature gradient method. The specimen was separated from the cold plate either by desiccant (a) or by a layer of polyvinylidenechloride (b) (Schwartz et al., 1989).

The cold plate was separated from the specimen either by desiccant, or a layer of low permeance polyvinylidenechloride. A benefit of producing this test setup was to eliminate the impact of the variation in relative humidity inside the chamber on the tested materials during the cup test methods which is occurring while the temperature is changed (Mukhopadhyaya et al., 2005). However, the process of weighting the sample which includes disassembling and re-assembling the setup can be a drawback for their test method as it increases the weighing time and can impact the accuracy of the measurement results.

Peuhkuri et al. (2008) introduced a special design and built climatic chamber for non-isothermal water vapor transmission measurement split the 'other' moisture transport from the total measured moisture flux and quantify its significance in the water vapor pressure-driven non-isothermal moisture transport process. Their test setup was called Megacup due to the similarity of the measurement principle with ordinary cups for water vapor permeability measurements, Figure 2-15. Utilizing this method, no uncontrolled condensation occurs, and the measured flux is an accurate representation of the actual flux produced by the driving potentials. The whole set-up was situated in a controlled climate room, where temperature and relative humidity were held constant at the desired levels.

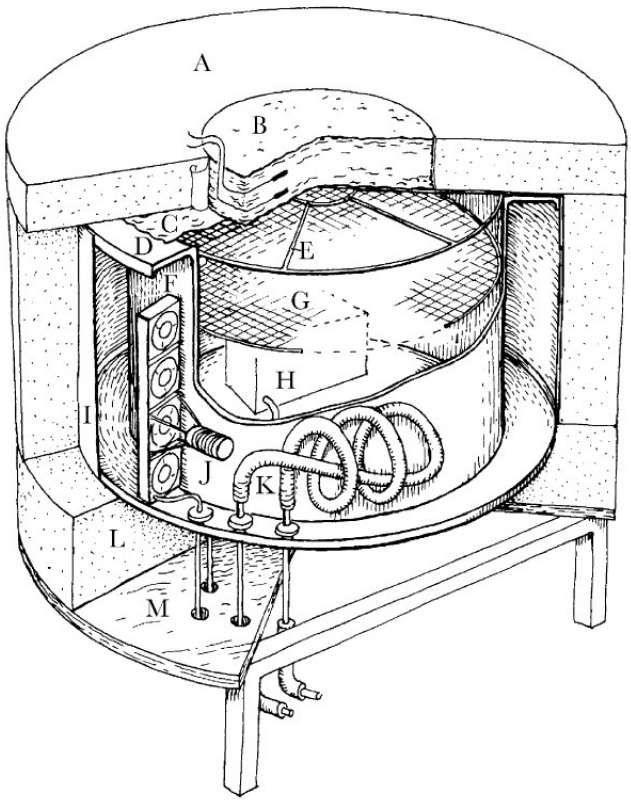

Figure 2-15. The cross-section of the experimental set-up and the construction principles: (A) thermal guard insulation, (B) sample (square shape in these experiments), (C) vapor barrier under the guard insulation, (D) flange over annular space, (E) open grid, (F) fans, (G) another grid (not used), (H) moisture control unit, (I) stainless-steel wall, (J) heating (electric resistance), (K) cooling (water circulating in coil), (L) bottom insulation,(M) table (Peuhkuri et al., 2008).

It has been proven that material structure such as: thickness, internal fiber direction and initial moisture content influence the vapor permeability.

2.4.2.2 Non-Steady State Methods

Vrána and Björk (2008) designed and built an equipment with the ability to controlled environmental condition on both sides of the tested material to enhance the accuracy of the property measurements. Their apparatus included an insulated testing box with controlled condition at inside which material samples could be sealed on the top side while the whole setup will be placed inside a climatic chamber, Figure 2-16.

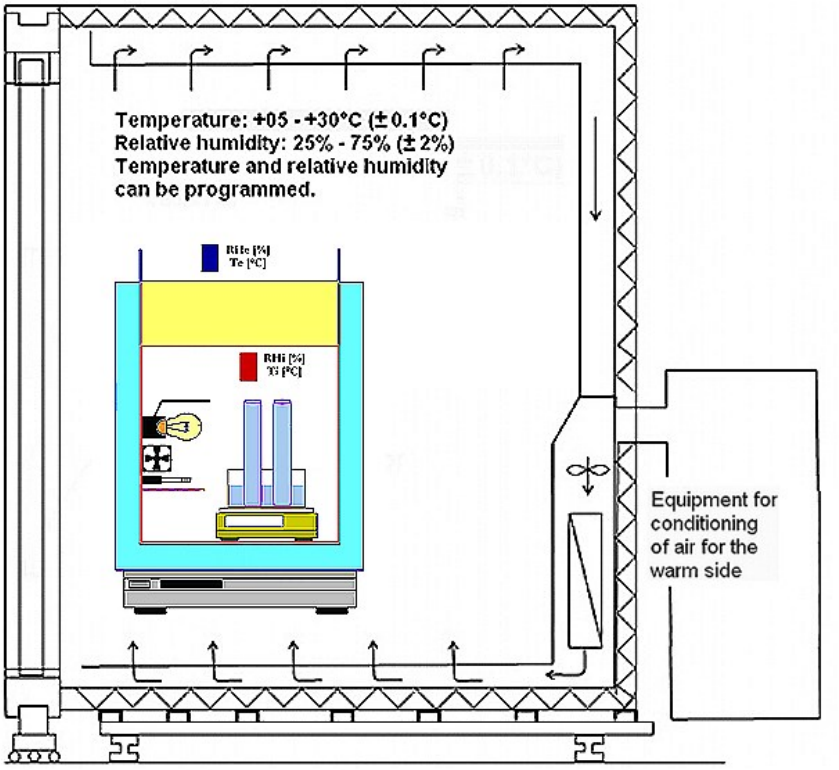

Figure 2-16. Section view of the climatic chamber with the testing box placed inside (Vrána and Björk, 2008).

There is a small water tank in the testing box. The inside of the box is heated electrically, and a fan is circulating the air. Therefore, different temperatures and relative humidities could be regulated at both sides of a specimen. The box is placed on a balance in order to record the mass loss during the test. The results of the apparatus performance were reported to be satisfactory.

2.4.3 **Temperature Dependency**

Temperature gradient exists in real configurations. As a result, building envelopes and consequently materials are exposed to different temperatures. Babbitt (1940) explored the idea that the permeability of hygroscopic materials can be determined in two distinct regions of low and high relative humidity using different forms of Fick's law. He carried out the vapor permeability test using a cup like assembly which enabled him to apply different relative humidities and temperatures across the material sample as: 85.5˚F (29.7˚C) and 75 % RH at the top surface and 102˚F (38.9˚C) and 67 % RH at the lower surface. His experimental results showed that the moisture transmission resistance of fiberboard is proportional to its thickness. After determining

the moisture content and vapor pressure gradient across the specimens which are opposite to each other, he pointed out that in relative humidities below 75%, the vapor pressure gradient is the driving force for moisture movement in fiberboard.

Doty et al. (1946) investigated the influence of temperature on vapor permeability of several types of self-supporting films from organic polymer. Their measurements were in a temperature range from -10˚C to 80˚C under the constant relative humidity. Their results represented that the effect of temperature on permeability constants is vary from no effect on polystyrene films to a doubling of permeability in every 5˚C for polyvinylidene chloride.

Chang and Hutcheon (1956) investigated the influence of different temperatures and relative humidities on the water vapor permeability of two building papers: asphalt saturated felt and a smooth, lightly saturated and waxed kraft building paper. Accordingly, the dry cup test method was carried out at different temperatures: -12.23˚C, -3.89˚C, 1.67˚C, 22.78˚C and 32.23˚C, and various relative humidities with increasing increments of 20%. Based on their study, increasing temperature at higher relative humidities has significant effects on asphalt-saturated sheathing felt while permeability in slightly-saturated waxed crafted building paper increased slightly by increasing temperature and relative humidity. They pointed out that the influence of temperature gradient cannot be calculated through a simple vapor flow equation. They explained that in order to obtain more realistic results for permeability the flow equation must include surface film and capillary transport under a moisture content gradient mixed by vapor diffusion under the vapor pressure gradient.

Tveit (1966) studied the vapor permeability of 48 materials under different fixed conditions for various temperatures and relative humidities within the hygroscopic range. He measured the vapor permeability under 24 different conditions of combination of temperatures and relative humidities in the range of 5-45˚C and 5-90% RH, using the cup method. His results represented an increase in vapor permeability with increasing the temperature in constant relative humidity. He concluded that vapor permeability depends on hygroscopicity, air permeability of materials and the capillary migration ability.

Hedlin (1977) simulated the roof with insulation on protected membrane in laboratory condition in order to study the moisture movement and absorption of several foam plastic insulation

subjected to temperature and moisture gradients. He examined closed cell insulations and one open cell material under different temperature gradients from 0˚C to 22˚C in the presence of free water. His results indicate that in almost all cases, the permeability values obtained during the experiment were higher than permeability values obtained through the wet cup test method according to ASTM C355. For instance, the permeability values for extruded polystyrene and urethane were approximately 50% higher, and for bead polystyrene and phenolic foam were 150 to 500% higher.

Schwartz (1988) examined a number of foam insulations under temperature gradients in laboratory as well as exposed to Ottawa weather in winter in order to study moisture gain and vapor permeability. The insulation included number of sprayed-in-place polyurethane (PUR), extruded polystyrene (XPS), and phenolic foam. The laboratory experiments were conducted under temperature gradient from 50˚C on the warm side to 5˚C on the cold side while material samples in the field test were exposed to 20˚C and 40 % RH on the room (warm) side and as low as -25˚C on the outside weather (cold side).

In the case of PUR, Schwartz (1988) noticed moisture accumulation in the laboratory test due to the different rates of moisture migration through the assembly from the warm side to the cold side. The lab results confirmed that the vapor permeability increased by temperature. However, in filed testing of PUR, the vapor permeability was constant with a low value across the sample under the temperature gradient and the potential for moisture accumulation was low. This study showed that contrary to PUR the vapor permeability in the XPS changed slightly with temperature below 45˚C.

In another research Schwartz et al. (1989) investigated the water vapor transport and moisture accumulation in polyurethane and polyisocyanurate foams using modified cup method under isothermal and non-isothermal conditions. They performed isothermal experiments at different temperatures between 10˚C and 51˚C and for the test under thermal gradient they applied temperatures of 5˚C and 50˚C on the cold and warm plates, respectively. By analyzing and comparing the results of the two techniques, they concluded that for both techniques the permeability of tested insulation materials was independent of temperature within the range of 10˚C to 21.5˚C. However, the vapor permeability dramatically increased linearly for temperatures above 21.5˚C. According to their results there was no moisture gain in isothermal conditions while,

under the presence of thermal gradient, moisture accumulation on warmer regions of materials was significant depending on the duration of the test.

Kumaran (1989) studied the impact of thickness on moisture transport characteristics with the influence of temperature gradient on vapor transmission through fiber glass insulation using heat flow meter apparatus with applying various temperature differences from 20.1˚C to 40.6˚C. According to his experiment process, a certain amount of water which was sprayed to the hot plate surface, was completely transported to the surface of the cold plate through the body of the insulation. The measurement of this process along with the heat flux at steady state provides information regarding simultaneous heat and moisture transport through the material sample (see Kumaran and Mitalas (1987) for theoretical analysis). The test results revealed an increase of vapor flux at higher temperature differences.

Douglas et al. (1992) conducted the permeability test with their self-designed and made experimental setup. Studying the low-permeance gypsum wallboard with the presence of only vapor pressure gradient or only temperature gradient, they observed high and low (near zero) water vapor transport rate, respectively. However, the moisture flux increased when the two gradients were applied together. They concluded that in water-resistant wallboard vapor pressure gradient associates much higher with moisture transport than the temperature gradient.

Burch et al. (1993) examined water vapor transmission of ten building materials under a wide range of relative humidities at two different temperatures of 7˚C and 24˚C. They provided different relative humidities for two sides of the materials using different saturated salt solutions in a large glass vessel. The whole glass vessel assembly was placed inside a conditioning chamber to achieve constant temperature during the test. Analyzing the cup measurements, they stated that although temperature considerably affected the diffusivity, it insignificantly influenced the permeability.

Galbraith et al. (1998) studied two cases of isothermal and non-isothermal test conditions in which they examined moisture flux on small-scale material samples under different temperatures and humidities using a device they developed shown in Figure 2-12. They tested particle board and polystyrene under the isothermal condition at temperatures of 20˚C and 42˚C and plasterboard and insulation under a temperature gradient between 23˚C and 15˚C. Their test results for the isothermal condition showed no substantive indication of a measurable thermal diffusion flux.

However, the results for the non-isothermal condition indicated a relationship between temperature gradient and moisture flow. Although a consistent value was observed for the average vapor permeability for insulation, a variation of 7 % was recorded for plasterboard. Previously, Galbraith and McLean (1990) stated no dependency of permeability on temperature when they investigated the vapor permeability of plasterboard, polystyrene, plywood, wood and brick over the range of temperatures from 10˚C to 25˚C.

(Galbraith et al., 2000a) studied the temperature dependency of vapor permeability in four common building materials (plasterboard, phenolic foam insulation, plywood and medium density fiberboard (MDF). They measure the permeability of tested materials at different temperatures between 10˚C and 30˚C using conventional gravimetric approach based on European Standard, prEN/ ISO 12572. At each temperature, four different relative humidity were considered in order to create the variation of moisture permeability with relative humidity. The results then were evaluated mathematically using the concept of differential permeability. In their experiment they constantly kept the relative humidity of chamber at 60% during all the measurements. Based on their experimental findings, they concluded except the two wood-based materials which had a significant temperature effect in the liquid flow regime, for other materials the impact of temperature was negligible. However, the authors could not establish a universal mathematical model that includes the temperature effect in an isothermal condition within the differential permeability concept.

Later the same author, further tested plywood and fiberboard (MDF) under different environmental conditions of various combinations of at least three temperatures and four relative humidities Galbraith et al. (2000b). Their investigation out lined that the effects of temperature on permeability was more considerable at relative humidities above 60% while it is negligible in low humidities. For example, with increasing temperature from 10˚C to 30˚C, at relative humidity near 100%, the permeability increased 51% and 29% for plywood and fiberboard, respectively.

Gibson (2000) investigated water vapor transmission properties of nine different polymer membranes and textile/membrane laminate exposed to different temperatures. He conducted the tests with the Dynamic Moisture Permeation Cell (DMPC) instrument. DMPC is an automated apparatus that is capable of testing the mass transport properties of very small samples of broad range of woven, nonwoven fabrics, membrane and foams. DMPC enables user to study nonlinear

transport properties coupled with vapor sorption under the full range of relative humidity at temperatures from -15˚C to 50˚C. The results exhibited an exponential increase in water vapor flux by the increase in temperature. However, he concluded that vapor transport property of all polymer membranes was influenced significantly by moisture content rather than temperature.

Jooss and Reinhardt (2002) investigated the influence of temperature on the water permeability and vapor diffusivity of 11 types of concrete including normal to high strength concrete, polymer modified and self-compacting concrete by using a custom maid instrument and the cup test method, respectively. Both experiments were carried out under temperature range of 20˚C to 80˚C by placing the test setups inside climatic chamber. Although, they did not use specific standard test procedure for water permeability, the diffusivity test was completed according to the DIN 52615, German standard for testing water vapor permeability. Additionally, through numerical methods, they predicted the coefficient for aforementioned properties for the temperature range of 20˚C – 80˚C. The theoretical based and experimental results for both properties indicated an upward trend in coefficients with increasing temperature within a good agreement to the literature. Analyzing the results, it was found that by rising temperature from 20˚C to 50˚C, the permeability to water rose by 13-62% and diffusivity to vapor increased by 10-21%. Furthermore, due to raising temperature from 50˚C to 80˚C, the permeability and diffusivity increased by 3-35 % and 8-21 %, respectively. In both cases, they concluded that the types of concrete were considered as an influential factor in variation of the results.

Valovirta and Vinha (2004) studied the relationship between water vapor transmission properties and thermal conductivity at various temperatures and relative humidities, particularly in Nordic climatic conditions. They used wet cup method to measure water vapor transmission properties of materials which are exposed to the exterior climate condition. Tests were performed inside a climatic chamber at 33% RH and temperatures of –10˚C, +5˚C, and +23˚C. The relative humidity inside the cups were 55%, 75%, 86%, and 97%, except in a –10˚C temperature test in which relative humidities of 45%, 76%, and 86% were provided. The reason as they described was because some salt solutions did not perform well below the freezing point of water. They concluded from the tests results that at the given relative humidities, the water vapor permeability increases with temperature. Some materials had constant water vapor permeability at one temperature, whereas at some other temperature it rose as a function of relative humidity.

However, the vapor transmission values of very permeable and impermeable materials were hard to fit in a mathematical model. For example, in highly permeable thermal insulation materials air convection contributes to moisture transfer in addition to diffusion. In testing impermeable materials such as concrete, assembling the cup with improper sealing of the specimen can cause more moisture leaks and consequently leading to error in the water vapor permeability measurement. After performing the tests, thermal conductivity seemed to change linearly even at temperatures below 0˚C, while moisture conditions were clearly below capillary range.

Using the modified cup method, Mukhopadhyaya et al. (2005) evaluated the vapor transmission properties of fiberboard and gypsum board under different temperatures and constant relative humidity. They performed the experiment at five temperatures of 7˚C, 16˚C, 23˚C, 34˚C, and 43˚C and verified the results by carrying out a limited number of 'conventional cup method' tests according to the ASTM standards Test Methods for Water Vapor Transmission of Materials (E96). During the test procedure, temperature levels below 22.8˚C were maintained inside a cooling chamber. Similarly, temperature levels above 22.8˚C were maintained inside an oven while in both cases the average relative humidity remained at around 50%. The results indicated that higher temperature causes higher rate of water vapor transmission. The interaction between water vapor transmission rate and temperature can be described as exponential. However, they concluded that water vapor permeabilities of both materials were almost independent of temperature conditions.

Utilizing their designed special climate chamber , Megacup, Peuhkuri et al. (2008) introduced new measurement method to investigate the magnitude of moisture transport due to temperature gradient in number of porous light-weight building materials. Based on published literature and their observations of tested materials, they concluded that some kind of 'other' transport processes exist against the gradient of vapor pressure. Using a special made setup and creating the temperature gradient of 10K, they experimentally attempted to split this 'other' moisture transport from the total measured moisture flux and quantify its significance in the water vapor pressure-driven non-isothermal moisture transport process. After performing the experiment on several materials, they could not confirm the hypothesis that relative humidity being a driving force for non-isothermal moisture transport in the hygroscopic part while, there are some indications that the temperature gradient itself is driving the moisture from the warm side towards the cold side.

Constructing a special setup to control the condition on both sides of the tested specimen, Vrána and Björk (2008) investigated moisture flow rate as well as moisture resistance factor of stone wool insulation under four temperature gradients and a constant relative humidity of 40%. The temperature gradients cross the specimen were obtained with changing the temperature of the climate chamber to 5˚C, 10˚C, 15˚C and 20˚C while maintaining the temperature inside the box at 20˚C. The result of the test indicated that the measured value of moisture resistance factor for mineral wool was aligned with values from the relevant standard (EN 12524). However, the moisture resistance factor declared by the manufacturer was 2.5 times higher than the measured value.

Baker et al. (2009) introduced an experimental protocol to solve the problems of the investigations from (Galbraith et al., 1998; Galbraith et al., 2000a) including:

- Difficulty of creating temperature differences in small samples
- Difficulty of estimating a concentration-driven flux from isothermal permeability measurements.

First, they used larger samples in guarded arrangement instead of small samples. This clearly helped them to establish 1D temperature gradient through the samples. Second, they performed the measurements under non-isothermal boundary conditions. Their experimental test protocol includes:

- small-scale isothermal permeability with cup test method at different temperatures between 10˚C to 30˚C,
- large-scale moisture flow tests under non-isothermal conditions either with temperature gradient of 7˚C – 10˚C and constant relative humidity or with zero vapor pressure gradient and different relative humidities.

The authors pointed out that although temperature gradient is a significant driving potential in moisture transfer through building materials in the non-isothermal tests, the vapor pressure gradient is more crucial driving potential. After evaluating the temperature dependent permeability, the results represented that except timber-based materials at higher humidities (RH>70%), the other types of materials showed no significant variation with temperature. Furthermore, their results also highlighted that the surface boundary conditions, i.e. the surface

thermal and vapor resistances had considerable impact on the moisture gradients through single layer materials as it was observed in the non-isothermal tests.

In another study, Trabelsi et al. (2012) investigated the influence of temperature on moisture transfer in a brick under isothermal and non-isothermal conditions. They evaluated two driving force for moisture flux as: water vapor content gradient and temperature gradient with average ΔT of 9.4˚C. They found a consistent difference between the mass flow under isothermal and non-isothermal regimes which its ratio did not exceed 10% for all the tested materials. They outlined that the effect of temperature gradient is significant and speeds up the flow of moisture particularly when the gradient of relative humidity is very low. According to their conclusion, the pore structure of material and the moisture content influence the water vapor permeability.

Pavlík et al. (2013) studied the effects of temperature and thickness on water vapor transport properties of cellular concrete. They conducted cup method with three thickness of samples under the range of temperatures between 10˚C and 50˚C at constant relative humidity. The results revealed an increase in water vapor diffusion coefficient and water vapor diffusion permeability with increasing temperature, while it has reverse effect on water vapor diffusion resistance. The obtained results also, showed a considerable effect from sample thickness on vapor transmission properties.

Following a similar approach as the previous study, Fořt et al. (2014) studied the influence of temperature and sample thickness on water vapor transport properties of calcium silicate. They measured the vapor diffusion permeability of samples under a range of temperatures from 10˚C to 50˚C and under a wide range of relative humidities from 0% to 98%. According to their results, water vapor diffusion coefficient increased by the temperature.

The full list of the literature reviewed along with the factors influences the water vapor permeability are shown in Table 2-6.

Table 2-6. Published Literature in Temperature Dependency of Vapor Permeability.

Article	Theoretical	Experimental	Properties	Temperature range	Materials	Remarks
Babbitt (1940)	•	•	Vapor Permeability	Temperature gradient between 85.5˚F (29.7˚C) and 102˚F (38.9˚C)	Fiberboard	The moisture transmission resistance of fiberboard is proportional to its thickness. In relative humidities below 75%, the vapor pressure gradient is the driving force for moisture movement in fiberboard.
Doty et al. (1946)	•	•	Vapor Permeability	-10˚C - +80˚C	Ten Homogeneous Polymer Films	The effect of temperature on permeability constants was vary from no effect on polystyrene films to a doubling of permeability in every 5˚C for polyvinylidene chloride.
Chang and Hutcheon (1956)	•	•	Vapor Permeability	-12.23˚C, -3.89˚C, 1.67˚C, 22.78˚C and 32.23˚C	Asphalt-Saturated Sheathing Felt, Asphalt-Saturated Building Paper and Waxed Craft Building Paper	The vapor permeability in asphalt-saturated sheathing felt was more sensitive to temperature change than waxed crafted building paper. They explained that in order to obtain more realistic results for permeability the flow equation must include surface film and capillary transport under a moisture content gradient mixed by vapor diffusion under the vapor pressure gradient.
Tveit (1966)		•	Sorption, Vapor Permeability	+5˚C - +45˚C	Wood-Based, Cementitious materials, Building paper, Insulations	His results represented an increase in vapor permeability with increasing the temperature in constant relative humidity. He concluded that vapor permeability depends on hygroscopicity, air permeability of materials and the capillary migration ability.
Hedlin (1977)	•	•	Vapor Permeability, Sorption Isotherm	Temperature gradients with ΔT: 0˚C, 2.8˚C, 11˚C and 22˚C	Extruded polystyrene, Bead Polystyrene, Polyurethane, Phenolic foam	In majority of cases, the permeability values obtained during the experiment were higher than permeability values obtained through the wet cup test method. For instance, the permeability values for extruded polystyrene and urethane were approximately 50% higher, and for bead polystyrene and phenolic foam were 150 to 500% higher.

Schwartz (1988)		•	Vapor Permeability	Temperature gradients of -25˚C to +20˚C And +5˚C to +50˚C	Sprayed in place polyurethane (PUR), extruded polystyrene (XPS), and phenolic foam insulations	The lab results confirmed that the vapor permeability increased by temperature. However, in filed testing of PUR, the vapor permeability was constant with a low value across the sample. In contrary to PUR the vapor permeability in the XPS changed slightly with temperature below 45˚C.
Schwartz et al. (1989)		•	Vapor Permeability	Isothermal conditions between 10˚C and 51˚C. Non-isothermal conditions from +5˚C to +50˚C	Rigid polyurethane foam and Polyisocyanurate foam	They concluded that for both techniques the permeability of tested insulation materials was independent of temperature within the range of 10˚C to 21.5˚C. However, the vapor permeability dramatically increased linearly for temperatures above 21.5˚C. There was no moisture gain in isothermal conditions while, under the presence of thermal gradient, moisture accumulation on warmer regions of materials was significant depending on the duration of the test.
Kumaran (1989)		•	Vapor Permeability	ΔT: 20.1˚C - 40.6˚C	Fiber Glass Insulation	The test results revealed an increase of vapor flux at higher temperature differences.
Galbraith and McLean (1990)	•	•	Vapor Permeability	10˚C - +25˚C	Plasterboard, Polystyrene, Plywood, Wood and Brick	No dependency of permeability on temperature was stated.
Douglas et al. (1992)		•	Vapor Permeability	Isothermal condition: at 23˚C Non-isothermal condition: 18˚C and 29˚C.	Regular, Fire-resistant, Water-resistant, and Pre-decorated wallboard	They observed high and low (near zero) water vapor transport rate with the presence of only vapor pressure gradient or only temperature gradient, respectively. However, the moisture flux increased when the two gradients were applied together.
Burch et al. (1993)	•	•	Vapor Permeability	7˚C and 24˚C	Wood-based, Gypsum and Foam core sheathing	Analyzing the cup measurements, they stated that although temperature considerably affected the diffusivity, it insignificantly influenced the permeability.
Galbraith et al. (1998)	•	•	Vapor Permeability	Isothermal condition at temperatures of 20˚C and 42˚C.	Particle board, Polystyrene. Plasterboard and insulation under a	A substantive evidence of a measurable thermal diffusion flux was observed only under non-isothermal condition with temperature gradient.

				Temperature gradient between 23˚C and 15˚C	temperature gradient.	
Gibson (2000)	•	•	Vapor Permeability	-15˚C - +50˚C	Polymer membrane and Membrane/Textile Laminates	The results exhibited an exponential increase in water vapor flux by the increase in temperature. However, it was concluded that vapor transport property of all polymer membranes was influenced significantly by moisture content rather than temperature.
Galbraith et al. (2000b)	•	•	Vapor Permeability	10˚C - 30˚C	Plywood, Fiberboard	The effects of temperature on permeability was more considerable at relative humidities above 60% while it is negligible in low humidities. For example, with increasing temperature from 10˚C to 30˚C, at relative humidity near 100%, the permeability increased 51% and 29% for plywood and fiberboard, respectively.
Galbraith et al. (2000a)	•	•	Vapor Permeability	10˚C - 30˚C	Plasterboard, Phenolic Foam Insulation, Plywood and Medium Density Fiberboard	They concluded except the two wood-based materials which had a significant temperature effect in the liquid flow regime, for other materials the impact of temperature was negligible.
(Jooss and Reinhardt, 2002)	•	•	Water Permeability and vapor diffusivity	20˚C, 50˚C and 80˚C	Normal to High Strength Concrete, Polymer Modified and Self-compacting Concrete	By rising temperature from 20˚C to 50˚C, the permeability to water rose by 13-62% and diffusivity to vapor increased by 10-21%. Furthermore, due to raising temperature from 50˚C to 80˚C, the permeability and diffusivity increased by 3-35 % and 8-21 %, respectively.
Valovirta and Vinha (2004)	•	•	Vapor Permeability, Thermal Conductivity	–10˚C, +5˚C, and +23˚C	Wood-based, Insulation, Building paper	They concluded from the tests results that at the given relative humidities, the water vapor permeability increases with temperature
(Mukhopadhyaya et al., 2005)	•	•	Vapor Permeability	7˚C, 16˚C, 23˚C, 34˚C, and 43˚C	Fiberboard, gypsum board	The results indicated that higher temperature causes higher rate of water vapor transmission.

						The interaction between water vapor transmission rate and temperature can be described as exponential. However, they concluded that water vapor permeabilities of both materials were almost independent of temperature conditions.
(Vrána and Björk, 2008)			Water Vapor resistance (Vapor Permeability)	Temperature gradient, ΔT: 0˚C, 5˚C, 10˚C, 15˚C	Stone Wool Insulation	The result of the test indicated that the measured value of moisture resistance factor for mineral wool was aligned with values from the relevant standard (EN 12524). However, the moisture resistance factor declared by the manufacturer was 2.5 times higher than the measured value.
(Peuhkuri et al., 2008)	•	•	Vapor Permeability	Temperature gradient of 10K	Glass wool, Rock wool, Cellular Concrete, Cellulose, Flax, Perlite	They could not confirm the hypothesis that relative humidity being a driving force for non-isothermal moisture transport in the hygroscopic part while, there are some indications that the temperature gradient itself is driving the moisture from the warm side towards the cold side.
(Baker et al., 2009)	•	•	Vapor Permeability	Isothermal condition at temperatures of 10˚C and 30˚C. Temperature gradient of 7˚C - 10˚C	Masonry, Insulation, Wood-based, Plasterboard	The authors pointed out that although temperature gradient is a significant driving potential in moisture transfer through building materials in the non-isothermal tests, the vapor pressure gradient is more crucial driving potential. The results represented that except timber-based materials at higher humidities (RH>70%), the other types of materials showed no significant variation with temperature.
(Trabelsi et al., 2012)	•	•	Sorption Isotherm, Moisture Transfer (water vapor transmission)	Temperature gradient of 9.4˚C	Brick, Calcium Silicate	They found a consistent difference between the mass flow under isothermal and non-isothermal regimes which its ratio did not exceed 10% for all the tested materials.
(Pavlík et al., 2013)		•	Sorption/Desorption Isotherm, Vapor Permeability	10˚C - 50˚C	Cellular Concrete	The results revealed an increase in water vapor diffusion coefficient and water vapor diffusion permeability with increasing temperature. Additionally, sample thickness influences vapor transmission properties.

(Fořt et al., 2014)		•	Vapor Permeability, Sorption-Desorption Isotherm	10˚C - 50˚C	Calcium Silicate Thermal Insulation Board	The water vapor diffusion coefficient increased by the temperature.

2.5 Liquid Transport

Liquid transport through porous building materials is more ambiguous not as well defined as vapor transport; since the processes such as liquid diffusion, capillary flow, and surface flow are very difficult to separate, Figure 2-17 (Kumaran et al., 1994).

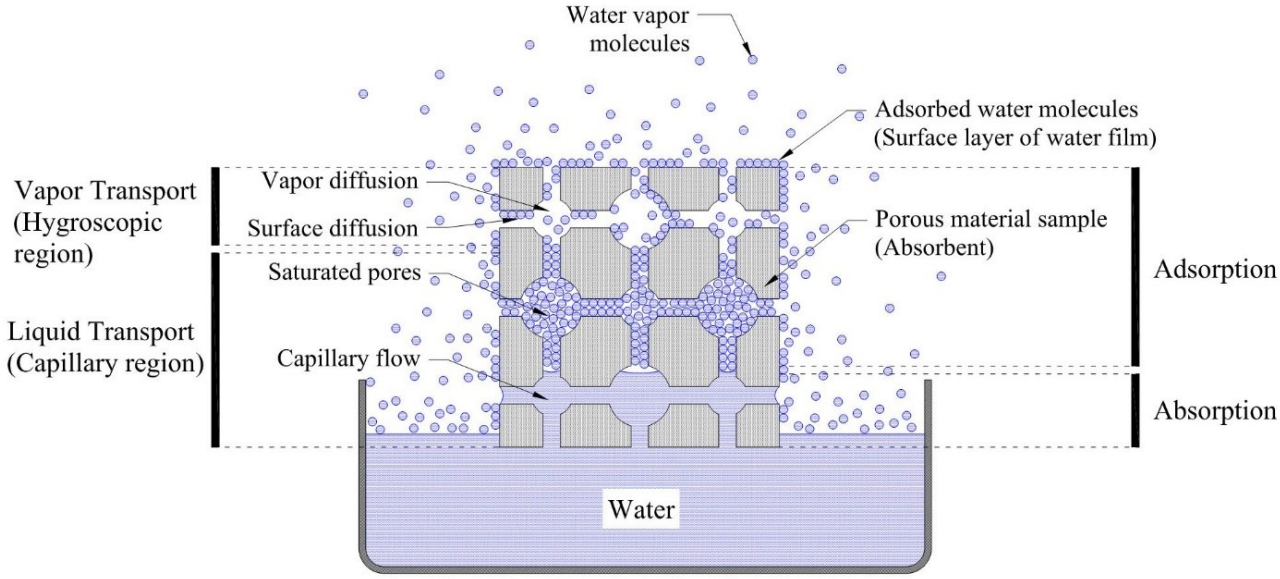

Figure 2-17. Schematic drawing of moisture transport process through porous building materials.

It is generally assumed that liquid transfer will begin when the moisture content of the material exceeds the critical level, w_{cr}, which is governed by the existence of a continuous liquid phase. Therefore, in studying the phenomena of liquid transport, it is necessary to dissect the sorption moisture region and the capillary water region, Figure 2-17 (Krus, 1996).

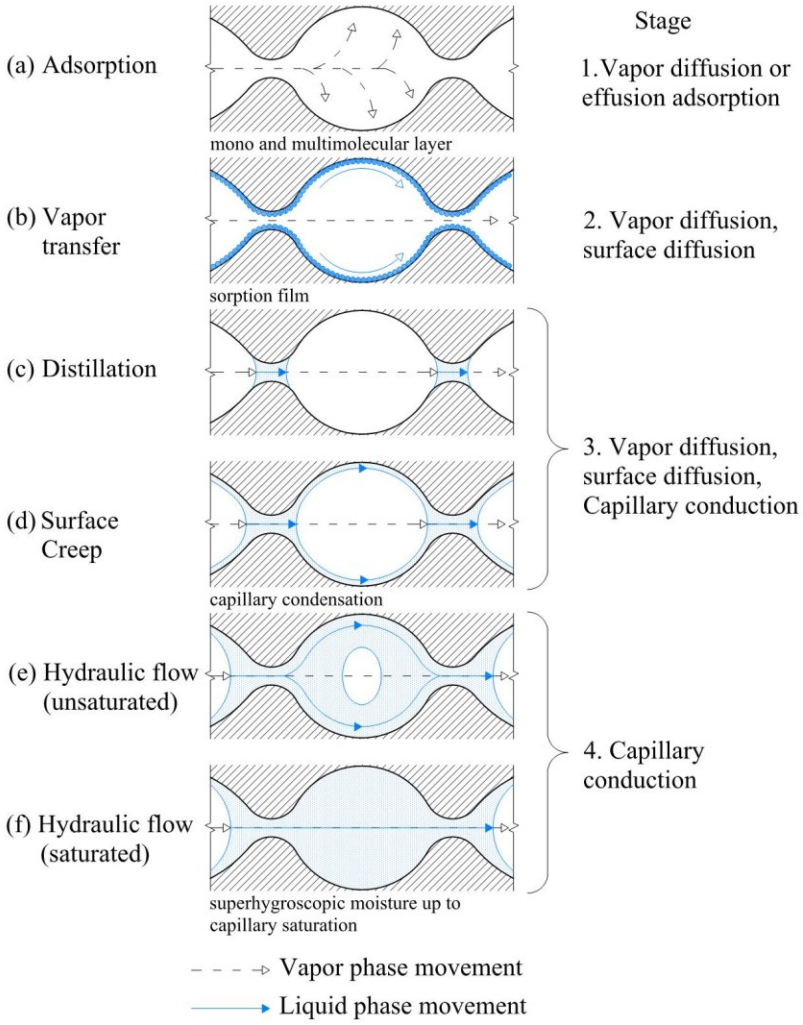

Figure 2-18. Different stages of liquid transport through material's pores (Rose, 1963).

Pure water vapor transfer will decrease from this point with increasing moisture content until vapor transfer will become zero at saturation. Another reason to differentiate vapor from liquid transport is that the migrate of soluble salts under thermal gradients takes place in the liquid phase (Peuhkuri, 2003a). According to Philip and De Vries (1957) the transport of pure liquid in saturated pores is liquid transfer and every other forms of combinations of liquid and vapor is considered as vapor transfer. Vapor and liquid transport are often distinguished with respect to the critical moisture content w_{cr}:

- $w < w_{cr}$ vapor transfer
- $w > w_{cr}$ continuous liquid phase / liquid transfer

Nevertheless, Krus (1996) believed that, in hygroscopic mineral building materials, surface diffusion can occur in the sorption moisture region as it has been depicted within stages two and three in Figure 2-18, while capillary suction takes place in the capillary water region.

According to the Brunauer-Emmett-Teller (BET) theory, when the molecules of water adsorb on the inner surfaces of the pores in an hygroscopic materials, they form an absorbed water film of which its thickness increases with rising relative humidity (Brunauer et al., 1938). If there exists a relative humidity gradient, a mass migration will occur in the water film on the pore wall due to the differences in the thickness of the layers of the water films, Figure 2-19.

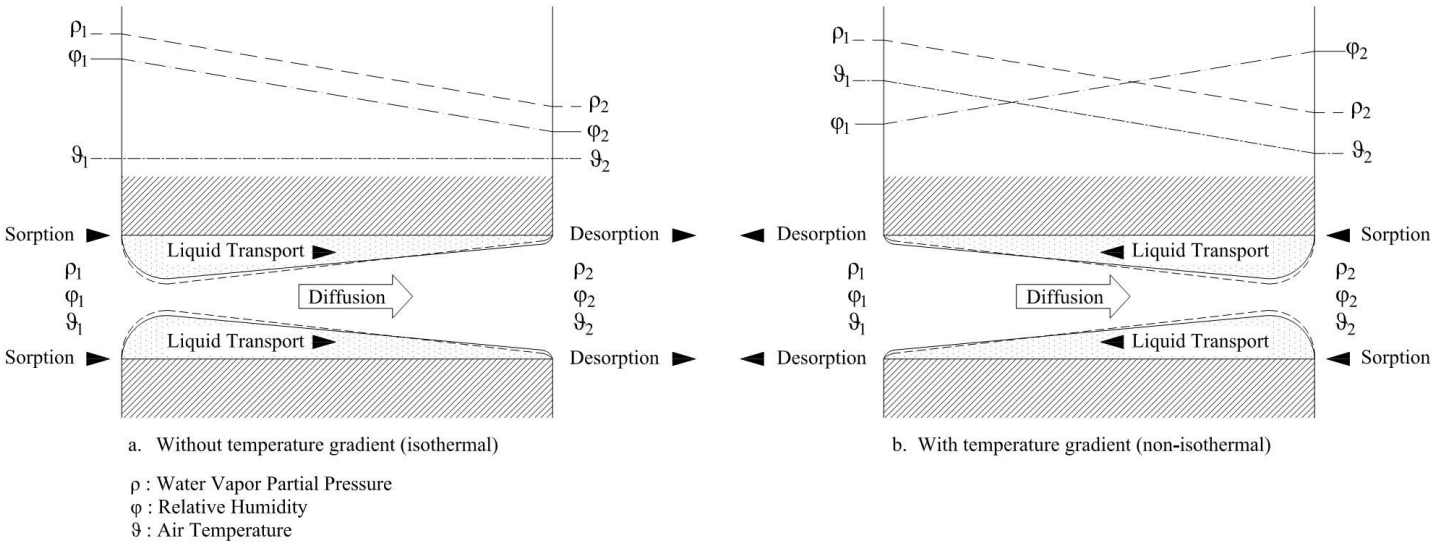

Figure 2-19. Model for superimposed liquid and vapor transport in the pore space of hygroscopic building materials under isothermal and non-isothermal conditions (Krus, 1996).

The dashed line shows the sorption moisture equilibrium in the sorbed phase that may obtained without liquid transport. The solid line indicates the dynamic equilibrium achieved due to liquid film transport. The sorption on the side with higher relative humidity and desorption on the side with lower relative humidity, permits a continuous liquid mass flow (Krus, 1996). As opposed to Philip and De Vries (1957), who considered surface diffusion to be negligible, Krus (1996) stated that the moisture transport through surface diffusion is significant in hygroscopic mineral building materials at relative humidities above 50% and it can even exceed sole vapor diffusion in some respects. The mass flow in surface diffusion can be proportional to the layer thickness gradient and thus to the concentration. It is assumed that surface diffusion increases with temperature rise

due to the decrease in viscosity of the liquid (Chang and Hutcheon, 1956; Galbraith and McLean, 1986; Krus, 1996).

2.5.1 **Isothermal Liquid Transport**

Liquid moisture transport can be expressed using Darcy's law:

$$g_l = -K \frac{\partial P_c}{\partial x} \qquad (2.25)$$

where g_l is the density of liquid flux [kg/m^2.s], K [kg/Pa.m.s] the hydraulic conductivity and P_c (Pa) is the suction pressure as driving force. It is practically impossible to determine the hydraulic conductivity experimentally (Peuhkuri, 2003b). Therefore, to determine the liquid moisture transport experimentally, Equation 2.26 is used, where the driving potential is replaced by moisture content w [kg/m^3]:

$$g_l = -D_{w,l} \frac{\partial w}{\partial x} \qquad (2.26)$$

where $D_{w,l}$ [m^2/s] is the coefficient for moisture content driven liquid diffusion. However, as discussed earlier, there exist some liquid transport due to the surface diffusion at moisture contents below critical capillary saturation level. Pedersen (1990) stated that the total moisture transport increases with increasing moisture content, as hydraulic conductivity in small pores is larger than water vapor permeability. Accordingly, Krus (1996) considered moisture content w, as a driving force for surface diffusion flow density $g_{s,l}$ [kg/(m^2.s)]:

$$g_{s,l} = -D_{s,l} \frac{\partial w}{\partial x} \qquad (2.27)$$

The mass flow in surface diffusion is considered to be proportional to the layer thickness gradient and consequently to the concentration gradient. Moreover, Künzel (1995) outlined relative humidity as a strong driving force in liquid conduction. Therefore, the diffusion coefficient $D_{w,l}$ [m^2/s] in equation 2.26 can also be given by the relative humidity as driving potential (Tariku, 2008):

$$g_l = -D_{\varphi,l} \frac{\partial \varphi}{\partial x} \qquad (2.28)$$

where $D_{\varphi,l}$ [kg/ (m.s)] is the coefficient for relative humidity driven liquid conduction and φ is the relative humidity (-). In the capillary region (RH > 98%), it is difficult to measure the RH

experimentally. Tariku (2008) explained that combining equations (2.26) and (2.28) establishes a relationship between moisture conduction coefficient D_φ and moisture diffusivity D_w:

$$D_{w,l}\frac{\partial w}{\partial \mathrm{x}} = D_{\varphi,l}\frac{\partial \varphi}{\partial \mathrm{x}} \qquad \xrightarrow{yields} D_\varphi = D_w \,.\frac{\partial w}{\partial \varphi} \tag{2.29}$$

where $\frac{\partial w}{\partial \varphi} = \Theta$ is the sorption capacity (slope of sorption-moisture retention curve).

This relation is given as equation 2.30 which yields the liquid conduction coefficient, D_ϕ, and liquid conductivity, D_l, from measurable quantities of moisture capacity, vapor permeability and moisture diffusivity:

$$D_\varphi = D_w.\Theta = \left(\delta_v \hat{P} + D_l \frac{\rho_w R}{M}\frac{T}{\varphi}\right) \qquad \xrightarrow{yields} D_l = \frac{M}{\rho_w R}.\frac{\varphi}{T}\left(D_w.\Theta - \delta_v \hat{P}\right) \tag{2.30}$$

Where $\hat{P}$ is the saturation vapor pressure, δ_v is vapor permeability, R is the universal gas constant (8.314 J/mol), M is the molecular weight of water molecule (0.01806 kg/mol).

Furthermore, it has been proposed that an average liquid diffusivity can also be determined by using the water absorption coefficients together with capillary saturation moisture content (de Wit and van Schindel, 1993; Krus and Künzel, 1993). Accordingly, Kumaran (1999) explained how those two factors together can define the moisture transport characteristic and the redistribution of moisture in materials while used the equation (2.31) to derive information on an average moisture diffusivity for building products:

$$D_w \approx \left(\frac{A_w}{w_c}\right)^2 \tag{2.31}$$

Where D_w is liquid diffusivity, A_w is the water absorption coefficient and w_c is the saturated volumetric moisture content of the material. Subsequently, if the profile of the advancing moisture front is considered (Krus and Künzel, 1993), the equation 2.31 can be modified as:

$$D_w = \frac{\pi}{4}\left(\frac{A_w}{w_c}\right)^2 \tag{2.32}$$

Derived from de Wit and van Schindel (1993), Kumaran (1999) presented an exponential equation to calculate D_w as a function of volumetric moisture content, w, as following:

$$D_w = \left(\frac{A_w}{w_c}\right)^2 \frac{b^2}{2b-1}\exp b\left(\frac{w}{w_c} - 1\right) \tag{2.33}$$

where $5 < b < 10$. Accordingly, Kumaran compared the moisture diffusivities of spruce calculated by equations 2.31, 2.32 and 2.33 with the result from a sophisticated gamma-ray method. He found a coherence between the values calculated from equations 2.31 and 2.32 and the measured results from the gamma-ray method. However, it was noted that the values from the equation 2.33 were harmonized with experimental results only at higher moisture content range. Furthermore, Mukhopadhyaya et al. (2002b) successfully derived the average liquid diffusivity D_w from water absorption coefficient A_w for eastern white pine, red clay brick and concrete by using equation 2.32.

However, Vejmelková et al. (2009) highlighted that the accuracy of moisture diffusivity results which are obtained based on manually operated water absorption test may be questionable. Particularly for fast water absorbing materials. They measured the water absorption coefficient and capillary moisture content for three building materials: high-performance concrete (HPC), hydrophilic mineral wool and autoclaved aerated concrete (AAC). Those material were selected due to the difference in the speed of water transport inside the materials. By analyzing the empirical results, Vejmelková et al. (2009) observed that the capillary moisture content for all material samples which derived from the second stage of the absorption test is very low considering the open porosity of the tested materials. For example, the capillary moisture content for mineral wool was 310 kg/m^3, which gave w_{cap}/w_{sat} =0.333. This is a very low value compare to its open porosity value of 93%. They explained that mineral wool is a fast water absorber which may lead to water loss and time delay during the weighing procedure.

2.5.2 **Non-Isothermal Liquid Transport**

When materials are exposed to a temperature gradient, the following mechanisms will impact liquid transport:

- The viscosity of a liquid reduces with rising temperatures (Pedersen, 1990) which yield increasing liquid transport. However, this impact is lower than the effect of increasing moisture content (Galbraith et al., 2000a).
- The Soret effect includes the transfer of liquid water along a temperature gradient from warm to cold (Peuhkuri, 2003a).

- There is a possibility for surface diffusion driven by the relative humidity and/or moisture content gradient, which is often against the temperature gradient (Krus, 1996).

Liquid flux due to a temperature gradient, which is called Soret effect or thermal diffusion, can be expressed as $g_{T,l}$ [kg/(m^2. s)]:

$$g_{T,l} = -D_{T,l}\frac{\partial \mathrm{T}}{\partial \mathrm{x}} \qquad (2.34)$$

where $D_{T,l}$ [kg/(K.m.s)] is the non-isothermal liquid transport coefficient. (Luikov, 1966) operated with a Soret coefficient, i.e. the ratio of thermal diffusivity D_T and moisture diffusivity D_w. Surface diffusion can also be considered as non-isothermal transport, since the relative humidity is a function of temperature (Peuhkuri, 2003a). According to Philip and De Vries (1957), the governing equation for liquid flux under non-isothermal conditions is:

$$g_l = -D_{w,l}\frac{\partial_w}{\partial \mathrm{x}} - D_{T,l}\frac{\partial \mathrm{T}}{\partial \mathrm{x}} \qquad (2.35)$$

2.5.3 **Combined Transport Forms**

The migration of pure water vapor at very low relative humidities, or liquid migration in a saturated material, occurs only for a very limited set of conditions. Often, diverse combinations of moisture transport forms exist within pores of material. Peuhkuri (2003a) called such combined transport as 'total moisture transport'. The total moisture flux g is not necessarily driven by just one potential, but according to Peuhkuri (2003a)is a linear combination of them and can be delineated as:

$$g = \sum -coefficient \times \nabla\,(Driving\ Force) \qquad (2.36)$$

The moisture permeability coefficients for different driving forces are dissimilar. As a result of thermodynamics, the number of driving forces is identical to the number of contributed flows. For instance, in coupled heat and moisture transport, only 2 forces are considered as required for a model. It is assumed that there is no distinction between vapor and liquid moisture transport while the air flux, the convective moisture transfer and transport due to gravitational forces are ignored (Peuhkuri, 2003a).

Although temperature which is commonly accepted as the reference driving force for heat transfer, moisture transport is linked to various arrays of driving forces such as moisture content and temperature, suction and vapor pressure, relative humidity and vapor pressure, suction and

temperature and so on (Hens, 1996). Nevertheless, the discourse is still ongoing regarding selecting appropriate potentials and how to apply them in modeling heat and moisture transfer. For instance, Peuhkuri (2003a) investigated driving forces which are continuously active on the material boundaries, including: temperature (T), relative humidity (φ) and various pressures (p, P_c) and concentration of water vapor ρ_v.

2.5.4 **Liquid Diffusivity Measurement Techniques**

Several advanced methods have been developed as transient non-destructive measurement techniques for analyzing the unsaturated flow and determining of the moisture diffusivity of porous building materials. The well-known methods are the nuclear magnetic resonance (NMR) and x-ray (Pel et al., 1995; Descamps, 1997; Brocken, 1998; Roels et al., 2004b). However, there are several other techniques such as the Gamma-ray attenuation which developed and used at National Research Council of Canada (NRC) (Kumaran and Bomberg, 1985), the positron emission tomography (Hoff et al., 1996), capacitance method (Voutilainen, 2005), and neutron radiography (Pražák et al., 1990; Pel et al., 1993). Plagge et al. (1996) applied time domain reflectometry (TDR) technique to building materials which is originally used for soil sciences. Likewise, in order to analyze the moisture transport in porous building materials, microfocus X-ray radiography has been evolved by Roels et al. (2003b) from well-known medical technique. The latter two techniques are instances which are transferred from other sciences into building physics. Description pertinent to those different techniques can be found in (Roels et al., 2003a; Roels et al., 2004b).

2.5.5 **Water Absorption Coefficient**

According to Hall (1977) the water absorption through a porous material is divided into three one directional configurations:

(a) horizontal flow, in which the gravitational forces can be neglected, but absorption is affected by hydrostatic pressure;

(b) vertically-downwards flow (infiltration), in which capillary and gravity impacted flows are in the same direction; and

(c) vertically-upwards flow (capillary rise), in which the gravity and capillary potentials are against each other.

These three configurations are inseparable in measuring the absorption rate of most of building materials, since the capillary potential is dominant (Hall, 1989). Therefore, because of its easy process and simplicity, the capillary rise technique is typically selected.

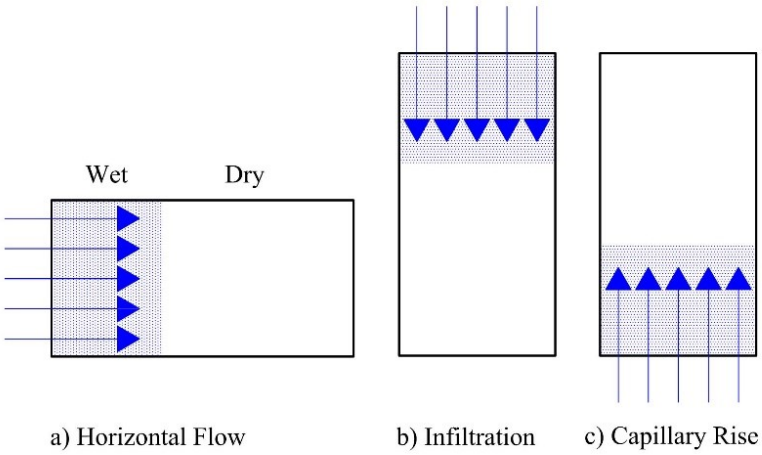

Figure 2-20. Different configurations of one-dimensional water absorption into a porous material (Hall, 1989).

The water absorption coefficient is the property of building materials which quantifies the water enters the materials due to absorption while its surface contacts the liquid water. This property is derived from the linear relation between the change of the amount of water entry across the unit area of the surface and the corresponding change in time expressed as the square root. From this experiment, the water absorption coefficient and the capillary moisture content can be derived. In the early part of an absorption process, this relation remains constant and that constant value is determined as the water absorption coefficient.

2.5.6 **Measurement Methods**

In literature, water absorption experiments are mainly given in the context of moisture profiles in materials. The water absorption or water uptake experiment measures the liquid water transport property of a material at given direction. The standard test methods (EN.ISO.15148, 2002; ASTM-C1794, 2015) can be applied in the determination of the water absorption coefficient by partial immersion, Figure 2-21.

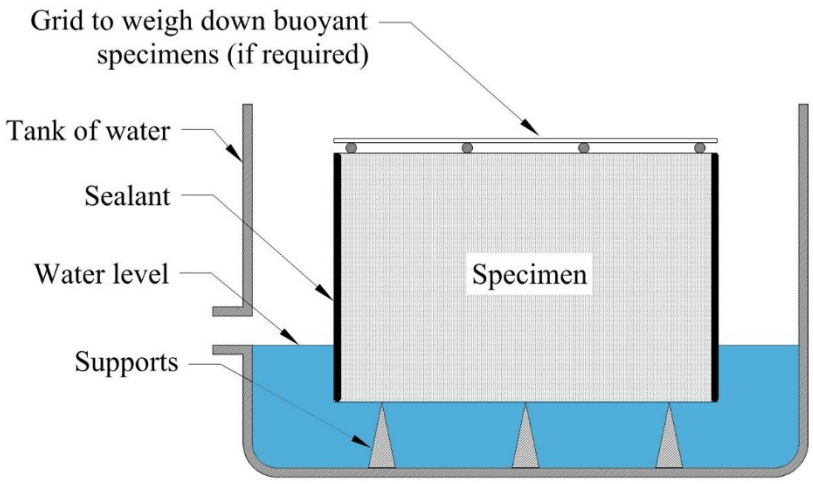

Figure 2-21. Example of appropriate testing apparatus (EN.ISO.15148, 2002; ASTM-C1794, 2015).

After preconditioning at normal laboratory conditions (between 18˚C and 28˚C, 40% to 60% relative humidity), the specimen is immersed (5 ± 2 mm) into water with one major surface. To provide one-dimensional transport, the lateral sides of the specimen have to be sealed. The increase in mass as a result of moisture absorption is recorded at time intervals defined according to a log scale during the first 24 h period and after that every 24 h. This has to be repeated several times to obtain a number of measurement points forming a characteristic water absorption versus time curve. According to the standards, when that relation is not verified, only the values registered at 4 h are used (EN.ISO.15148, 2002; ASTM-C1794, 2015). Usually, for many building materials the plot of the mass of water versus the square root of time during the initial part of the absorption process, is a straight line (Kumaran et al., 1994). The slope of the line divided by the area of the surface in contact with water is the water absorption coefficient A_w in [$kg/(m^2\sqrt{s})$] (Kumaran, 1999) which can be written as:

$$A_w = \left(\frac{m_t - m_i}{A\sqrt{t}}\right) \qquad (2.37)$$

Where m_t (kg) is weight of the specimen after time t (s), m_i (kg) initial mass of the specimen, and A (m^2) liquid contact area of the specimen. The experiment in general is briefly summarized, among others by (Mukhopadhyaya et al., 2002b; Bomberg et al., 2005) where Mukhopadhyaya also investigated the influence of water temperature on the absorption coefficient.

Besides the typical procedures of standards specification, Scheffler (2007) outlined a number of factors to be considered with more care:

- duration of the whole experiment and amount of data points collected during measurement,
- sealing of the upper side to prevent evaporation /moisture absorption due to boundary conditions,
- dipping / water contact at the bottom surface of the specimen

The duration is seen as the most crucial part of the experiment. Since the time of which the moisture front requires to reach the top of the specimen is dependent on both, the transport properties of the material and the height of the specimen. Therefore, the material behavior should be taken as the criterion when to stop the experiment. For homogeneous and isotropic materials, in general, a free water uptake experiment can be split into two distinct phases (Roels et al., 2004a). During the first phase, the position of the waterfront slowly approaches the top surface of the sample. Water absorption is governed by capillary and viscous forces. During the second phase, the waterfront has reached the upper side of the sample and any further increase of the moisture content can be due to the dissolution and relieve of the entrapped air in water which typically proceeds very slowly (Plagge et al., 2007). The capillary moisture content w_{cap} is usually taken as the moisture content of the specimen at the end of the transition from the first to the second phase or as the moisture content at the end of the experiment (Plagge et al., 2007). However, on the contrary, as explained earlier, Vejmelková et al. (2009) pointed out that the value of the capillary moisture content which is obtained from the free water uptake experiment is appeared to be very low.

The single coefficient, as A_w is only useful for a rough approximation. Therefore, for interpreting the hygric transport functions, especially with regard to the calibration of material performance, the whole water absorption curve is considered (Scheffler, 2007). To overcome this problem, some research measures the mass increase continuously using an automatic balance delivering the whole curve. Thus, the duration of the experiment can be adjusted exactly to the material behavior by evaluating the recorded data. Moreover, by using this method, the water absorption behavior of building materials which do not follow the ideal square root of time course, can be observed and determined (Plagge et al., Unpublished).

In order to analyze the experiment by numerical simulation, it is important to precisely know the boundary conditions. As the moisture storage function is normally defined only in the capillary pressure range, i.e. for suction pressures, but not for overpressures, it is recommended to perform the experiment under conditions where no overpressure is applied. Ideally, a zero-pressure condition is considered, which means that the bottom surface of the specimen is equal to the water surface and neither a small water column is hanging nor a small overpressure due to the dipping is applied. However, achieving such conditions is rather difficult. Thus, as Scheffler (2007) discussed, a small hanging water column at the bottom surface is to be preferred.

There are several different studies in the literature in which the impact of different factors on water absorption of materials has been investigated.

Focused on wood fiber direction, Candanedo and Derome (2005) studied the water uptake and moisture diffusivity characteristics in a softwood through comparing an experimental result with numerical simulations. Water absorption coefficient (WAC) test was carried out with a similar experimental procedure to the study of (Mukhopadhyaya et al., 2002b) under the laboratory environment condition. However, different wood grain orientation was examined while the water temperature was maintained at 20˚C through the tests. The experimental results indicated that the water absorption coefficient in longitudinal wood fiber direction was significantly higher than other directions while the water absorption flow in radial direction was the lowest value with a slight difference from the tangential direction. The measured results for WAC were used to calculate the average liquid water diffusivity based on the developed equation from Krus and Künzel (1993). Eventually, the experimental results were compared to the results of numerical 3D transient simulations which authors developed based on (Roels, 2000; Bird et al., 2002). Although their model did not consider the complex internal structure of wood and the relation between the moisture transfer path and the wood grain orientations, a good agreement was observed between the results particularly for long period of water absorption.

2.5.7 **Temperature Dependency**

Water absorption coefficient is a property that can be used directly to evaluate wind-driven rain penetration through the surface of exterior cladding materials in a building envelope (Mukhopadhyaya et al., 2002b). The results of numerical simulation represent that the variation of the liquid diffusivity and therefore, the water absorption coefficient of exterior cladding materials

can significantly impact the building envelope response to the moisture (Mukhopadhyaya et al., 2002a). Thus, it appears to be important for building scientists to study the water absorption coefficient of a building materials under different temperature regimes.

Hedlin (1977) simulated the roof with insulation on protected membrane in laboratory condition in order to study the moisture movement and absorption of several foam plastic insulation subjected to temperature and moisture gradients. He examined a closed cell (Extruded polystyrene) as well as an open cell (Phenolic foam) insulation materials under different temperature gradients of 0˚C, 2.8˚C, 11˚C and 22˚C in the presence of free water. His results indicated that:

1. The rate of gaining moisture increased by applying vapor pressure gradient. Then it decreased as the moisture content increased and eventually stopped absorbing moisture once the moisture content reached 50 to 60%.
2. The rate of moisture absorption was low at lower temperatures.

Gummerson et al. (1980) studied the sorptivity of a clay brick for four organic liquids and water at several temperatures between 5˚C and 36˚C. Based on the measurements at different temperatures, they pointed out a linear relationship between sorptivity of clay brick and temperature. They explained that the capillary absorption in a porous solid is influenced by the properties of the liquid and the microstructure of the solid and therefore, it depends on surface tension and viscosity of the liquid.

Reinhardt and Jooss (1998) examined the temperature dependency of water absorption property in concrete, high performance concrete and a French brick at temperatures of 20˚C, 50˚C and 80˚C. The Capillary absorption test was carried out according to the standard: DIN 52617, “Determination of the water absorption coefficient of building materials”. Their results indicated a linear increase in water absorption coefficient of all materials with rising temperature.

Mukhopadhyaya et al. (2002b) investigated the water absorption characteristics of three common building materials including eastern white pine, red clay brick and concrete at the four temperature levels between 3˚C and 35˚C. They set up an experiment based on the partial immersion method from the European standard CEN/TC 89/WG10 N70 (1994) thermal performance of buildings and building components called determination of water absorption coefficient. The test was performed for each material at 3˚C, 12˚C, 21˚C and 35˚C. Based on their experiment they concluded that

eastern white pine has the most visible and consists change in liquid moisture transport property with the variation of temperature. Conversely, temperature variation has virtually no effect on the average liquid diffusivity of concrete, which has the highest density and liquid diffusivity. They also suggested that materials with lower water absorption coefficient or liquid diffusivity values could be more susceptible to the effect of surface temperature variation, in contract to materials with high water absorption coefficients, which are less or not at all susceptible to the impact of temperature variation.

Karagiannis et al. (2016) investigated the influence of temperature on the capillary water absorption coefficient in different clay bricks, stones, and natural hydraulic lime mortars. They carried out the experiment according to Italian Normal 11/85 and at three different temperatures: 20˚C, 25˚C and 30˚C while the relative humidity was constant at 45±5% during all tests. They concluded that water absorption coefficient increases with the increase in temperature with a linear relationship. Additionally, brick showed the higher absorption coefficient among other materials in their study with a clear and straightforward two stages of cumulative mass of capillary water uptake curve versus time. Mortar composites showed some irregularities in their curve shape which authors believed that it can be associated with their different microstructure. Moreover, by comparing the empirical results with the estimated values through the equations suggested by other researchers, they found that the current models are not capable of predicting absorption coefficient adequately for all cases (also see (Feng et al., 2017)). It was highlighted by the authors that the capillary water absorption coefficient is reliant on both hygric transport properties and the intrinsic properties of each building materials.

Feng and Janssen (2016) investigated the hygroscopic properties of three building materials: autoclaved aerated concrete (AAC), calcium silicate board (CS), and ceramic brick (CB) under the temperatures: 11.2˚C, 22.5˚C and 38˚C. Based on the results from water absorption experiment, they concluded that the impact of temperature on capillary moisture content was negligible. However, a direct relationship was observed between the capillary water absorption coefficient and temperature. Similar to Gummerson et al. (1980), Feng and Janssen (2016) emphasized the significance of the characteristics of water and microstructure of the material when they are exposed to temperature variation. They pointed out that with increasing temperature

from 11.2˚C to 38˚C the surface tension and the viscosity of water decrease by 5.55% and 46.4%, respectively.

Guizzardi et al. (2016) made an effort to produce a dataset of water uptake in clay brick at different temperature and compared them with the results obtained from two numerical simulations in order to evaluate their effectiveness in considering liquid viscosity and density as temperature dependents. The experiments were carried out according to a modified system for electrical conductivity measurement which detects the position of the water front in the material at six different temperature: 5˚C, 15˚C, 25˚C, 35˚C, 45˚C and 55˚C. Their experimental results showed a clear impact of increasing temperature on enhancing the speed of capillary water travel through the clay brick which was more noticeable in temperatures above 15˚C.

Later in another research, Karagiannis et al. (2019) studied the effects of various environmental conditions on the capillary water uptake in different types of clay bricks, stones and mortars. Additional to the temperature changes (15˚C, 30˚C and 40˚C), they exposed the experiments to various air velocities (1,3 and 5 m/s) and relative humidities (20%, 35% and 50%). They concluded that although, increasing the temperature increases the rate of water uptake for all material samples, rising the air velocity and relative humidity decreased the rate of capillary uptake in all tested materials.

The full list of the literature reviewed along with the factors influences the water vapor permeability are tabulated in the following table.

Table 2-7. Published Literature in Temperature Dependency of Water Absorption Coefficient.

Article	Theoretical	Experimental	Properties	Temperature range	Materials	Remarks
Hedlin (1977)		•	Water absorption	Temperature gradients ΔT: 0˚C, 2.8˚C, 11˚C and 22˚C	Extruded polystyrene (closed cell), Phenolic foam (open cell)	The rate of gaining moisture increased by applying vapor pressure gradient. Then it decreased as the moisture content increased and eventually stopped absorbing moisture once the moisture content reached 50 to 60%. The rate of moisture absorption was low at lower temperatures.
Gummerson et al. (1980)	•	•	Water sorptivity	5˚C - 36˚C	Clay brick	they pointed out a linear relationship between sorptivity of clay brick and temperature. They explained that the capillary absorption in a porous solid is influenced by the properties of the liquid and the microstructure of the solid and therefore, it depends on surface tension and viscosity of the liquid.
(Reinhardt and Jooss, 1998)		•	Water Absorption Coefficient	20˚C, 50˚C and 80˚C	9 kinds of concrete	Their results indicated a linear increase in water absorption coefficient of all materials with rising temperature.
Mukhopadhyaya et al. (2002b)		•	Water absorption coefficient	3˚C, 12˚C, 21˚C and 35˚C	Eastern white pine, Red clay brick and Concrete	They pointed out that materials with lower water absorption coefficient or liquid diffusivity values could be more susceptible to the effect of surface temperature variation, in contract to materials with high water absorption coefficients, which are less or not at all susceptible to the impact of temperature variation.
(Karagiannis et al., 2016)	•	•	Water Absorption Coefficient	20˚C, 25˚C and 30˚C	Stones, clay bricks and natural hydraulic	They concluded that water absorption coefficient increases with the increase in temperature with a linear relationship

					lime mortars	They found that the current numerical models are not capable of predicting absorption coefficient adequately for all cases. The capillary water absorption coefficient is reliant on both hygric transport properties and the intrinsic properties of each building materials.
Feng and Janssen (2016)	•	•	Water Absorption Coefficient	11.2˚C, 22.5˚C and 38˚C	Autoclaved aerated concrete, calcium silicate board, and ceramic brick	a direct relationship was observed between the capillary water absorption coefficient and temperature. They emphasized the significance of the characteristics of water and microstructure of the material when they are exposed to temperature variation.
Guizzardi et al. (2016)	•	•	Capillary water uptake	5˚C, 15˚C, 25˚C, 35˚C, 45˚C and 55˚C	Clay brick	Their experimental results showed a clear impact of increasing temperature on enhancing the speed of capillary water travel through the clay brick which was more noticeable in temperatures above 15˚C.
Karagiannis et al. (2019)	•	•	Water Absorption Coefficient	15˚C, 30˚C and 40˚C	Clay brick, stone and mortar	They concluded that although, increasing the temperature increases the rate of water uptake for several building materials, rising the air velocity and relative humidity decreased the rate of capillary uptake in all tested materials.

3 Problem Statement

Climate conditions significantly change the properties of materials. Physical properties of building materials should always be measured at conditions that prevail in real life conditions. Due to significant changes in climate conditions as well as the geographical locations of different buildings, the exterior material layers of the building envelope components are exposed to cold or hot temperature (seasonal temperature changes) and solar radiation gain and long-wave radiation exchanges with the surrounding environment. It is known that building envelopes in North America are exposed to an extreme temperature regime, ranging from +50˚C to -50˚C (Environment-Canada, 2015; NRC, 2015). Local temperature may influence the heat and moisture transport characteristics of building materials (Mukhopadhyaya et al., 2005). Quite naturally it is to be expected that temperature variations have direct or indirect effects on the material properties. According to the literature review, some of the properties are more sensitive to temperature changes, such as thermal conductivity, vapor permeability, vapor diffusivity, and sorption/desorption isotherms (Chahal, 1965; Galbraith et al., 2000a; Budaiwi et al., 2002; Mukhopadhyaya et al., 2002b; Valovirta and Vinha, 2004; Karamanos et al., 2008; Ochs et al., 2008; Delgado et al., 2012; Jerman and Černý, 2012; Pavlík and Černý, 2012; Trabelsi et al., 2012; Vololonirina et al., 2014). However, often, changes of temperature are accompanied with changes in moisture content and moisture transmission. Regardless of the nature of materials, higher moisture content increases thermal conductivity of porous materials, (Karamanos et al., 2008; Jerman and Černý, 2012). The water vapor diffusion coefficient of materials is also temperature dependent (Mills, 1985; Kumaran, 1987; Kumaran et al., 2003; Pavlík and Černý, 2012). These impacts are significant when considering modeling of building physical behavior with simulation tools. In other word, it is impossible to get full benefits of those tools without correct material data. The influence of temperature on material properties must be determined to allow practicing building physicists and engineers to evaluate realistic moisture movement inside and across the building envelope appropriately and more accurately.

Material properties values measured at standard laboratory conditions are not necessarily valid in extreme conditions. According to published literature, almost all of the standard testing instructions are accomplished within a limited range of temperature and relative humidity, e.g. 21˚C to 23˚C and 50% to 75% RH. Consequently, these limited conditions would limit the outputs of such experiments. Unfortunately, these conditions make material properties less valuable in

simulating real-life climate conditions. For instance, the effective thermal conductivity of insulation material in service can be higher by a factor of 4 to10 compare to manufacturer or DIN specifications, which are given for 10˚C (Ochs et al., 2008). Considering the material properties dependence on local temperature conditions, it is important to better evaluate the hygrothermal performance of building envelope components that are exposed to real environmental conditions.

Furthermore, experimental testing under outside extreme climate condition is challenging. All tests standards and devices are designed for conducting tests under normal conditions and are not appropriate for performing under different conditions. However, a few researchers have attempted to create the specific devices such as megacup (Peuhkuri et al., 2008), specific climate chambers (Delgado et al., 2012) in order to determine materials' characteristics in reaction to ranges of climate conditions. Due to high uncertainties and rare/singular values of properties at high temperature, specific and detailed experiments are required to obtain more valuable measured data.

There is no coherent summary of material properties data available for extreme temperatures. Among the published literature, there are some studies that evaluated specific material properties which are temperature dependent. But they are still not complete and comprehensive, or they are for decades ago. The old data for material properties are outdated due to the constant evolution in manufacturing process and technologies. In recent years, the impact of mass transfer on heat transfer has attracted the attention of researchers and industry because of the potential energy savings associated with latent flux, which is not included in the current regulations and thermal tools (Vololonirina et al., 2014). Moreover, building materials are developing regularly due to the advances in manufacturing technology, therefore, a constant updating of information of their hygrothermal properties is necessary (Kumaran et al., 2003).

4 Research Approach

4.1 Research Objectives

The aim of this experimental research project is to investigate the potential effects of relative humidity and temperature ranges on hygrothermal properties of building materials. Accordingly, the objectives of this thesis project are to:

- Acquire rigorous knowledge and fundamental understanding of material behaviors through review of published literature and laboratory measurements.
- Modify and optimize extensions to current standard test methods to conduct experiments at different conditions than the standards recommend currently.
- Characterize the hygrothermal properties of materials at different temperatures and relative humidities and develop a temperature dependent material properties database.
- Compare the obtained results with current available data. Where it is needed, update the hygrothermal properties of selected materials as their properties may have evolved gradually due to change in manufacturing process or raw materials.

4.2 Methodology

In order to achieve the scopes of this project, the following approach was developed:

1. Review previous research and knowledge about measuring hygrothermal properties of building materials under different conditions.

2. Investigate the validity of proposed new test methods to measure the material properties under ranges of temperatures. Since the test conditions in this research was expanded to include hot and cold temperature, I had to modify the available test method or develop new test procedures to measure the properties of the tested materials.

3. The proposed new test methods were calibrated according to the available standards and their validity were confirmed considering the scattered but similar published literature.

4. Determine a set of different types of common building materials within the wall assembly which are either exposed or are affected by outside extreme temperature.

5. Determine the material properties which change with respect to variation in temperature and relative humidity.

6. Systematically select building materials from different categories considering the length of the test periods. For example, roof membranes are excluded due to the long time of their measurement tests.

7. Propose test conditions other than the normal routine defined in standard test methods in order to create realistic conditions representing range of exposure end.

8. Set up relevant test standards and perform the experiments under normal and proposed conditions.

5 Description of Building Materials

Building envelope components are typically composed of several layers of materials, including the exterior cladding, water resistive barriers (e.g., building paper/housewrap), sheathing, studs with insulation and interior gypsum board Figure 5-1.

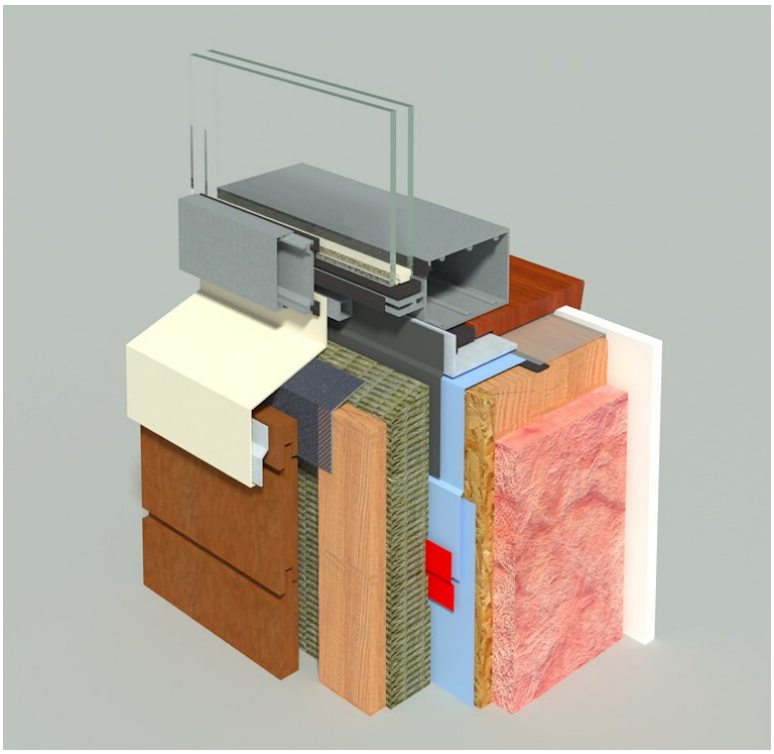

Figure 5-1. Schematic 3D Section of an exterior wall

The building materials which are considered in this thesis research, are usually used as exterior layers in building envelope in North America including cladding, sheathing, framing, insulation and building wrap. An attempt has been made to have at least one material from each relevant

building material group. The number of materials considered in the study is limited by the length of time to complete the various testing and the planned project period.

The building materials are classified in different categories and general information on each product is given as following:

5.1 Claddings

1. **Clay Brick:** The selected brick is manufactured in Canada and is identified as Inca red brick. Test specimens were prepared from a production batch of ECON shape bricks with dimension of 89 × 89 × 292 mm. The bricks are reddish brown in color and referred to as "common extruded clay brick." The bulk density is (2080 ± 27) kg/m^3.
2. **Fiber Cement Board:** The tested product is known commercially as James Hardie's HardiePanel. The samples were cut from 4 × 8 ft (1219.2 mm × 2438.4 mm) boards with cray smooth texture at a nominal thickness of 5/16 ± 0.04 in (7.9 mm). The bulk density is (1348 ± 12) kg/m^3.
3. **Stucco:** This product was made as three-coat stucco using commercially available mixtures for base coat and finish coat stucco. Scratch and Brown Base Coat Stucco are a Portland cement-based stucco which is polymer modified, used for construction and repair of stucco walls. It complies with ASTM C 926 requirements for cement-based mortars. Finish Coat Stucco is also a Portland cement-based stucco finishing plaster which is polymer modified designed for use as the color and texture coat over the base coat. The white finishing is used in this project. The bulk density is (2400 ± 40) kg/m^3.
4. **Western Red Cedar:** The specimens used for various tests are taken from 1.5 in. (nominal thickness) × 12 in. × 8 ft (38.1 × 304.8 × 2438.4 mm) planks. The bulk density is (380 ± 4) kg/m^3. The product is commonly available at Dick's Lumber and Building Supplies store.

5.2 Weather Resistive Barriers (WRB)

5. **60 Minute Paper (**Extra-Heavy building paper). The test samples are taken from 4ft. × 120 ft. (1219.2 mm × 36576 mm) roll known as HAL-TEX 60" and manufactured by HAL Industries Inc. Its component is asphalt-saturated paper. Mass per area is approximately

310.5 g/m^2. The product thickness is (0.34 ± 0.01) mm and compliant with standard CAN 2-51.32M77. This product is commonly available at RONA stores.

6. **Spun Bonded Polyolefin (Tyvek):** This Tyvek home wrap is manufactured by DuPond company. The samples of this study were cut from a 3 ft. × 100 ft. (914.4 mm × 30480 mm) roll. Mass per area is approximately 65 g/m^2. The thickness is from 0.14 to 0.15 mm.

5.3 Wall Sheathing Boards

7. **Plywood**: This product is manufactured by West Fraser Timber Co. Ltd. in Canada and is available as 4 × 8 ft (1219.2 mm × 2438.4 mm) boards at a nominal thickness of ½ in (12.7 mm). It is certified as conforming to Canadian plywood manufacturing standard CSA O121, Spruce Plywood. The bulk density is (461 ± 8) kg/m^3.

8. **Oriented Strand Board (OSB**): The sample are taken from 4 × 8 ft (1219.2 mm × 2438.4 mm) boards at a nominal thickness of 7/16 in (11.12 mm). The product is known as Trubord sheathing manufactured by Norbord Inc which is commonly available at Homedepot stores. The bulk density is (620 ± 12) kg/m^3.

9. **Densglass Gold Gypsum Sheathing:** This product is manufacture by Georgia-Pacific Gypsum LLC. The samples are cut from a 4 × 8 ft (1219.2 mm × 2438.4 mm) boards at a nominal thickness of 5/8 in (15.8 mm) Fireguard type X sheathing. It qualifies for fire-resistant construction when tested in accordance with ASTM E 119. A glass fiber mat layer is adhered to one side surface. Labels on the product say the following: Manufactured to conform with ASTM C 1177. The bulk density is (755± 7) kg/m^3.

5.4 Wood Studs

10. **Spruce:** The specimens used for various tests are taken from 1.5 in. (nominal thickness) × 12 in. × 8 ft (38.1 × 304.8 × 2438.4 mm) planks. The bulk density is (469 ± 1.7) kg/m^3. The product is commonly available at Dick's Lumber and Building Supplies store.

11. **Douglas Fir:** The specimens used for various tests are taken from 1.5 in. (nominal thickness) × 12 in. × 8 ft (38.1 × 304.8 × 2438.4 mm) planks. The bulk density is (572 ± 9) kg/m^3. The product is provided from Dick's Lumber and Building Supplies store as Weyerhaeuser kiln-dried Douglas-fir lumber.

5.5 Insulations

Materials which the thermal conductivity is below or between 0.006 and 0.10 W/m.K are generally regarded as insulation materials (Koru, 2016). Thermal insulation materials are usually produced as either open-cell or closed-cell materials. Materials such as fiberglass, mineral wool, glass wool, rock wool, wood wool and ceramic fiber are considered as open-cell. While materials such as expanded polystyrene (EPS), extruded polystyrene (XPS), expanded nitrile rubber (ENR), polyurethane (PUR), polyethylene (PE) and ethylene vinyl acetate (EVA) are examples of some closed-cell insulation materials. In this research we have selected various types of insulating materials in order to cover and investigate wide range of available insulation materials.

12. **Cellulose Fiber Insulation**: All test specimens are prepared from samples blown from a commercial cellulose insulation product according to the manufacturer's directions. The product is prepared from recycled newspaper as the starting material using a dry fiberization technology. The fire retardant and fungicide are also applied as dry raw materials during the production process. The applied density of the insulation is 79.24 kg/m^3.

13. **Expanded Polystyrene Insulation (EPS)**: The specimens are taken from 4 × 8 ft (1219.2 mm × 2438.4 mm) boards of Envirosheet EPS at a nominal thickness of 1 in (25.4 mm). This insulation product is produced by Amvic Building System. This product meets ASTM C578 and CAN/ULC-S701-01 requirements for Type 2 expanded polystyrene insulation. The bulk density is (21.6 ± 0.1) kg/m^3. This product was provided from Lowe's store.

14. **Extruded Polystyrene Insulation (XPS)**: The specimens are taken from 4 × 8 ft (1219.2 mm × 2438.4 mm) boards of Owens Corning- FOAMULAR C-200 XPS at a nominal thickness of 1 in (25.4 mm). The product meets CAN-ULC-S701: 13431-L and is type 3. The bulk density is (26.6 ± 0.15) kg/m^3. This product was provided from Home Depot store.

15. **Open Cell Sprayed Polyurethane**: Test specimens are taken from a 1 × 2 ft (304.8 x 609.6 mm) sample prepared using a commercial product commonly known as half-pound SPF sprayed 1-2 in (25.4-50.8 mm). thick. The bulk density is 6.5 to 8.5 kg/m^3.

16. **Polyisocyanurate Insulated Sheathing Board**: Test specimens are taken from a 4 ft × 8 ft board (1219.2 mm × 2438.4 mm) at a nominal thickness of 1 in. which is manufactured by IKO Industries Ltd. Except for thermal conductivity measurement, the facers were removed from both major surfaces before specimens were prepared for the other tests. The product meets ASTM C1289 and CAN-ULC-S704: 13188-L and is type 1-class 1. The bulk density is (27.5 ± 0.16) kg/m^3. This product was provided from Lowe's store.

17. **Mineral Fiber (Stone Wool):** Test specimens are taken from a 2 ft × 4 ft (609.6 mm × 1219.2 mm) ComfortBoard 80 with nominal R6.0 at a nominal thickness of 1.5 in (38.1 mm). manufactured by ROCKWOOL Group. ComfortBoard IS is classified as "non-combustible" as determined by ASTM E136 and CAN4-S114. The product meets ASTM C612 and CAN/ULC S702 for mineral fiber thermal insulation for buildings and is Type 1 compliant. The bulk density is (128 ± 4) kg/m^3. This product was provided from Lowe's store.

6 Experimental Determination of Material Properties

Table 6-1 presents a list of materials studied in this project along with their hygrothermal properties measured in this project. Due to the different structures and compositions of building materials, for some products not all the hygrothermal properties could be measured according to the selected measurement methods.

Based on the literature review of material properties and their dependency on temperature, the material properties along with the pertinent experiments and proposed conditions listed in Table 6-2 are used to characterize the hygrothermal property of a material. Consequently, this thesis was focused on measurement and analysis of these properties. The planned test conditions include nine combinations of three temperature set points 3˚C, 21˚C and 45˚C and three relative humidities of 50%, 70% and 90%. The test procedures have been developed through evaluation of different sets of ISO and ASTM Standards as well as other published measurement techniques.

Table 6-1. Matrix showing selected materials and the properties which are proposed for measurement.

		1	2	3	4							5									6									7								
Materials		Dry Density	Porosity	Heat Capacity	Thermal Conductivity							Vapour Permeability									Sorption Isotherms									Water Absorption Coefficient								
	Symbol	Kg/ m^3	m^3/ m^3	J/(kgK)	w/(mK)							kg/(Pa.s.m)									kg/kg									kg/(m2√s)								
					Temperature							Temperature 3°C			Temperature 21°C			Temperature 45°C			Temperature 3°C			Temperature 21°C			Temperature 45°C			Temperature 3°C			Temperature 21°C			Temperature 45°C		
					5°C	10°C	21°C	24°C	35°C	50°C	60°C	50% RH	70% RH	90% RH	50% RH	70% RH	90% RH	50% RH	70% RH	90% RH	50% RH	70% RH	90% RH	50% RH	70% RH	90% RH	50% RH	70% RH	90% RH	50% RH	70% RH	90% RH	50% RH	70% RH	90% RH	50% RH	70% RH	90% RH	50% RH	70% RH	90% RH
	Claddings																																					
1	Clay Brick	•	•									•	•	•	•	•	•	•	•	•	•	•	•	•	•	•	•	•	•	•	•	•	•	•	•	•	•	•
2	Fiber Cement Board	•	•	•	•	•	•	•	•	•	•	•	•	•	•	•	•	•	•	•	•	•	•	•	•	•	•	•	•	•	•	•	•	•	•	•	•	•
3	Stucco	•	•		•	•	•	•	•	•	•	•	•	•	•	•	•	•	•	•	•	•	•	•	•	•	•	•	•	•	•	•	•	•	•	•	•	•
4	Western Red Cedar	•	•		•	•	•	•	•	•	•	•	•	•	•	•	•	•	•	•	•	•	•	•	•	•	•	•	•	•	•	•	•	•	•	•	•	•
	Building Membranes																																					
5	Tyvek	•										•	•	•	•	•	•	•	•	•										•	•	•	•	•	•	•	•	•
6	60 min Paper	•										•	•	•	•	•	•	•	•	•	•	•	•	•	•	•	•	•	•	•	•	•	•	•	•	•	•	•
	Sheathing Boards																																					
7	OSB	•	•	•	•	•	•	•	•	•	•	•	•	•	•	•	•	•	•	•	•	•	•	•	•	•	•	•	•	•	•	•	•	•	•	•	•	•
8	Plywood	•	•	•	•	•	•	•	•	•	•	•	•	•	•	•	•	•	•	•	•	•	•	•	•	•	•	•	•	•	•	•	•	•	•	•	•	•
9	Densglass gold gypsum sheathing	•	•	•	•	•	•	•	•	•	•	•	•	•	•	•	•	•	•	•	•	•	•	•	•	•	•	•	•	•	•	•	•	•	•	•	•	•
	Wood Studs																																					
10	Spruce	•	•		•	•	•	•	•	•	•	•	•	•	•	•	•	•	•	•	•	•	•	•	•	•	•	•	•	•	•	•	•	•	•	•	•	•
11	Douglas Fir	•	•		•	•	•	•	•	•	•	•	•	•	•	•	•	•	•	•	•	•	•	•	•	•	•	•	•	•	•	•	•	•	•	•	•	•
	Insulations																																					
12	Cellulose Fibre	•	•	•	•	•	•	•	•	•	•	•	•	•	•	•	•	•	•	•	•	•	•	•	•	•				•	•	•	•	•	•	•	•	•
13	Expanded Polystyrene	•	•	•	•	•	•	•	•	•	•	•	•	•	•	•	•	•	•	•	•	•	•	•	•	•	•	•	•									
14	Extruded Polystyrene	•	•	•	•	•	•	•	•	•	•	•	•	•	•	•	•	•	•	•	•	•	•	•	•	•	•	•	•									
15	Open Cell Spray polyurethane	•	•		•	•	•	•	•	•	•	•	•	•	•	•	•				•	•	•	•	•	•	•	•	•	•	•	•	•	•	•	•	•	•
16	Polyisocyanurate	•	•	•	•	•	•	•	•	•	•	•	•	•	•	•	•	•	•	•	•	•	•	•	•	•	•	•	•									
17	Mineral Fiber	•	•	•	•	•	•	•	•	•	•	•	•	•	•	•	•	•	•	•	•	•	•	•	•	•	•	•	•	•	•	•	•	•	•	•	•	•

Table 6-2. A set of proposed properties and test methods under different indicated conditions.

Property	Test method	Temperature and relative humidity ranges
Dry Density	Dry weight measurement	Not applicable
Porosity	Fully saturation method	Not applicable
Thermal Conductivity	Heat flow meter	5˚C, 10˚C, 21˚C, 24˚C, 35˚C, 50˚C and 60˚C
Specific Heat Capacity	Heat flow meter	15°C, 17°C, 19°C, 21°C, 23°C, 25°C, 27°C, 29°C, 31°C and 41°C
Adsorption Isotherm	Adsorption measurement using climatic chamber	Temperature: 3˚C, 21˚C and 45˚C RH: 50%, 70% and 90%
Vapor Permeability	Cup methods and climatic chamber	Temperature: 3˚C, 21˚C and 45˚C RH: 50%, 70% and 90%
Water Absorption Coefficient	Water uptake experiment / Partial immersion	Temperature: 3˚C, 21˚C and 45˚C RH: 50%, 70% and 90%

As a part of a test protocol, three specimen replicas of each material were prepared for every property test identified in the table above. All experiments were performed at BCIT Building Science Centre of Excellence, Hygrothermal Property Measurement Laboratory (HPML).

Thickness and density were measured for all the building materials using caliper with the accuracy of 0.01 mm, Figure 6-1, and an electronic balance with the accuracy of ± 0.0001 g Figure 6-2, respectively. Depending on the specimen size, 4 to 10 measurement points were taken to determine the thickness of each specimen.

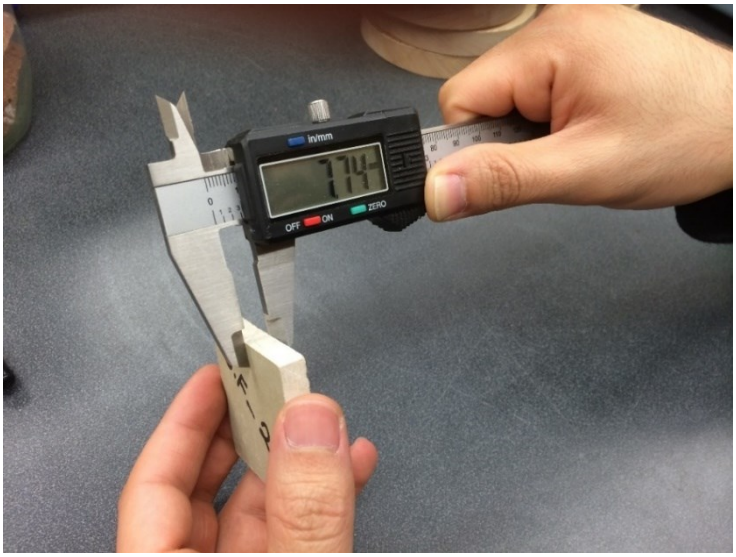

Figure 6-1. Caliper with the accuracy of 0.01 mm.

Figure 6-2. Electronic balance with the accuracy of ± 0.0001 g.

To measure the dry density, the specimens were dried in an Convective-drying oven Figure 6-3, at either 40°C, 72°C or 110°C depending on the type of materials.

Figure 6-3. Air drying oven.

It is widely accepted that the drying temperature and method have considerable impact on the results of the absorption isotherm (Wilkes and Karagiozis, 2004; Peuhkuri et al., 2005; Kumaran et al., 2006). All the test specimens were dried until the weight change for each specimen was less than 0.1% for five consecutive measurements in 24 hours time interval. There is a risk that some building materials change structure or dimension at high temperature and some materials experience chemical or physical alteration. Therefore, all test specimens were grouped in different categories. Densglass Gold Gypsum Board, XPS, EPS and Polyisocyanurate were dried in the oven

with 40°C, while wood-based materials were dried with 72°C oven. The other materials were dried at 110°C.

6.1 Thermal Conductivity and Specific Heat Capacity

This property was measured by the following standards:

- ASTM C518–10 *Standard Test Method for Steady-State Thermal Transmission Properties by Means of the Heat Flow Meter Apparatus* (ASTM-C518, 2010).
- ISO 8301:1991- Thermal insulation - Determination of steady-state thermal resistance and related properties - Heat flow meter apparatus (EN.ISO.8301:1991, 2014).
- ASTM-C1784-14 *Standard Test Method for Using a Heat Flow Meter Apparatus for Measuring Thermal Storage Properties of Phase Change Materials and Products* (ASTM-C1784-14, 2014)

6.1.1 Specimens Preparation and Test Conditions

A 300 × 300 mm specimen with a thickness ranging from 5 to 100 mm can be tested with the HFM apparatus. The test specimen should be the size as to cover both cold and hot plate surfaces, and the actual thickness to be applied in use or of sufficient thickness to give a true average representation of the material to be tested. Except Clay Brick and Building Papers, four samples of 300 × 300 mm from all tested building materials were cut preferably with maintaining the original thickness of materials in real application. During the period of this study, the selected samples were kept at normal lab conditions for an adequate period of time (at least six months) to satisfy the testing method instruction. Any small changes in testing conditions that was not observed by the operator, might yield significant deviations in measured results, depending on the nature of the tested material. The thermal conductivity of each of the selected samples was measured at five different mean temperatures: 5˚C, 10˚C, 21˚C, 24˚C, 35˚C, 50˚C and 60˚C.

In general, before testing the specimen some preparation was performed on samples. Surfaces of the material samples were prepared to ensure that they are parallel with and have uniform thermal

contact with the hot and cold plates. In some cases, it was necessary to smooth the specimen surfaces to achieve better plate-to-specimen contact. For example, in this study, both surfaces of sprayed foam and cellulose fiber insulation samples were rough and uneven, Figure 6-4. Therefore, two layers at both sides were cut considering maintaining enough thickness. Furthermore, a 5 mm thick soft foam was used on both rough surfaces of concrete samples to provide a better contact to the HFM plates. The solid woods samples had a small bending with the maximum depth of 4-5 mm at the middle of both surfaces. Therefore, thicker pads of 1/2-inch low density EPS was used at both sides during the test. The thermal resistance of both types pads was measured separately and considered in the final calculation of the thermal conductivity of the tested materials.

Figure 6-4. Sprayed foam insulation samples with rough and uneven surface.

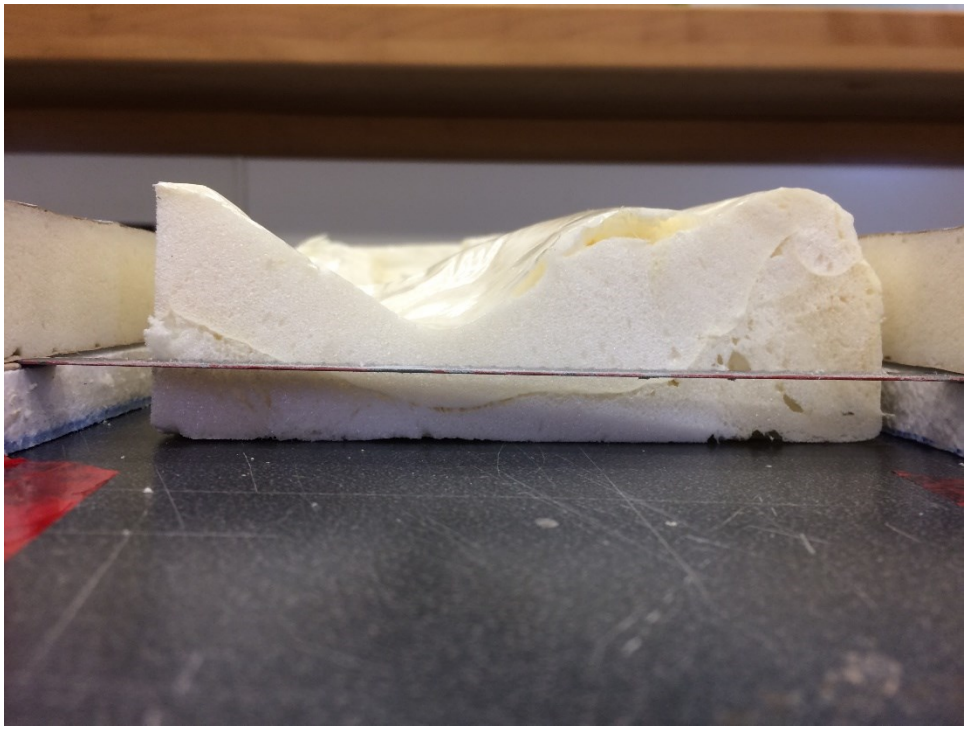

Figure 6-5. Rough and uneven surfaces were removed on the samples of sprayed foam insulation.

Furthermore, for materials' samples which were slightly smaller than the plates surfaces, all the surfaces exposed to the air were covered with insulation material (XPS) during the test in order to limit the edge heat losses on the measurement. Extreme environmental condition during the test might impact the thermal conductivity values. However, it has been found that the measured k values of building material are not considerably influenced by relative humidity until dew point is reached to the temperature of the cold side of the test specimen (Hansen et al., 2001). Material samples with the dimension of 600 mm × 600 mm were used for measuring specific heat capacity. The samples were prepared following the same procedure as for thermal conductivity measurement.

6.1.2 **Experimental Methods and Equipment**

6.1.2.1 Thermal conductivity

The thermal conductivities of building products were determined using the heat flow meter apparatus as shown in Figure 6-6, following the instruction described in ASTM standard C518-04.

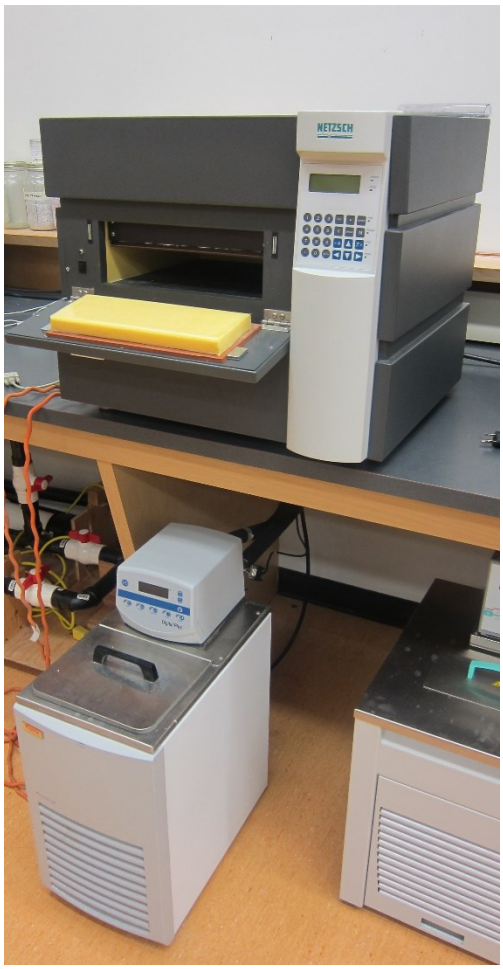

Figure 6-6. Heat Flow Meter Apparatus.

At BCIT Building Science Centre of Excellence the HFM Lambda 2000 apparatus with working thickness range between 6 and 100 mm was used to test thermal insulations. The heat flow meter apparatus establishes steady state one-dimensional heat flux through a test specimen between two 300 mm × 300 mm parallel plates at constant but different temperatures. The metering area is a thermopile with many copper-constantan junctions. The temperature control system is thermoelectric. Thermal conductivity is determined, upon achieving thermal equilibrium and establishing a uniform temperature gradient throughout the sample. The general principle of the heat flow meter instruments is based on one-dimensional equation for Fourier law in steady state (Yener et al., 2018):

$$q = -\lambda A \frac{dT}{dx} \qquad (6.1)$$

where

q = heat flux through the specimen (W/m^2),
$\lambda = k$ = thermal conductivity (W/mK),
A = the area through which the heat flows (m^2),
dT/dx = temperature gradient (K/m).

One or two heat flow transducers measured the heat flow across the specimen through the area of the transducer which is the same for all specimens (Lakatos and Kalmár, 2013b). The signal of a heat flow transducer is proportional to the heat flux through the transducer which is expressed in equation (6.2):

$$q = SV \qquad (6.2)$$

Where S (W/(m^{2}V) is the calibration factor pertinent to the voltage signal (V) of the heat flux transducer. Therefore, combining equations (6.1) and (6.2) established the relation between the thermal conductivity and heat flux transducer output:

$$\lambda = S\frac{V\Delta x}{\Delta T} \qquad (6.3)$$

This equation was used for calibrating of the HFM apparatus which is described further in this study.

The following characteristics related to temperature measurement was assessed (Bomberg et al., 1985):

- temperature uniformity - differences in temperatures measured over the surface of the plates,
- temperature stability with time, and
- repeatability of temperature measurements.

The standard deviation for each thermocouple recording indicates stability, while the range between minimum and maximum measured surface temperatures indicates temperature uniformity. The precision of temperature difference was calculated based on the measurement of temperature difference across the specimen. Bomberg et al. (1985) for example, outlined the characteristics of a reliable HFM apparatus as temperature uniformity better than ±0.15°C,

temperature stability better than ± 0.02°C, and repeatability precision (preferably with readings on DVM) of 1.0%.

Since, the heat flow meter apparatus is a comparative or secondary method of measurement, it requires to be calibrated to specimens of known thermal transmission properties which were tested using an absolute measurement method such as the guarded-hot-plate apparatus (Scott and Bell, 1994). To minimize errors, the apparatus should be calibrated with the Calibrated Transfer Specimen (CTS) or Standard Reference Material (SRM) to measure the response of the heat flow transducer at different temperatures.

Before testing the selected samples in this study, the measuring instrument (i.e., the Lambda 2000 heat flow meter) was calibrated using the Standard Reference Material (SRM) 1450c at various temperatures. The SRM 1450c was a 24.7 mm thick semi-rigid glass fiber board with the dimension of 300 × 300 mm and density of 165 kg/m^3. The calibration procedure was carried out according to ASTM-C518 (2010). The calibration factor was calculated using the following equation:

$$S = \frac{C.(T_h - T_c)}{(E_1 + E_2)} \qquad (6.4)$$

Where:

S = calibration coefficient of the heat flux transducer, $(W/m^2)/V$.

C = thermal conductance, $W/(m^2.K)$.

T_h = temperature of the hot plate surface, K.

T_c = temperature of the cold plate surface, K.

E_1 = heat flux transducer output of hot plate, V.

E_2 = heat flux transducer output of cold plate, V.

The equation (6.1) also can be written as:

$$S = \frac{\Delta T}{(E_1 + E_2)} \frac{1}{R} \qquad (6.5)$$

Where according to Newton et al. (1985) R is the thermal resistance measured on the GHP apparatus at the same thickness and mean temperature, with a known confidence interval. We obtained the certified value for thermal conductivity of SRM at 24°C from equation (2.11). The reference sample was tested 6 times at 24°C over an extended period to ensure accuracy and

repeatability. The thermal conductivity at 24°C was determined based on three configurations of the heat flux transducers' outputs as both, only upper and only lower. Accordingly, the calibration factor *S* was calculated. The results for standard deviation, mean error and repeatability for all three tests are tabulated in Table 6-3.

Table 6-3. The results of calibration of HFM apparatus with SRM 1450c based on heat flux transducer outputs.

Heat Flow Transducer	**Thickness (mm)**	**T_h (°C)**	**T_c (°C)**	**ΔT (°C)**	**Mean Temperature (T_m (°C))**	**Mean Thermal Conductivity (W/m.K)**	**St. Deviation of λon HFM (%)**	**Difference to the certified thermal**	**Mean Error**	**Repeatability**
Both	24.71	33.97	13.97	20	23.97	0.03382	1.9	0.4	0.0093	0.55
Upper	24.72	34.01	14.01	20	24.01	0.03365	1.9	1.02	0.0097	0.58
Lower	24.71	33.95	13.95	20	23.95	0.03360	1.9	0.79	0.0097	0.58

According to the measured thermal conductivities, the test based on both transducers output showed a better accuracy because its difference to the predicted certified value was 0.4 % compared to the tests with upper and lower transducer outputs of 1.02 % and 0.79 %, respectively. Therefore, the former test was considered for measuring the thermal conductivity values of the investigated building materials in this study. Then the calibration factor for each mean temperature was calculated accordingly, Table 6-4.

Table 6-4. The calculated calibration factors for all designated mean temperatures.

	Mean Temperature (°C)						
	5	10	21	24	35	50	60
Calibration Factor, S ($W/m^2.V$)	5870.15	5929.52	6045.28	6047.39	6152.41	6226.06	6281.7
St. Deviation	29.8	20.9	19.78	26	18.47	15.86	13.89

After determining the calibration factor, the thermal conductivity of tested materials was calculated using equation (6.6) by considering both transducers output (ASTM-C518, 2010):

$$\lambda = \mathrm{S}.(E_1 + E_2).\frac{L}{\Delta T} \qquad (6.6)$$

Where:

λ = thermal conductance, $W/(m^2.K)$.

S = calibration coefficient of the heat flux transducer, $(W/m^2)/V$.

E_1 = heat flux transducer output of hot plate, V.

E_2 = heat flux transducer output of cold plate, V.

ΔT = temperature difference between two plates surfaces, K.

L = thickness of the specimen, m.

6.1.2.2 Heat Capacity

The specific heat capacity of the tested materials was measured using the LaserComp Fox 600 HFM. The measurement method follows the American Standard ASTM-C1784-14 (2014) which is based on the principle of calculating the amount of absorbed heat by the specimen from the HFM outputs. Its working area range is 610 mm × 610 mm equipped with two built-in 254 mm × 254 mm transducer on both upper and lower plates and a maximum tested thickness of 203 mm. The HFM apparatus was calibrated using NIST SRM 1450b. It has an ability to measure the thermal conductivity of materials in the range between 0.005 to 0.35 W/m.K and accuracy and temperature control of ±1 % and ±0.01°C, respectively.

Figure 6-7. The LaserComp Fox 600 HFM in the material lab at BCIT center of excellence.

The FOX 600 uses WinTherm32 software for full PC control including setting experimental parameters and data handling. In order to calculate the volumetric specific heat capacity $C_p\rho$(J/m^3.K) of materials, the set points for both plates should be the same with step between the set points. In this study, the set points were selected as 15°C, 17°C, 19°C, 21°C, 23°C, 25°C, 27°C, 29°C, 31°C and 41°C with steps of 2°C and 10°C. The set points should be within the calibration's temperatures range provided by the 1450b NIST calibration file in the WinTherm32 software database which are from 5°C and 5°C up to 50°C and 50°C for both plates. The amount of time required at each temperature step varied depending on the size of the temperature step, the thermal diffusivity of the specimen, the material thickness and the amount of energy that was stored in tested materials over the temperature step. By selecting 2°C steps, it took 4-5h for each temperature set to reach the steady state of full thermal equilibrium. The control software calculated the total

heat H (J/m^2) which was absorbed within the material sample and the instrument's HFMs themselves using the conservation equation (6.7):

$$H_{total} = \sum_{i=0}^{N}\left[S_U\left(QU_i - QU_{equil}\right) + S_L(QL_i - QL_{equil})\right].\tau \qquad (6.7)$$

where

H_{total} = total heat energy per square meter (J/m^2),

S_U = transducers calibration factors for upper plate (W/m^2.μV),

S_L = transducers calibration factors for lower plate (W/m^2.μV),

QU_i = heat flux transducer (HFT) output for upper plate (μV),

QL_i = HFT output for lower plate (μV),

QU_{equil} = final equilibrium value of HFT output at upper plate (μV),

QL_{equil} = final equilibrium values of HFT output at lower plate (μV)

τ = time interval (s).

The heat absorbed by the two plates' transducers should be subtracted from the results. Heat capacity of the transducers $C_p`\rho`2\delta x`$ can be obtained from equation (6.8) (Tleoubaev and Brzezinski, 2007):

$$C_p\rho x + C_p`\rho'2\delta x` = H_{total}/\Delta T \qquad (6.8)$$

where

$C_p\rho$ = volumetric specific heat of the specimen (J/(m^{3}K) and ρ is density (kg/m^3),

x = thickness of the specimen (m),

$C_p`\rho`$ = volumetric specific heat of two plates' transducers (J/(m^{3}K),

$2\delta x`$ = thickness of two transducers (m),

ΔT = temperature change (K).

Then the correct volumetric specific heat capacity of the specimen which is temperature dependent is calculated by the equation (6.9):

$$C_p\rho = \left(\frac{H_{total}}{\Delta T} - C_p`\rho'2\delta x`\right)/x \qquad (6.9)$$

The control software of the HFM apparatus was pre-programmed to calculate H_{HFMs} (C_p`$\rho$`$2\delta x$`) using transducers heat capacity coefficients pre-determined by the manufacturer and automatically subtract it from H_{total} using the equation (6.10) in order to obtain $C_p\rho$ (LaserComp, 2007):

$$C_p\rho x = \left(\frac{H_{total}}{\Delta T} - H_{HFMs}\right)/x \qquad (6.10)$$

Measuring the thermal conductivity and volumetric heat capacity of the tested building materials, two other thermophysical properties including thermal diffusivity, a (m^2/s) and thermal effusivity, ε ($W.s^{½}/m^2K$) can be calculated using equation 6.11 and 6.12 (Tleoubaev et al., 2008):

$$a = \lambda/C_p\rho \qquad (6.11)$$

and

$$\varepsilon = \sqrt{\lambda.C_p\rho} \qquad (6.12)$$

While the thermal diffusivity characterizes the rate of heat transfer through the material from the hot side to the cold side, the thermal effusivity represent the material ability to exchange thermal energy with its surroundings.

6.2 Adsorption Isotherm

This property was measured by the following standards:

- ASTM C1498–04a (2010)e1 *Standard Test Method for Hygroscopic Sorption Isotherms of Building Materials* (ASTM-C1498−04a, 2011).
- ISO 12571- Hygrothermal performance of building materials and products-Determination of hygroscopic sorption properties(EN.ISO.12571, 2013).

As mentioned in Chapter 2, the moisture storage characteristics are presented in a different way in hygroscopic range and capillary range. In this project, ASTM C l498 was used for determination of sorption isotherms for building products in the hygroscopic range.

6.2.1 **Specimens Preparation and Test Conditions**

Prior to adsorption isotherm testing, each test specimen was dried to a constant mass. The test specimen was dried at an appropriate drying temperature based on the nature of the building materials. The drying temperatures for woods, stucco, gypsum sheathing and insulations were selected as 105°C, 80°C, 40°C and 50°C following the procedure described in (Kumaran et al., 2006). For example, the wood samples first dried at 95°C for several days to constant mass and then were kept at 105°C for 2 h. Additionally, in order to avoid chemical reaction of the epoxy agent in plywood and OSB, their samples were dried at 70°C. Furthermore, the mineral fiber specimens, were dried at 121°C for according to (ASTM-C1104/C1104M-13a, 2013) until two successive weighings agreed to within 0.2 % of the specimen weight in the last weighing. For each weighing process, the samples were taken out from the oven and placed immediately into an air sealed weighing container to cool down to the room temperature and using the balance. The drying process was continued until three successive daily weighings are within 0.1 % of the specimens' weight measured in the latest weighing. The average of the three last weights was recorded as a dry weight of the specimen.

According to (ASTM-C1498−04a, 2011; EN.ISO.12571, 2013) the test specimens for measuring the sorption isotherm should have a mass of at least 10 g and smaller material samples reduce the time to reach equilibrium with the environment. However, EN.ISO.12571 (2013) recommends that the area of specimens of materials with a dry density less than 300 kg/m^3 should be at least 100 mm × 100 mm. Therefore, for the sorption isotherms test of the materials in this study, 81 specimens, with the size of 50 mm × 50 mm, were used for each of the solid building product and 42 specimens with the size of 150 mm × 150 mm, were used for each of the insulating materials and the 60 min building paper. However, for achieving better and faster sorption results a grid of perpendicular cuts with 10 mm distance were made through one face of specimens of EPS, XPS and polyisocyanurate insulation, Figure 6-8. Applying cuts, allowed three-dimensional flow through multiple surfaces while the surface area also increased by a factor of 1.5. Before the test, all the specimens were oven dried as mentioned in Section 5. The test specimens in each category for each material were grouped into three batches to be tested in each temperature. The dried Specimens were stored in air sealed containers prior using for the sorption test.

Figure 6-8. A grid of cuts on one side of EPS samples for sorption test.

6.2.2 **Experimental Methods and Equipment**

In the standard test method ASTM C1498, the primary emphasis is on the adsorption (sorption) isotherm that describes the wetting process of the material from the oven-dry condition. Following the test method presented in the standard, the dried specimens were placed in the environment conditions of constant temperature and different relative humidities starting from 50 % to 70 % and then 90%RH. Typically, the test environment condition is achieved either in a desiccator containing a salt solution or in the climatic chamber. At BCIT Building Science Centre of Excellence, three temperature-humidity chambers were used to provide environment conditions as nine different combination of temperature and RH, Figure 6-9. They can maintain the temperature and relative humidity of the air inside at a constant level. The chamber recorded tolerances for the temperature and for the relative humidity in the nine conditions are presented in the Table 6-5. All nine conditions of the chambers are presented in Figure 6-10, Figure 6-11 and Figure 6-12. Those chambers gave very precise control of temperature and humidity levels.

Figure 6-9. Climate chambers at BCIT Building Science Centre of Excellence.

Table 6-5. Standard Deviations (SDs) for temperature and relative humidity in nine conditions at the three climate chambers.

Conditions	Temperature and Relative Humidity	SD
One	T = 3°C	0.13
	RH = 50%	0.8
Two	T = 3°C	0.14
	RH = 70%	1.09
Three	T = 3°C	0.16
	RH = 90%	0.9
Four	T = 21°C	0.19
	RH = 50%	1.05
Five	T = 21°C	0.15
	RH = 70%	0.93
Six	T = 21°C	0.15
	RH = 90%	0.42
Seven	T = 45°C	0.003
	RH = 50%	0.31
Eight	T = 45°C	0.02
	RH = 70%	0.5
Nine	T = 45°C	0.03
	RH = 90%	0.41

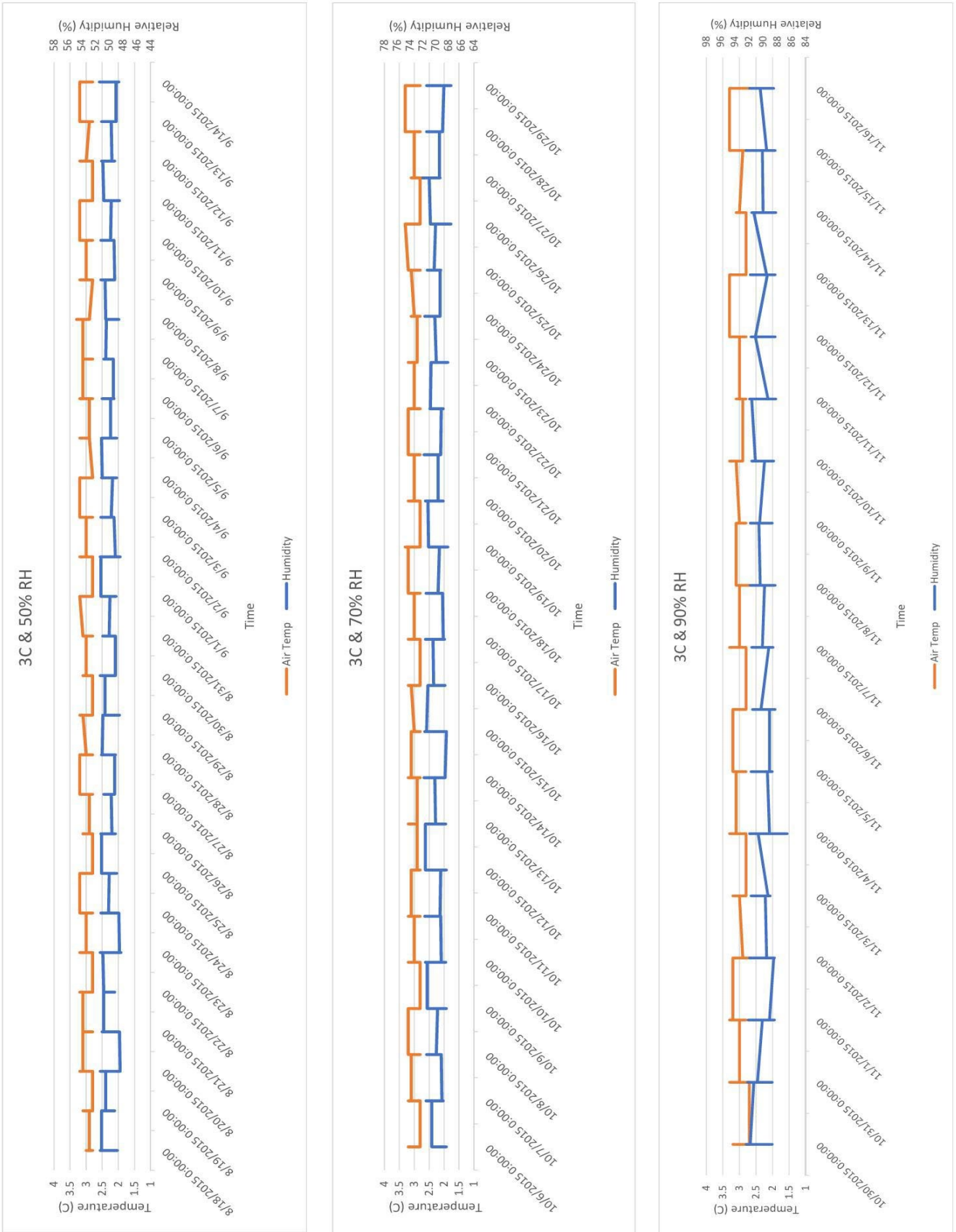

Figure 6-10. Three climate conditions in chamber one. Constant temperature: 3°C and three steps of relative humidities: 50%, 70% and 90%.

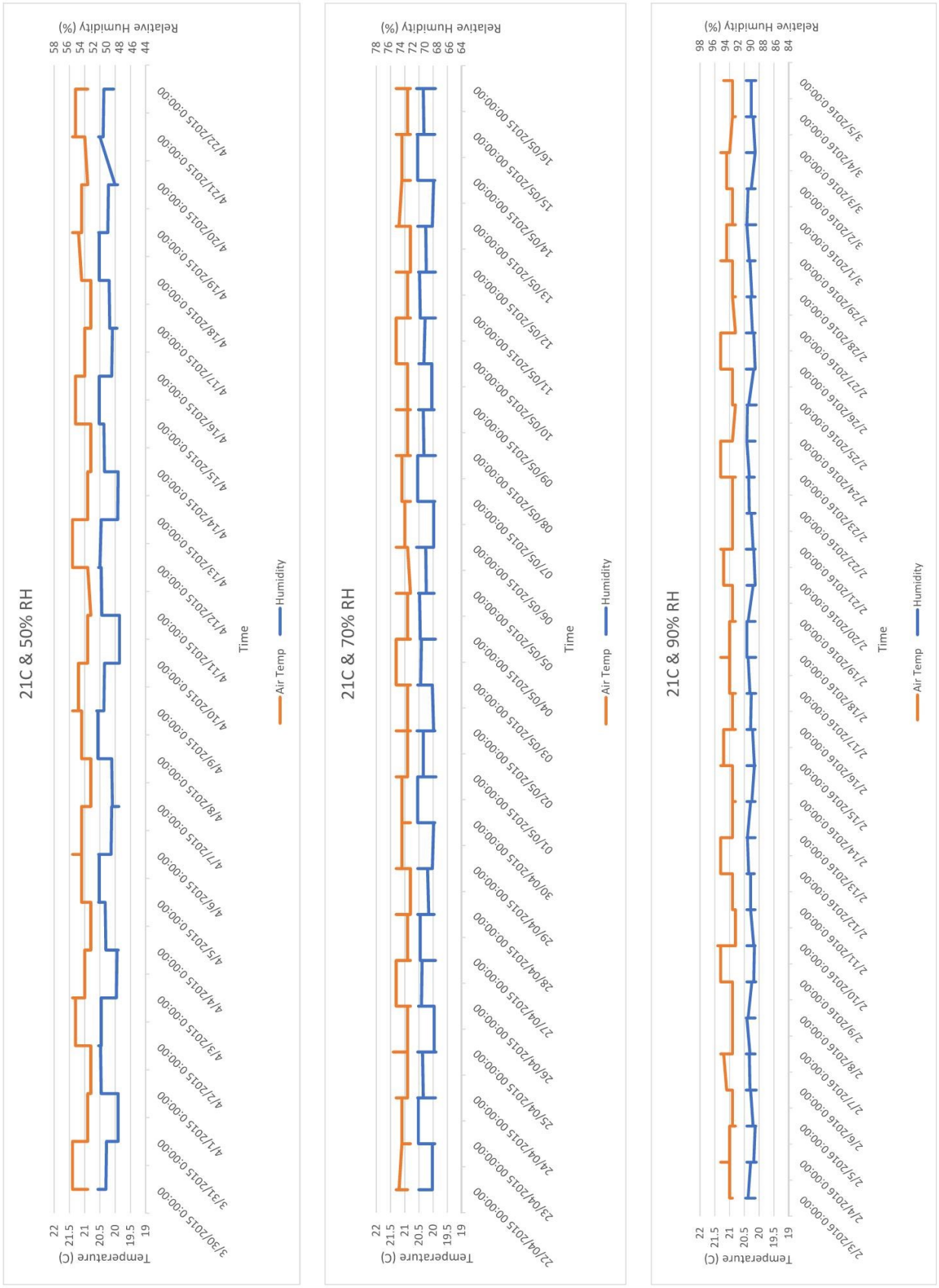

Figure 6-11. Three climate conditions in chamber two. Constant temperature: 21°C and three steps of relative humidities: 50%, 70% and 90%.

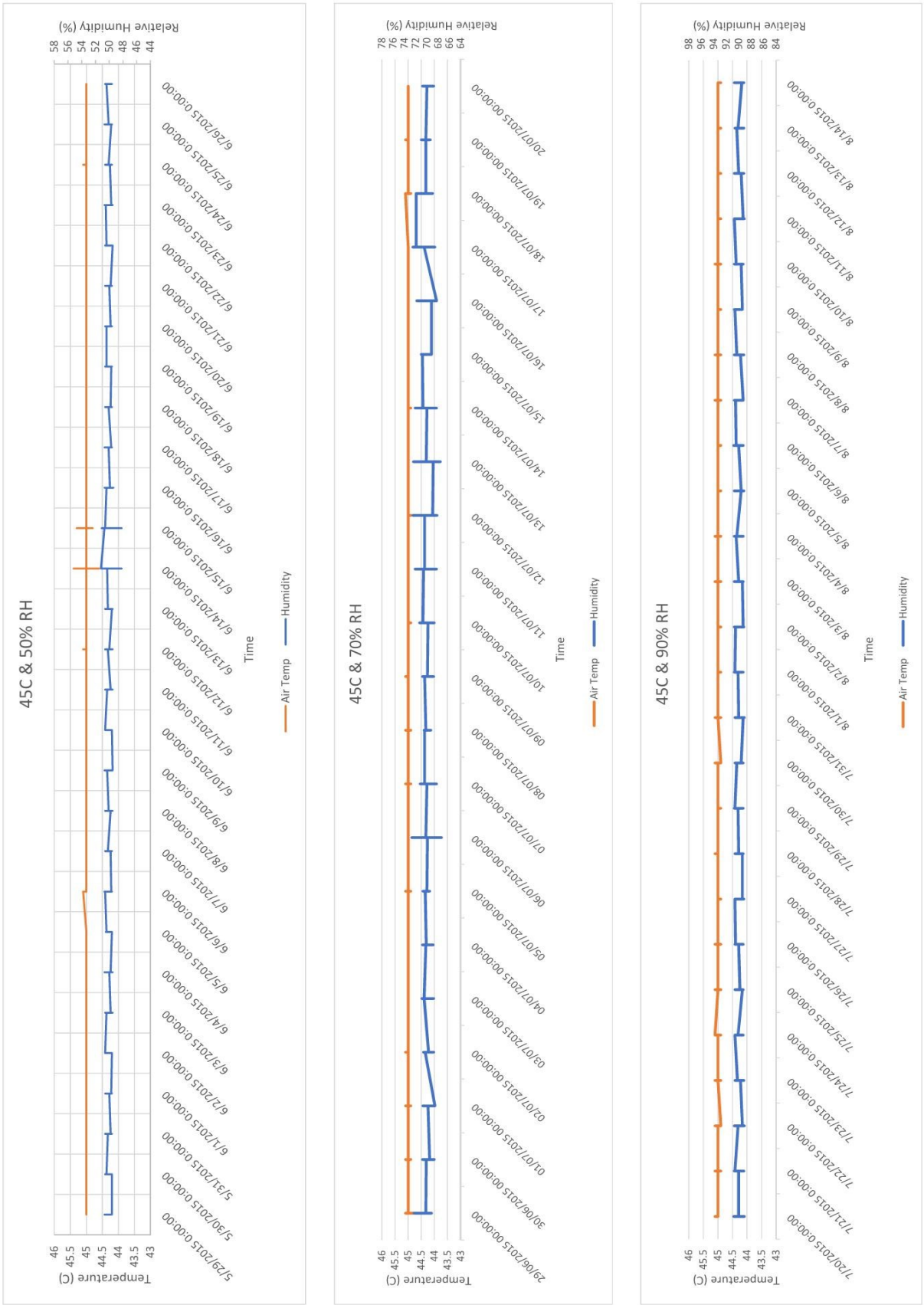

Figure 6-12. Three climate conditions in chamber three. Constant temperature: 45°C and three steps of relative humidities: 50%, 70% and 90%.

In order to eliminate mass gain or loss during the weighing process, extra precaution was taken, and each specimen was placed in an airtight glass container, Figure 6-13. Furthermore, the cellulose fiber samples were covered by a plastic mesh to prevent losing detached pieces of fibers due to the air circulation inside the chambers and during the weighing procedure, Figure 6-14. However, to expedite the process, the specimens were kept inside the open containers while exposed to designated condition of temperature and relative humidity within the climatic chambers, Figure 6-15.

Figure 6-13. The plywood specimens inside the airtight glass containers during the weighing process.

Figure 6-14. The cellulose fiber samples wrapped by a plastic mesh and kept in containers.

Figure 6-15. The OSB and plywood specimens remained in the open containers while exposed to the condition inside the climatic chambers.

Accordingly, for the larger material samples, Ziploc plastic bags were used in transit from the chamber to the weighing table. All weighing process on balance were carried out inside the plastic box to reduce impact of local airflow and ambient conditions on the measurement, Figure 6-16. The weights of specimens were determined by an electronic analytical balance with an accuracy of 0.00l g.

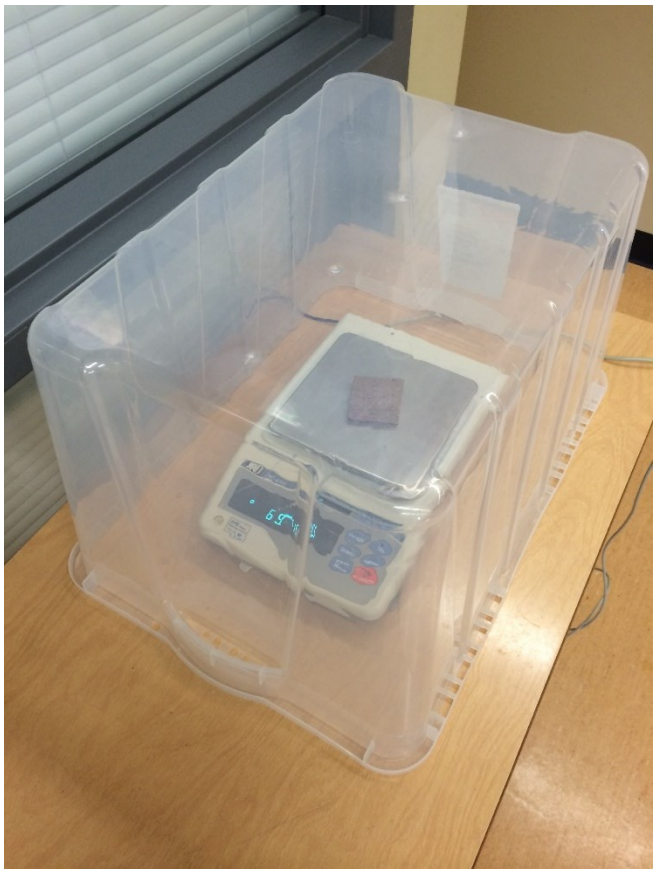

Figure 6-16. A clay brick sample on the balance inside a plastic box to reduce the impact of local airflow on measurement.

When the specimen reached the equilibrium moisture content (EMC) at each condition of relative humidity, then it was placed in the next environment condition with the next higher relative humidity step. The EMC in each material was reached when the change of mass between five consecutive weighing, with 24 h intervals, was less than 0.1% of the specimen mass. Then EMC at each condition was calculated as a difference between the constant mass at each RH and the dry weight of the specimen using the following equation:

$$u = \frac{m_w - m_d}{m_d} \qquad (6.13)$$

where

u = moisture content (kg/kg)

m_w = the mass of the specimen at equilibrium (kg),

m_d = the dry mass of the specimen (kg).

6.3 Capillary Saturation and Open Porosity

After completing the sorption isotherms tests, in order to calculate the porosity of the solid materials, specimens were finally immersed in water for eight days while there was at least 150 mm of water over the specimens, Figure 6-17. As described in ASTM-C1498−04a (2011), in practice, the moisture content measured for a specimen after three days of immersion in water under a reduced air pressure (less than 0.4 atm) can be considered as water saturation. Alternatively, the specimen can be immersed for seven days in water with a lab temperature while 100 mm water head is maintained on its top surface.

Figure 6-17. Specimens were kept under at least 15 cm of water for 8 days to reach full fiber saturation equivalent.

In this study, the specimens were saturated in the water after 8 days, then the weight of the wet specimens were used as saturated weight. When saturating Densglass Gold gypsum board products, special care was taken. Gypsum board specimens were soaked into plaster solution according to Wu (2007). Since gypsum loses its rigidity easily and dissolves with water, plaster powder was used in the solution to prevent its structural dispersal. In order to make a saturated solution of plaster, the drywall compound (commercially available) was added to water until no more powder dissolved. The apparent porosity was determined using equation (6.14) following (ASTM-C20-00, 2015).

$$V_{Pores} = \frac{W-D}{\rho_w} \quad \text{and} \quad \varepsilon = \frac{V_{Pores}}{V_e} \times 100 \qquad (6.14)$$

where

V_{Pores} = the volume of the open pores inside the specimen (m^3),
W = saturated weight of the water-saturated material sample (kg),
D = dry weight of the material sample (kg),
ρ_w = density of water (kg/m^3),
V_e = exterior volume of the specimen (m^3).

6.4 Water Vapor Permeability

This property was measured by the following standards:

- ASTM E96 / E96M–10 *Standard Test Methods for Water Vapor Transmission of Materials* (ASTM-E96/E96M, 2013).
- ISO 12572- Hygrothermal performance of building materials and products-Determination of water vapor transmission properties (EN.ISO.12572, 2001).

The dry cup and wet cup methods were used for the determination of water vapor permeabilities of building materials. The experimental procedure was based on an extension (Kumaran, 1998a) of the cup methods described by ASTM standard E96 and ISO 12572.

6.4.1 Specimens Preparation and Test Conditions

A round shallow transparent glass cup was selected to perform the water permeability test as it enabled observation of the water level, desiccant condition and monitoring the lower side of the specimen in wet cups for the risk of wetting by water. In vapor permeability test method, the specimen was sealed to the mouth of the cup. The dry cups, the cup contained desiccant while the wet cups contained distilled water. In order to be secured on the cup, the materials samples were cut with the external diameter of the cup so that they can be supported by the wall of the cups. Therefore, the specimens were cut into the circle shape with the diameter of 115 mm, Figure 6-18. However, according to the standard (ASTM-E96/E96M, 2013) the area of the supporting wall shall not exceed 10% of the sample area as this may cause error in the measured vapor permeability particularly for thick specimens (Joy and Wilson, 1966). A similar criterion was applied when the

edge of the top surface of the specimens were sealed to prevent any vapor passage into or out of the cup assembly around the edge of the sample. The area of the cup wall and the sealing mask at the edge of the top surface of the samples were subtracted from the samples area to calculate the effective exposed surface of the specimen to both inside and outside the cup. Prior to the measurement, the mass and dimensions of the specimen were recorded, Figure 6-19.

The specimen was sealed to the cup by a mixture of molten wax. The molten wax was made of 60% beeswax and 40% paraffin wax warmed to 100°C. However, I found that this mixture was not suitable to use with lower and higher temperatures than 21°C as it became very brittle and fragile (Figure 6-20) and melts and start running (Figure 6-21) at the 3°C and 45°C temperature, respectively.

Figure 6-18. Densglass (left) and spruce (right) specimens cut and labeled for vapor permeability cup tests.

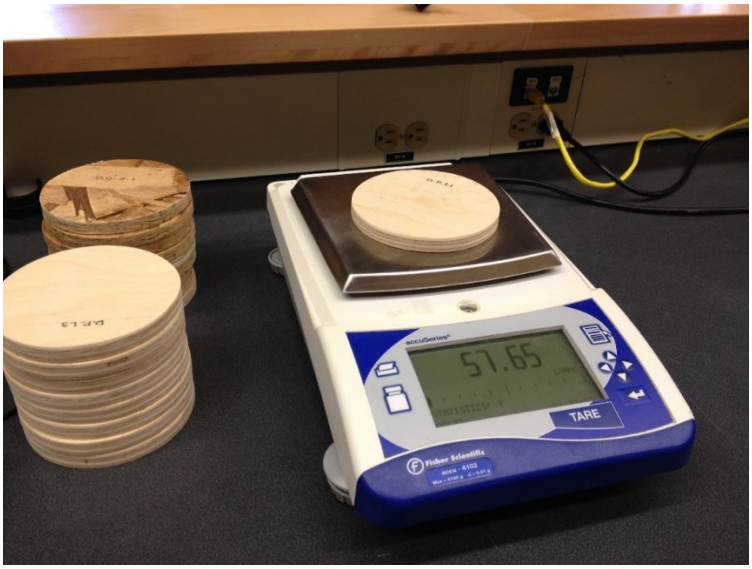

Figure 6-19. The mass and dimensions of the specimen were recorded before attaching to the cups.

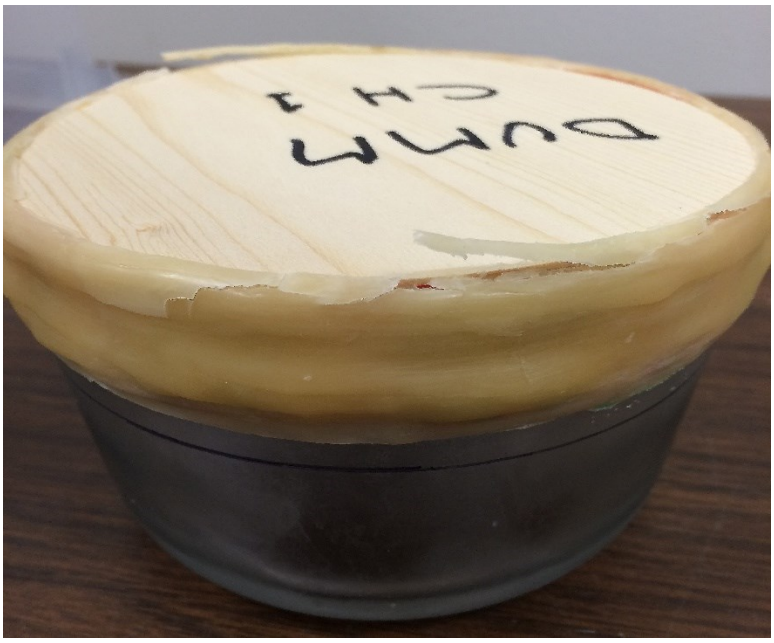

Figure 6-20. The normal wax mixture sealing getting brittle at temperature 3°C.

Figure 6-21. Melted normal wax mixture with air bubbles at temperature 45°C.

Therefore, I made different mixture portions of synthetic beeswax and paraffin wax with lower and higher melting temperatures than the normal ones as presented in Table 6-6.

Table 6-6. Different mixture configuration of beeswax and paraffin wax for sealing material samples to the cup in permeability test.

Permeability test temperature	Component	Melting point	Mass portion rate
3°C	Beewax	62°C	50%
	Parafin wax #1	50°C	50%
21°C	Beewax	62°C	60%
	Paraffin wax #2	60°C	40%
45°C	Beewax	62°C	10%
	Microcrystaline wax	86°C	90%

The dry cup was filled with desiccant (Calcium Chloride), and with distilled water for the wet cup. Both dry and wet cups were filled to 15 mm below the specimen, Figure 6-22. A series of weighings of the empty cups and cups with desiccant were carried out to determine the mass of the dry desiccant.

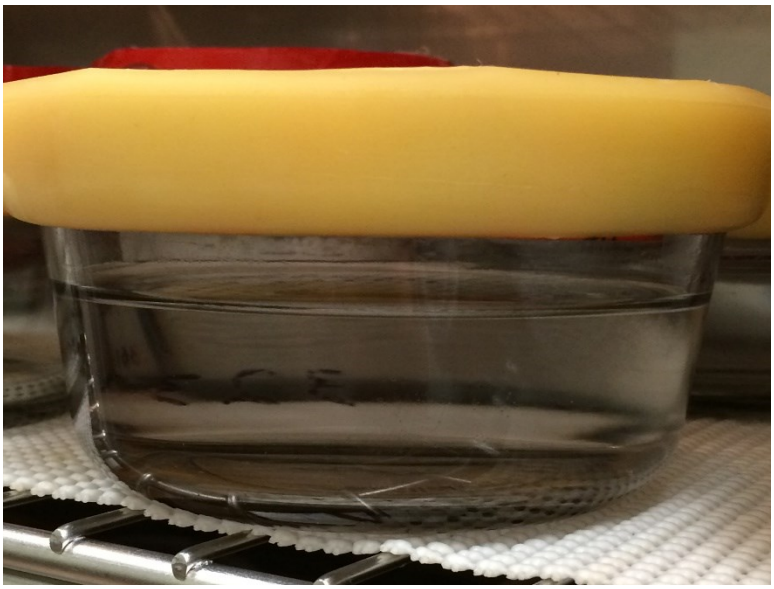

Figure 6-22. A sample wet cup filled with distilled water to 15 mm below the specimen.

At the next step, the lateral edge of the specimens was covered by tape to protect the penetration of hot wax mixture. Then, they were mounted on top of the cups where the joint between material samples and the cup were covered by another band of tape in order to block entering wax into the desiccant and water inside the cups, Figure 6-23.

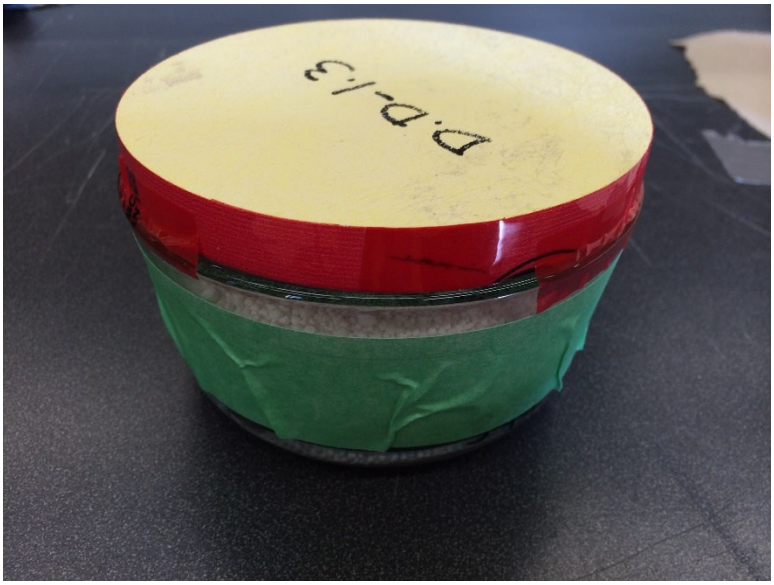

Figure 6-23. A material sample is placed on the mouth of the cup and the joint is covered with the tape.

Before applying wax, a band of gauze was attached around the joint to reinforce the wax sealing, Figure 6-24.

Figure 6-24. The joint between the specimen and the cup is reinforced by using a band gauze.

The specimen and cup assembly then were fully sealed with the proper wax mixture considering the temperature of the test.

Figure 6-25. Sealing the specimen on the cup with applying wax mixture.

Eventually, the edge of the top surface of the specimen was sealed while the material surface was protected by a cardboard template, Figure 6-26.

Figure 6-26. During sealing test cups, the top surface of the material samples was protected by a cardboard template.

Due to the brittle nature of the cellulose fiber samples, a plastic cylindrical frame was prepared in which the lower opening was closed by a highly porous stainless-steel mesh to prevent losing fibers into the cup during the test, Figure 6-27. The cellulose fiber samples were secured carefully inside the frame without applying excessive compression and then was secured on top of the cups using the previous sealing procedure, Figure 6-28. Similar to the other materials sealing procedure, the edge of the top surface of cellulose fiber samples inside the frame was sealed using sealant. Cups were placed into the climate-controlled chamber Figure 6-29, and the assemblies were weighed at different intervals depending on materials.

Figure 6-27. A plastic cylindrical frame with stainless-steel mesh on one side.

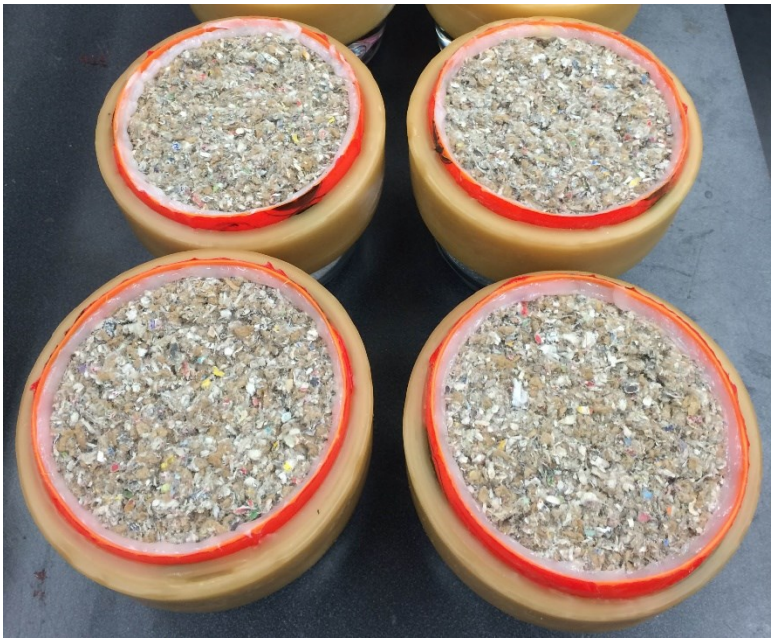

Figure 6-28. Cups with cellulose fiber samples.

Figure 6-29. Dry and wet cup samples inside a climate chamber.

Kumaran (1998a) suggested an extension of the cup methods described by ASTM standard E96. In the Standard, the dry cup method gives the results as an average value of the property at a mean relative humidity of 25 % and the wet cup at 75 %. This information is not enough for detailed hygrothermal analysis of building components. The complete dependence of water vapor permeability data on relative humidity and temperature is required by most computer models for hygrothermal simulation. Therefore, in this work three series of dry cups and wet cups were tested at each temperature exposing to 50 %, 70% and 90 % RH (nine conditions in total for each building material) in other to achieve complete dependence of water vapor permeability on relative humidity of each material at different temperatures.

6.4.2 **Experimental Methods and Equipment**

For each material three dry cups, three wet cups and a dummy cup were used in each chamber with different temperature. Then, the cups were placed in the climate chamber to exposed to the different environment conditions. The controlled temperature-humidity chambers were utilized to provide climate conditions the same as those used to determine the sorption isotherms of building materials. The rate of the water vapor movement through the specimen into desiccant in dry cups and towards outside in wet cups were measured by periodic weighing of the cups. Desiccant absorbed moisture during the test. Since, it loses its drying capacity after absorbing water vapor equivalence to 10% of its weight (ASTM-E96/E96M, 2013), the weight of desiccant was recorded

so it could be easier to judge when to terminate the test at a 10% desiccant moisture content. There was not a similar issue with the wet cups and so they were used continuously from 50% to 90% RH for each temperature set. However, the level of water inside the cups maintained constant during the experiment by injecting water into the cup with small syringe, Figure 6-30.

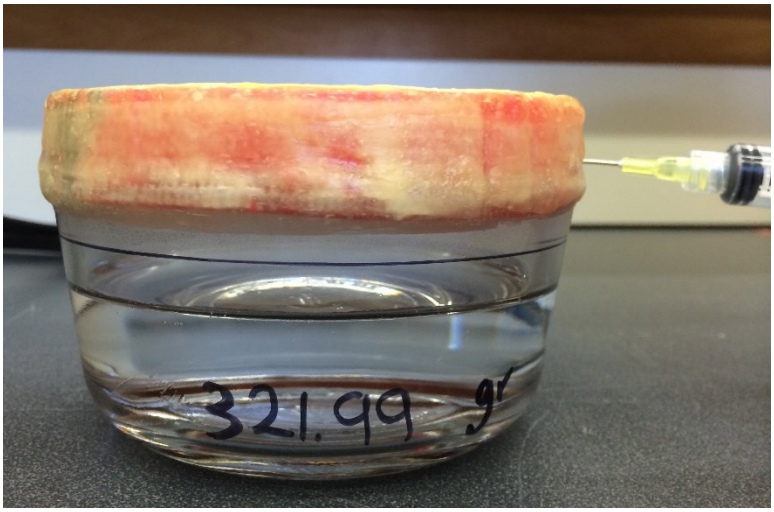

Figure 6-30. Carefully adding distilled water into a wet cup using syringe.

The injection was done carefully through the gap between the specimen and cup without wetting the lower surface of the material. The wet cups, however, were disassembled after each temperature set test. The electrical balance, shown in Figure 6-31, with 5 kg maximum capacity and the resolution is ± 0.01 g used for weighing the specimens and test assemblies, to satisfy the criteria specified in the ASTM E96 standard.

As the air movement of the laboratory air conditioning system caused fluctuation in balance readings so, all the measurements of all properties tests were performed while the balance was covered by a clear plastic box. Furthermore, all the measurements were read within 10 seconds after placing the specimen on the balance in order to decrease the risk of evaporation or condensation in the hot and cold conditions. Additionally, the climate chambers were located in a separate room with an independent condition allowed us to lower the temperature and RH to avoid condensation on the cups at tests with temperature of 3°C.

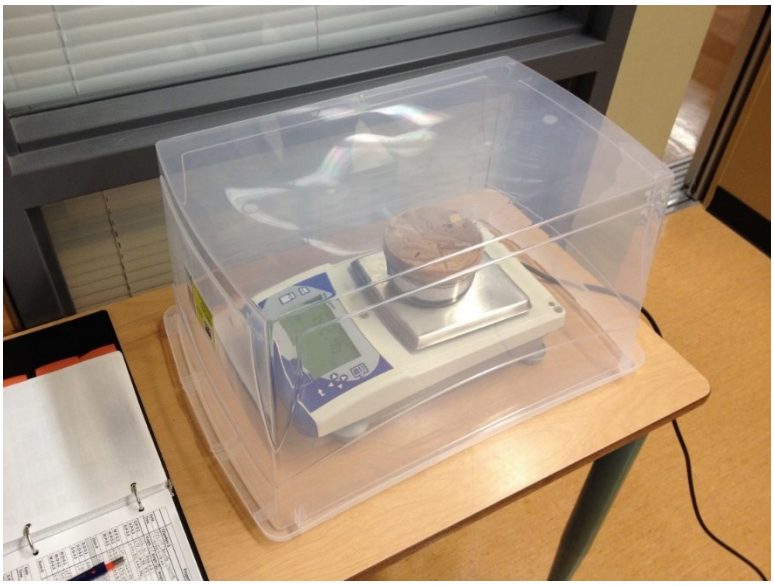

Figure 6-31. Electric balance with the accuracy of 0.01 g and a clear cover box.

In order to monitor the mass gain or loss in the specimens throughout the test, an additional specimen as a dummy was tested exactly like others while it was attached to an empty cup. Having a dummy specimen to determine modified dish weights may considerably decrease the time required to complete the test. Since, in some thick hygroscopic materials, time to reach equilibrium water permeance increases as square of the thickness up to two months (ASTM-E96/E96M, 2013). The measurement results were analyzed based on the principles used in (EN.ISO.12572, 2001); ASTM-E96/E96M (2013). These test methods cover the determination of water vapor transmission (WVT) of materials through which the passage of water vapor may be of importance.

6.4.2.1 Water Vapor Transmission

The change in mass gain of the cup weight was plotted against the elapsed time. A straight line was observed which, involved measurements of at least eight properly spaced points, indicated the establishment of the steady state water vapor transmission process. The slope of this straight line is the rate of water vapor transmission (WVT). The WVT rate was thus calculated using the following equation:

$$WVT = \frac{\mathrm{G}}{tA} = \frac{(G/t)}{A} \qquad (6.15)$$

where, G [kg] is the weight change of desiccant or water, t [s] is time, G/t [kg/s] is the slope of the straight line, A [m^2] is the cup mouth area, and WVT [kg/s·m^2] is the rate of water vapor

transmission. To achieve the true steady state of each set of measurements, the results obtained in this study, when plotted and curve fitted, showed a very clear straight line with the linear least-squares regression coefficient (R-square) value 0.99 or higher.

6.4.2.2 Water Vapor Permeance

Water vapor permeance (WVP) is calculated using equation (6.16):

$$WVP = \frac{\text{WVT}}{\Delta \text{P}} = \frac{WVT}{S(\varphi_1 - \varphi_2)} \qquad (6.16)$$

Where, S [Pa] is saturation vapor pressure at test temperature, φ_1 is relative humidity at the source expressed as a fraction (the test chamber for desiccant method; in the dish for water method), φ_2 relative humidity at the vapor sink expressed as a fraction, and WVP [kg/m^2.s.Pa] is the water vapor permeance.

6.4.2.3 Water Vapor Resistance

The water vapor resistance WVR [m^2.s.Pa/kg] of a building component is articulated as the reciprocal of the water vapor permeance (WVP) of the same.

$$WVR = \frac{1}{WVP} \qquad (6.17)$$

In addition, the corrections for resistance due to the still air layer and specimen surface are applied to the test results.

6.4.2.4 Resistance Due to Still Air Layer

If a layer of the still air with known thickness presents between the desiccant or water and specimen, then the equivalent water vapor resistance can be calculated using the following equation of permeability.

$$\delta_a = \frac{2.306 \times 10^{-5} . P_0}{R_v T P_a} \left(\frac{T}{273.13}\right)^{1.81} \qquad (6.18)$$

Where δ_a [kg/m.s.Pa] is water vapor permeability of the still air, P_0 [101325 Pa] standard atmospheric pressure, P_a [Pa] is ambient air pressure, T [K] the temperature, and R_v [461.5 J/K.kg] gas constant for water.

AR is the resistance presented by still air [m.s.Pa/kg],

$$AR = \frac{l}{\delta_a} \qquad (6.19)$$

Where, l [m] is the thickness of the air layer and has a direct relationship with the air resistance. Therefore, it is important to maintain the thickness of the air layer constant during the test.

6.4.2.5 Resistance Due to Specimen Surface Boundary Layer

The surface diffusion resistances, i.e. inside and outside surfaces of the specimen, may be derived using Lewis' law which governs the relation between heat and mass transfer coefficients at an interface with surrounding air (Pedersen, 1990). Using the convection heat transfer coefficient, the convection mass transfer coefficient is calculated as (Hansen and Lund, 1990):

$$\beta_p = \frac{h_c}{R_v.T.\rho.c_p} \qquad (6.20)$$

where β_p is convection mass transfer coefficient, h_c is convection heat transfer coefficient, R_v is gas constant for water vapor, T is temperature, ρ is density of air, and c_p is specific heat capacity of air. Then, the surface diffusion resistance for each side, is calculated as $Z = \frac{1}{\beta_p}$.

For the cup method, where the measured data is not available, the total surface diffusion resistance offered by two surfaces is judged to be approximately 4×10^7 [Pa.s.m^2/kg] (ASTM-E96/E96M, 2013).

6.4.2.6 Water Vapor Permeability of the Materials

Corrected WVR of the specimen = (WVR from Equation 6.17) - (resistance offered by still air (Equation 6.18)) for a known thickness in the cup and specimen surfaces (i.e., 4×10^7 [Pa.s.m^2/kg]), i.e.

$$WVR_{corrected} = \frac{1}{WVP} - \frac{l}{\delta_a} - S_R \qquad (6.21)$$

where S_R [Pa.s.m /kg] is the resistance offered by specimen surfaces. Corrected WVP of the specimen = l/ (Corrected WVR of the specimen):

$$WVP_{corrected} = \frac{1}{WVR_{corrected}} \qquad (6.22)$$

Corrected water vapor permeability $\delta_{corrected}$ [kg/m.s.Pa] of the material is calculated as:

$$\delta_{corrected} = WVP_{corrected} \times d \qquad (6.23)$$

Where *d* [m] is the thickness of the specimen. Another type of correction that cannot be ignored is the buoyancy correction (Lackey et al., 1997). The property measurement of some materials such as XPS and stucco can take many days or weeks. The atmospheric pressure may noticeably change during such long periods. The effect of buoyancy appears to be significant in tests measurements on building materials which are highly vapor resistant. In those cases, the measured masses should be corrected for the fluctuations in atmospheric pressure which may take many weeks to produce analyzable results. Corrections made for the impact of buoyancy can considerably reduce the duration of the test. The effect of buoyancy can be corrected by applying the following equation:

$$\frac{m_2}{m_1} = 1 + \frac{\rho_a(\rho_1 - \rho_2)}{\rho_1(\rho_2 - \rho_a)} \qquad (6.24)$$

Where, m_1 [kg] is the weight recorded by the balance, m_2 [kg] is the mass corrected for buoyancy effect, ρ_a [kg/m^3] is density of air, ρ_1 [kg/m^3] is density of the material of the balance weight and ρ_2 [kg/m^3] is bulk density of the test assembly.

6.5 Water Absorption Coefficient

This property was measured by the following standards:

- ASTM C1794-15 Standard Test Method for Determination of the Water Absorption by Partial Immersion (ASTM-C1794, 2015).
- ISO 15148- Hygrothermal performance of building materials and products- Determination of water absorption coefficient by partial immersion (EN.ISO.15148, 2002).

Water absorption coefficient is defined as the ratio between the change of the amount of water entry across unit area of the surface and the corresponding change in the square root of the time (see section 2.5.6

6.5.1 Specimens Preparation and Test Conditions

Four cubic specimens of each product with the touching surface area of 100 mm × 100 mm were tested. Twenty-seven specimens of each material (except EPS, XPS and Polyiso) in nine set of three were tested at nine different combinations of temperatures and relative humidities. It is

recommended in the literature to cover the upper surface of material specimen to prevent drying by evaporation. Though, the cover must enable air pressure equilibration with the atmosphere, therefore, the top sealing should be pierced or some gaps should be left for the air pressure to equilibrate (Descamps, 1997). In my research, however, similar to Karagiannis et al. (2019), I decided to conduct our measurements in climatic chambers and expose material samples to the different relative humidities since air temperature and relative humidity were the variables taken into consideration during the experiments. The four lateral sides in each specimen were sealed with sealant or adhesive tape, based on the type of the tested materials. For wood material samples, I particularly used sealant instead of normal wax mixture because of two reasons, first, at temperature 3°C, the wax cracked due to the wood dimensional expansion, Figure 6-32.

Figure 6-32. A crack in wax sealing even with gauze reinforcement on a Douglas fir sample during the water absorption test.

Second, hot wax could penetrate into the wood fiber during applying wax and melt during the test at temperature 45°C, Figure 6-33. Therefore, in contact with water, the specimen did not absorb the water through the full surface area, Figure 6-34.

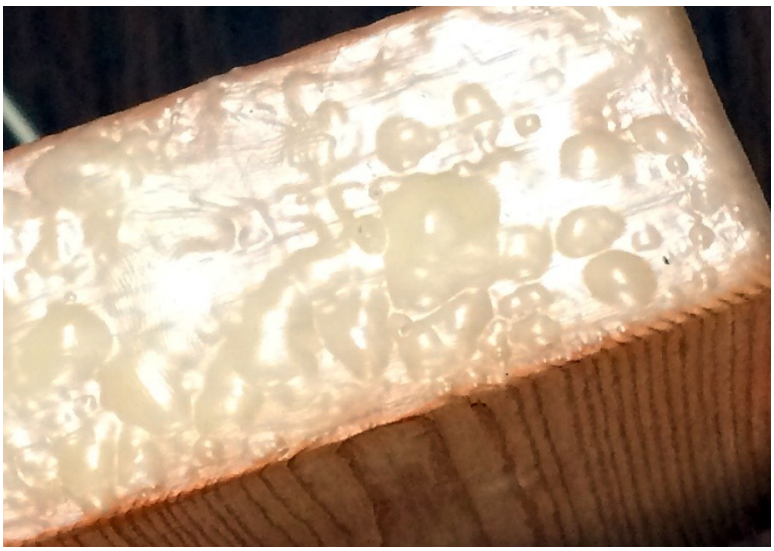

Figure 6-33. The normal mixture wax melted during water absorption test at 45°C.

Figure 6-34. The penetrated wax into the wood fiber limited absorbing water through the full area of the surface.

The top was left uncovered to be exposed to the test environment conditions and to prevent any build-up of entrapped air pressure during the water absorption test which might slow down the

imbibition processes. Cellulose fiber samples were prepared by using the same cylindrical plastic frame with double metal mesh, Figure 6-35.

Figure 6-35. A cylindrical plastic frame with a stainless-steel mesh was made for the water absorption test of cellulose fiber samples.

The building membranes were tested following the procedure suggested by Kumaran (2002). However, in this study gypsum compound paste was poured inside the 100 mm × 100 × 20 mm boxes which were pre-made of building membranes and allowed to dry, Figure 6-36. The sides were then sealed using wax or adhesive tape. Water was allowed to touch the exposed surface of the membrane.

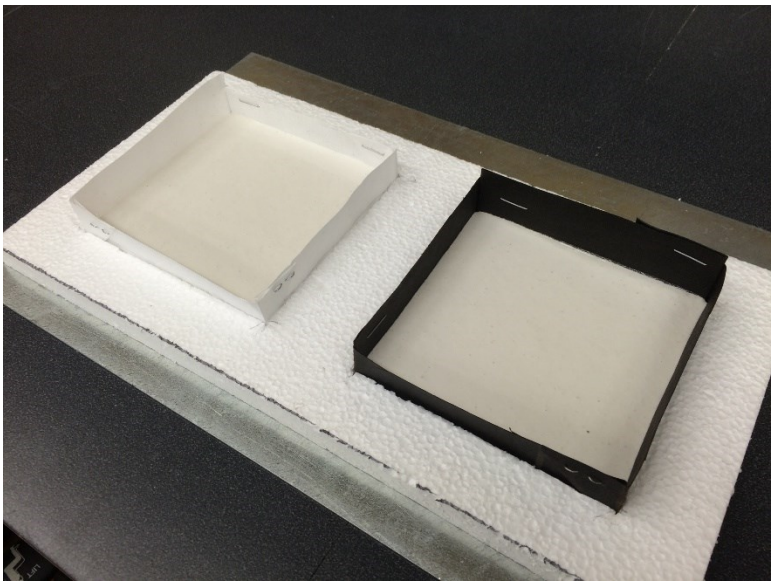

Figure 6-36. The gypsum compound paste was poured inside the 100 mm × 100 mm boxes which were pre-made of building membranes.

Before the test, all the specimens were conditioned inside the chambers at the designated conditions until the weight of each specimen reached a steady state as described in sorption isotherm test procedure.

6.5.2 **Experimental Methods and Equipment**

The current standard test methods (EN.ISO.15148, 2002; ASTM-C1794, 2015) are intended to be used for the characterization of materials in the laboratory condition. They are not intended to simulate any particular environmental condition encountered in building construction applications. Accordingly, there is no specific procedure in the standards for preparing the specimens for different conditions. However, it specifies how to prepare a suitable apparatus carefully. A decent description of the water absorption test method based on the partial immersion method is available in Mukhopadhyaya et al. (2002b).

The technical drawings which are shown in Figure 6-37 is the water tank and circulation bath which I designed through this research for this measurement method according to the designated standards and published relevant research at the BCIT Building Science lab.

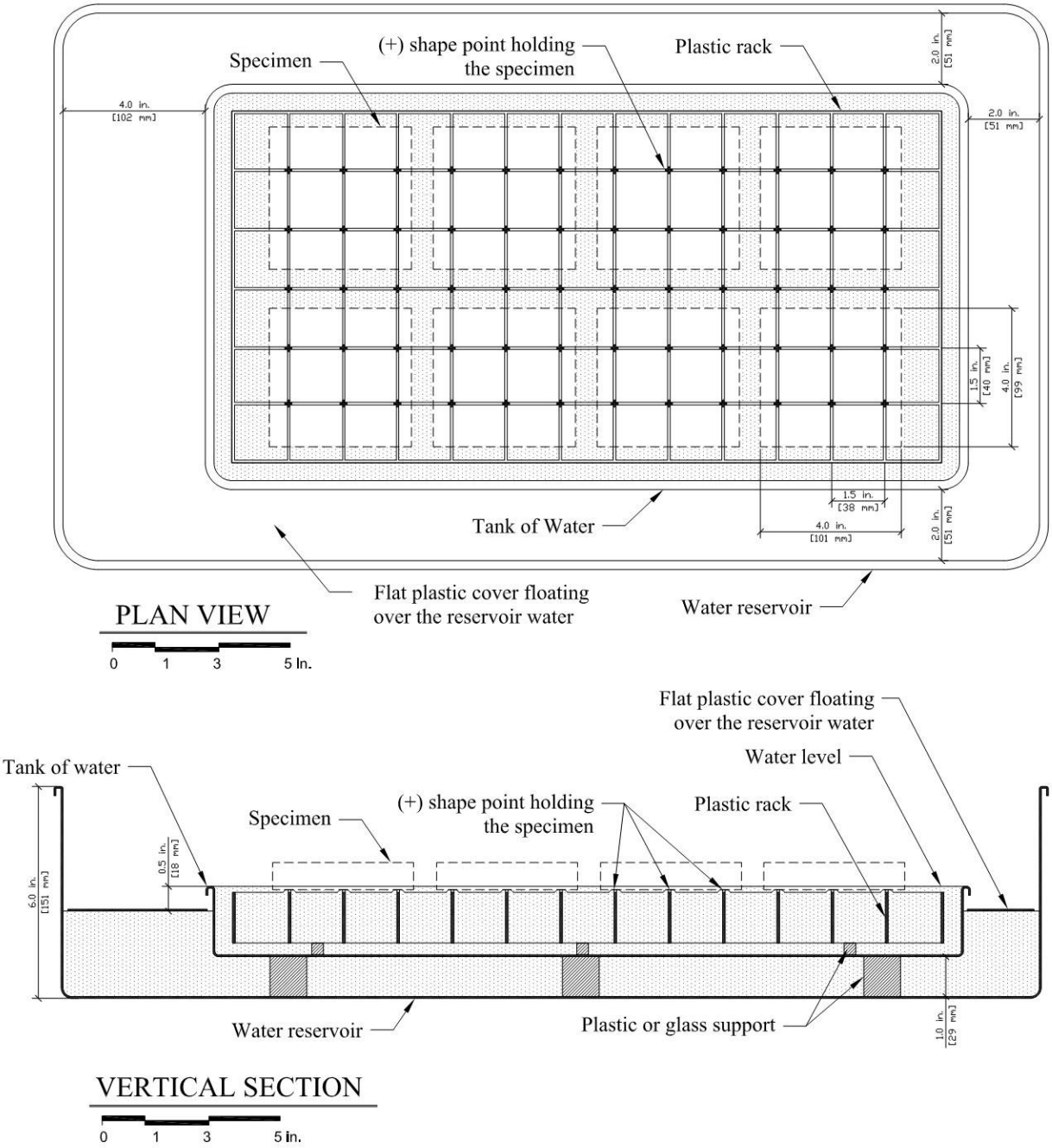

Figure 6-37. Detailed drawings of the custom-made apparatus for water absorption test designed in this study.

The water tank must contain certain level of distilled/deionized water and be able to maintain the level of the water surface inside the circulation bath at all times during the test. Each specimen was placed on six (+) points of a plastic rack. The rack was able to be adjusted vertically to control the immersion depth of the specimen or to be just touching the surface of water. A transparent lid with several holes at all sides was initially designed to maintain a certain level of relative humidity around the tested material samples and protect the top surface of materials from excessive evaporation due to the air circulation inside chambers as depicted in Figure 6-38. Several experimental tests were carried out while the condition under the lid was recorded. It was realized that using lid significantly decreased the air circulation over the samples which caused a high relative humidity between 80% and 90% at all nine relative humidity conditions. On the other hand, it was found that when the absorption setup was placed on the bottom floor of the chamber, the 6 in. lateral walls of the reservoir tank already, prevented the excessive air circulation over the samples. Therefore, the clear led was eventually removed as the specimen were supposed to be exposed to the different relative humidities inside the chambers. Additionally, since evaporation through the open water surface of the reservoir tank created uncontrol fluctuation in the condition inside chambers, a plastic sheet was designed to cover the surface of the reservoir water. The plastic rack can hold six specimens during the test. Two absorption test setups were placed inside each of the three climate chambers while running at different temperatures during the process of measurement the water absorption coefficient of the building materials, Figure 6-39.

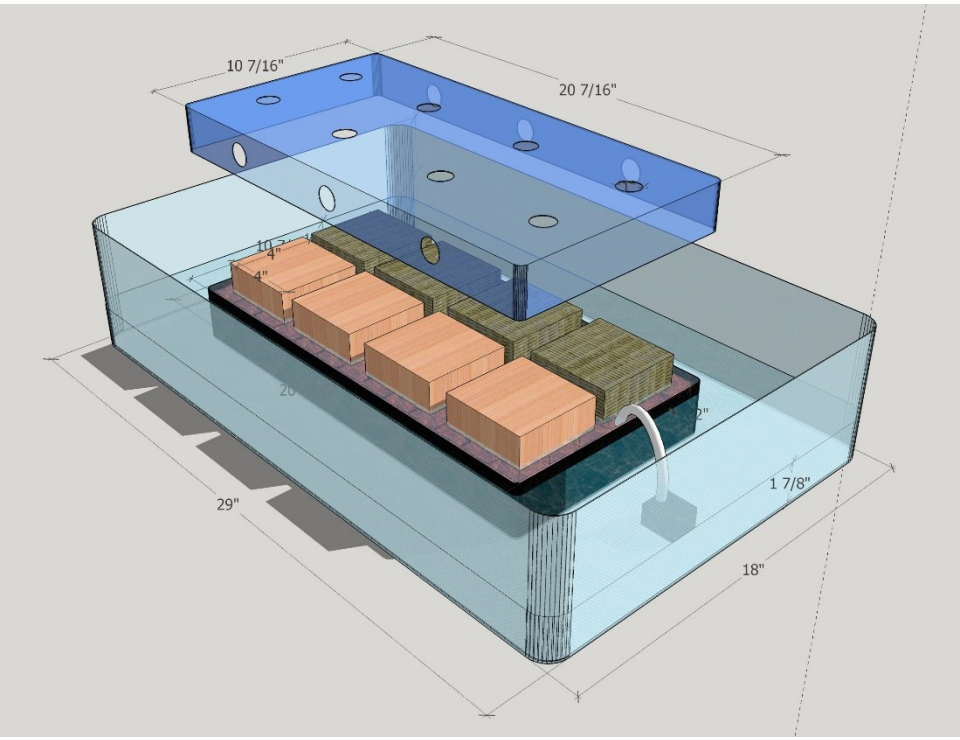

Figure 6-38. The schematic diagram of the water tank and circulation bath we designed at BCIT's Building Science center of excellence.

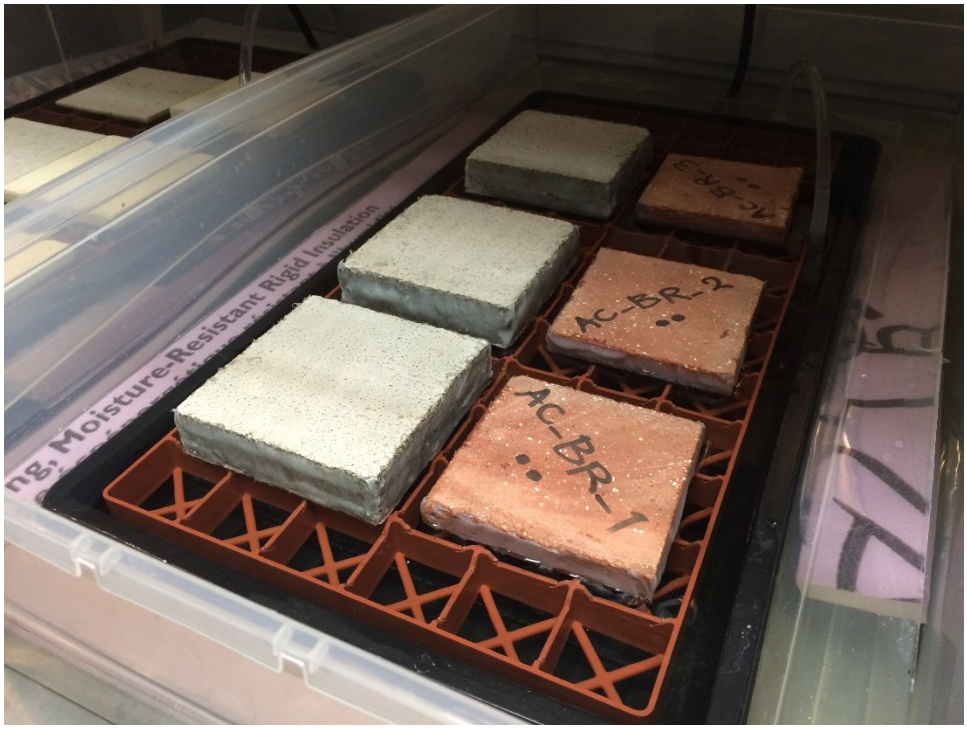

Figure 6-39. The Water absorption test setup in operation.

During the absorption test, one side of the material samples was immersed in the water tank. The specimen was weighed periodically while the water is continuously circulated in the bath to keep the constant water level. For recording the weight, the specimen was taken out of the water and its bottom side was dried out with a towel then it was placed on the balance. The process of weighing was successfully shortened to less than 10 seconds. This was done to prevent any undesired drainage and moisture loss during recording the mass gain. The calculation of the water absorption coefficient and expression of results in this study were carried out based on procedure described in (EN.ISO.15148, 2002; ASTM-C1794, 2015). The difference between the mass (m_t) at time t and the initial mass (m_i) of the specimen per area was calculated as Δm_t using the equation:

$$\Delta m_t = \frac{m_t - m_i}{A} \qquad (6.25)$$

The results were plotted against the square root of the time √t.

Depending on their nature, in some of the building materials, liquid water reached the top surface of the specimen during the test while in the others water did not reach the top surface. Accordingly, the graph resulting from the equation (6.25) for the former group is called type B (Figure 6-42) which expresses a nonlinear relationship between m_t and t and for the latter group the graph is called type A (Figure 6-40 and Figure 6-41) which shows a linear relationship between m_t and t until the end of the test. In both cases the $\Delta m`_0$ was determined by extending the regression curve back to time zero where it cuts the vertical axis.

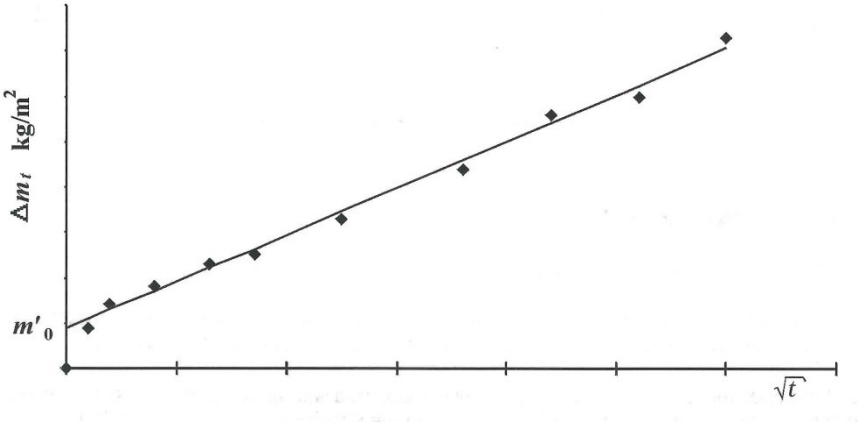

Figure 6-40. Type A graphs without liquid water on the top surface (EN.ISO.15148, 2002).

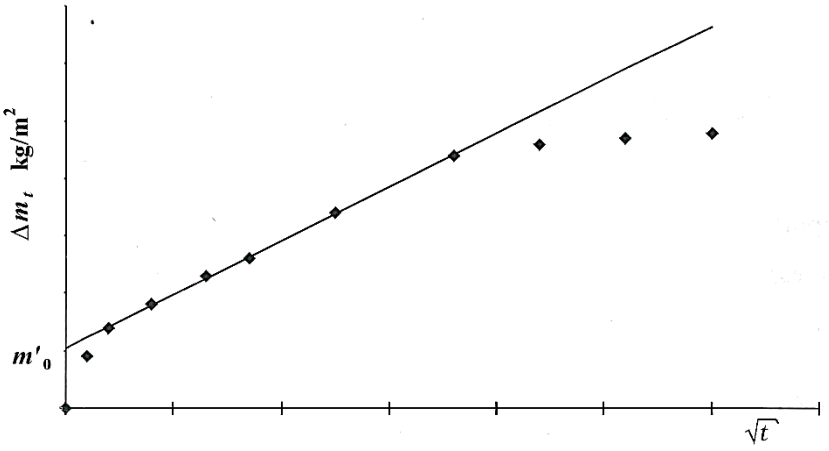

Figure 6-41. Type A graphs without liquid water on the top surface (EN.ISO.15148, 2002).

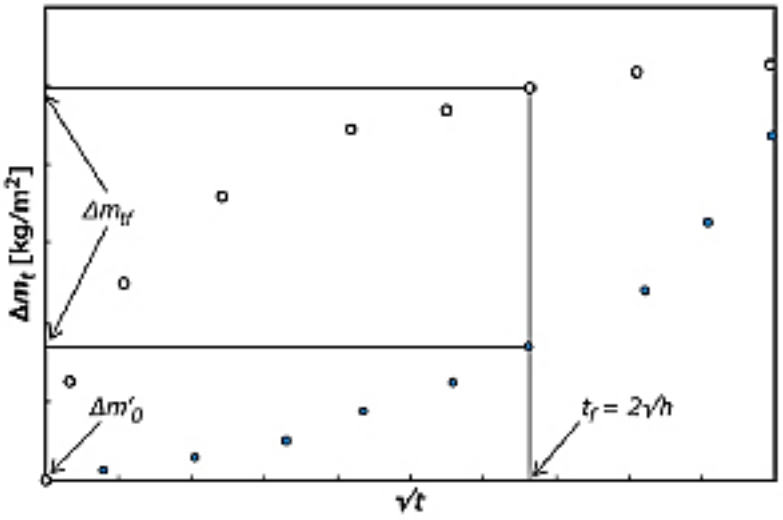

Figure 6-42. Type B graphs (ASTM-C1794, 2015).

Then the water absorption coefficient in Type A was calculated from:

$$A_w = \frac{\Delta m`_{tf} - \Delta m`_0}{\sqrt{t_f}} \qquad (6.26)$$

where

$\Delta m`_{tf}$ = is the value of Δm (kg/m^2) on the regression curve at time t_f (s) which is generally one day,

Or

$$W_w = \frac{\Delta m`_{tf} - \Delta m`_0}{\sqrt{t_f}} \qquad (6.27)$$

where

t_f = the duration of the test (generally one day), (h).

When the liquid water reaches the top surface of the specimen in less than a 24 h which is considered as type B, different approaches are offered by ASTM-C1794 (2015) and EN.ISO.15148 (2002). According to ASTM-C1794 (2015) which is followed in this study, A_w and W_w of the type B cases are calculated by equations (6.28) and (6.29), respectively at time t_f = 14400 (s) (4 h) while no values shall be reported in case of observing water at the top surface in less than 4 h.

$$A_{w,4} = \frac{\Delta m`_{tf} - \Delta m`_0}{\sqrt{14400s}} \qquad (6.28)$$

where

$\Delta m`_{tf}$ = is the value of Δm (kg/m^2) on the regression curve at time t_f = 4 h.

And

$$W_{w,4} = \frac{\Delta m`_{tf} - \Delta m`_0}{2\sqrt{h}} \qquad (6.29)$$

EN.ISO.15148 (2002) recommends calculating A_w and W_w at time t_f = 24 h using equations (6.30) and (6.31) and no values will be reported for the times below 24 h.

$$A_{w,24} = \frac{\Delta m_{tf}}{\sqrt{86400s}} \qquad (6.30)$$

$$W_{w,24} = \frac{\Delta m_{tf}}{\sqrt{24}} \qquad (6.31)$$

7 Results and Discussion

Advanced building envelope HAM models require a set of accurate input data, which include the properties of different building materials. This chapter presents the measured four hygrothermal properties of each building product under nine combinations of different temperatures and relative humidities. As explained, for material reasons all properties for all building materials were not measured due to sample size, incompatibility of the nature of the material, and the test setup.

7.1 Thermal Conductivity and Heat Capacity of Building Materials

The results were obtained through three/four tests with different 300 mm × 300 mm samples of each building material. The thermal conductivity (k value) of selected samples of each material was then measured at six different mean temperatures (5°C, 10°C, 20°C, 24°C, 34°C, 50°C and 60°C) and ΔT of 20°C. The k value variation of four samples of each material with respect to temperature was plotted accordingly in a graph. Accordingly, another set of two 600 mm × 600 mm samples of each material were used for measuring the specific heat capacity. The measurements were carried out at temperatures 16°C, 18°C, 20°C, 22°C, 24°C, 26°C, 28°C, 30°C and 36°C. We were not able to run the test at mean temperatures below the lab air dew points as condensation and frost around the cooling pipe of the instrument were noticed. The results for the specific heat capacity measurement are plotted in a separate graph. Furthermore, the thermal conductivities and specific heat capacity of the tested building materials are compared with the results extracted from the ASHRAE research project 1018 (Kumaran, 2002).

7.1.1 **Fiber Cement**

According to the measured k values for the fiber cement samples presented in the Figure 7-1, the thermal conductivity increased with rising the temperature. Although the graph expressed a plateau trend between 21.37°C and 49.03°C for samples two and three, the overall trend for all samples of fiber cement is upward. The conductivity values from the ASHRAE RP-1018 (Kumaran, 2002) have been obtained at mean temperatures of 1.5°C and 25°C with average temperature difference (ΔT) of 3.75°C across the specimen which represent a small increase in thermal conductivity of fiber cement samples and they were slightly higher than the conductivity values measured in this study.

Table 7-1. The measured density and thickness of the tested building material and the corresponding RP-1018 material.

Material	**Density (kg/m^3)**	**Thickness (mm)**
Fiber Cement Board	1358 ± 12	7.7
Fiber Cement Board (ASHRAE RP-1018)	1380 ± 40	7.9

The specific heat capacity measurements showed an increase while the temperature elevated. In addition, the variation in specific heat capacity is more significant in both samples at low temperatures between 16°C and 20°C and at higher ranges between 30°C and 36°C. In comparison with the reported values in IEA-Annex 24 (Kumaran, 1996b), our measured specific heat capacities appeared to be slightly higher.

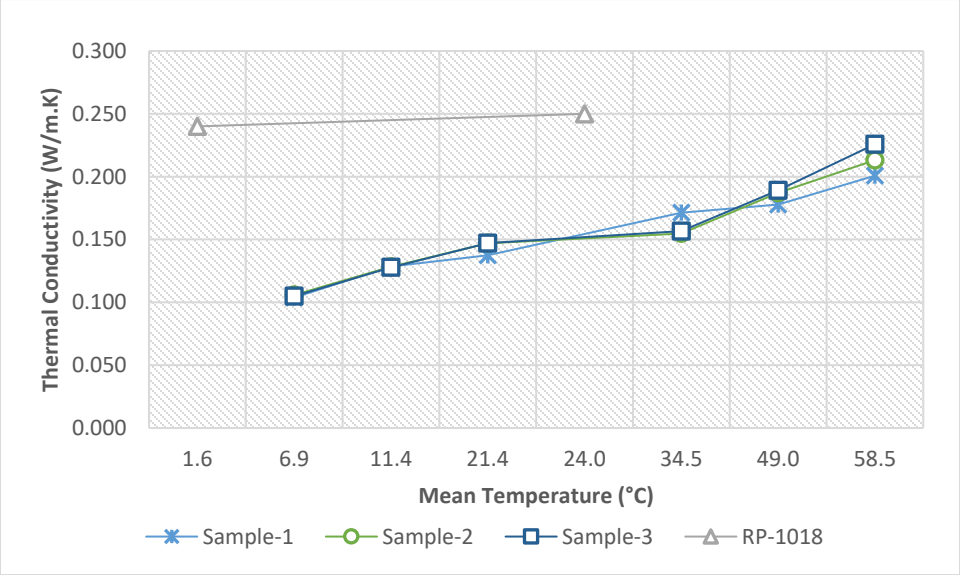

Figure 7-1. Fiber Cement-Thermal Conductivity.

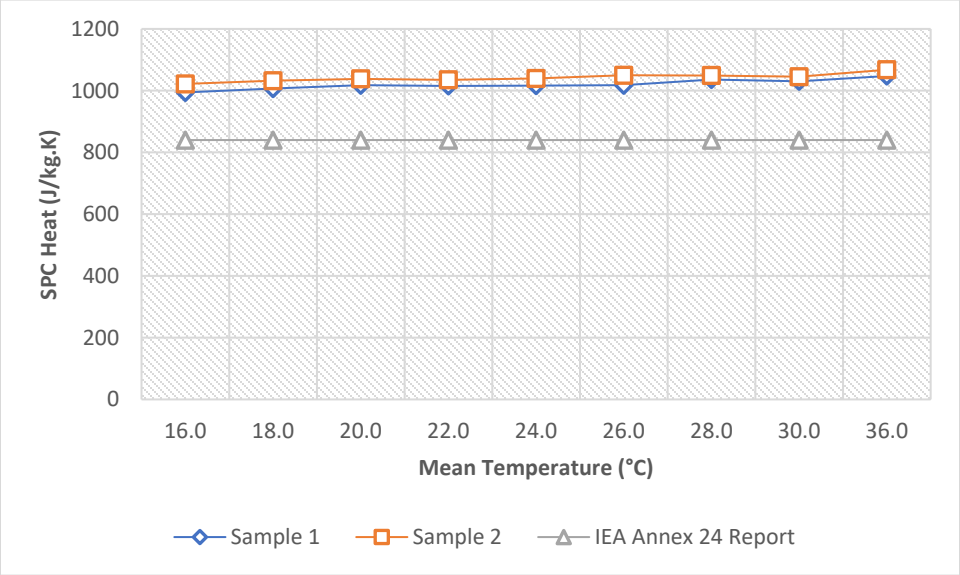

Figure 7-2. Fiber Cement-Specific Heat Capacity.

7.1.2 **Stucco**

The measured values of thermal conductivity for stucco samples presented an increase with respect to temperature. In all samples, the upward trend was observed to be more notable when temperature rose above 24°C.

The results from RP-1018 represented slightly lower values and a small increase with rising mean temperatures while average ΔT was 4.7°C. The discrepancy between our measured k values and the ASHRAE report (RP-1018) can be due to higher density of our stucco samples, different mean temperature, material components and their ratio (polymer modified stucco mixture was used in this study) and the workmanship.

Table 7-2. The measured density and thickness of the tested building material and the corresponding RP-1018 material.

Material	**Density (kg/m^3)**	**Thickness (mm)**
Stucco	2389 ± 39	25.9
Stucco (ASHRAE RP-1018)	1985 ± 30	14.69, 12.87

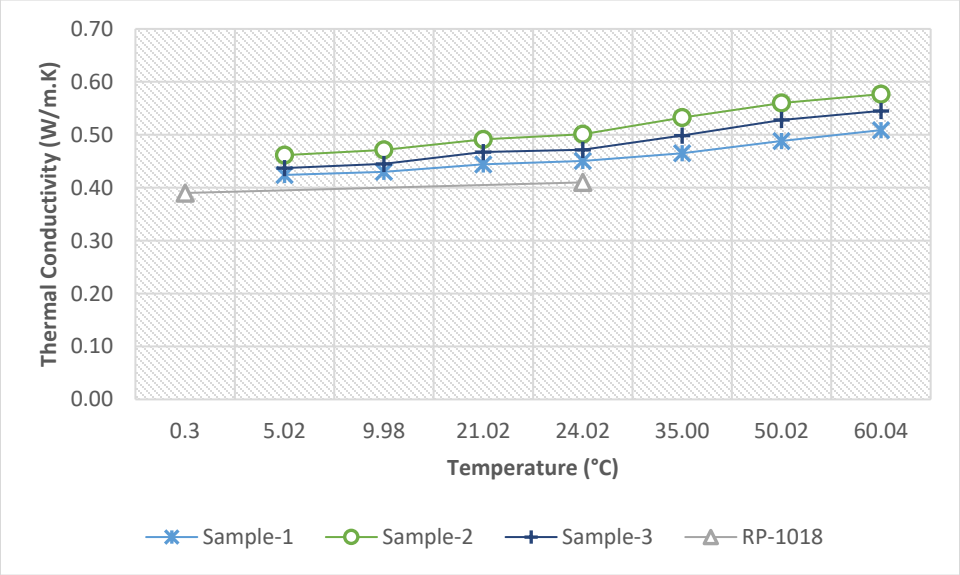

Figure 7-3. Stucco-Thermal Conductivity.

7.1.3 **Western Red Cedar**

The measured values of thermal conductivity in western red cedar samples showed an overall increase with temperature while the changes observed to be noticeable at mean temperatures below 24°C. The results for thermal conductivity for the same material from RP-1018 with two ΔTs of 19.64°C and 15.1°C also, expressed an upward trend with rising temperature and were slightly lower than our measured values.

Table 7-3. The measured density and thickness of the tested building material and the corresponding RP-1018 material.

Material	**Density (kg/m^3)**	**Thickness (mm)**
Western Red Cedar	380 ± 4	42.9
Western Red Cedar (ASHRAE RP-1018)	350 ± 20	17.8

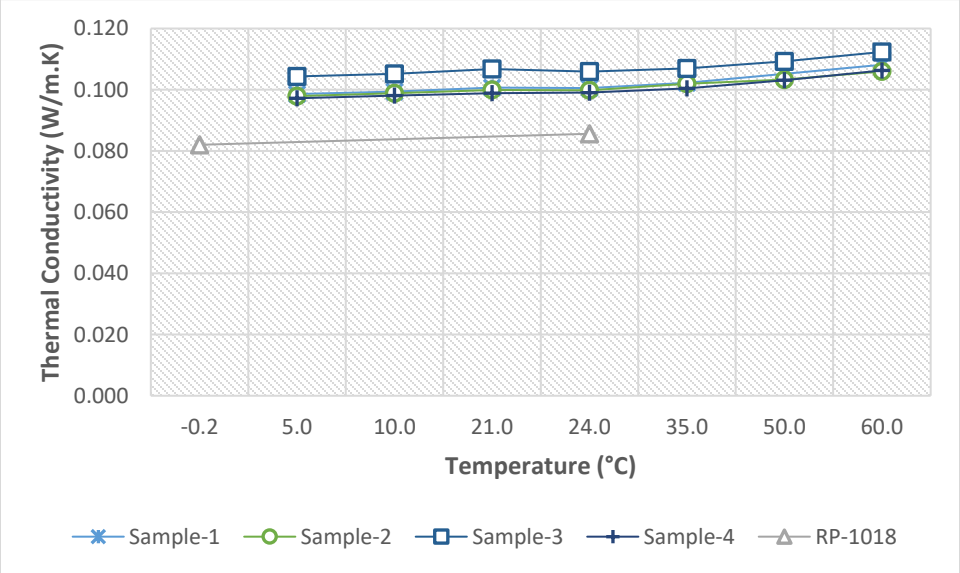

Figure 7-4. Western Red Cedar-Thermal Conductivity.

7.1.4 **Oriented Strand Board (OSB)**

The thermal conductivity measurements in all samples of OSB showed a steady upward trend with temperature rise. Comparing with the results from RP-1018 with average $\Delta T=5.75°C$, showed a slightly higher thermal conductivity value with increasing mean temperature. The measured specific heat capacity for OSB represented a smooth rise with increasing temperature. However, according to IEA-Annex 24 results, OSB represented slightly higher values than our measured specific heat capacity.

Table 7-4. The measured density and thickness of the tested building material and the corresponding RP-1018 material.

Material	**Density (kg/m^3)**	**Thickness (mm)**
OSB	620 ± 12	11.4
OSB (ASHRAE RP-1018)	650 ± 30	10.87

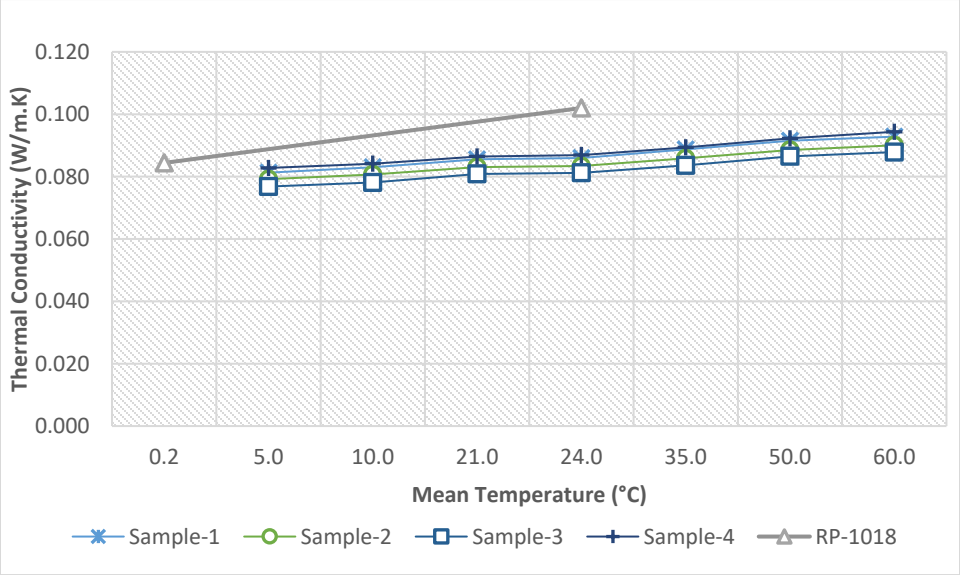

Figure 7-5. OSB-Thermal Conductivity.

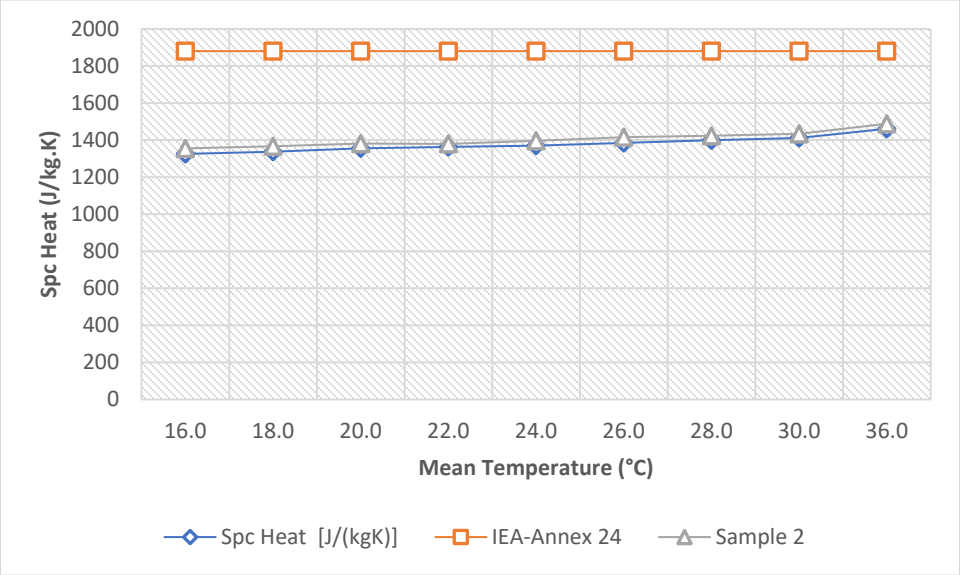

Figure 7-6. OSB-Specific Heat Capacity.

7.1.5 **Plywood**

According to the results of thermal conductivity measurements for plywood, it appeared that the conductivity values increased slightly with the rise of temperature. However, an increase in thermal conductivity was observed in the sample one between temperatures 34.99°C and 60°C. The results for thermal conductivity from ASHRAE RP-1018 for plywood material with temperature difference of 6.3°C represents an increase with temperature which we found our measured values to be in a good agreement with them.

Accordingly, the measured specific heat capacity for plywood represented a smooth and slight rise with increasing temperature. However, compared to the results of IEA-Annex 24, our obtained results were lower.

Table 7-5. The measured density and thickness of the tested building material and the corresponding RP-1018 material.

Material	**Density (kg/m^3)**	**Thickness (mm)**
Plywood	461 ± 8	12.9
Plywood (ASHRAE RP-1018)	470 ± 5	12.03

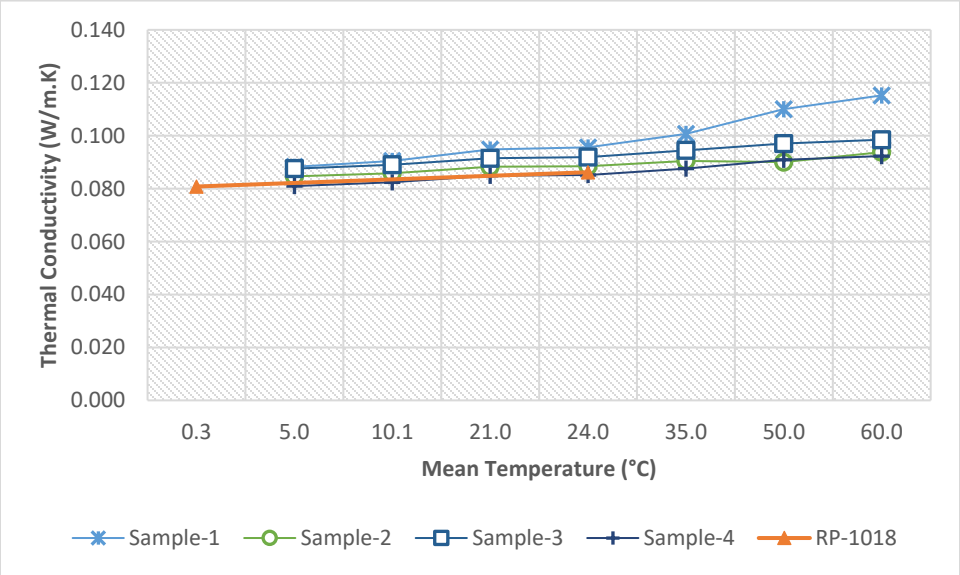

Figure 7-7. Plywood-Thermal Conductivity.

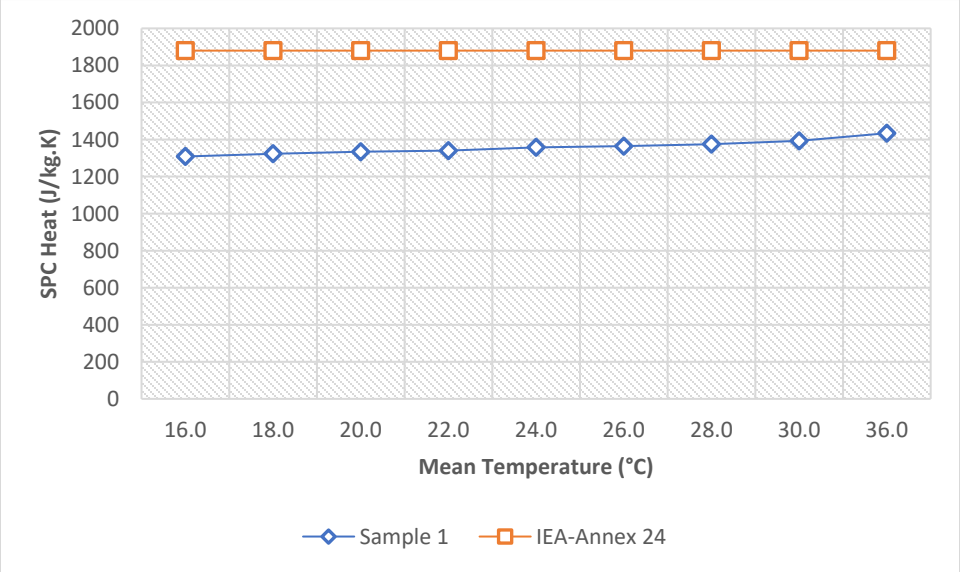

Figure 7-8. Plywood-Specific Heat Capacity.

7.1.6 **Densglass Gold Gypsum Sheathing Board**

The measured thermal conductivity values from three samples of Densglass gold gypsum sheathing board showed a considerable discrepancy between three samples. Samples one and three represented a slightly downward trend in their thermal conductivity with rising temperature whereas the trend in sample two was slightly upward. The RP-1018 report does not include Densglass exterior gypsum sheathing board. However, their measurement results of thermal conductivity for interior gypsum with $\Delta T=10.35°C$ showed a constant value against temperature which was slightly lower than our measured data.

Unlike the thermal conductivity results, the measurements of specific heat capacity of Densglass gold gypsum sheathing showed similar small increase with rising temperature in both samples. The results of both samples showed a steady trend from 16.01°C to 26.02°C and a small increase from 26.02°C to 28.02°C. Comparing with the result of specific heat capacity from IEA-Annex24, our results observed to be slightly higher.

Table 7-6. The measured density and thickness of the tested building material and the corresponding RP-1018 material.

Material	**Density (kg/m^3)**	**Thickness (mm)**
Densglass Gold Gypsum Sheathing	755 ± 7	13.3
Interior Gypsum Board (ASHRAE RP-1018)	625 ± 7	12.51

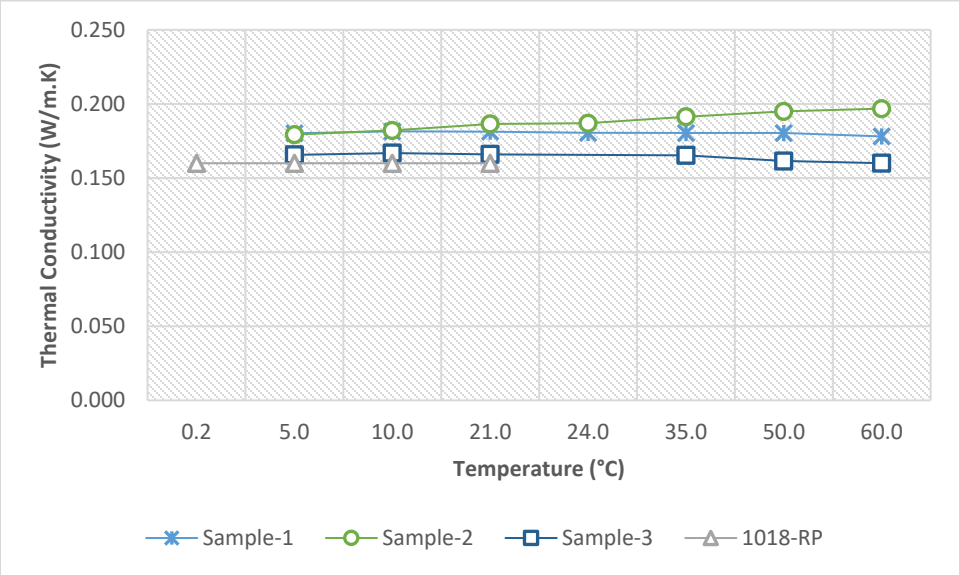

Figure 7-9. Densglass Gypsum Sheathing-Thermal Conductivity.

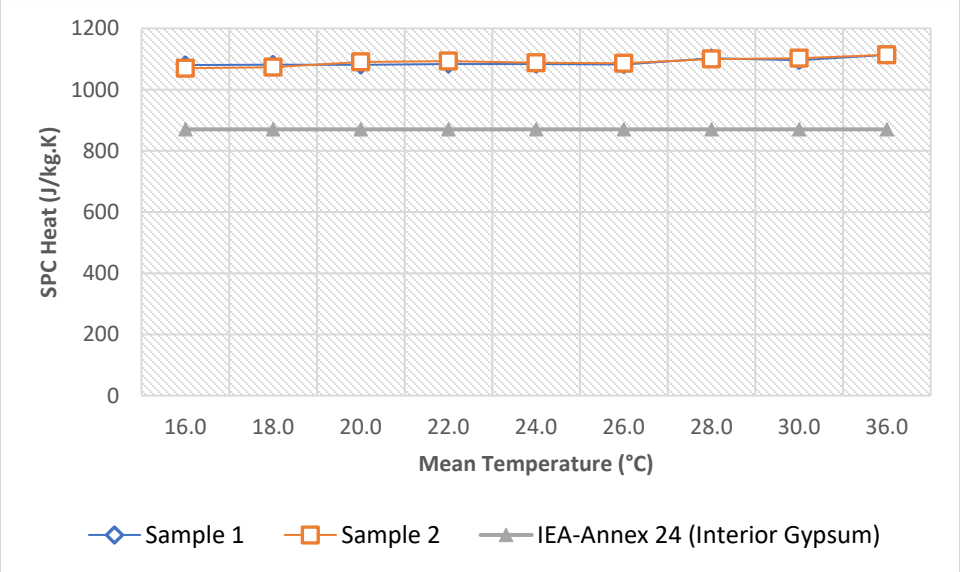

Figure 7-10. Densglass Gypsum Sheathing-Specific Heat Capacity.

7.1.7 **Spruce**

The measured thermal conductivity for all four samples of spruce plank expressed linear graphs with an increase with escalating temperature which was more noticeable at temperatures lower than 21°C and higher than 34.97°C. Comparing to the results from RP-1018 with ΔT of 20.5°C, both results indicated a rise in thermal conductivity of spruce samples with temperature whereas our values appeared to be higher and presenting less increase with respect to temperature.

Table 7-7. The measured density and thickness of the tested building material and the corresponding RP-1018 material.

Material	**Density (kg/m^3)**	**Thickness (mm)**
Spruce	469 ± 17	37.3
Spruce (ASHRAE RP-1018)	400 ± 50	19.5

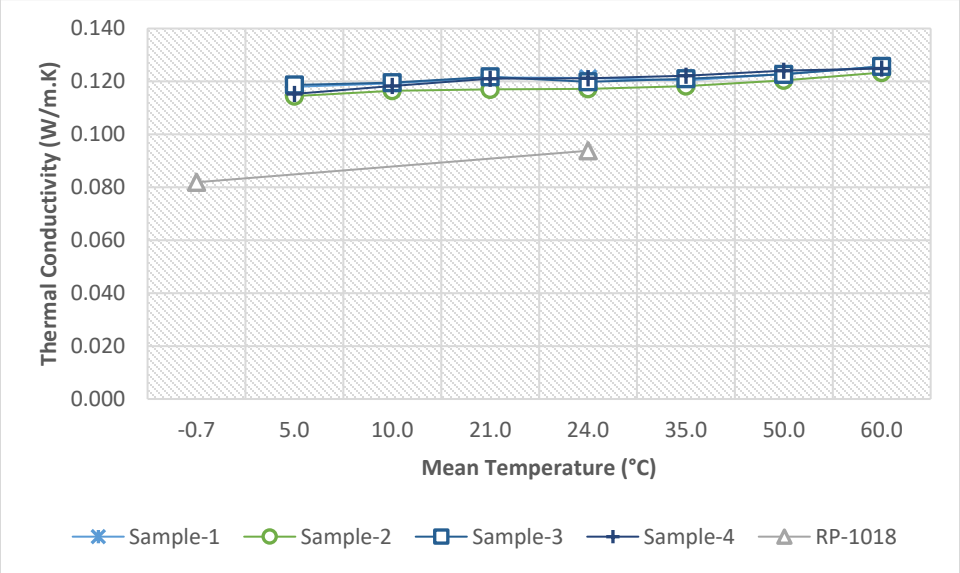

Figure 7-11. Spruce-Thermal Conductivity.

7.1.8 **Douglas Fir**

The measured thermal conductivity for Douglas fir with respect to elevated mean temperatures showed slightly increase. The changes in k values were not considerable between temperatures 21.05°C and 35.01°C in all samples. Among all samples, the results for the sample two exhibited higher values for thermal conductivity than the others. There was no measured thermal conductivity for Douglas fir in ASHRAE RP-1018.

Table 7-8. The measured density and thickness of the tested building material and the corresponding RP-1018 material.

Material	**Density (kg/m^3)**	**Thickness (mm)**
Douglas Fir	572 ± 9	36.2
(ASHRAE RP-1018)	-	-

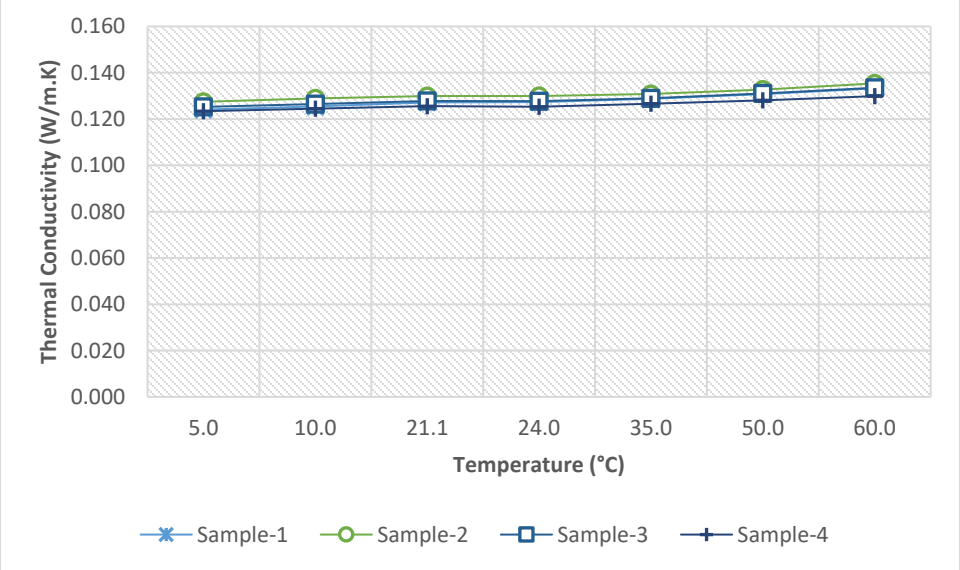

Figure 7-12. Douglas Fir-Thermal Conductivity.

7.1.9 **Cellulose Fiber**

Analyzing the results for cellulose fiber insulation samples revealed a coherence between measured thermal conductivity in samples except for sample one which appeared to be higher than the others while maintained the same upward trend in thermal conductivity with increasing temperature. Comparing with the results from RP-1018 with ΔT of 22.95°C, we found our results to be slightly higher. The results of measuring the specific heat capacity for cellulose fiber insulation presented an increase with temperature. According to the graph presented below, the influence of temperature on specific heat capacity was less considerable between 20.02°C and 28.02°C. Although, the measured specific heat capacity at 20°C in this research project was the same as values reported in IEA-Annex 24, we noted that our results to be a little lower and higher at temperatures below and above 20°C.

Table 7-9. The measured density and thickness of the tested building material and the corresponding RP-1018 material.

Material	**Density (kg/m^3)**	**Thickness (mm)**
Cellulose Fiber	57.6	48.7
Cellulose Fiber (ASHRAE RP-1018)	30 ± 4	88.53

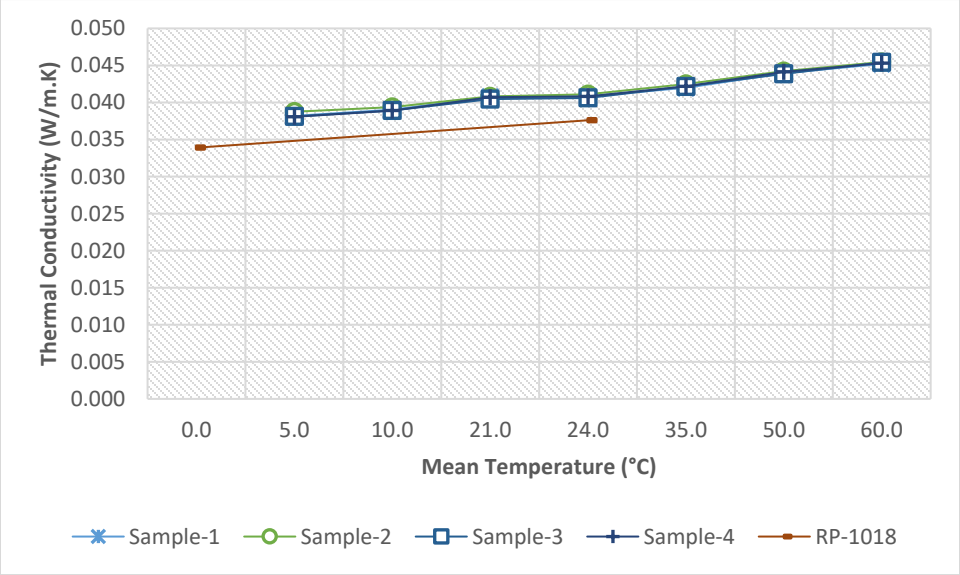

Figure 7-13. Cellulose Fiber-Thermal Conductivity.

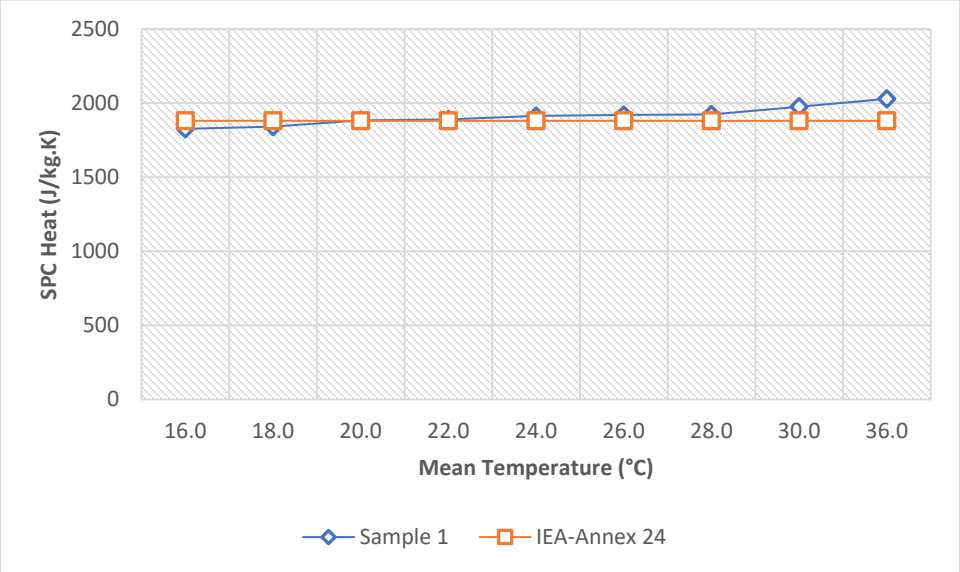

Figure 7-14. Cellulose Fiber-Specific Heat Capacity.

7.1.10 **Expanded Polystyrene (EPS)**

The measured results from heat flow meter test for EPS showed that the thermal conductivity increased upon rising the temperature. There was a coherence between the thermal conductivities of all samples. The results from IEA-Annex 24 operated with average ΔT of 22.5°C also showed that the thermal conductivity increased with temperature rise and in a good coherence with our results.

The measured specific heat capacity for EPS presented a horizontal graph against temperature and appeared to be lower than the IEA-Annex 24 result. Although, there was a slight decrease in our measured values from 16°C and 20°C and from 28°C to 36°C, the rest of the graph projected an upward trend in measured specific heat values.

Table 7-10. The measured density and thickness of the tested building material and the corresponding IEA-Annex 24 material.

Material	**Density (kg/m^3)**	**Thickness (mm)**
Expanded Polystyrene	21.9 ± 0.1	24.5
Expanded Polystyrene (IEA-Annex 24)	23.2	79

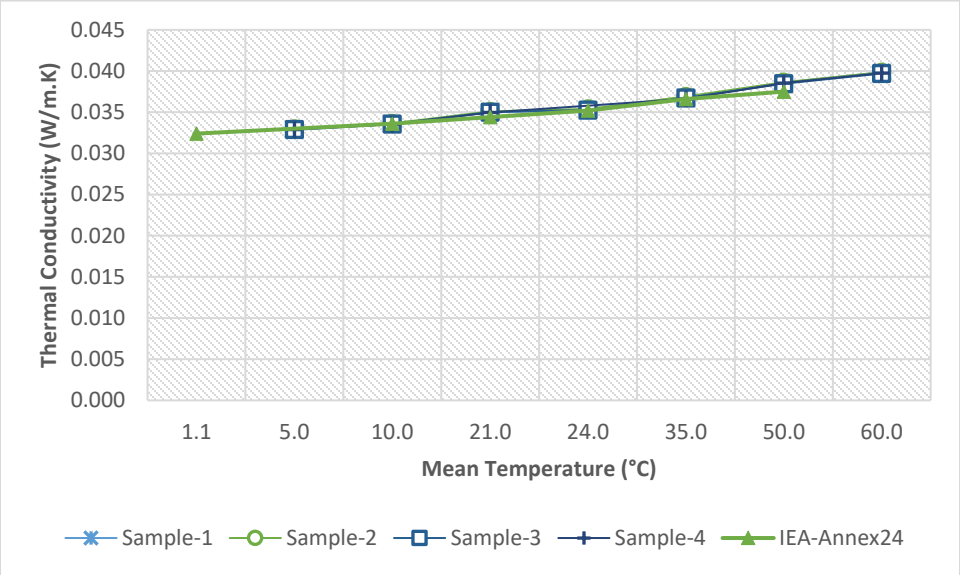

Figure 7-15. EPS-Thermal Conductivity.

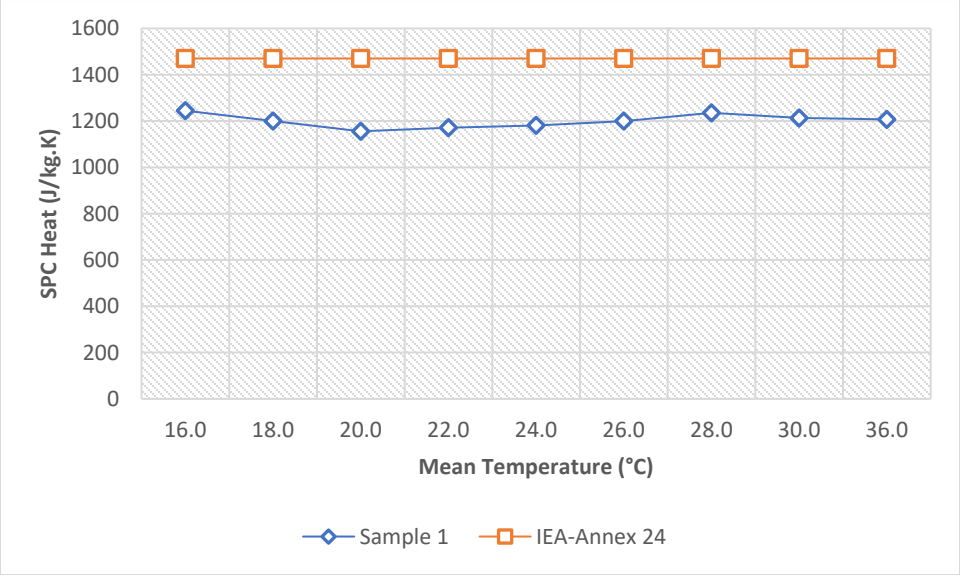

Figure 7-16. EPS-Specific Heat Capacity.

7.1.11 **Extruded Polystyrene (XPS)**

Analyzing the measured thermal conductivity of XPS samples at increasing steps of mean temperatures, we observed a coherence between all samples' results with an upward trend in k values by rising temperature. The results from this research noted to be in good agreement with the measured k values for XPS material from IEA-Annex 24 with operating temperature of 8.9°C.

Unlike the thermal conductivity measurements, the results for specific heat capacity for two samples of XPS presented a variation in values through all mean temperatures. The results were also lower compared with IEA-Annex 24 value for specific heat capacity of XPS.

Table 7-11. The measured density and thickness of the tested building material and the corresponding IEA-Annex 24 material.

Material	**Density (kg/m^3)**	**Thickness (mm)**
Extruded Polystyrene	26.6 ± 0.15	25.5
Extruded Polystyrene (IEA-Annex 24)	30.6	19.6

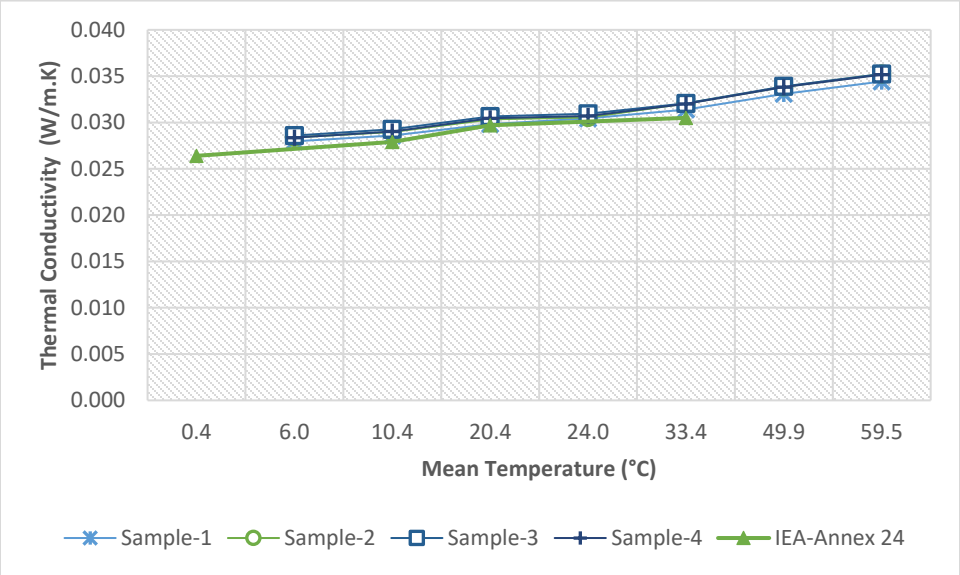

Figure 7-17. XPS-Thermal Conductivity.

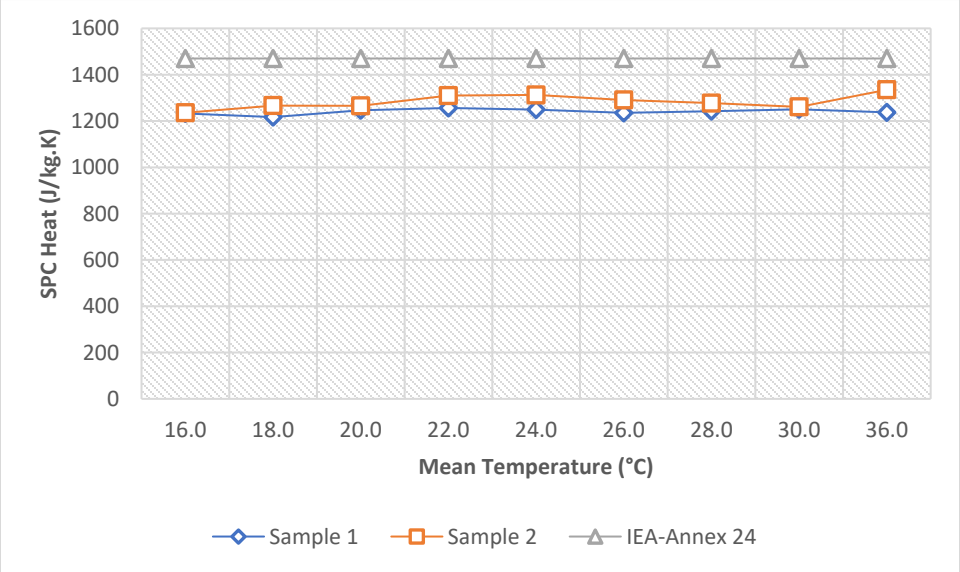

Figure 7-18. XPS-Specific Heat Capacity (J/kg.K).

7.1.12 **Open Cell Sprayed Polyurethane**

According to the measured thermal conductivity at different temperatures for open cell sprayed polyurethane insulation, the k value increased with temperature rise. The obtained results presented a similar upward trend for all three tested open-cell sprayed polyurethane samples. A good agreement was found with the RP-1018 results where their temperature difference was 22.15°C.

Table 7-12. The measured density and thickness of the tested building material and the corresponding RP-1018 material.

Material	**Density (kg/m^3)**	**Thickness (mm)**
Open Cell Spray polyurethane	14.75 ± 1.2	41.5
Low-Density Spray polyurethane (ASHRAE RP-1018)	8.4	19.7

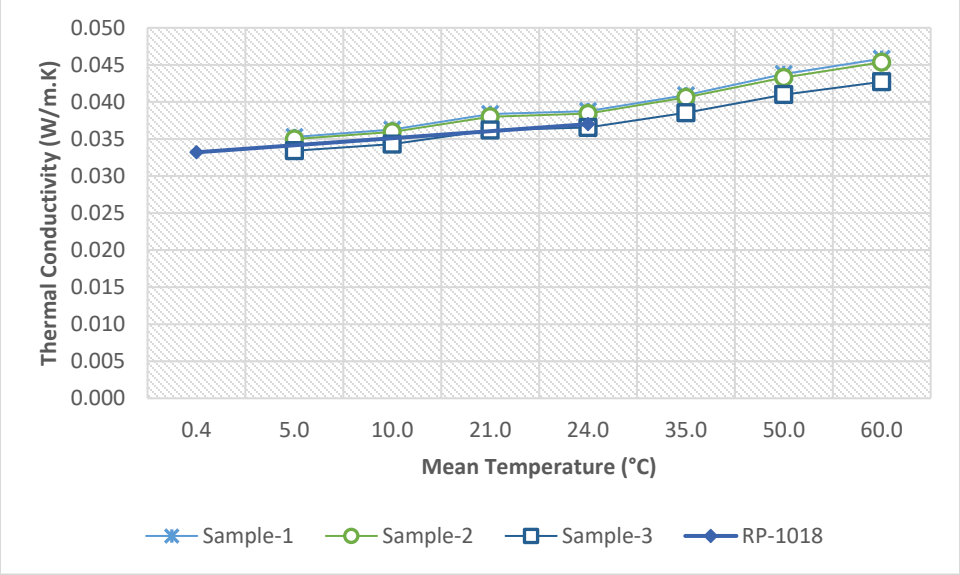

Figure 7-19. Open Cell Spray Polyurethane-Thermal Conductivity.

7.1.13 **Polyisocyanurate**

Unlike the other insulation materials, the thermal conductivity test for polyisocyanurate insulation board at different mean temperatures showed a non-linear trend with rising temperature. Through all four samples the thermal conductivity was observed to be lowest at 20.98°C while increased at lower and higher tested mean temperatures. This non-linear behavior of thermal conductivity is due to the existence of blowing agent inside the microstructure of polyisocyanurate. At lower temperatures, it starts condensing which determines the rise of conductivity (Berardi et al., 2018). However, the results presented in ASHRAE RP-1018 showed the thermal conductivity only for temperatures 23.99°C to 24.47°C with ΔT of 21.5°C, where they were in good agreement with the values for this project.

Similar to the thermal conductivity results, the specific heat capacity measurements revealed a decrease from lower temperatures to 22°C and an increase towards higher temperatures. IEA-Annex 24 however, reported a single value for the specific heat capacity which was slightly lower than all our measurement values.

Table 7-13. The measured density and thickness of the tested building material and the corresponding RP-1018 material.

Material	**Density (kg/m^3)**	**Thickness (mm)**
Polyisocyanurate	27.5 ± 0.16	25.4
Polyisocyanurate (ASHRAE RP-1018)	26.5 ± 0.2	68.58

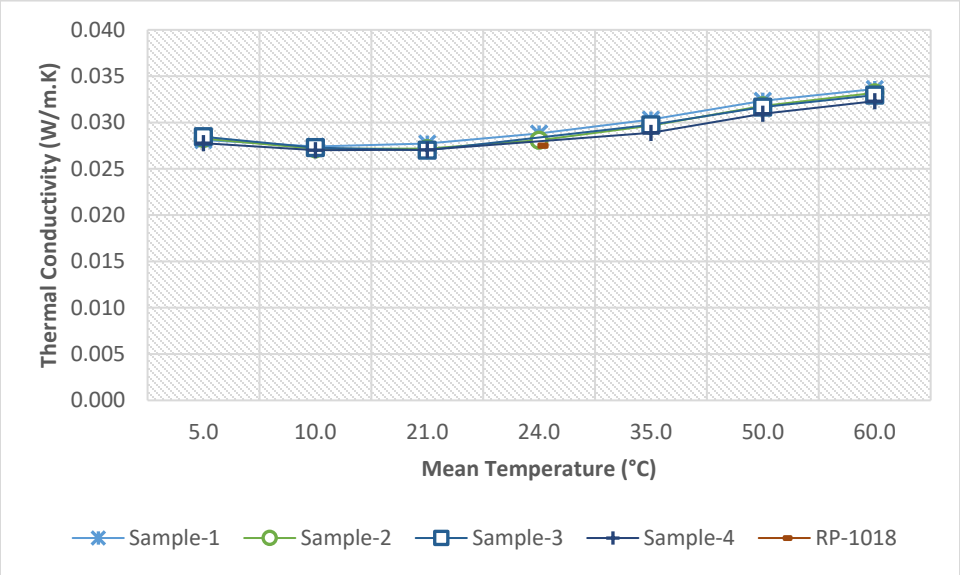

Figure 7-20. Polyisocyanurate-Thermal Conductivity.

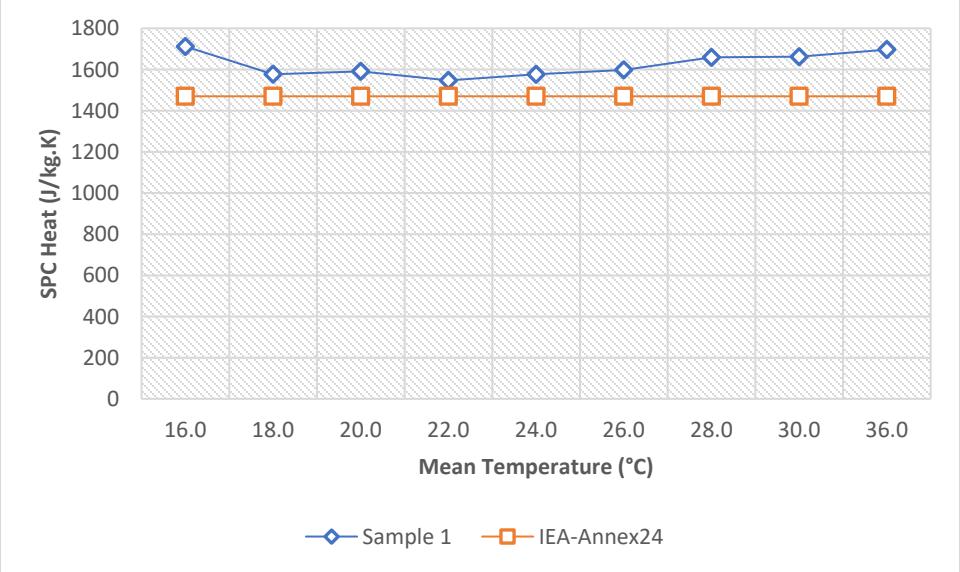

Figure 7-21. Polyisocyanurate-Specific Heat Capacity.

7.1.14 **Mineral Fiber (Stone Wool)**

The results of thermal conductivity measurements of mineral wool presented a rise in conductivity values when the mean temperature increased. Although our measured k values were slightly lower than the results from IEA-Annex24 (Kumaran, 1996b) operated with temperature difference of 22°C, a good coherence was observed between all samples with a similar upward trend IEA-Annex24 reported. The results of specific heat capacity measurements at different temperatures, showed small fluctuation with different trends upon rising temperature. There were two main deviation points through the measurements at temperatures 18.01°C and 28.02°C where the trend changed from decreasing to increasing at these temperatures in both tested samples. The results from IEA-Annex 24 indicated a single value which was slightly higher than our results at temperatures below 24.02°C.

Table 7-14. The measured density and thickness of the tested building material and the corresponding IEA-Annex 24 material.

Material	**Density (kg/m^3)**	**Thickness (mm)**
Mineral Fiber (Stone Wool)	128 ± 4	39.5
Mineral Fiber (IEA-Annex 24)	155	140

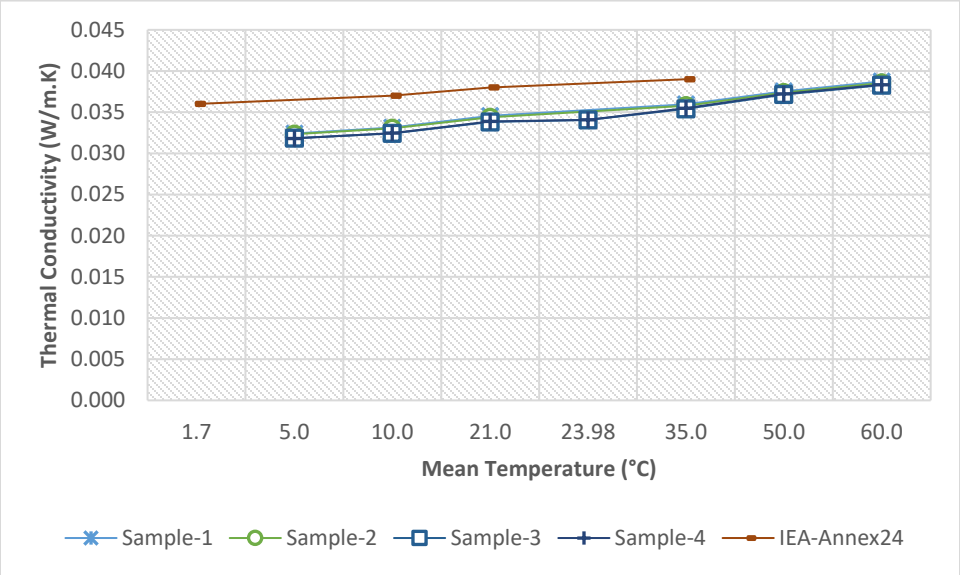

Figure 7-22. Mineral Fiber-Thermal Conductivity.

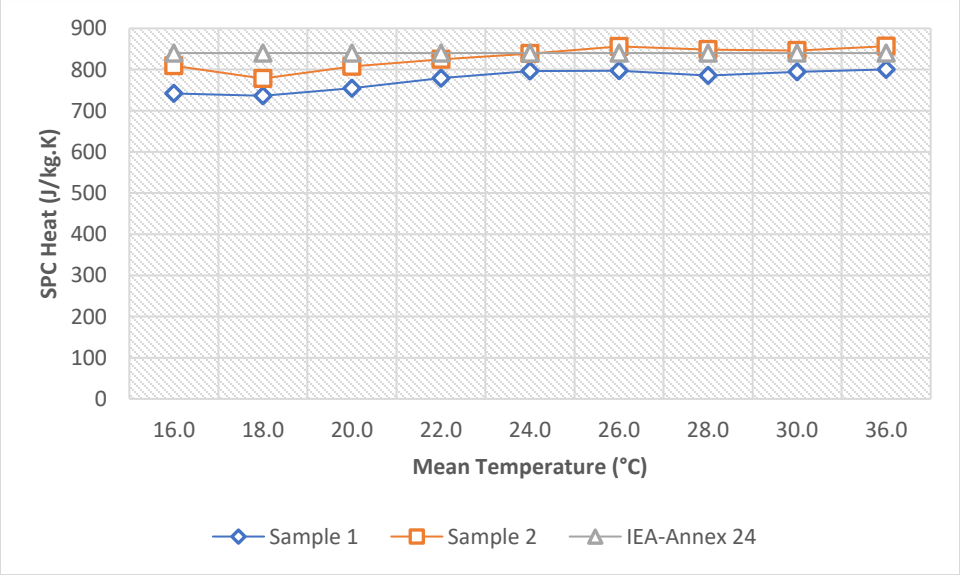

Figure 7-23. Mineral Fiber-Specific Heat Capacity.

7.1.15 **Summary**

Analyzing the results showed that the thermal conductivity in all materials increased with rising the mean temperature. Difference of measured thermal conductivities for different materials at lowest and highest mean temperatures are tabulated in Table 7-15. Similar to the thermal conductivity, the specific heat capacity of the materials increased with the mean temperature. Comparison of measured heat conductivities for different materials is presented in Figure 7-24. Results showed that regardless of the operating mean temperature, among all materials, stucco possessed the highest thermal conductivity as 0.544 (W/m.K) and polyisocyanurate had the lowest conductivity as 0.0272 (W/m.K). The tested building materials in this project can be classified in three categories including materials with high, medium and low thermal conductivities. Fiber cement, stucco and Densglass gold gypsum sheathing board with k value range between 0.1- 0.544 are determined as high conductive materials to heat. All wood and wood-based materials with k value range of 0.08-0.133 are noted to have a medium range of thermal conductivity. Eventually, all insulation building materials with k value range of 0.0272-0.0453 presented the lowest thermal conductivity under all operating temperatures. Among all tested materials, Densglass gold gypsum sheathing with 5% variation in measured k values at different temperatures noted to be less influenced by rising temperature while fiber cement with 103.3% increase appeared to be more impacted by temperature. During the tests I found that the apparatus performance was extremely sensitive and affected with numbers of factors including the level mean temperature itself in the apparatus and the surrounding environmental conditions (room temperature and relative humidity). The small discrepancies between some of our measured K values and RP-1018 results are within our expectation, as the density and composition of the tested building materials in both projects are different.

Table 7-15. Difference of measured thermal conductivities for different materials at different mean temperatures.

Material	Density (kg/m^3)	Thickness (mm)	Thermal conductivity within the measurement range (T_m 50°C – 60°C)		Thermal conductivity increase (%)
			Minimum	Maximum	
Claddings					
Fiber Cement Board	1358.1	7.7	0.105	0.213	**103.3**
Stucco	2399.5	25.9	0.441	0.544	**23.3**
Western Red Cedar	380	42.9	0.100	0.108	**8.7**
Wall Sheathing Boards					
OSB	620.7	11.4	0.080	0.091	**14.1**
Plywood	460.1	12.9	0.085	0.100	**17.1**
Densglass Gold Gypsum Sheathing	757	13.3	0.175	0.184	**5.0**
Wood Studs					
Spruce	469.8	37.3	0.117	0.125	**7.1**
Douglas Fir	567.1	36.2	0.125	0.133	**6.4**
Insulations					
Cellulose Fiber	57.6	48.7	0.038	0.045	**18.5**
Expanded Polystyrene (EPS)	21.1	24.5	0.033	0.040	**20.9**
Extruded Polystyrene (XPS)	25.5	25.5	0.028	0.035	**23.6**
Open Cell Spray polyurethane	14.75	41.5	0.035	0.045	**29.2**
Polyisocyanurate	27.8	25.4	0.027	0.033	**21.3**
Mineral Fiber (Stone Wool)	127.4	39.5	0.032	0.038	**19.9**

Figure 7-24. Comparison of measured heat conductivities for different tested building materials.

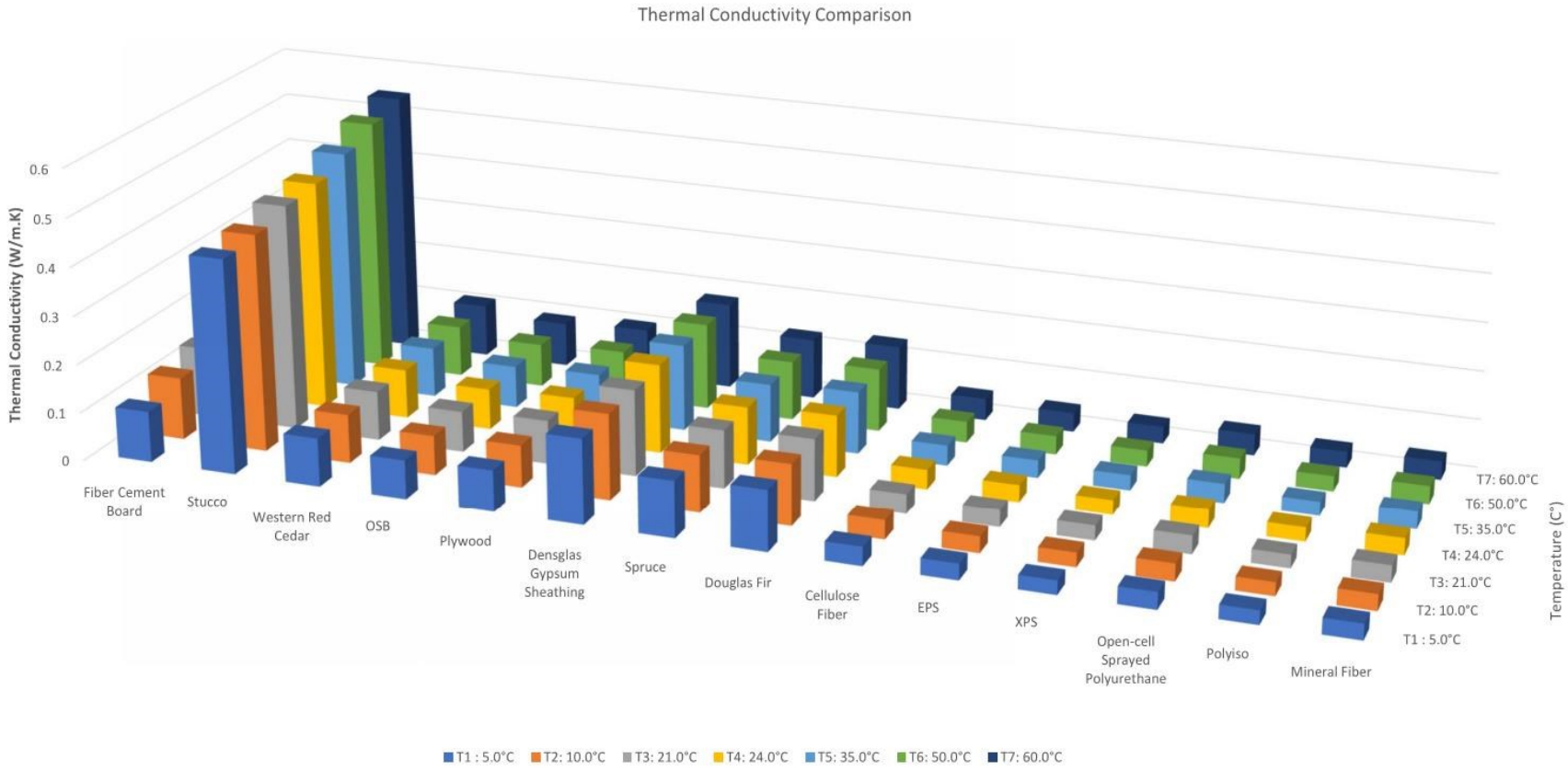

7.2 Adsorption Isotherms of Building Materials

The average equilibrium moisture content was gravimetrically determined after conditioning the samples at a relative humidity of 50%, 70% and 90% in each temperature. The average adsorption isotherms of each tested building material in three temperatures: 3°C, 21°C and 45°C are tabulated in a table. Accordingly, two graphs are plotted in which the influence of relative humidity and temperature on the equilibrium moisture content is evaluated for each material. Furthermore, the effects of variations in temperature and relative humidity are assessed quantitatively.

7.2.1 **Clay Brick**

The measured moisture contents within the hygroscopic range from 50% RH to 90% RH in all temperatures represented a rising with increasing RH. However, the increase in moisture content at higher relative humidities was more significant at temperatures 3°C and 45°C. The measured moisture content at temperature 45°C was lower than the other temperatures at all relative humidities tested. Analyzing the influence of temperature on moisture content showed that at the same relative humidity level, rising temperature led to lower moisture content. Additionally, more effect of temperature on moisture content was observed from 21°C to 45°C. The maximum increase in moisture content in brick samples influenced by relative humidity was observed as 96% between relative humidities 50% and 90% at temperature 45°C while the maximum decrease affected by temperature was noted to be -56% between temperatures of 3°C and 45°C at relative humidity of 50%.

In comparison with RP-1018, our results of sorption isotherms in brick samples at 21°C presented a good alignment at 50% RH. However, by increasing the relative humidity to 70% and 90%, our results projected lower and higher values than ASHRAE RP-1018, respectively. Given the fact of huge variability in brick samples depending on manufacturing and composition, the provided comparison in this study is for general reference as the two brick types are different.

Table 7-16. Clay Brick-Adsorption Isotherms at Different Temperatures and Relative Humidities.

Clay Brick-EMCs at Different Temperatures and Relative Humidities				Difference between RHs		
EMC at	**50% RH**	**70% RH**	**90% RH**	**70%-50%**	**90%-70%**	**90%-50%**
3°C	9.42E-04	1.05E-03	1.30E-03	12%	24%	38%
21°C	7.97E-04	1.02E-03	1.23E-03	28%	21%	55%
45°C	4.12E-04	4.96E-04	8.07E-04	20%	63%	96%
Difference between 21°C and 3°C	-15%	-3%	-5%			
Difference between 45°C and 21°C	-48%	-51%	-35%			
Difference between 45°C and 3°C	-56%	-53%	-38%			

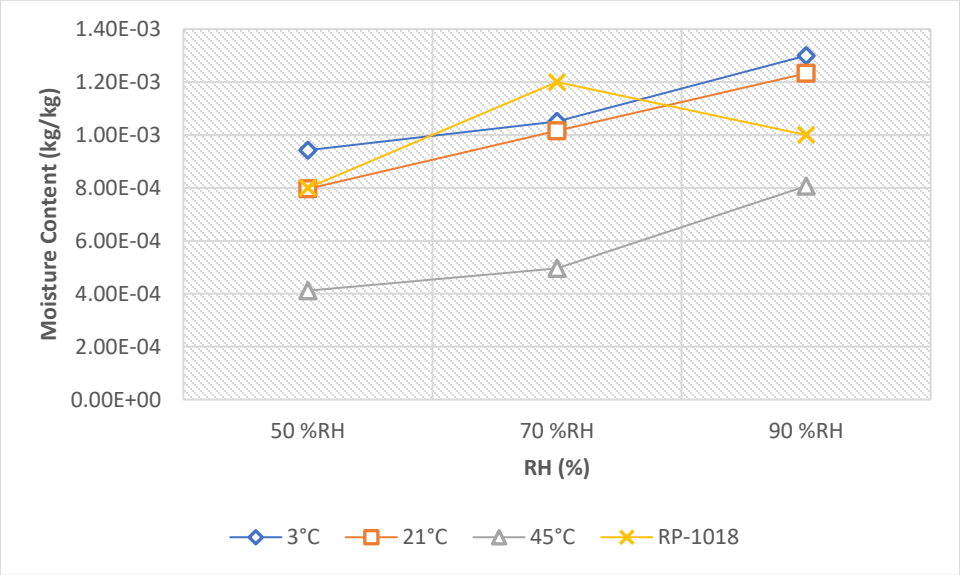

Figure 7-25. Effect of Relative Humidity on Adsorption Isotherms- Clay Brick.

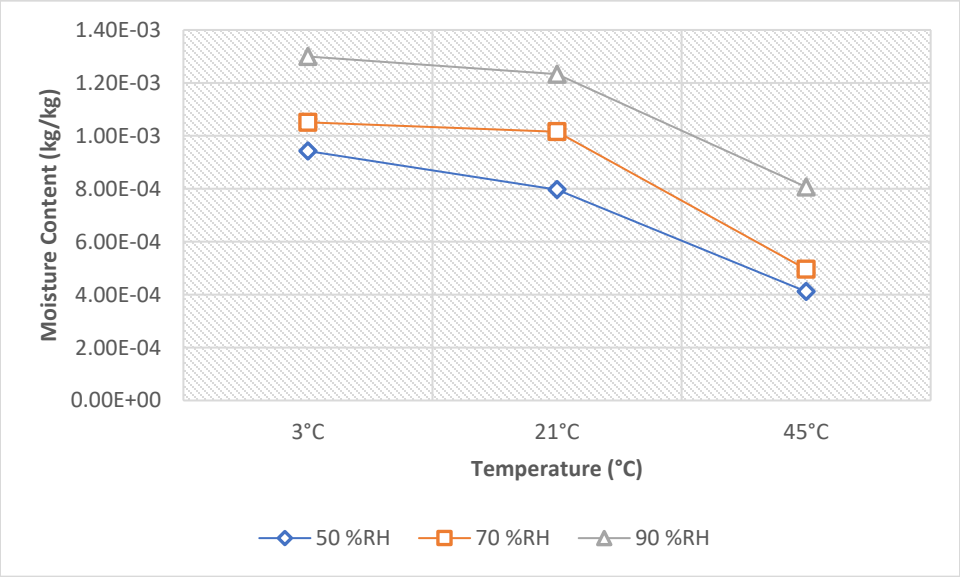

Figure 7-26. Effect of Temperature on Adsorption Isotherms- Clay Brick.

7.2.2 **Fiber Cement**

The measured moisture content of fiber cement samples exposed to different temperatures at three relative humidities revealed that their sorption increased and reduced with relative humidity and temperature, respectively. However, according to the influence of temperature was much lower than the relative humidity. The maximum increase in moisture content in fiber cement samples influenced by relative humidity was noted as 177% between relative humidities 50% and 90% at temperature 45°C while the maximum decrease affected by temperature was noted to be -22% between temperatures of 3°C and 45°C at relative humidity of 50%. We found a good correlation between our results of sorption isotherms measured at 21°C and the results from RP-1018 at relative humidities of 50% and 70% while at 90% RH we measured relatively lower.

Table 7-17. Fiber Cement-Adsorption Isotherms at Different Temperatures and Relative Humidities.

Fiber Cement-EMCs at Different Temperatures and Relative Humidities				**Difference between RHs**		
EMC at	**50% RH**	**70% RH**	**90% RH**	**70%-50%**	**90%-70%**	**90%-50%**
3°C	5.05E-02	6.28E-02	1.18E-01	24%	88%	134%
21°C	4.30E-02	5.78E-02	1.09E-01	34%	88%	153%
45°C	3.94E-02	5.74E-02	1.09E-01	46%	90%	177%
Difference between 21°C and 3°C	-15%	-8%	-8%			
Difference between 45°C and 21°C	-8%	-1%	0%			
Difference between 45°C and 3°C	-22%	-9%	-8%			

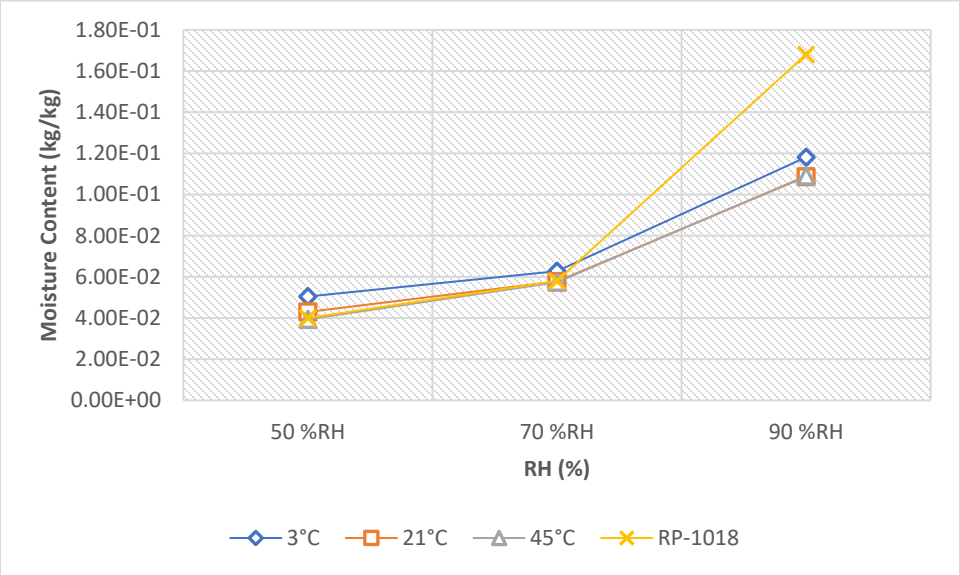

Figure 7-27. Effect of Relative Humidity on Adsorption Isotherms- Fiber Cement.

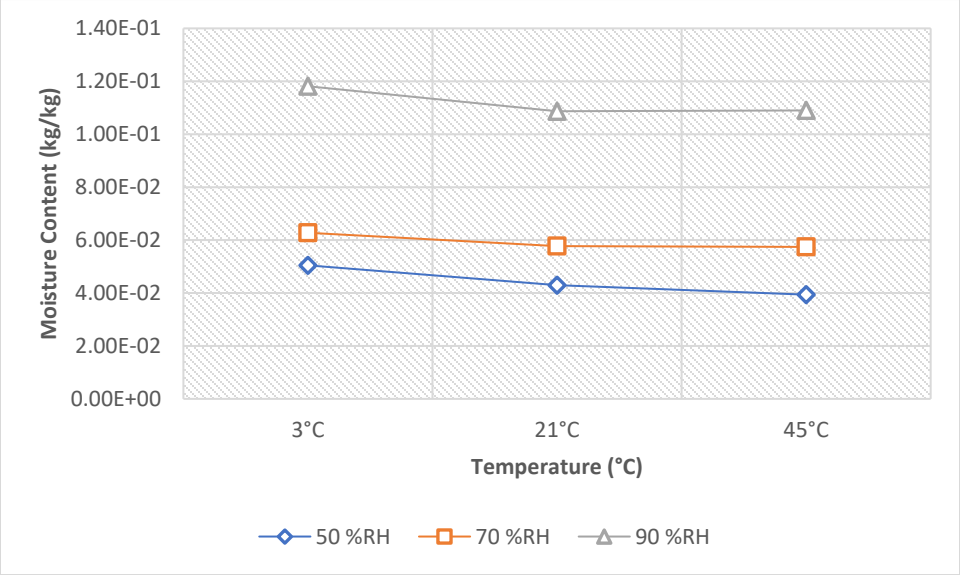

Figure 7-28. Effect of Temperature on Adsorption Isotherms- Fiber Cement.

7.2.3 **Stucco**

The measurements for equilibrium moisture content of stucco samples showed that while moisture content increased considerably at higher relative humidities, it decreased slightly with rising temperature. Based on the measurements, the moisture content of tested samples of stucco at 90% RH were higher than the measured values at 50% RH by a factor of 2-3. It is notable that the absorption process for cementitious product such as stucco and fiber cement board was rather time consuming compared to other materials. The maximum decrease in moisture content due to increasing the temperature from 3°C to 45°C was observed as -39% at relative humidity of 70% while the maximum increase in moisture content due to increasing relative humidity from 50°C to 90°C was observed as 116% at temperature of 21°C. Our recorded data for moisture content of stucco samples at temperature of 21°C showed a good alignment with the results from RP-1018.

Table 7-18. Stucco-Adsorption Isotherms at Different Temperatures and Relative Humidities.

Stucco-EMCs at Different Temperatures and Relative Humidities				**Difference between RHs**		
EMC at	**50% RH**	**70% RH**	**90% RH**	**70%-50%**	**90%-70%**	**90%-50%**
3°C	3.58E-02	5.36E-02	6.60E-02	50%	23%	84%
21°C	2.63E-02	3.78E-02	5.69E-02	44%	50%	116%
45°C	2.58E-02	3.27E-02	5.18E-02	27%	58%	101%
Difference between 21°C and 3°C	-27%	-29%	-14%			
Difference between 45°C and 21°C	-2%	-13%	-9%			
Difference between 45°C and 3°C	-28%	-39%	-22%			

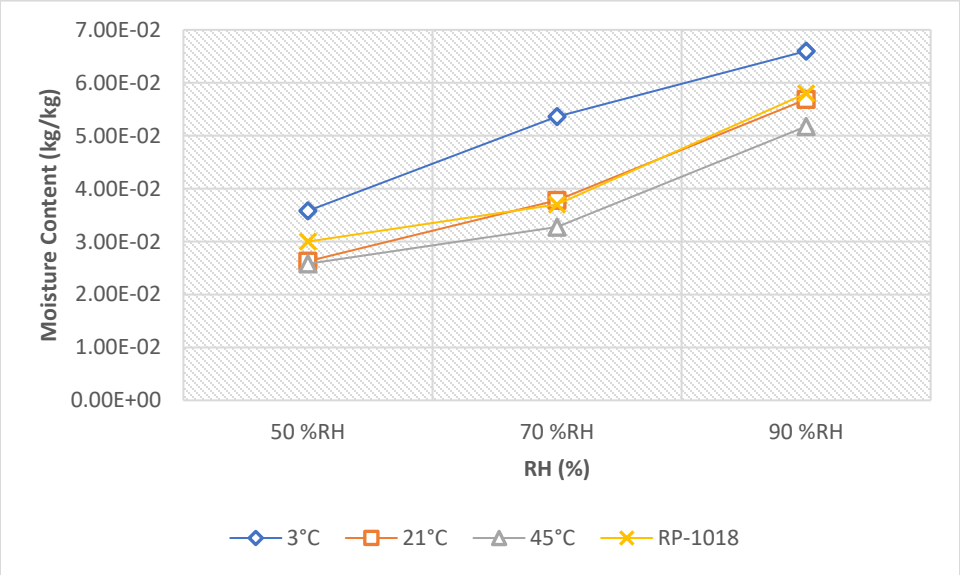

Figure 7-29. Effect of Relative Humidity on Adsorption Isotherms- Stucco.

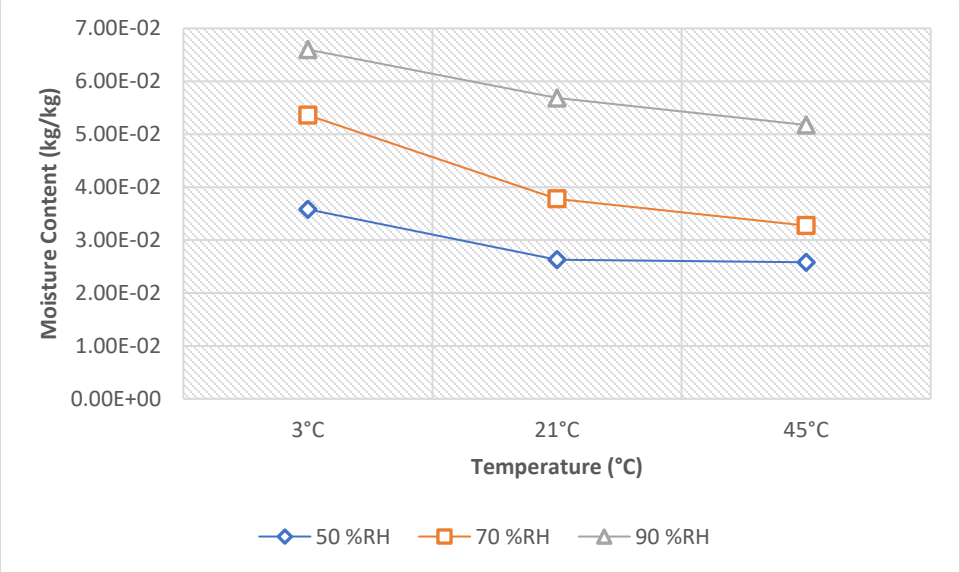

Figure 7-30. Effect of Temperature on Adsorption Isotherms- Stucco.

7.2.4 **Western Red Cedar**

The equilibrium moisture content of western red cedar samples decreased slightly with escalating temperature whereas increased significantly with relative humidity at each temperature set. The maximum increase in moisture content due to increasing relative humidity from 50C to 90C was observed as 146% at temperature of 45°C while the maximum decrease in moisture content due to increasing the temperature from 3°C to 45°C was observed as -15% at relative humidity of 50%. Our results of sorption isotherms at 21°C were higher through all tested relative humidities in comparison with RP-1018.

Table 7-19. Western Red Cedar-Adsorption Isotherms at Different Temperatures and Relative Humidities.

Western Red Cedar-EMCs at Different Temperatures and Relative Humidities				**Difference between RHs**		
EMC at	**50% RH**	**70% RH**	**90% RH**	**70%-50%**	**90%-70%**	**90%-50%**
3°C	6.65E-02	9.70E-02	1.49E-01	46%	54%	125%
21°C	6.15E-02	9.29E-02	1.48E-01	51%	60%	141%
45°C	5.68E-02	8.81E-02	1.40E-01	55%	59%	146%
Difference between 21°C and 3°C	-8%	-4%	-1%			
Difference between 45°C and 21°C	-8%	-5%	-6%			
Difference between 45°C and 3°C	-15%	-9%	-6%			

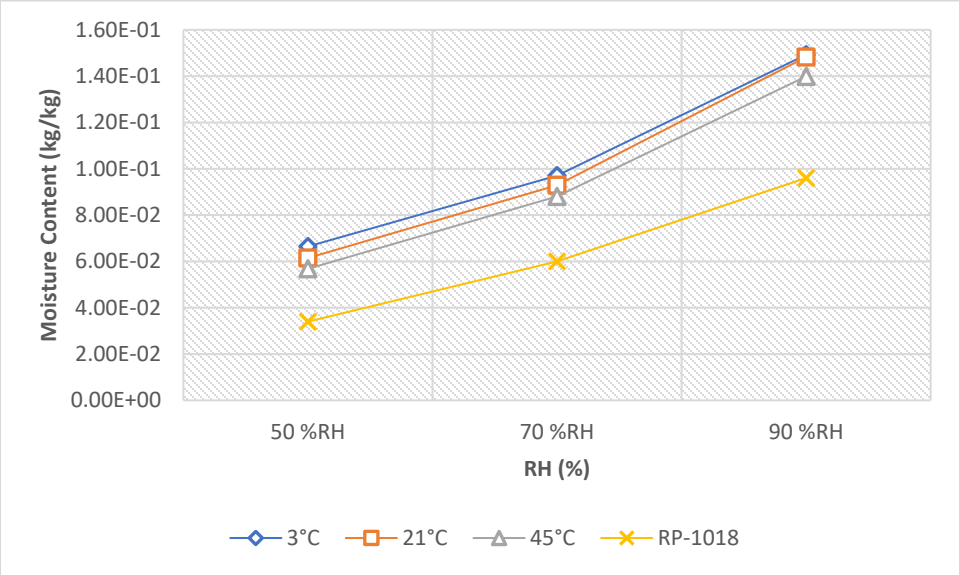

Figure 7-31. Effect of Relative Humidity on Adsorption Isotherms- Western Red Cedar.

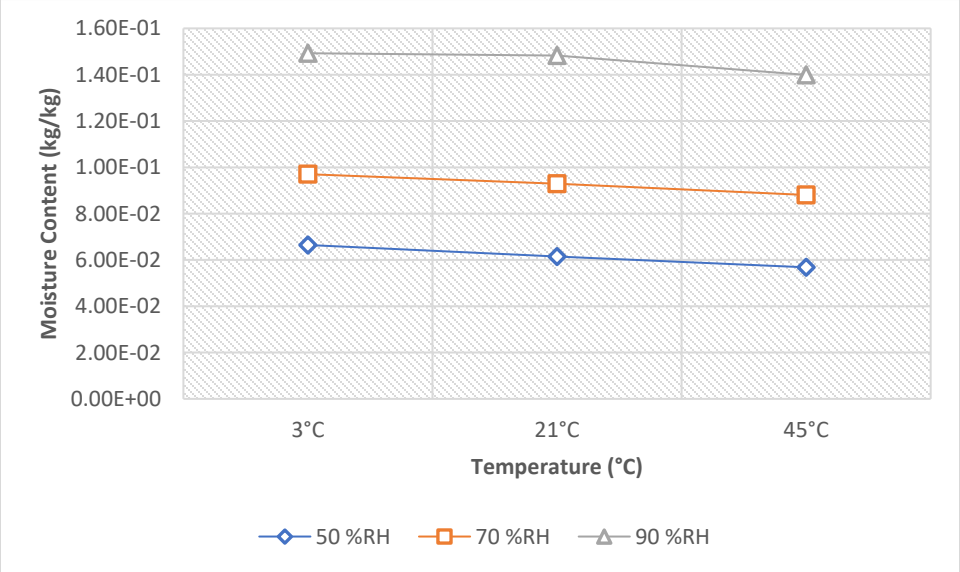

Figure 7-32. Effect of Temperature on Adsorption Isotherms- Western Red Cedar.

7.2.5 **60 Min Building Paper**

The measurement data for the sorption isotherm of 60-minute building paper at different temperature showed that influence of temperature on water vapor adsorption of building paper can be as high as the impact of relative humidity. According to the results, the moisture content of building paper samples at temperatures of 3°C and 21°C, increased significantly and linearly with the relative humidity while at temperature of 45°C, the changes were significantly higher at relative humidities above 50%. The maximum increase in moisture content due to increasing relative humidity from 50°C to 90°C was observed as 152% at temperature of 45°C while the maximum decrease in moisture content due to increasing the temperature from 3°C to 45°C was observed as -53% at relative humidity of 70%.

Comparing the moisture contents of building paper samples at the same relative humidity throughout different temperatures, the impact of temperature was observed to be considerably low at relative humidity of 90% between temperatures of 21°C and 45°C. There was no information pertinent to sorption isotherms of 60 min building paper in RP-1018 to compare with our measured results.

Table 7-20. 60 Min Building Paper -Adsorption Isotherms at Different Temperatures and Relative Humidities.

60 Min Building Paper -EMCs at Different Temperatures and Relative Humidities				**Difference between RHs**		
EMC at	**50% RH**	**70% RH**	**90% RH**	**70%-50%**	**90%-70%**	**90%-50%**
3°C	9.48E-02	1.20E-01	1.47E-01	27%	23%	56%
21°C	6.87E-02	8.57E-02	1.25E-01	25%	45%	81%
45°C	4.93E-02	5.66E-02	1.24E-01	15%	120%	152%
Difference between 21°C and 3°C	-28%	-29%	-16%			
Difference between 45°C and 21°C	-28%	-34%	0%			
Difference between 45°C and 3°C	-48%	-53%	-16%			

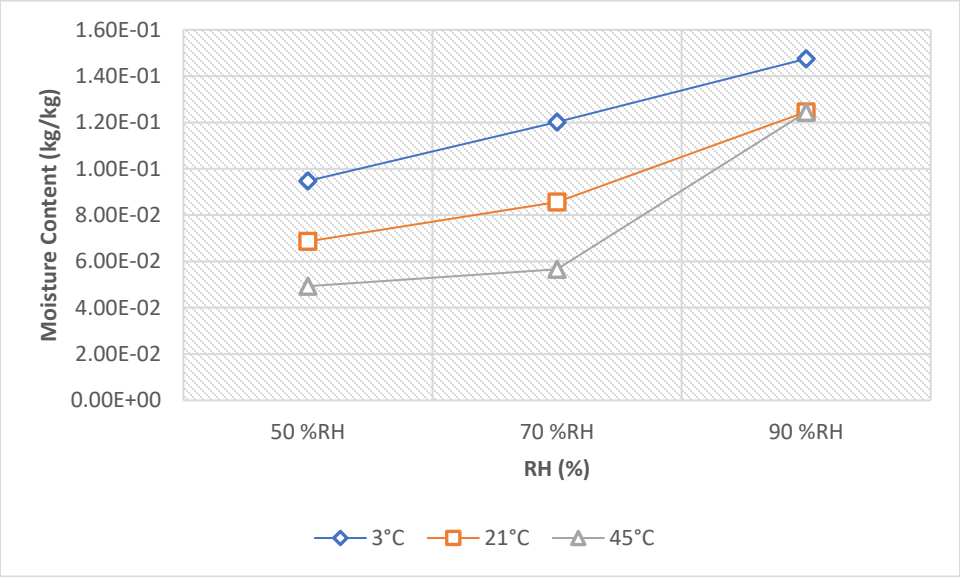

Figure 7-33. Effect of Relative Humidity on Adsorption Isotherms- 60 Min Building Paper.

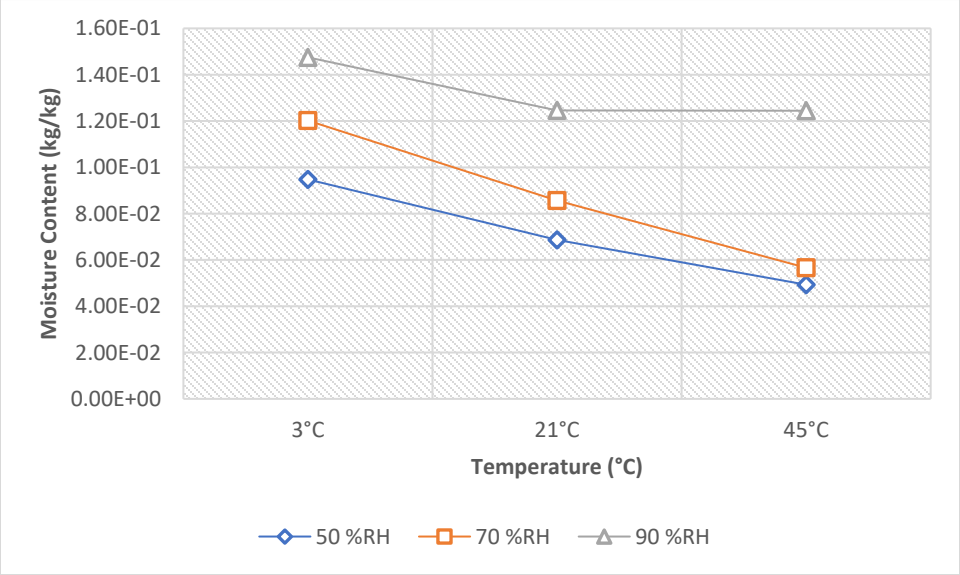

Figure 7-34. Effect of Temperature on Adsorption Isotherms- 60 Min Building Paper.

7.2.6 **Oriented Strand Board (OSB)**

According to the measured moisture contents for OSB samples in this project, the influence of temperature changes on sorption isotherms was observed to be less significant than relative humidity. By escalating the relative humidity from 50% to 70% and 90%, the sorption isotherm increased at least by the factor of 2 as the maximum increase was observed as 195% for temperature 21°C. However, analyzing the measured equilibrium moisture content of OSB samples at one relative humidity through different temperatures we observed a small decrease in sorption isotherm with rising the temperature since the maximum difference was -16% between 3°C and 45°C at 50% RH. A good agreement was observed comparing our measurements at temperature of 21°C with the results of RP-1018.

Table 7-21. OSB-Adsorption Isotherms at Different Temperatures and Relative Humidities.

OSB-EMCs at Different Temperatures and Relative Humidities				**Difference between RHs**		
EMC at	**50% RH**	**70% RH**	**90% RH**	**70%-50%**	**90%-70%**	**90%-50%**
3°C	6.42E-02	1.24E-01	1.72E-01	94%	38%	167%
21°C	5.38E-02	8.61E-02	1.59E-01	60%	84%	195%
45°C	5.38E-02	7.80E-02	1.58E-01	45%	102%	194%
Difference between 21°C and 3°C	-16%	-31%	-8%			
Difference between 45°C and 21°C	0%	-9%	0%			
Difference between 45°C and 3°C	-16%	-37%	-8%			

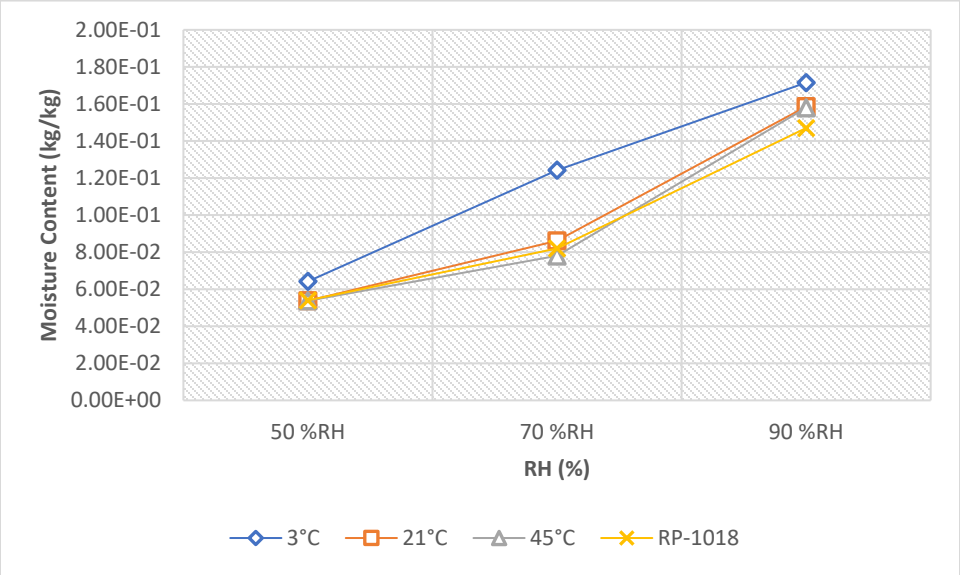

Figure 7-35. Effect of Relative Humidity on Adsorption Isotherms- OSB.

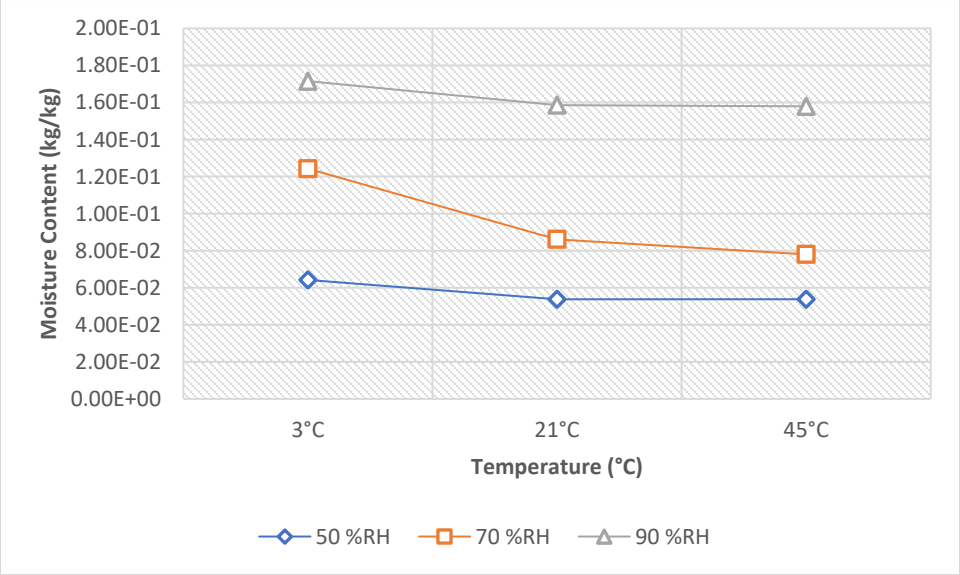

Figure 7-36. Effect of Temperature on Adsorption Isotherms- OSB.

7.2.7 **Plywood**

Analyzing the results for measured moisture contents of plywood samples showed that the sorption isotherms increased and decreased with rising relative humidity and temperature, respectively. Additionally, the impact of temperature was noted to be considerably lower than relative humidity. The maximum increase was observed as 168% between relative humidities 50% and 90% at temperature 45°C while the maximum decrease was noted to be -21% between temperatures of 3°C and 45°C at relative humidity of 50%.

Compared our measurements with the results from RP-1018 at the temperature 21°C, the differences observed to be very low and negligible.

Table 7-22. Plywood -Adsorption Isotherms at Different Temperatures and Relative Humidities.

Plywood -EMCs at Different Temperatures and Relative Humidities				**Difference between RHs**		
EMC at	**50% RH**	**70% RH**	**90% RH**	**70%-50%**	**90%-70%**	**90%-50%**
3°C	7.60E-02	9.36E-02	1.66E-01	23%	78%	119%
21°C	6.77E-02	9.28E-02	1.62E-01	37%	74%	139%
45°C	6.02E-02	8.30E-02	1.62E-01	38%	95%	168%
Difference between 21°C and 3°C	-11%	-1%	-3%			
Difference between 45°C and 21°C	-11%	-11%	0%			
Difference between 45°C and 3°C	-21%	-11%	-3%			

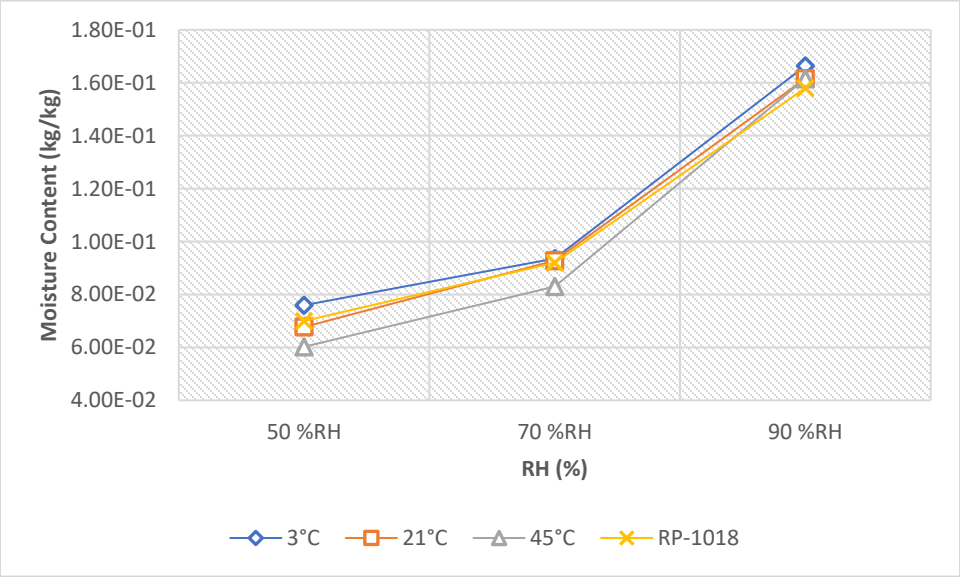

Figure 7-37. Effect of Relative Humidity on Adsorption Isotherms- Plywood.

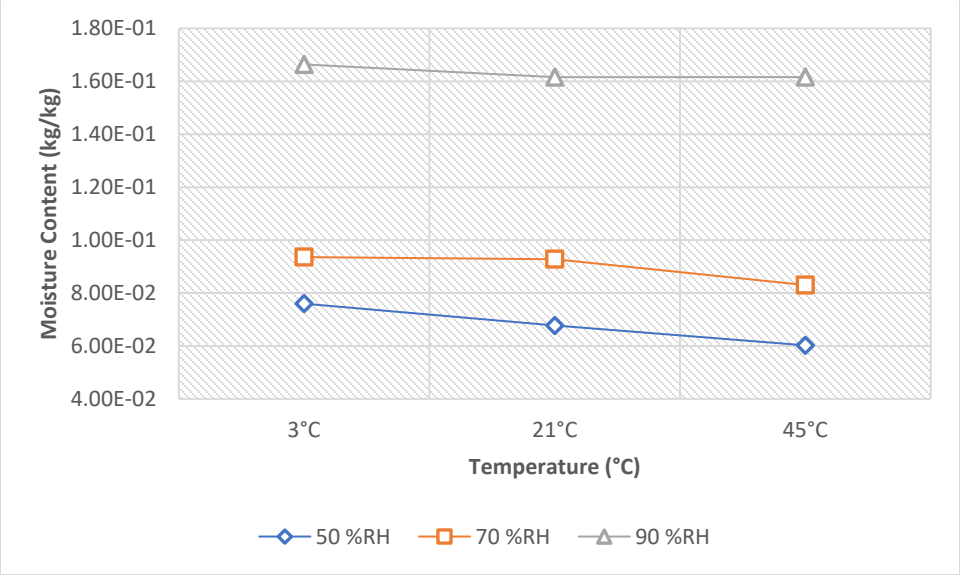

Figure 7-38. Effect of Temperature on Adsorption Isotherms- Plywood.

7.2.8 **Densglass Gold Gypsum Sheathing Board**

According to the measurements of the equilibrium moisture content in the samples of Densglass gypsum sheathing board, their sorption isotherms increased more significantly with relative humidity while decreased slightly when temperature rose. The highest increase in moisture content was observed as 492% for the rise of relative humidity from 50% to 90% at the temperature of 45°C. However, the maximum decrease in moisture content due to the rise in temperature from 3°C to 45°C was noted as -74% for relative humidity of 50%.

Comparing our measured results at 21°C with the associated results from RP-1018 for interior gypsum board, we obtained lower values for sorption isotherms for Densglass material samples expressing lower temperature impact.

Table 7-23. Densglass Gold Gypsum -Adsorption Isotherms at Different Temperatures and Relative Humidities.

Densglass Gold Gypsum -EMCs at Different Temperatures and Relative Humidities				**Difference between RHs**		
EMC at	**50% RH**	**70% RH**	**90% RH**	**70%-50%**	**90%-70%**	**90%-50%**
3°C	2.12E-03	2.59E-03	4.15E-03	22%	60%	96%
21°C	1.17E-03	2.10E-03	3.86E-03	79%	83%	229%
45°C	5.55E-04	1.19E-03	3.29E-03	114%	177%	492%
Difference between 21°C and 3°C	-45%	-19%	-7%			
Difference between 45°C and 21°C	-53%	-44%	-15%			
Difference between 45°C and 3°C	-74%	-54%	-21%			

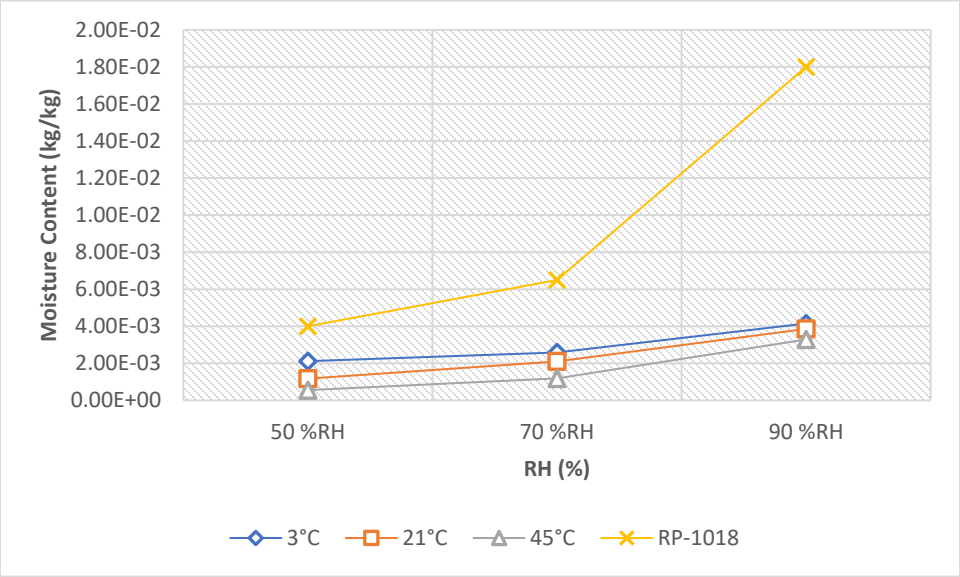

Figure 7-39. Effect of Relative Humidity on Adsorption Isotherms- Densglass Gold Gypsum.

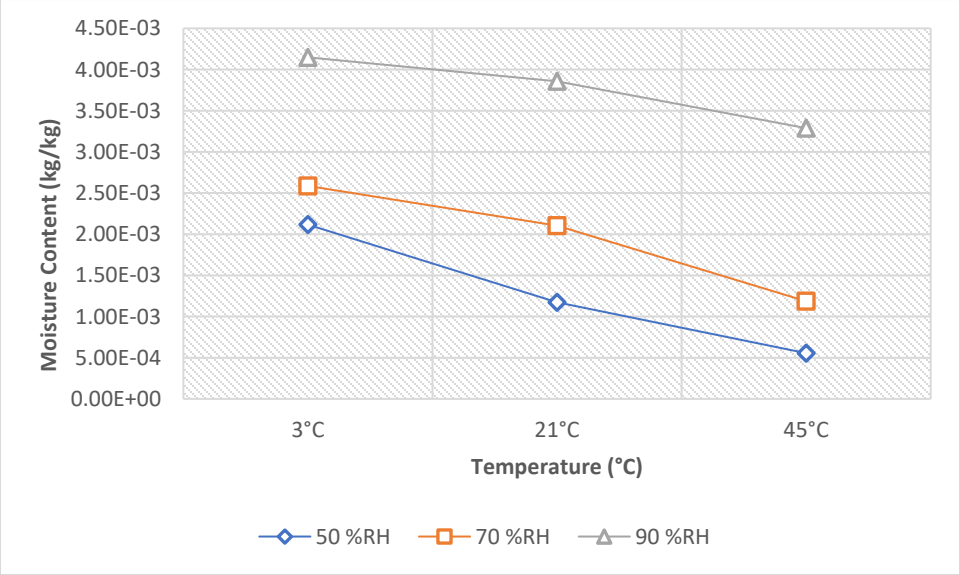

Figure 7-40. Effect of Temperature on Adsorption Isotherms- Densglass Gold Gypsum.

7.2.9 **Spruce**

The measured results for the moisture content of spruce samples at different temperature and relative humidities showed an increase with escalating the relative humidity and decrease with rising temperature. However, the influence of temperature was noted to be lower than the relative humidity as the maximum changes in moisture contents of our samples due to the rise in relative humidity and temperature was observed to be 148% at temperature 45°C and -20% at 50% RH, respectively.

In comparison with RP-1018 results, although the differences between our results at 21°C were insignificant, our results appeared to be slightly higher.

Table 7-24. Spruce -Adsorption Isotherms at Different Temperatures and Relative Humidities.

Spruce -EMCs at Different Temperatures and Relative Humidities				**Difference between RHs**		
EMC at	**50% RH**	**70% RH**	**90% RH**	**70%-50%**	**90%-70%**	**90%-50%**
3°C	8.91E-02	1.27E-01	1.92E-01	43%	51%	116%
21°C	7.88E-02	1.17E-01	1.88E-01	49%	60%	139%
45°C	7.13E-02	1.10E-01	1.77E-01	55%	60%	148%
Difference between 21°C and 3°C	-12%	-8%	-2%			
Difference between 45°C and 21°C	-9%	-6%	-6%			
Difference between 45°C and 3°C	-20%	-13%	-8%			

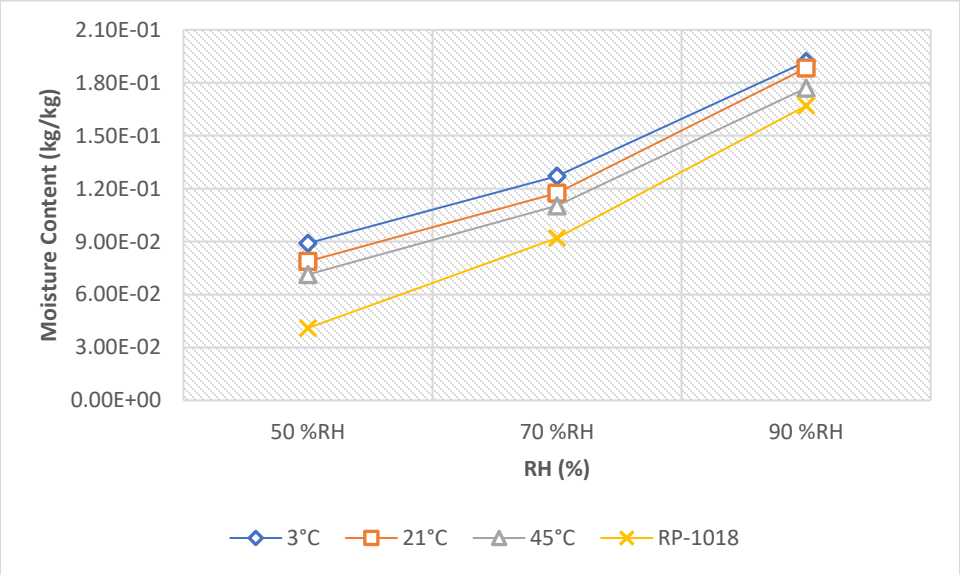

Figure 7-41. Effect of Relative Humidity on Adsorption Isotherms- Spruce.

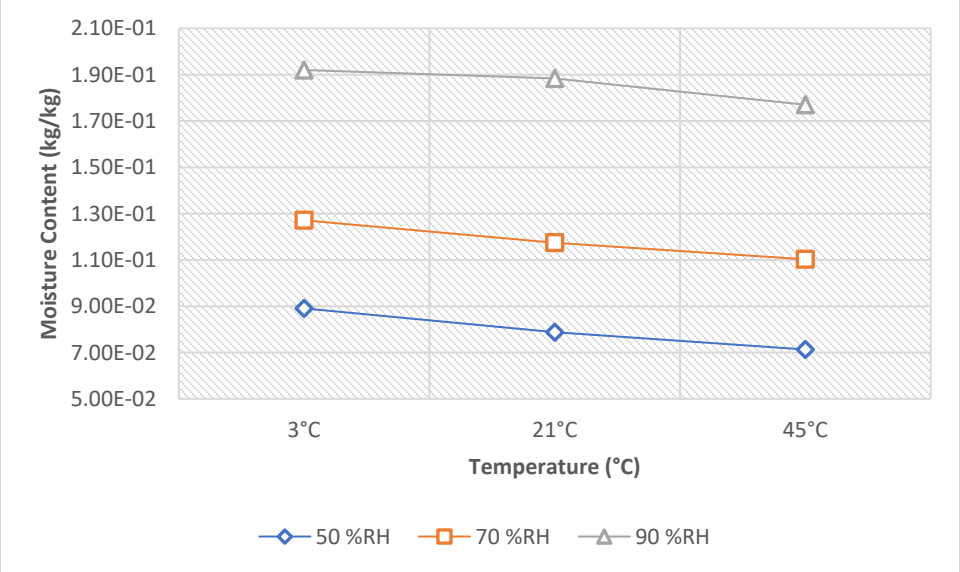

Figure 7-42. Effect of Temperature on Adsorption Isotherms- Spruce.

7.2.10 **Douglas Fir**

According to the measured moisture content of Douglas fir samples, the adsorption capacity of the tested samples was significantly increased with relative humidity while decreased a little with temperature. The maximum decrease in moisture content due to the rise in temperature from 3°C to 45°C was observed as -30% at relative humidity of 50% and the highest increase in moisture content was noted as 138% for the rise of relative humidity from 50% to 90% at the temperature of 45°C. There was no information pertinent to Douglas fir wood in RP-1018 to compare with our measured results.

Table 7-25. Douglas Fir -Adsorption Isotherms at Different Temperatures and Relative Humidities.

Douglas Fir -EMCs at Different Temperatures and Relative Humidities				**Difference between RHs**		
EMC at	**50% RH**	**70% RH**	**90% RH**	**70%-50%**	**90%-70%**	**90%-50%**
3°C	1.04E-01	1.41E-01	2.04E-01	36%	45%	97%
21°C	7.85E-02	1.17E-01	1.82E-01	49%	56%	132%
45°C	7.22E-02	1.04E-01	1.72E-01	43%	66%	138%
Difference between 21°C and 3°C	-24%	-17%	-11%			
Difference between 45°C and 21°C	-8%	-12%	-6%			
Difference between 45°C and 3°C	-30%	-27%	-16%			

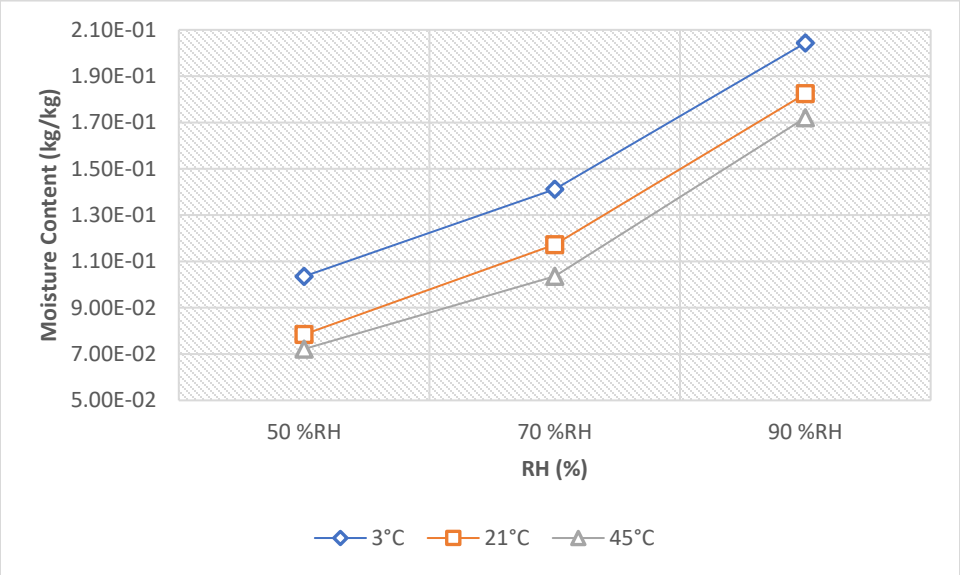

Figure 7-43. Effect of Relative Humidity on Adsorption Isotherms- Douglas Fir.

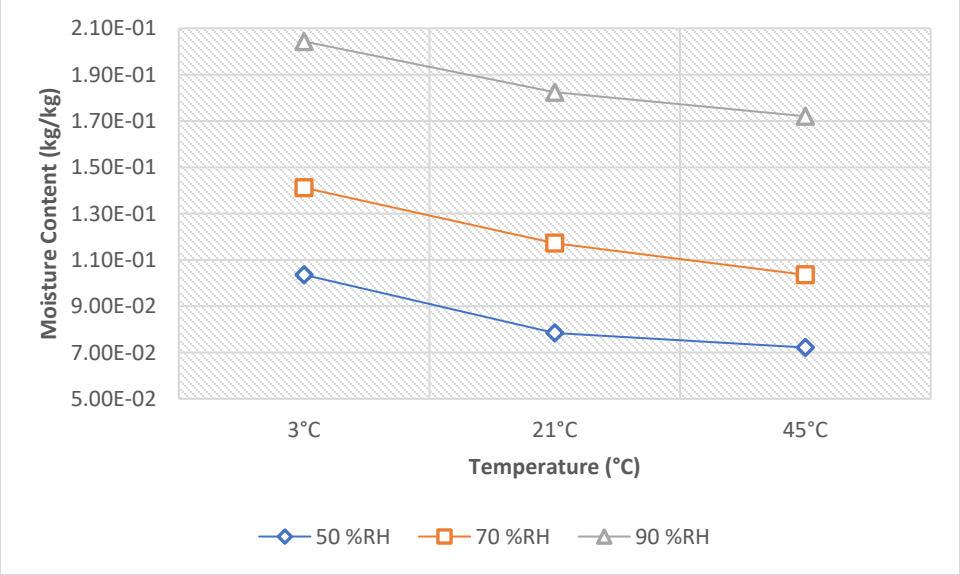

Figure 7-44. Effect of Temperature on Adsorption Isotherms- Douglas Fir.

7.2.11 **Cellulose Fiber**

Due to the time constraint, we were not able to run the sorption isotherm test at temperature 45°C. Therefore, our analysis is limited to temperatures of 3°C and 21°C. The obtained results of moisture content in cellulose fiber samples showed an increase in water vapor sorption capacity of cellulose insulation at higher relative humidities while it expressed a decrease with rising temperature from 3°C to 21°C. Our results indicated a maximum increase of 126% between 50% and 90% RH at temperature 21°C. Accordingly, the maximum decrease was observed as -45% when the temperature rose from 3°C to 21°C.

Comparing our sorption measurements at 21°C with the corresponding results from RP-1018 for cellulose fiber insulation, we obtained a slightly higher values at 50% RH and 70% RH and lower value at 90% RH.

Table 7-26. Cellulose Fiber -Adsorption Isotherms at Different Temperatures and Relative Humidities.

Cellulose Fiber -EMCs at Different Temperatures and Relative Humidities				**Difference between RHs**		
EMC at	**50% RH**	**70% RH**	**90% RH**	**70%-50%**	**90%-70%**	**90%-50%**
3°C	1.61E-01	1.70E-01	2.20E-01	6%	30%	37%
21°C	8.89E-02	1.25E-01	2.01E-01	41%	61%	126%
Difference between 21°C and 3°C	-45%	-26%	-8%			

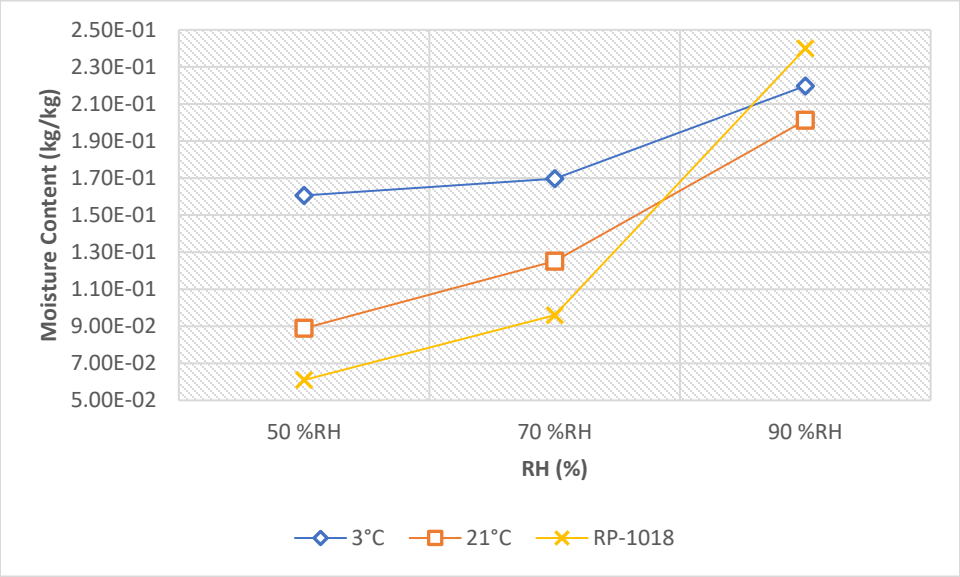

Figure 7-45. Effect of Relative Humidity on Adsorption Isotherms- Cellulose Fiber.

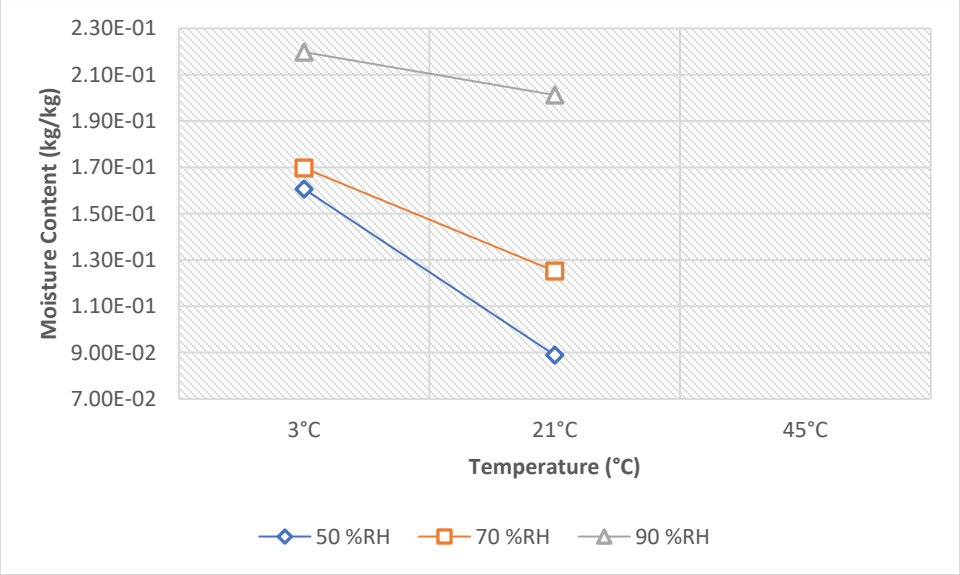

Figure 7-46. Effect of Temperature on Adsorption Isotherms- Cellulose Fiber.

7.2.12 **Expanded Polystyrene (EPS)**

Similar to other tested building materials in this project, the measured moisture content for EPS showed an increase with relative humidity rises and decrease with temperature. It was noted that the influence of changes in relative humidity was more pronounced at temperature of 45°C as the moisture content of EPS samples increased by 183%, 70 and 383% due to increasing relative humidity from 50% to 70% and 90%, respectively. In contrast with the RP-1018 results at temperature of 21°C which showed a downward trend in the sorption isotherm graph, our results represented an upward trend. However, a good correlation between the sorption isotherm values was observed at 70% RH.

Table 7-27. EPS-Adsorption Isotherms at Different Temperatures and Relative Humidities.

EPS-EMCs at Different Temperatures and Relative Humidities				**Difference between RHs**		
EMC at	**50% RH**	**70% RH**	**90% RH**	**70%-50%**	**90%-70%**	**90%-50%**
3°C	6.08E-03	6.40E-03	7.37E-03	5%	15%	21%
21°C	2.87E-03	3.02E-03	3.66E-03	5%	21%	27%
45°C	3.50E-04	9.91E-04	1.69E-03	183%	70%	383%
Difference between 21°C and 3°C	-53%	-53%	-50%			
Difference between 45°C and 21°C	-88%	-67%	-54%			
Difference between 45°C and 3°C	-94%	-85%	-77%			

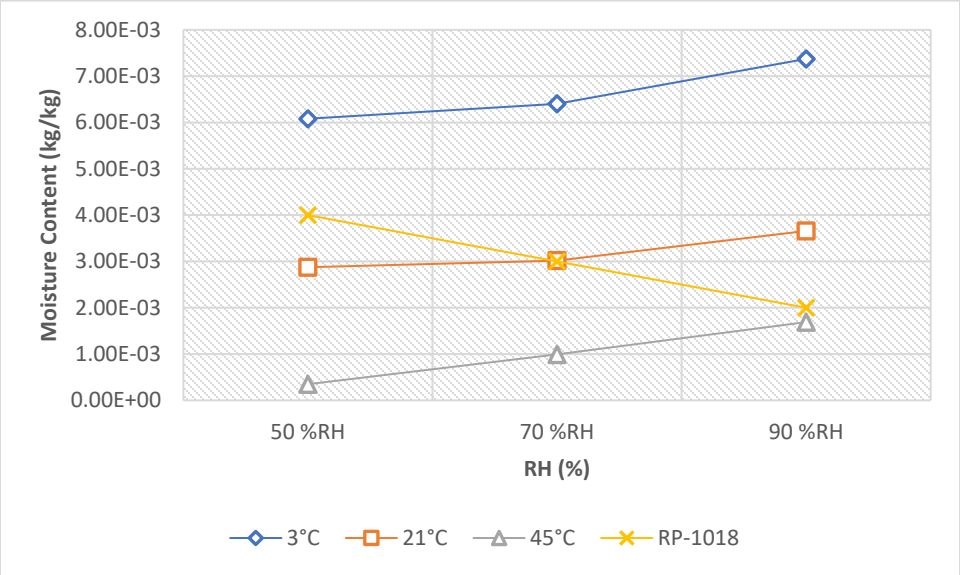

Figure 7-47. Effect of Relative Humidity on Adsorption Isotherms- EPS.

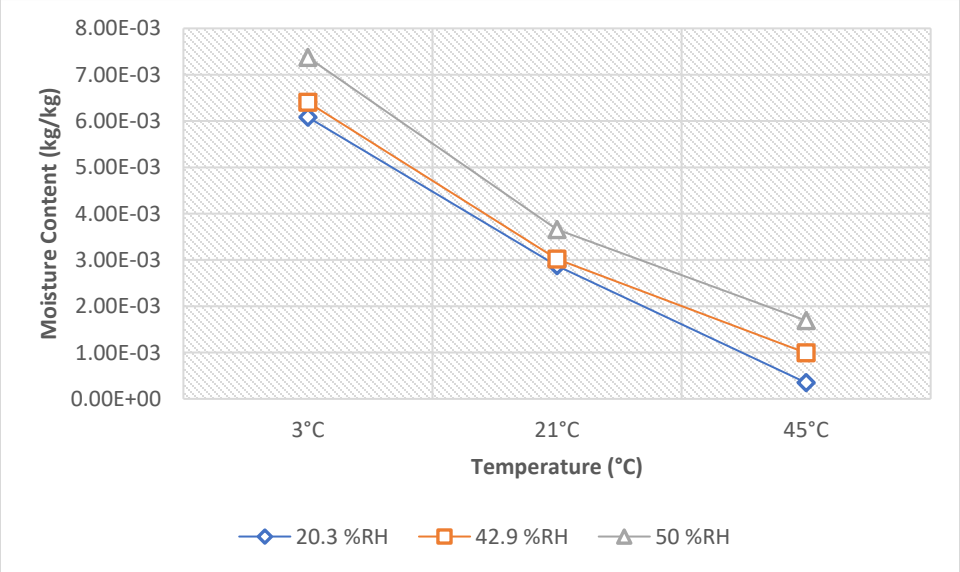

Figure 7-48. Effect of Temperature on Adsorption Isotherms- EPS.

7.2.13 **Extruded Polystyrene (XPS)**

According to the measured moisture content of XPS at different conditions of different temperatures and relative humidities, the sorption isotherms increased with relative humidity and decreased very slightly with temperature. The maximum decrease in moisture content due to the rise in temperature from 3°C to 45°C was observed as -12% at relative humidity of 90% and the highest increase in moisture content due to the rise of relative humidity from 50% to 90% was noted as 52% for at the temperature of 45°C.

Comparing our measurements at temperature 21°C, we found that they were higher than the results from RP-1018 where the difference was more considerable at higher relative humidities.

Table 7-28. XPS-Adsorption Isotherms at Different Temperatures and Relative Humidities.

XPS-EMCs at Different Temperatures and Relative Humidities				**Difference between RHs**		
EMC at	**50% RH**	**70% RH**	**90% RH**	**70%-50%**	**90%-70%**	**90%-50%**
3°C	9.70E-03	1.08E-02	1.34E-02	11%	24%	38%
21°C	9.29E-03	1.01E-02	1.18E-02	8%	17%	27%
45°C	6.97E-03	9.19E-03	1.06E-02	32%	15%	52%
Difference between 21°C and 3°C	-4%	-7%	-12%			
Difference between 45°C and 21°C	-25%	-9%	-10%			
Difference between 45°C and 3°C	-28%	-15%	-21%			

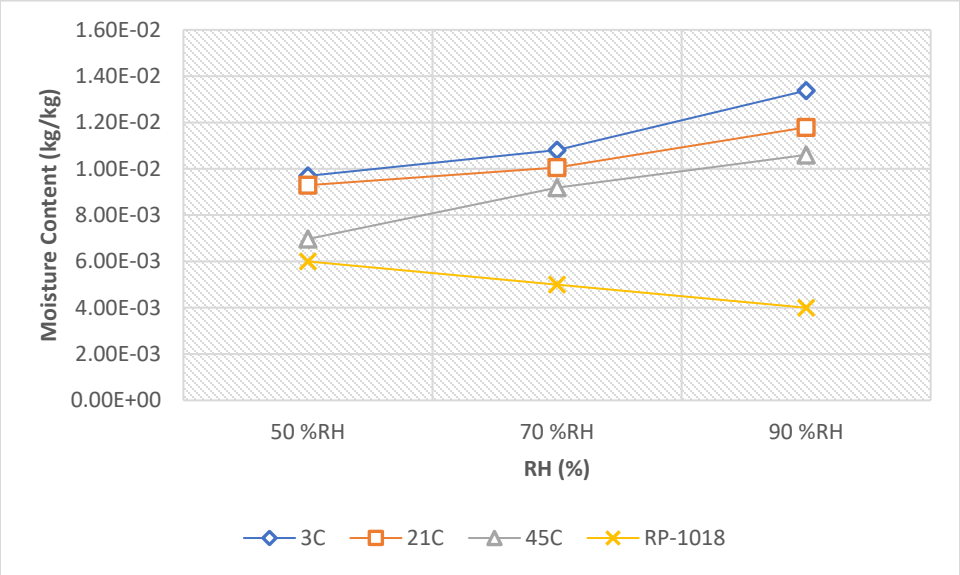

Figure 7-49. Effect of Relative Humidity on Adsorption Isotherms- XPS.

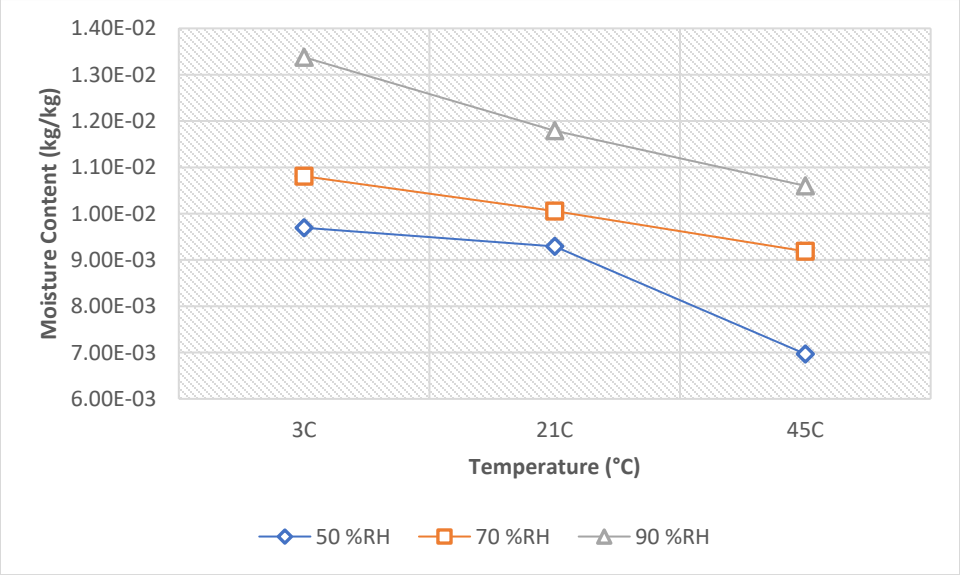

Figure 7-50. Effect of Temperature on Adsorption Isotherms- XPS.

7.2.14 **Open Cell Sprayed Polyurethane**

Analyzing the obtained data from the moisture content measurements of open cell sprayed polyurethane foam at different temperature sets represented an increase and decrease with escalating relative humidity and temperature, respectively. Based on our measurements, it appeared that higher relative humidities had more impact on water vapor sorption characteristics of open cell polyurethane foam while temperatures below 21°C had the highest influence. Additionally, the results showed that the water vapor adsorption capacity in open cell sprayed foam from 50% to 90% RH was significantly higher at 3°C (127%) which was approximately 21 times higher than the measurement values from 45°C (6%). The maximum decease in moisture content due to increasing the temperature from 3°C to 45°C was observed as -54% at relative humidity of 90%. In general, our measured values at temperature 21°C were higher than the corresponding results from RP-1018.

Table 7-29. Open Cell Sprayed Polyurethane -Adsorption Isotherms at Different Temperatures and Relative Humidities.

Open Cell Sprayed Polyurethane -EMCs at Different Temperatures and Relative Humidities				**Difference between RHs**		
EMC at	**50% RH**	**70% RH**	**90% RH**	**70%-50%**	**90%-70%**	**90%-50%**
3°C	3.56E-02	5.35E-02	8.07E-02	50%	51%	127%
21°C	3.23E-02	3.64E-02	3.70E-02	13%	2%	14%
45°C	2.10E-02	2.15E-02	2.22E-02	3%	3%	6%
Difference between 21°C and 3°C	-9%	-32%	-54%			
Difference between 45°C and 21°C	-35%	-41%	-40%			
Difference between 45°C and 3°C	-41%	-60%	-73%			

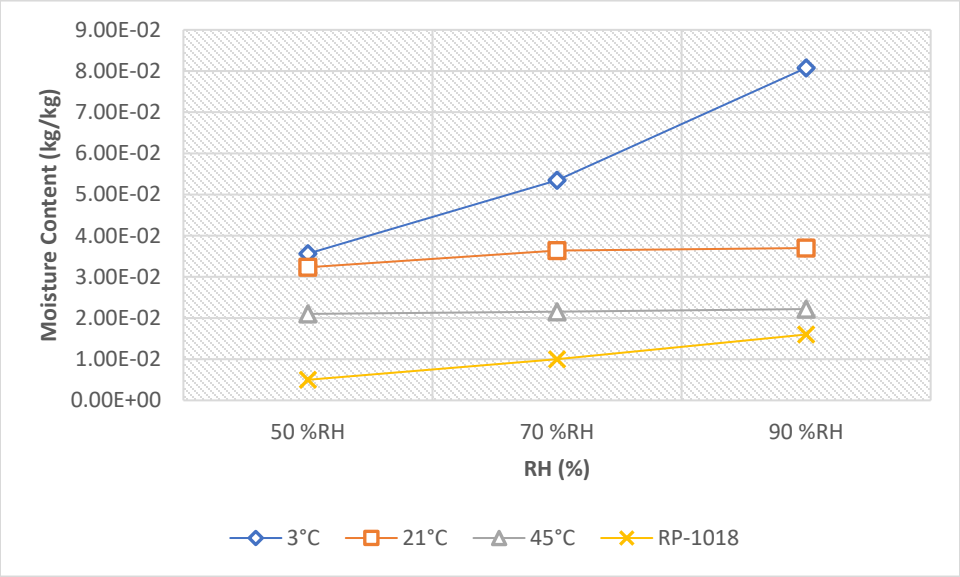

Figure 7-51. Effect of Relative Humidity on Adsorption Isotherms- Open Cell Sprayed Polyurethane.

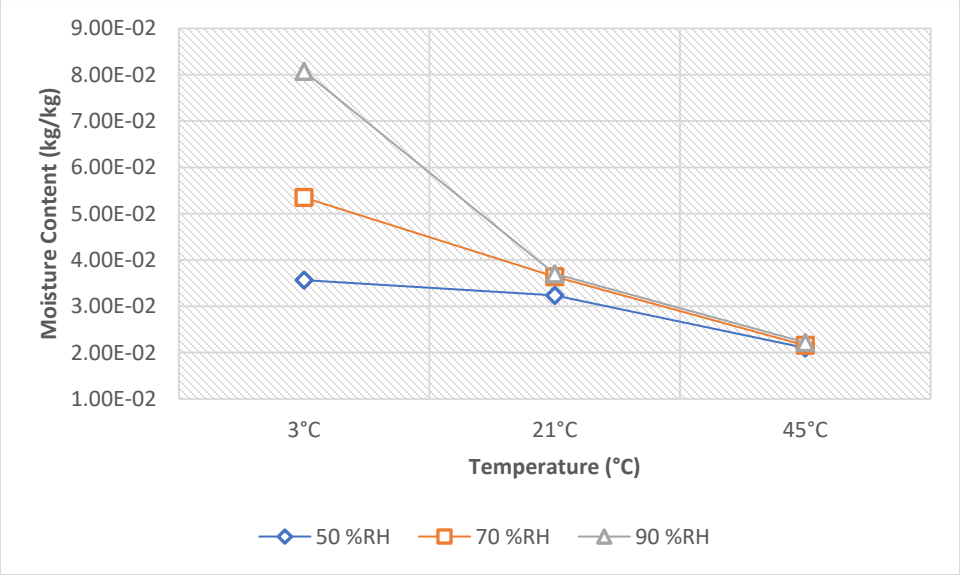

Figure 7-52. Effect of Temperature on Adsorption Isotherms- Open Cell Sprayed Polyurethane.

7.2.15 **Polyisocyanurate**

The obtained sorption isotherm from the measurements of moisture content of Polyisocyanurate insulation samples at different temperatures and relative humidities, revealed a considerable increase at higher relative humidities and a slight decrease with rising temperature. The maximum decrease in moisture content due to increasing the temperature from 3°C to 45°C was observed as -23% at relative humidity of 50% while the maximum increase in moisture content due to increasing relative humidity from 50°C to 90°C was observed as 202% at temperature of 21°C.

Our measurements at temperature 21°C appeared to be lower at relative humidities 50% RH and 70% RH and with a good agreement at 90% RH compared to the results from RP-1018.

Table 7-30. Polyisocyanurate-Adsorption Isotherms at Different Temperatures and Relative Humidities.

Polyisocyanurate-EMCs at Different Temperatures and Relative Humidities				**Difference between RHs**		
EMC at	**50% RH**	**70% RH**	**90% RH**	**70%-50%**	**90%-70%**	**90%-50%**
3°C	9.06E-03	1.10E-02	2.23E-02	22%	102%	146%
21°C	7.01E-03	1.09E-02	2.12E-02	56%	94%	202%
45°C	5.44E-03	8.98E-03	1.48E-02	65%	65%	172%
Difference between 21°C and 3°C	-23%	-1%	-5%			
Difference between 45°C and 21°C	-22%	-18%	-30%			
Difference between 45°C and 3°C	-40%	-19%	-34%			

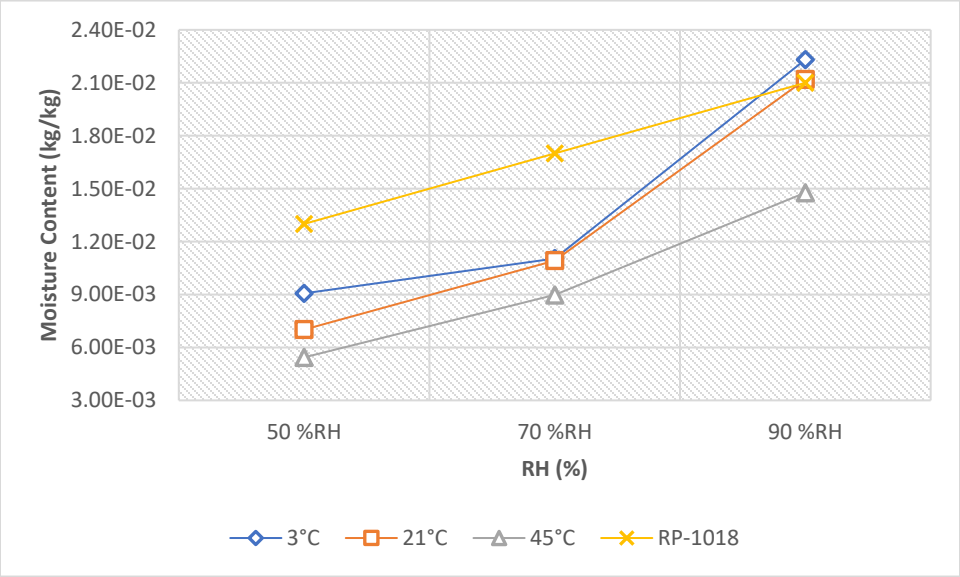

Figure 7-53. Effect of Relative Humidity on Adsorption Isotherms- Polyisocyanurate.

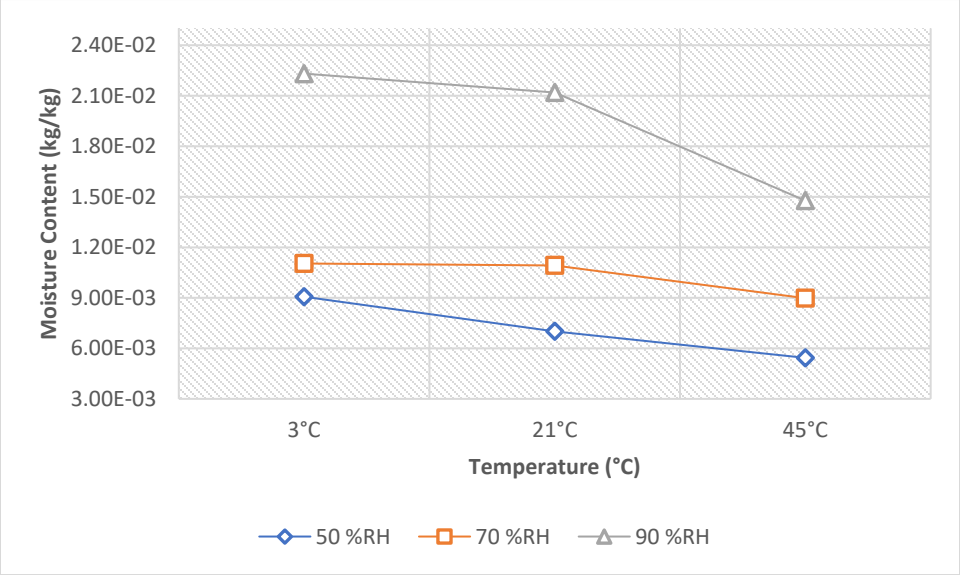

Figure 7-54. Effect of Temperature on Adsorption Isotherms- Polyisocyanurate.

7.2.16 **Mineral Fiber (Stone Wool)**

According to the measured moisture content of mineral fiber samples, their water vapor sorption capacity increased with relative humidity while decreased with rising temperature. The most impact of relative humidity increase was observed at the temperature of 45°C when the equilibrium moisture content radically jumped by 413% from 50%RH to 90% RH. The maximum decrease in moisture content duo to rising temperature, however, was noted as -54% at 50% relative humidity.

Comparing our sorption measurements at 21°C with the corresponding results from IEA-Annex24 for mineral fiber insulation, we found a good correlation between the results.

Table 7-31. Mineral Fiber -Adsorption Isotherms at Different Temperatures and Relative Humidities.

Mineral Fiber -EMCs at Different Temperatures and Relative Humidities				**Difference between RHs**		
EMC at	**50% RH**	**70% RH**	**90% RH**	**70%-50%**	**90%-70%**	**90%-50%**
3°C	1.25E-02	1.34E-02	1.61E-02	7%	20%	29%
21°C	5.79E-03	7.07E-03	9.16E-03	22%	29%	58%
45°C	1.62E-03	2.91E-03	8.31E-03	80%	186%	413%
Difference between 21°C and 3°C	-54%	-47%	-43%			
Difference between 45°C and 21°C	-72%	-59%	-9%			
Difference between 45°C and 3°C	-87%	-78%	-48%			

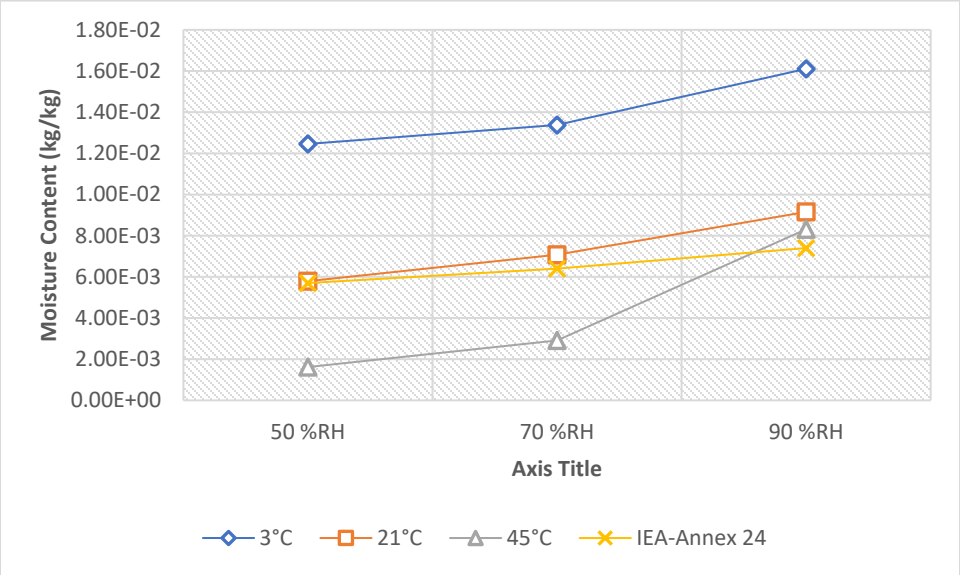

Figure 7-55. Effect of Relative Humidity on Adsorption Isotherms- Mineral Fiber.

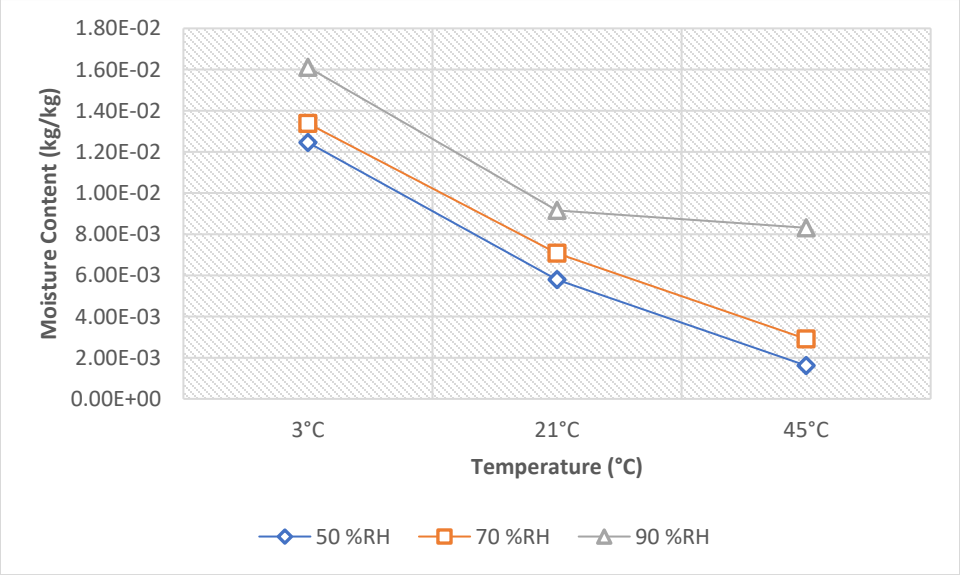

Figure 7-56. Effect of Temperature on Adsorption Isotherms- Mineral Fiber.

7.2.17 **Summary**

The basic properties of the tested building materials including bulk and dry densities, saturated moisture content and porosity are presented at Table 7-32. Additionally, a summary of differences between EMCs in all materials with regards to changes of temperature and relative humidity are tabulated in Table 7-33. According to the obtained results, there was a direct relationship between moisture content and relative humidity i.e. increasing relative humidity lead to higher moisture content, while there was an inverse relationship between moisture content and temperature i.e. increasing temperature lead to lower moisture content. Figure 7-57 shows a comparison between EMC of all tested materials at different temperatures and relative humidities. Based on the measurement data, it was found that wood-based materials along with cellulose fiber had higher moisture storage capacity than others. For instance, the moisture content of Douglas fir and cellulose fiber reached to 20% and 22%, respectively. On the other hand, Brick, Densglass gold gypsum and EPS products had lowest moisture content under different relative humidity conditions as 0.13%, 0.41% and 0.73%, respectively. Even though the Densglass gold gypsum board has lower moisture storage capacity than other materials, it showed the most impacted by relative humidity. Additionally, it reached the equilibrium state from dry condition in a week, while the others such as stucco took several months. Among building materials tested, Densglass gold gypsum showed to be more influenced by temperature followed by clay brick, open cell sprayed foam and mineral wool insulations while XPS insulation appeared to be less impacted by temperature variations. Comparing the measured data with ASHRAE research project 1018 (Kumaran, 2002) we found that our measurements data for most of the tested materials indicated a good agreement with the RP-1018 results. However, we observed noteworthy discrepancies between the two results for open cell sprayed foam, XPS and 60 min building paper products.

Table 7-32. Representative properties of tested materials.

Material	Thickness (mm)	Bulk Density (kg/m^3)	Dry Density (kg/m^3)	Saturated Moisture Content (kg/kg)	Porosity (%)
Claddings					
Clay Brick	11.5	2080.78 ± 27	2074.36 ± 27	0.056	11
Fiber Cement	7.7	1358 ± 12	1260 ± 8	0.331	42
Stucco	11.7	2399 ± 39	2400 ± 40	0.132	32
Western Red Cedar	20.29	380 ± 4	337 ± 3	0.898	3
Weather Resistive Barriers (WRB)					
Tyvek	0.14	65 g/m^2		-	-
60 Min Building Paper	0.14	310.5 g/m^2	281 g/m^2	-	-
Wall Sheathing Boards					
OSB	11.4	620 ± 12	595 ± 12	1.257	71
Plywood	12.39	461 ± 8	439 ± 7	0.947	41
Densglass Gold Gypsum	13.35	755 ± 7	753 ± 7	0.182	14
Wood Studs					
Spruce	17.25	469 ± 1.7	428 ± 1.6	0.914	39
Douglas Fir	17.7	572 ± 9	502 ± 7	0.830	4
Insulations					
Cellulose Fiber	59.89	79.24	42.88	-	-
EPS	12.6	21.9 ± 0.1	21.8 ± 0.1	-	-
XPS	15.3	26.6 ± 0.15	26.2 ± 0.2	-	-
Open Cell Sprayed Polyurethane	5 × 5.9	14.75 ± 1.2	14.75 ± 0.9	-	-
Polyisocyanurate	24.2	27.5 ± 0.16	27.3 ± 0.16	-	-
Mineral Fiber	3 × 9.8	128 ± 4	125 ± 4	-	-

Table 7-33. The dependency of adsorption isotherms of building materials on temperature and relative humidity.

Material	Relative Humidity Dependency of EMC (@90% - @50%)			Temperature Dependency of EMC (@3°C - @45°C)		
	3°C	**21°C**	**45°C**	**50% RH**	**70% RH**	**90% RH**
Clay Brick	38%	55%	96%	-56%	-53%	-38%
Fiber Cement	134%	153%	177%	-22%	-9%	-8%
Stucco	84%	116%	101%	-28%	-39%	-22%
Western Red Cedar	125%	141%	146%	-15%	-9%	-6%
60 Min Building Paper	56%	81%	152%	-48%	-53%	-16%
OSB	167%	195%	194%	-16%	-37%	-8%
Plywood	119%	139%	168%	-21%	-11%	-3%
Densglass Gold Gypsum	96%	229%	492%	-74%	-54%	-21%
Spruce	116%	139%	148%	-20%	-13%	-8%
Douglas Fir	97%	132%	138%	-30%	-27%	-16%
Cellulose Fiber *(Difference between 21°C and 3°C)*	37%	126%	_	-45%	-26%	-8%
EPS	21%	27%	383%	-94%	-85%	-77%
XPS	38%	27%	52%	-28%	-15%	-21%
Open Cell Sprayed Polyurethane	127%	14%	6%	-41%	-60%	-73%
Polyisocyanurate	146%	202%	172%	-40%	-19%	-34%
Mineral Fiber	29%	58%	413%	-87%	-78%	-48%

Figure 7-57. Comparing the adsorption isotherms of building materials at different temperatures and relative humidities.

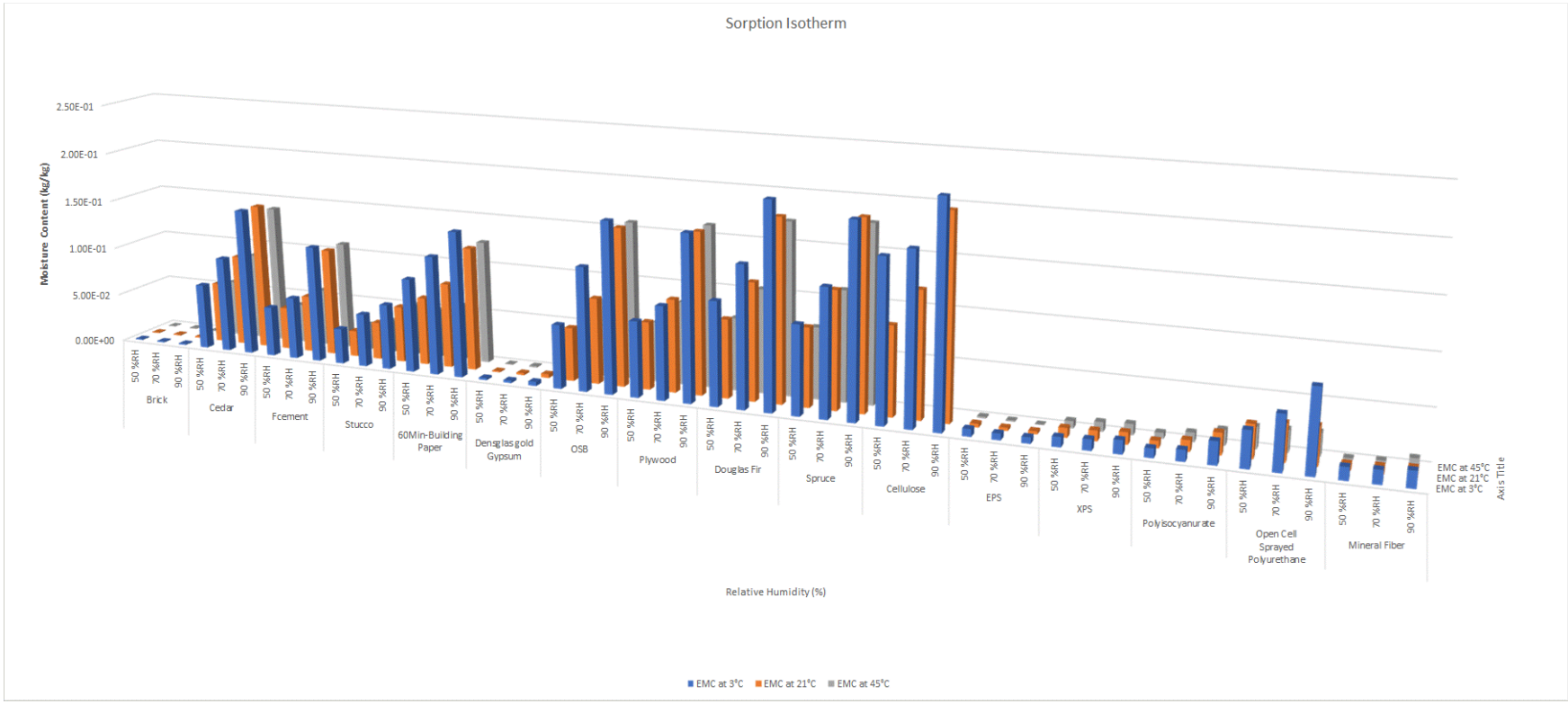

7.3 Water Vapor Permeabilities of Building Materials

The measured data for water vapor transmission rate, permeance and water vapor permeability for each tested building material from wet and dry cup tests are collected under three relative humidities. Then the whole process is repeated at three temperatures: 3°C, 21°C and 45°C. The dataset regarding each temperature is tabulated in separate table. Accordingly, the obtained water vapor permeability for each tested building material are given here, while the water vapor transmission rate of each specimen of tested building materials are separately presented in Appendix B.

7.3.1 Clay Brick

The results of measured water vapor permeability (WVP) and water vapor transmission rate (WVT) of clay brick samples at different temperatures indicated an increase of WVP and WVT with rising temperature. According to the results, the permeability of brick was more influenced by relative humidity than temperature. The highest impact was observed at temperature 45°C and when the relative humidity across the specimen was higher than 75% which is associated to the wet cup test. For example, under the relative humidities of 85% and 95%, by increasing the temperature from 3°C to 45°C, the WVP increased by 116% and 249%, respectively.

Comparing our measured permeability for clay brick at 21°C with the result from RP-1018, we found our values for permeability were lower than the ASHRAE report.

Table 7-34. Clay Brick-Water Vapor Permeability.

Clay Brick-Water Vapor Permeability (kg/m.s.Pa)							Difference between 50% and 90% RH
	25% RH	**35% RH**	**45% RH**	**75% RH**	**85% RH**	**95% RH**	
	Dry Cups			**Wet Cups**			
	50% RH	70% RH	90% RH	50% RH	70% RH	90% RH	
Permeability at 3°C	1.53E-12	1.98E-12	2.1E-12	2.15E-12	2.5E-12	3.32E-12	116%
Permeability at 21°C	2.23E-12	2.53E-12	2.6E-12	2.88E-12	3.13E-12	4.24E-12	89%
Permeability at 45°C	2.45E-12	2.68E-12	3.62E-12	3.66E-12	5.4E-12	1.16E-11	371%
Difference between 21°C and 3°C	46%	28%	24%	34%	25%	28%	
Difference between 45°C and 21°C	10%	6%	39%	27%	73%	173%	
Difference between 45°C and 3°C	60%	35%	73%	70%	116%	249%	

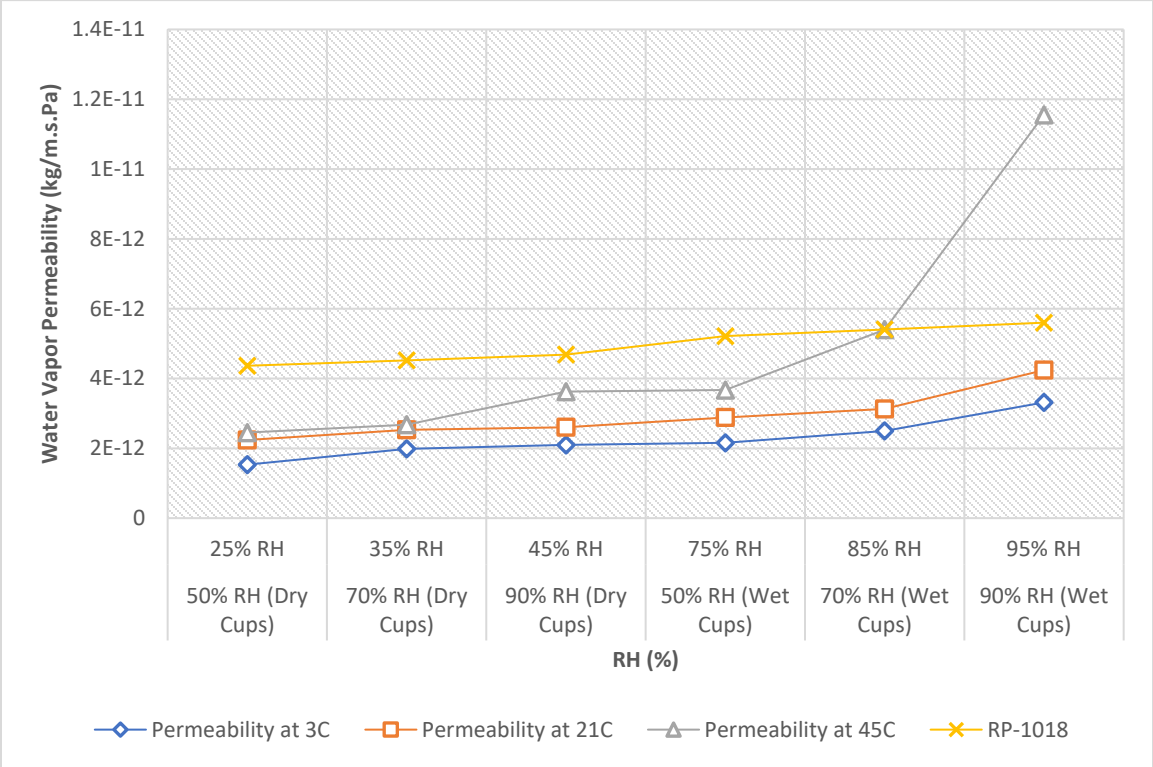

Figure 7-58. Clay Brick-Water Vapor Permeability.

7.3.2 **Fiber Cement**

The measured data for water vapor permeability (WVP) and water vapor transmission rate (WVT) of fiber cement samples at different temperatures indicated an increase of WVP and WVT with rising temperature. However, the permeability of fiber cement was impacted by relative humidity more than temperature. The highest impact was observed at temperature 45°C and when the relative humidity inside the specimen was higher than 50% which is associated to the wet cup test results. For example, under the relative humidities of 75%, 85% and 95%, by increasing the temperature from 3°C to 45°C, the WVP increased by 105%, 110% and 188%, respectively.

Comparing our measured permeability for fiber cement at 21°C with the result from ASHRAE report RP-1018, we noted a good agreement at relative humidities lower than 50% while our values for permeability at relative humidities above 50% were slightly higher than the ASHRAE report.

Table 7-35. Fiber Cement-Water Vapor Permeability.

Fiber Cement-Water Vapor Permeability (kg/m.s.Pa)							Difference between 50% and 90% RH
	25% RH	**35% RH**	**45% RH**	**75% RH**	**85% RH**	**95% RH**	
	Dry Cups			**Wet Cups**			
	50% RH	70% RH	90% RH	50% RH	70% RH	90% RH	
Permeability at 3°C	5.74E-13	6.08E-13	1.28E-12	2.89E-12	4.56E-12	6.14E-12	970%
Permeability at 21°C	6.52E-13	6.87E-13	1.4E-12	3.50E-12	5.44E-12	9.87E-12	1412%
Permeability at 45°C	6.96E-13	8.11E-13	1.53E-12	5.92E-12	9.59E-12	1.77E-11	2435%
Difference between 21°C and 3°C	14%	13%	9%	21%	19%	61%	
Difference between 45°C and 21°C	7%	18%	10%	69%	76%	79%	
Difference between 45°C and 3°C	21%	33%	20%	105%	110%	188%	

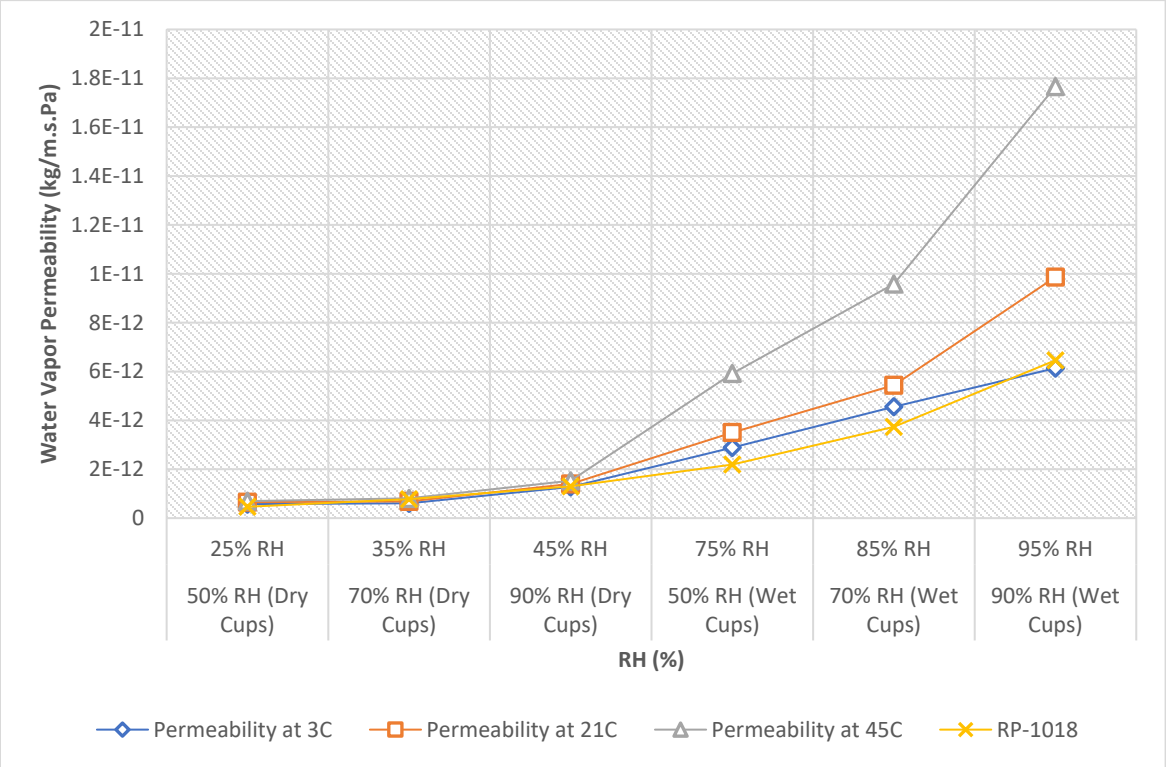

Figure 7-59. Fiber Cement-Water Vapor Permeability.

7.3.3 **Stucco**

The measured data for water vapor permeability (WVP) and water vapor transmission rate (WVT) of stucco samples at different temperatures indicated an increase of WVP and WVT with increasing temperature. The permeability of stucco was influenced more by temperature than relative humidity. A significant impact was observed at temperature 45°C through all range of relative humidities in both dry and wet cup test results. For example, by rising temperature from 3°C to 45°C, the permeability of stucco samples from dry cup test at 50% RH increased dramatically by 522%. Other permeability results under 45°C operating temperature, increased between 387% and 490%. However, the permeability of stucco samples from the lowest to the highest relative humidity increased by 224% at temperature of 3°C.

Comparing our measured permeability for stucco at 21°C with the result from ASHRAE report RP-1018, a similar upward trend was noted in both results graphs. However, our values for permeability at all tested relative humidities were observed to be higher than the ASHRAE report.

Table 7-36. Stucco-Water Vapor Permeability.

Stucco-Water Vapor Permeability (kg/m.s.Pa)							
	25% RH	**35% RH**	**45% RH**	**75% RH**	**85% RH**	**95% RH**	Difference between 50% and 90% RH
	Dry Cups			**Wet Cups**			
	50% RH	70% RH	90% RH	50% RH	70% RH	90% RH	
Permeability at 3°C	8.84E-13	1.03E-12	1.21E-12	1.77E-12	2.04E-12	2.86E-12	224%
Permeability at 21°C	2.67E-12	2.95E-12	3.55E-12	3.893E-12	4.88E-12	6.06E-12	126%
Permeability at 45°C	5.50E-12	6.02E-12	6.87E-12	8.63E-12	1.05E-11	1.12E-11	207%
Difference between 21°C and 3°C	203%	185%	193%	120%	140%	112%	
Difference between 45°C and 21°C	105%	104%	94%	122%	115%	178%	
Difference between 45°C and 3°C	522%	482%	468%	387%	414%	490%	

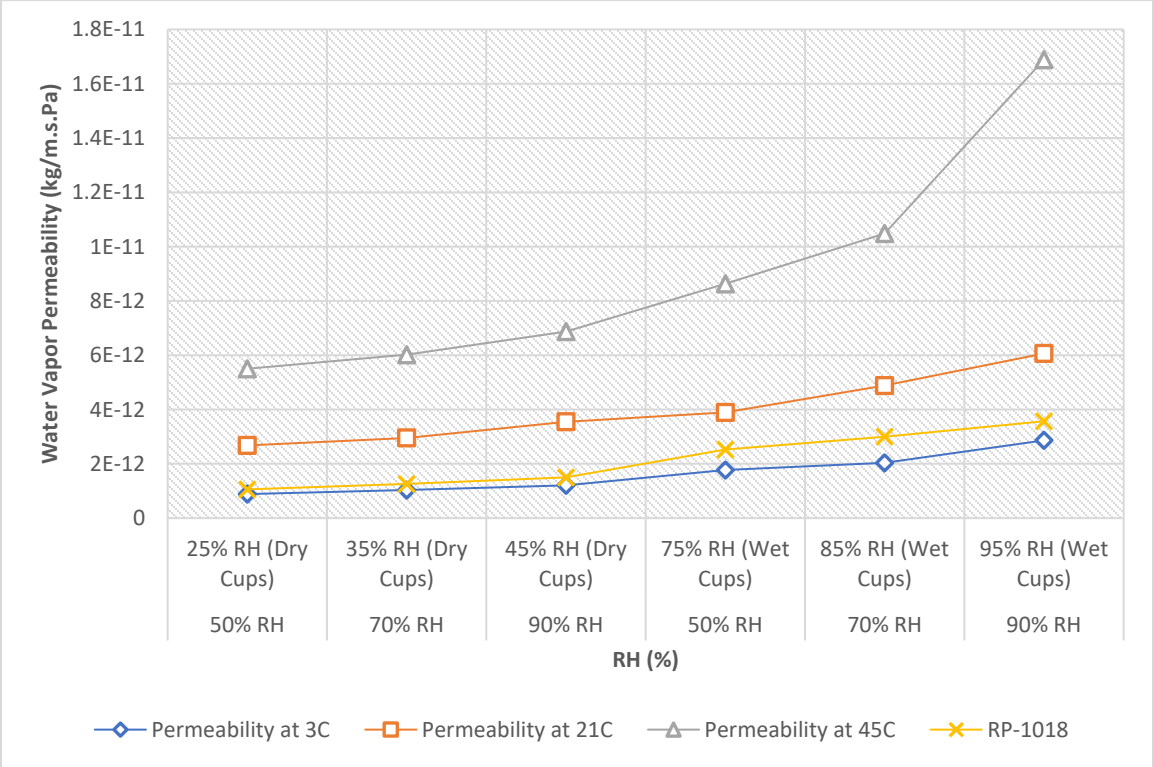

Figure 7-60. Stucco-Water Vapor Permeability.

7.3.4 **Western Red Cedar**

The measured data for water vapor permeability (WVP) and water vapor transmission rate (WVT) of western red cedar samples at different temperatures indicated an increase of WVP and WVT with increasing temperature. The permeability of tested cedar samples was influenced more by relative humidity than temperature. The vapor permeability of samples increased as 501%, 572% and 628% at temperatures 3°C, 21°C and 45°C, respectively for increasing relative humidity across the specimen from 25% to 95%. However, the impact of temperature was observed to be between 104% and 165% for relative humidities of 75% and 95% when the temperature rose from 3°C to 45°C.

In Comparison with the result from ASHRAE report RP-1018, our measured permeability for western red cedar at 21°C appeared to represent the same behavior against temperature as the wet cup results in both projects were more influenced by temperature changes.

Table 7-37. Western Red Cedar-Water Vapor Permeability.

Western Red Cedar-Water Vapor Permeability (kg/m.s.Pa)							
	25% RH	**35% RH**	**45% RH**	**75% RH**	**85% RH**	**95% RH**	Difference between 50% and 90% RH
	Dry Cups			**Wet Cups**			
	50% RH	70% RH	90% RH	50% RH	70% RH	90% RH	
Permeability at 3°C	7.36E-13	9.6E-13	1.59E-12	2.39E-12	3.33E-12	4.43E-12	501%
Permeability at 21°C	1.05E-12	1.38E-12	2.28E-12	3.72E-12	4.75E-12	7.09E-12	572%
Permeability at 45°C	1.61E-12	2.53E-12	3.38E-12	4.88E-12	7.7E-12	1.18E-11	628%
Difference between 21°C and 3°C	43%	44%	44%	56%	43%	60%	
Difference between 45°C and 21°C	53%	83%	48%	31%	62%	66%	
Difference between 45°C and 3°C	119%	164%	113%	104%	131%	165%	

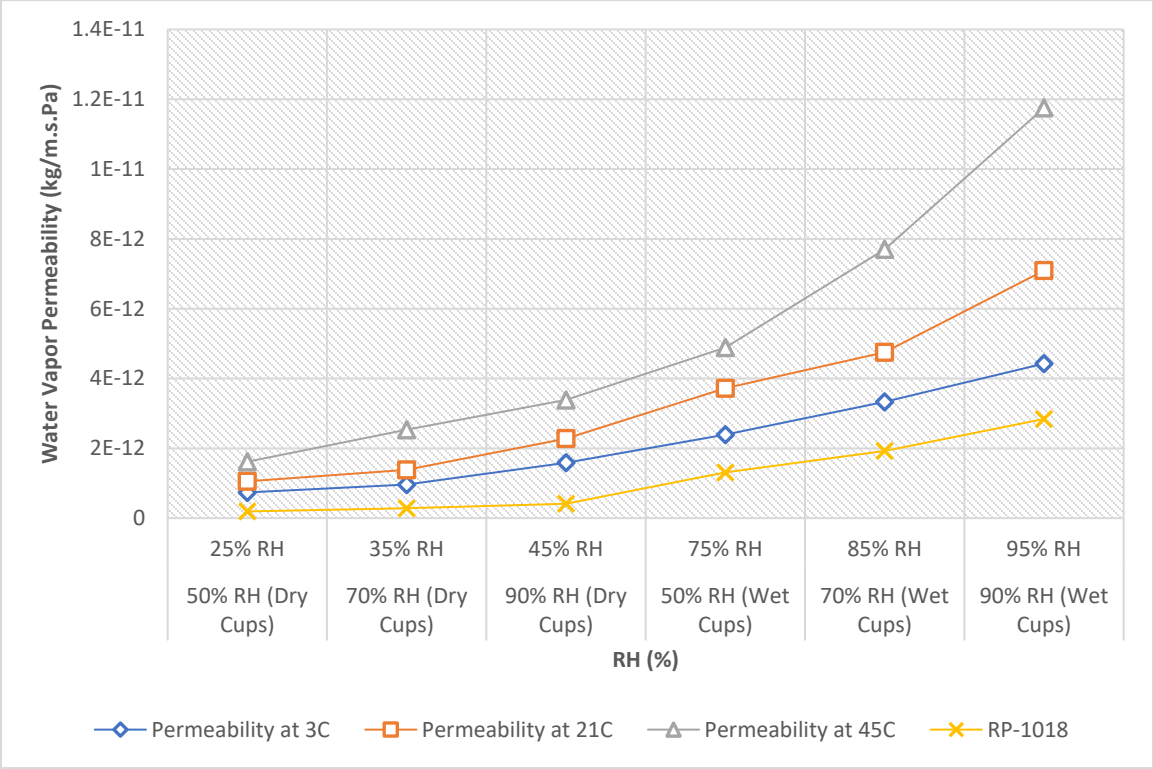

Figure 7-61. Western Red Cedar-Water Vapor Permeability.

7.3.5 **Tyvek**

The measured data for water vapor permeability (WVP) and water vapor transmission rate (WVT) of Tyvek samples at different temperatures indicated an increase of WVP and WVT with increasing temperature. According to the obtained results, it was noted that the permeability of tested Tyvek samples was equally influenced by relative humidity and temperature. The vapor permeability of samples increased as 16%, 35% and 42% at temperatures 3°C, 21°C and 45°C, respectively by increasing relative humidity from 25% to 95%. However, the impact of temperature was observed to be between 12% and 37% for relative humidities of 25% and 95% for rising temperature from 3°C to 45°C.

The permeability results for Tyvek at 21°C from ASHRAE report RP-1018 showed a constant value with no changes upon increasing relative humidity while our measured values projected an impact of relative humidity.

Table 7-38. Tyvek-Water Vapor Permeability.

Tyvek-Water Vapor Permeability (kg/m.s.Pa)							
	25% RH	**35% RH**	**45% RH**	**75% RH**	**85% RH**	**95% RH**	Difference between 50% and 90% RH
	Dry Cups			**Wet Cups**			
	50% RH	70% RH	90% RH	50% RH	70% RH	90% RH	
Permeability at 3°C	3.19E-09	3.32E-09	3.38E-09	3.55E-09	3.63E-09	3.70E-09	16%
Permeability at 21°C	3.39E-09	3.68E-09	3.88E-09	3.99E-09	4.30E-09	4.58E-09	35%
Permeability at 45°C	3.57E-09	3.92E-09	4.21E-09	4.47E-09	4.93E-09	5.08E-09	42%
Difference between 21°C and 3°C	6%	11%	15%	12%	18%	24%	
Difference between 45°C and 21°C	5%	7%	8%	12%	14%	11%	
Difference between 45°C and 3°C	12%	18%	24%	26%	36%	37%	

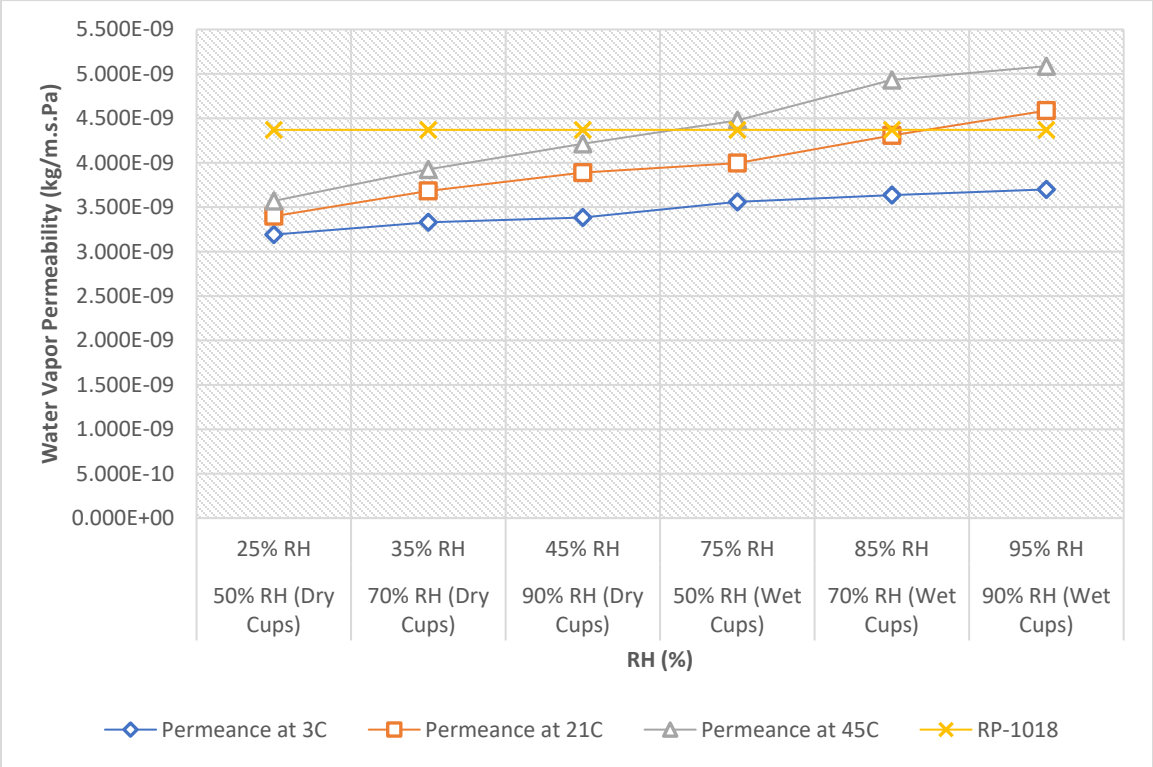

Figure 7-62. Tyvek-Water Vapor Permeance.

7.3.6 **60 Min Building Paper**

The measured data for water vapor permeability (WVP) and water vapor transmission rate (WVT) of samples of 60-min building paper at different temperatures showed that the WVP and WVT increased with rising temperature. However, it was noted that the permeability of tested building paper samples was influenced more significantly by relative humidity escalation than temperature. For example, the vapor permeability of samples increased by 284%, 547% and 459% at temperatures 3°C, 21°C and 45°C, respectively by increasing relative humidity from 25% to 95%. Nevertheless, the impact of temperature was observed to be between 74% and 180% for relative humidities of 25% and 75% for rising temperature from 3°C to 45°C.

Although our result presented the same upward trend with RP-1018 results in permeability graph against relative humidity, our results appeared to be lower than the values from ASHRAE report.

Table 7-39. Building Paper 60 min-Water Vapor Permeability.

Building Paper 60 min-Water Vapor Permeability (kg/m.s.Pa)							
	25% RH	**35% RH**	**45% RH**	**75% RH**	**85% RH**	**95% RH**	Difference between 50% and 90% RH
	Dry Cups			**Wet Cups**			
	50% RH	70% RH	90% RH	50% RH	70% RH	90% RH	
Permeability at 3°C	4.77E-10	5.07E-10	5.85E-10	8.17E-10	1.36E-09	1.83E-09	284%
Permeability at 21°C	5.22E-10	5.61E-10	8.79E-10	1.94E-09	2.70E-09	3.37E-09	547%
Permeability at 45°C	8.29E-10	1.18E-09	1.31E-09	2.29E-09	3.55E-09	4.63E-09	459%
Difference between 21°C and 3°C	9%	11%	50%	137%	98%	84%	
Difference between 45°C and 21°C	59%	110%	48%	18%	32%	37%	
Difference between 45°C and 3°C	74%	132%	123%	180%	161%	153%	

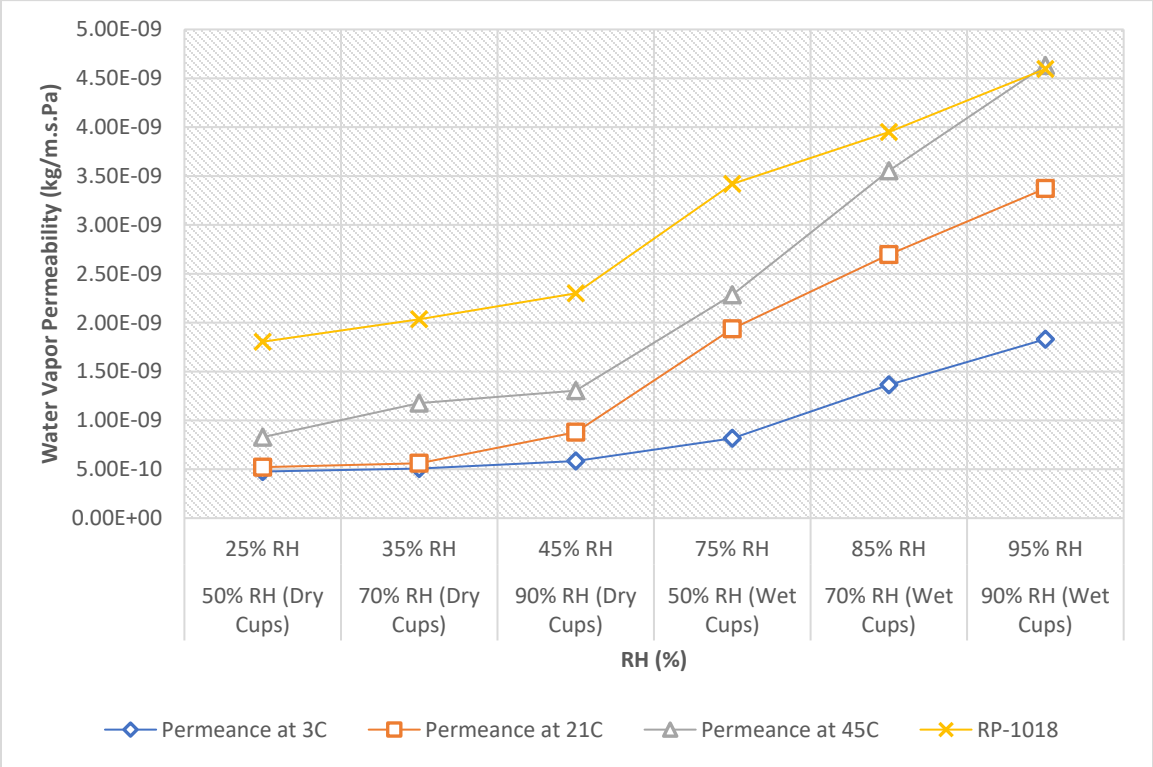

Figure 7-63. Building Paper 60 mins-Water Vapor Permeance.

7.3.7 **Oriented Strand Board (OSB)**

The measured data for water vapor permeability (WVP) and water vapor transmission rate (WVT) of samples of OSB at different temperatures presented that the WVP and WVT increased with temperature. However, it was noted that the permeability of tested OSB samples was influenced more significantly by relative humidity rise than temperature. For example, the vapor permeability of samples increased by 277%, 651% and 593% at temperatures 3°C, 21°C and 45°C, respectively by increasing relative humidity from 25% to 95%. However, the impact of temperature was observed to be between 38% and 155% for relative humidities of 25% and 95% for rising temperature from 3°C to 45°C.

Comparing our measured permeability for OSB at 21°C with the result from ASHRAE report RP-1018, we noted the same upward trend in both results graphs whereas our measured values for all tested relative humidities were observed to be higher than the values from ASHRAE report.

Table 7-40. OSB-Water Vapor Permeability.

OSB-Water Vapor Permeability (kg/m.s.Pa)							
	25% RH	**35% RH**	**45% RH**	**75% RH**	**85% RH**	**95% RH**	Difference between 50% and 90% RH
	Dry Cups			**Wet Cups**			
	50% RH	70% RH	90% RH	50% RH	70% RH	90% RH	
Permeability at 3°C	7.32E-13	8.59E-13	8.31E-13	1.66E-12	2.27E-12	2.76E-12	277%
Permeability at 21°C	7.45E-13	8.98E-13	1.43E-12	2.52E-12	4.06E-12	5.6E-12	651%
Permeability at 45°C	1.01E-12	1.26E-12	1.67E-12	3.02E-12	4.33E-12	7.03E-12	593%
Difference between 21°C and 3°C	2%	4%	72%	52%	79%	103%	
Difference between 45°C and 21°C	36%	40%	17%	20%	7%	26%	
Difference between 45°C and 3°C	38%	47%	101%	82%	90%	155%	

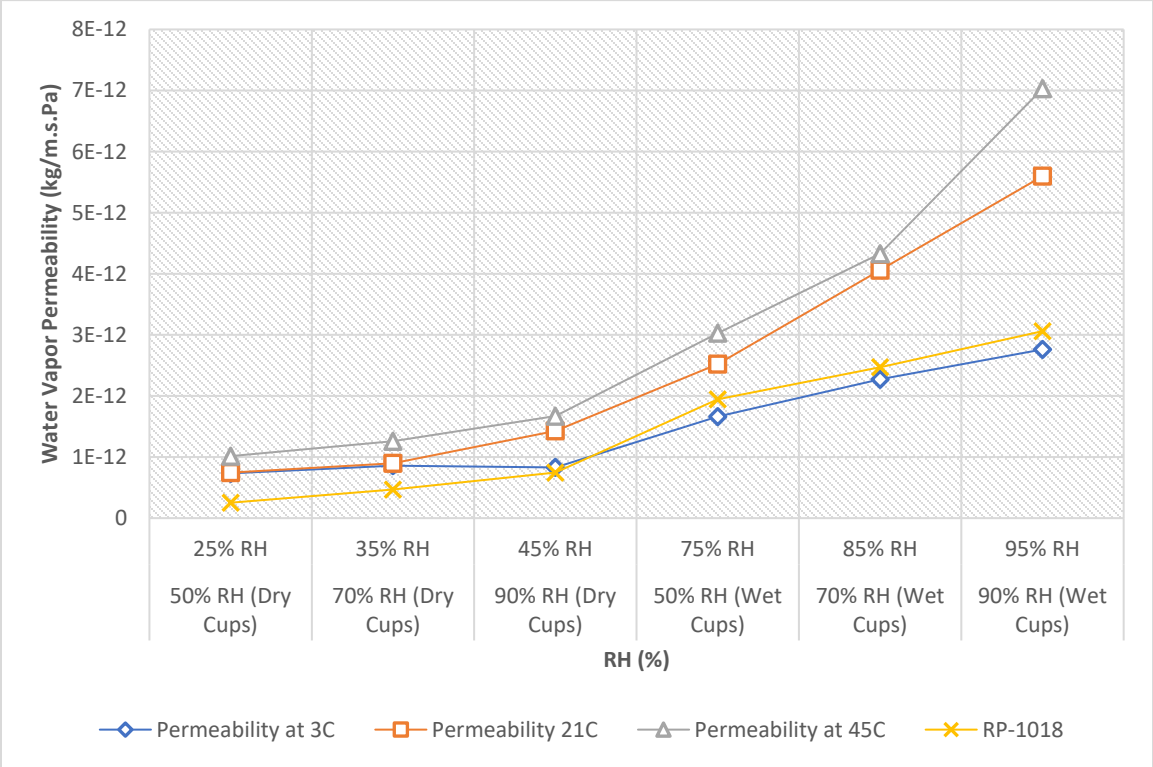

Figure 7-64. OSB-Water Vapor Permeability.

7.3.8 **Plywood**

The measured data for water vapor permeability (WVP) and water vapor transmission rate (WVT) of samples of plywood at different temperatures presented that the WVP and WVT increased with temperature. It was noted that the permeability of tested plywood samples was influenced more significantly by relative humidity rise than temperature. For example, the vapor permeability of samples increased by 772%, 1256% and 1411% at temperatures 3°C, 21°C and 45°C, respectively by increasing relative humidity from 25% to 95%. However, the impact of temperature was observed to be between 32% and 129% for relative humidities of 25% and 95% for rising temperature from 3°C to 45°C.

Our measured permeability for OSB at 21°C from dry cups appeared to be in a good agreement with the result from ASHRAE report RP-1018. However, our results from wet cups was noted to be slightly higher than corresponding results from RP-1018 while both showing a similar trend.

Table 7-41. Plywood-Water Vapor Permeability.

Plywood-Water Vapor Permeability (kg/m.s.Pa)							
	25% RH	**35% RH**	**45% RH**	**75% RH**	**85% RH**	**95% RH**	Difference between 50% and 90% RH
	Dry Cups			**Wet Cups**			
	50% RH	70% RH	90% RH	50% RH	70% RH	90% RH	
Permeability at 3°C	5.89E-13	7.55E-13	1.26E-12	2.89E-12	4.45E-12	5.14E-12	772%
Permeability at 21°C	6.68E-13	8.22E-13	1.57E-12	4.75E-12	6.85E-12	9.06E-12	1256%
Permeability at 45°C	7.80E-13	1.02E-12	1.85E-12	6.22E-12	9.56E-12	1.18E-11	1411%
Difference between 21°C and 3°C	13%	9%	24%	64%	54%	76%	
Difference between 45°C and 21°C	17%	24%	18%	31%	40%	30%	
Difference between 45°C and 3°C	32%	34%	46%	115%	115%	129%	

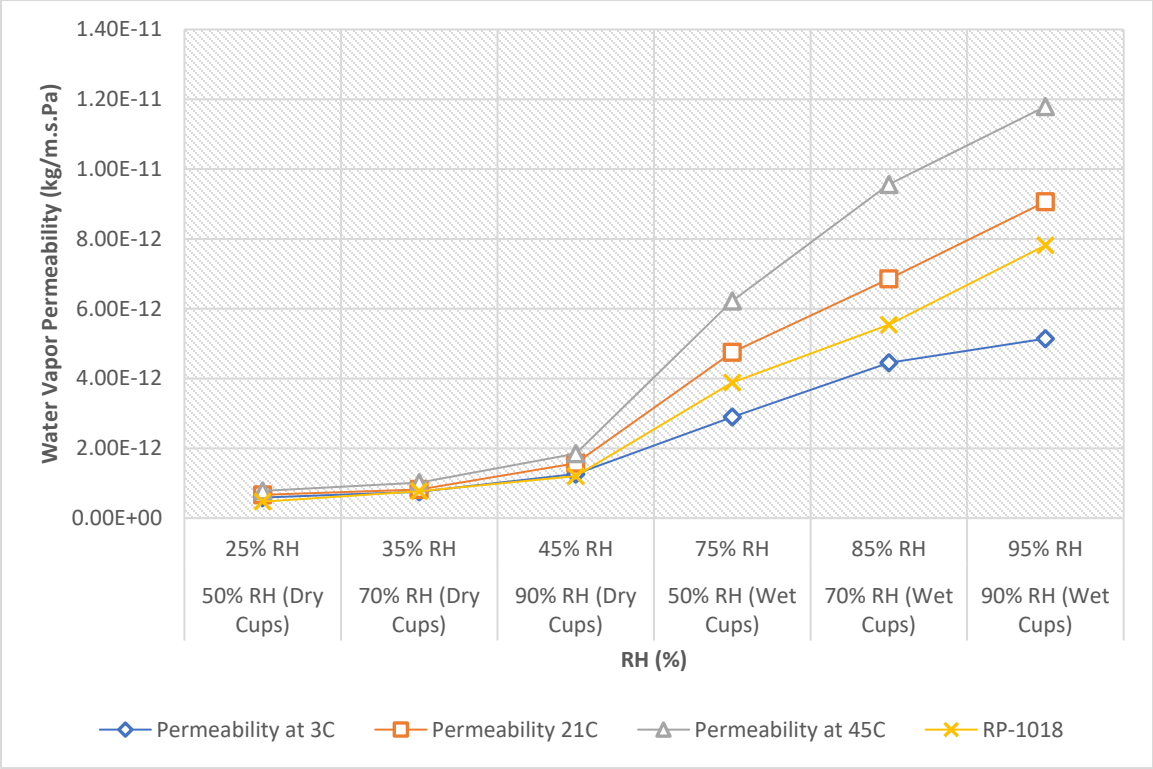

Figure 7-65. Plywood-Water Vapor Permeability.

7.3.9 **Densglass Gold Gypsum Sheathing Board**

The measured data for water vapor permeability (WVP) and water vapor transmission rate (WVT) of samples of Densglass at different temperatures presented that the WVP and WVT increased with temperature. It was noted that the permeability of tested Densglass gold gypsum samples was influenced by relative humidity rise slightly more than temperature. The vapor permeability of the samples increased by 40%, 96% and 142% at temperatures 3°C, 21°C and 45°C, respectively by increasing relative humidity from 25% to 95%. The impact of temperature on permeability was observed to be more significant at relative humidities above 50%. Due to rising temperature from 3°C to 45°C, the maximum increases at relative humidities below and above 50% were 11% and 91% at 25% RH and 95% RH, respectively.

The available information in ASHRAE report RP-1018 is for interior gypsum board. However, comparing our measured permeability for exterior gypsum sheathing at 21°C with the result from ASHRAE report RP-1018, a very small discrepancy was found.

Table 7-42. Densglass Gold Gypsum Sheathing-Water Vapor Permeability.

Densglass Gold Gypsum Sheathing-Water Vapor Permeability (kg/m.s.Pa)							
	25% RH	**35% RH**	**45% RH**	**75% RH**	**85% RH**	**95% RH**	Difference between 50% and 90% RH
	Dry Cups			**Wet Cups**			
	50% RH	70% RH	90% RH	50% RH	70% RH	90% RH	
Permeability at 3°C	3.27E-11	3.55E-11	3.76E-11	3.94E-11	3.95E-11	4.59E-11	40%
Permeability at 21°C	3.31E-11	3.56E-11	3.81E-11	4.73E-11	5.20E-11	6.48E-11	96%
Permeability at 45°C	3.63E-11	3.84E-11	3.96E-11	5.51E-11	6.22E-11	8.78E-11	142%
Difference between 21°C and 3°C	1%	0%	1%	20%	32%	41%	
Difference between 45°C and 21°C	10%	8%	4%	17%	20%	36%	
Difference between 45°C and 3°C	11%	8%	5%	40%	58%	91%	

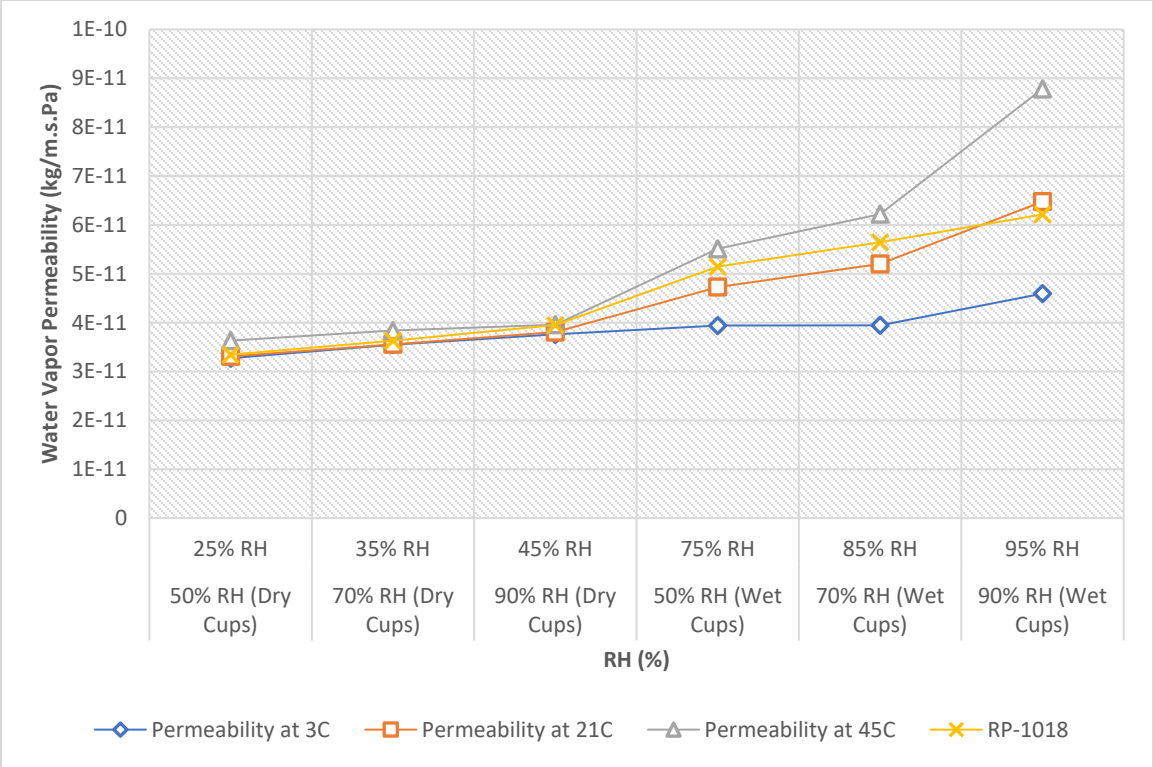

Figure 7-66. Densglass Gypsum-Water Vapor Permeability.

7.3.10 **Spruce**

The measured data for water vapor permeability (WVP) and water vapor transmission rate (WVT) of samples of spruce at different temperatures expressed that the WVP and WVT increased with temperature. It was noted that the permeability of tested spruce samples was influenced more significantly by relative humidity rise than temperature. For example, the vapor permeability of samples increased by 3055%, 5322% and 6928% at temperatures 3°C, 21°C and 45°C, respectively by increasing relative humidity from 25% to 95%. However, the impact of temperature was also observed to be considerable as the permeability increased between 49% and 311% for relative humidities of 45% and 85% when temperature rose from 3°C to 45°C.

The same uprising trends were observed in both our measured data and the result from ASHRAE report RP-1018 for the permeability of spruce at 21°C. Comparing both project results, we noted a better alignment between the dry cup test results than the wet cup.

Table 7-43. Spruce-Water Vapor Permeability.

Spruce-Water Vapor Permeability (kg/m.s.Pa)							Difference between 50% and 90% RH
	25% RH	**35% RH**	**45% RH**	**75% RH**	**85% RH**	**95% RH**	
	Dry Cups			**Wet Cups**			
	50% RH	70% RH	90% RH	50% RH	70% RH	90% RH	
Permeability at 3°C	4.45E-13	5.76E-13	2.03E-12	5.33E-12	6.25E-12	1.40E-11	3055%
Permeability at 21°C	6.23E-13	1.18E-12	2.77E-12	1.07E-11	1.64E-11	3.38E-11	5322%
Permeability at 45°C	8.04E-13	1.31E-12	3.03E-12	1.57E-11	2.57E-11	5.65E-11	6928%
Difference between 21°C and 3°C	40%	105%	36%	101%	162%	140%	
Difference between 45°C and 21°C	29%	11%	10%	46%	57%	67%	
Difference between 45°C and 3°C	81%	127%	49%	194%	311%	302%	

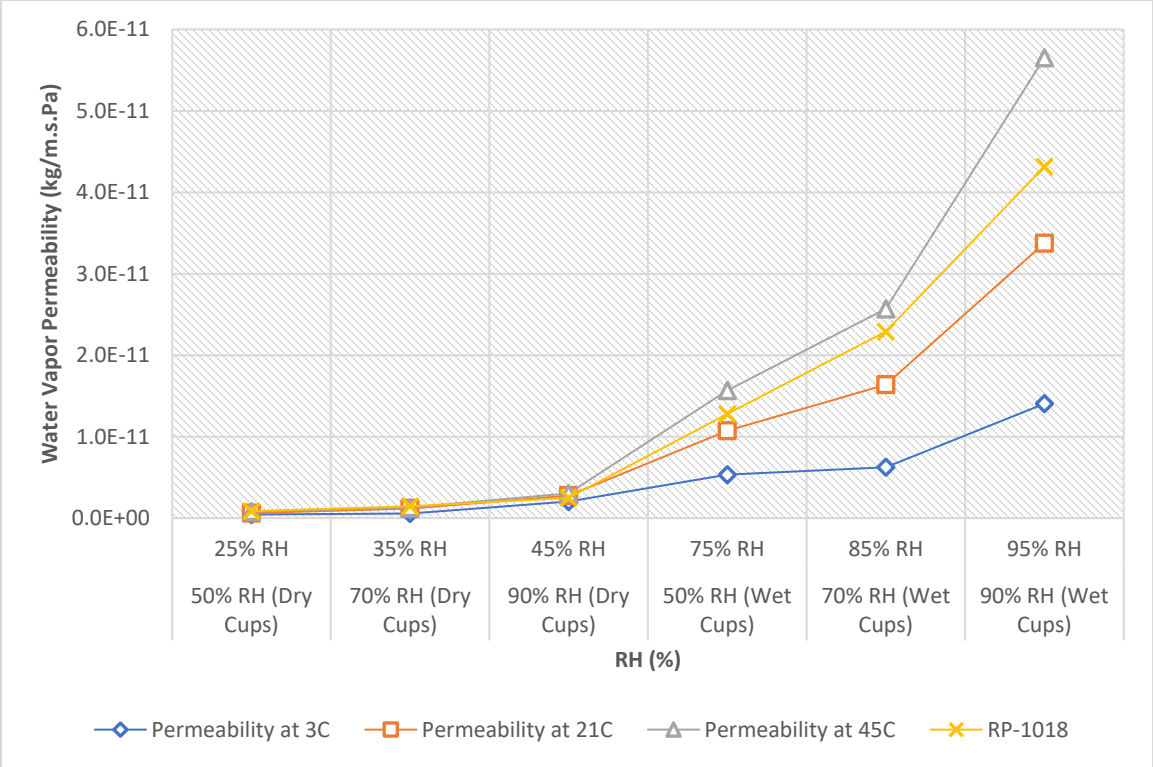

Figure 7-67. Spruce-Water Vapor Permeability.

7.3.11 **Douglas Fir**

The measured data for water vapor permeability (WVP) and water vapor transmission rate (WVT) of samples of Douglas fir at different temperatures expressed that the WVP and WVT increased with temperature. It was noted that the permeability of tested douglas fir samples was influenced more significantly by relative humidity rise than temperature. For example, the vapor permeability of samples increased by 3055%, 2677% and 1765% at temperatures 3°C, 21°C and 45°C, respectively by increasing relative humidity from 25% to 95%. Surprisingly, the impact of temperature was also observed to be considerable at lower relative humidities as by rising temperature from 3°C to 45°C, the maximum increases at relative humidities below and above 50% were 183% and 68% at 25% RH and 95% RH, respectively.

There was no available information regarding the water vapor permeability of Douglas fir wood in ASHRAE report, RP-1018.

Table 7-44. Douglas Fir-Water Vapor Permeability.

Douglas Fir-Water Vapor Permeability (kg/m.s.Pa)							
	25% RH	**35% RH**	**45% RH**	**75% RH**	**85% RH**	**95% RH**	Difference between 50% and 90% RH
	Dry Cups			**Wet Cups**			
	50% RH	70% RH	90% RH	50% RH	70% RH	90% RH	
Permeability at 3°C	2.86E-13	4.85E-13	1.59E-12	3.18E-12	6.74E-12	9.04E-12	3055%
Permeability at 21°C	4.08E-13	8.58E-13	2.09E-12	4.32E-12	6.76E-12	1.13E-11	2677%
Permeability at 45°C	8.11E-13	1.33E-12	2.16E-12	5.20E-12	8.69E-12	1.51E-11	1765%
Difference between 21°C and 3°C	42%	77%	31%	36%	0%	25%	
Difference between 45°C and 21°C	99%	55%	3%	20%	29%	34%	
Difference between 45°C and 3°C	183%	174%	36%	63%	29%	68%	

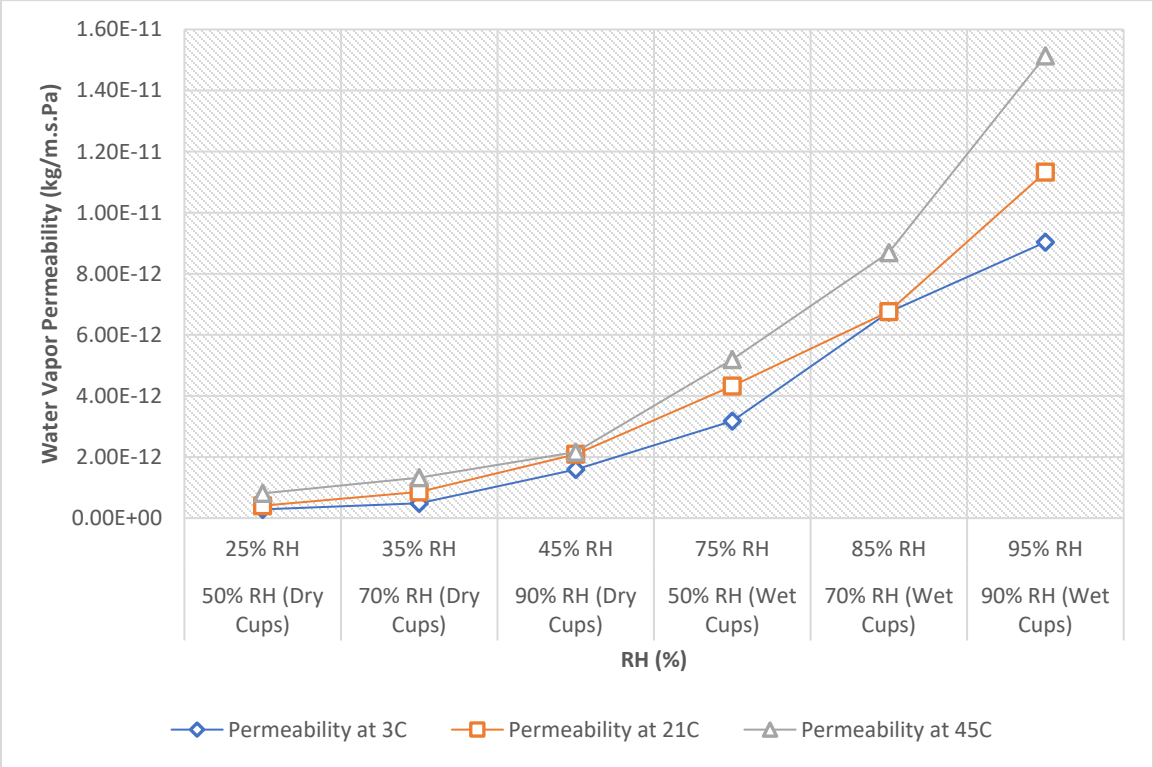

Figure 7-68. Douglas Fir-Water Vapor Permeability.

7.3.12 **Cellulose Fiber**

The measured data for water vapor permeability (WVP) and water vapor transmission rate (WVT) of samples of cellulose fiber insulation at different temperatures expressed that the WVP and WVT increased with temperature. It was noted that the permeability of tested cellulose samples was influenced by relative humidity rise slightly more than temperature. For example, the vapor permeability of samples increased by 111%, 151% and 79% at temperatures 3°C, 21°C and 45°C, respectively by increasing relative humidity from 25% to 95%. Nevertheless, the impact of temperature was observed to be considerable at lower relative humidities. Since by escalating temperature from 3°C to 45°C, the maximum increases at relative humidities below 50 % was 151% at 25% RH then decreased to 75% at 45% RH and increased again slightly at 95% RH.

Although, both the result from ASHRAE report RP-1018 and our measured permeability for spruce at 21°C presented an increase with elevating temperature, our results showed more variation with rising relative humidity. Except for high relative humidities above 50%, our measured values for permeability at 21°C were noted to be lower than the values from ASHRAE report.

Table 7-45. Cellulose Fiber-Water Vapor Permeability.

Cellulose Fiber-Water Vapor Permeability (kg/m.s.Pa)							
	25% RH	**35% RH**	**45% RH**	**75% RH**	**85% RH**	**95% RH**	Difference between 50% and 90% RH
	Dry Cups			**Wet Cups**			
	50% RH	70% RH	90% RH	50% RH	70% RH	90% RH	
Permeability at 3°C	6.18E-11	6.46E-11	9.40E-11	9.82E-11	1.21E-10	1.31E-10	111%
Permeability at 21°C	8.33E-11	1.11E-10	1.23E-10	1.62E-10	1.92E-10	2.09E-10	151%
Permeability at 45°C	1.55E-10	1.60E-10	1.64E-10	1.82E-10	2.26E-10	2.77E-10	79%
Difference between 21°C and 3°C	35%	71%	30%	65%	60%	60%	
Difference between 45°C and 21°C	86%	44%	34%	12%	18%	33%	
Difference between 45°C and 3°C	151%	147%	75%	85%	87%	112%	

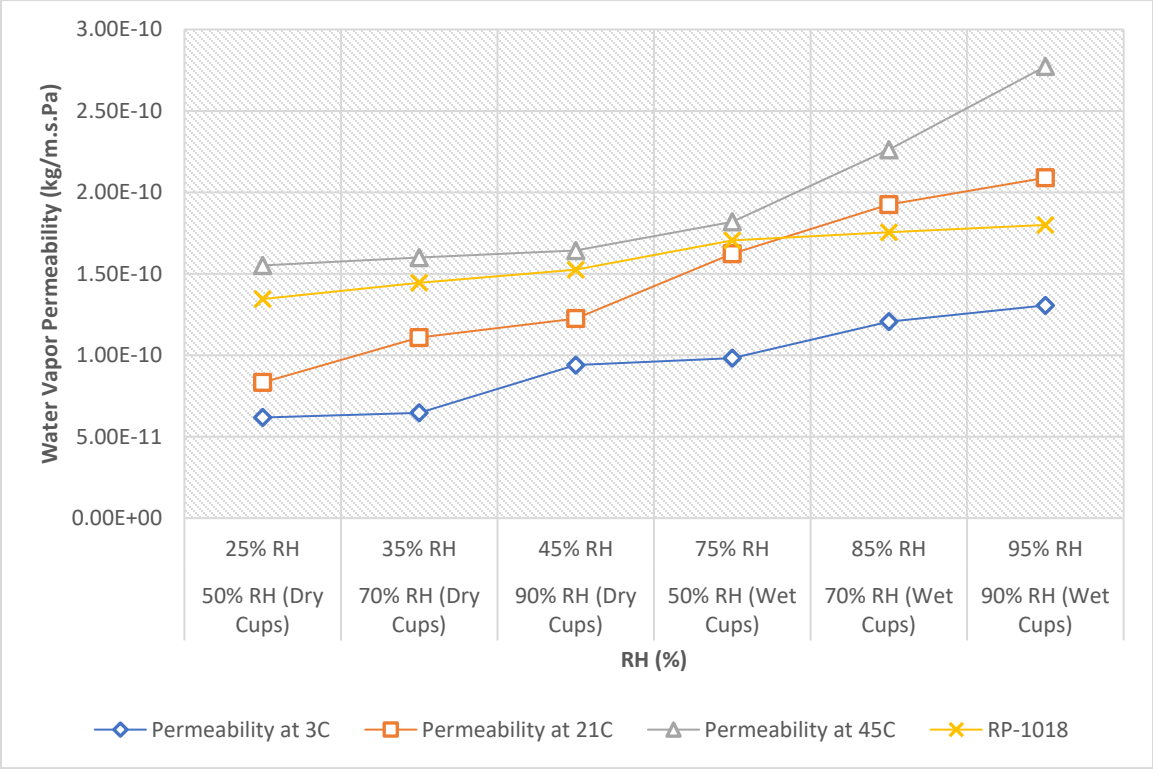

Figure 7-69. Cellulose Fiber-Water Vapor Permeability.

7.3.13 **Expanded Polystyrene (EPS)**

The measured data for water vapor permeability (WVP) and water vapor transmission rate (WVT) of EPS samples at different temperatures indicated an increase of WVP and WVT with increasing temperature. According to the obtained results, it was noted that the permeability of tested EPS samples was influenced by relative humidity slightly more than temperature. The vapor permeability of samples increased as 49%, 55% and 77% at temperatures 3°C, 21°C and 45°C, respectively by increasing relative humidity from 25% to 95%. However, the impact of temperature was observed to be between 31% and 56% for relative humidities of 25% and 95% for rising temperature from 3°C to 45°C.

Additionally, we noted a good correlation between our measured permeability for EPS at 21°C with the result from ASHRAE report RP-1018, particularly for the wet cup results (i.e. at higher relative humidities).

Table 7-46. EPS-Water Vapor Permeability.

EPS-Water Vapor Permeability (kg/m.s.Pa)							
	25% RH	**35% RH**	**45% RH**	**75% RH**	**85% RH**	**95% RH**	Difference between 50% and 90% RH
	Dry Cups			**Wet Cups**			
	50% RH	70% RH	90% RH	50% RH	70% RH	90% RH	
Permeability at 3°C	3.05E-12	3.22E-12	3.45E-12	3.79E-12	4.15E-12	4.54E-12	49%
Permeability at 21°C	3.71E-12	4.12E-12	4.51E-12	5.09E-12	5.43E-12	5.75E-12	55%
Permeability at 45°C	4.00E-12	4.46E-12	4.96E-12	5.78E-12	6.46E-12	7.07E-12	77%
Difference between 21°C and 3°C	22%	28%	31%	34%	31%	27%	
Difference between 45°C and 21°C	8%	8%	10%	14%	19%	23%	
Difference between 45°C and 3°C	31%	38%	44%	53%	55%	56%	

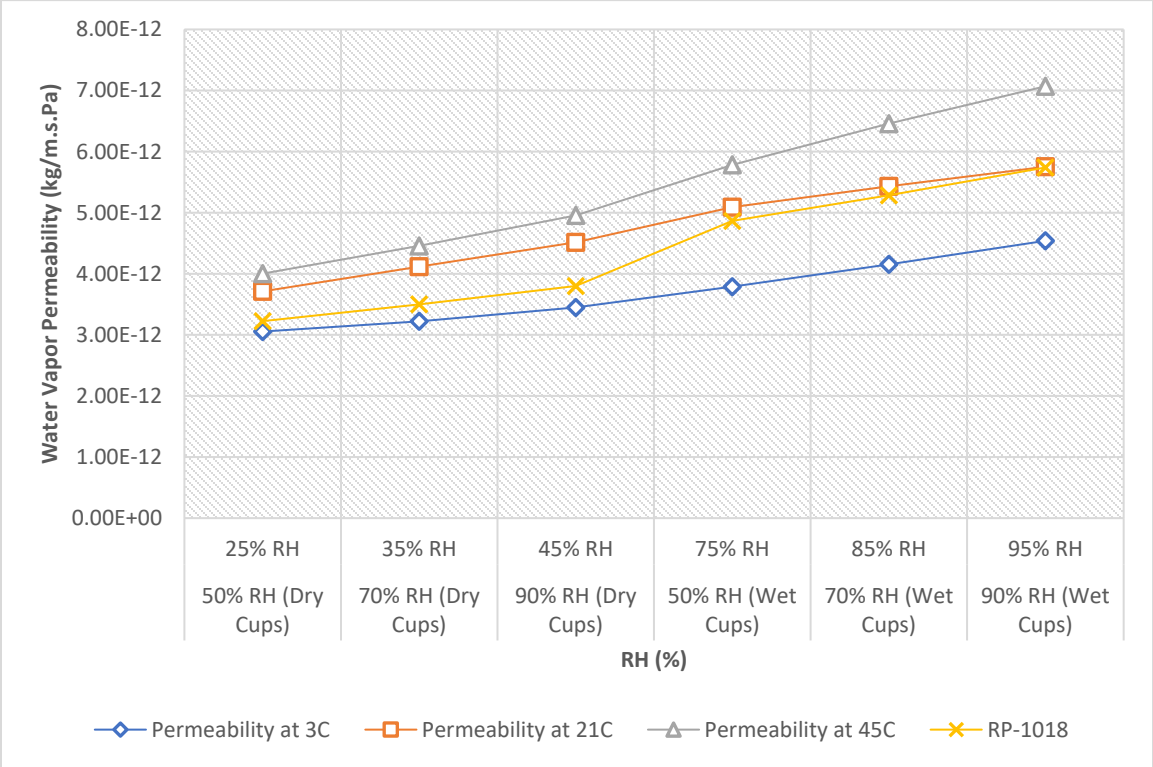

Figure 7-70. EPS-Water Vapor Permeability.

7.3.14 **Extruded Polystyrene (XPS)**

The measured data for water vapor permeability (WVP) and water vapor transmission rate (WVT) of XPS samples at different temperatures indicated an increase of WVP and WVT with increasing temperature. Based on the results, it was noted that the permeability of tested XPS samples was influenced more by relative humidity than temperature. The vapor permeability of samples increased as 66%, 65% and 60% at temperatures 3°C, 21°C and 45°C, respectively by increasing relative humidity from 25% to 95%. However, the impact of temperature was observed to be between 8% and 26% for relative humidities of 85% and 75% for rising temperature from 3°C to 45°C.

Unlike the result from ASHRAE report RP-1018 which showed a constant value through all tested relative humidities, our measured permeabilities for XPS at 21°C expressed an impact of relative humidity on the permeability of XPS. The effects were more significant in wet cup results as the representative of higher relative humidities.

Table 7-47. XPS-Water Vapor Permeability.

XPS-Water Vapor Permeability (kg/m.s.Pa)							
	25% RH	**35% RH**	**45% RH**	**75% RH**	**85% RH**	**95% RH**	Difference between 50% and 90% RH
	Dry Cups			**Wet Cups**			
	50% RH	70% RH	90% RH	50% RH	70% RH	90% RH	
Permeability at 3°C	8.97E-13	9.09E-13	9.48E-13	1.02E-12	1.37E-12	1.48E-12	66%
Permeability at 21°C	9.54E-13	9.78E-13	9.94E-13	1.19E-12	1.38E-12	1.57E-12	65%
Permeability at 45°C	1.02E-12	1.03E-12	1.14E-12	1.29E-12	1.48E-12	1.63E-12	60%
Difference between 21°C and 3°C	6%	8%	5%	16%	1%	6%	
Difference between 45°C and 21°C	7%	6%	14%	8%	7%	3%	
Difference between 45°C and 3°C	14%	14%	20%	26%	8%	10%	

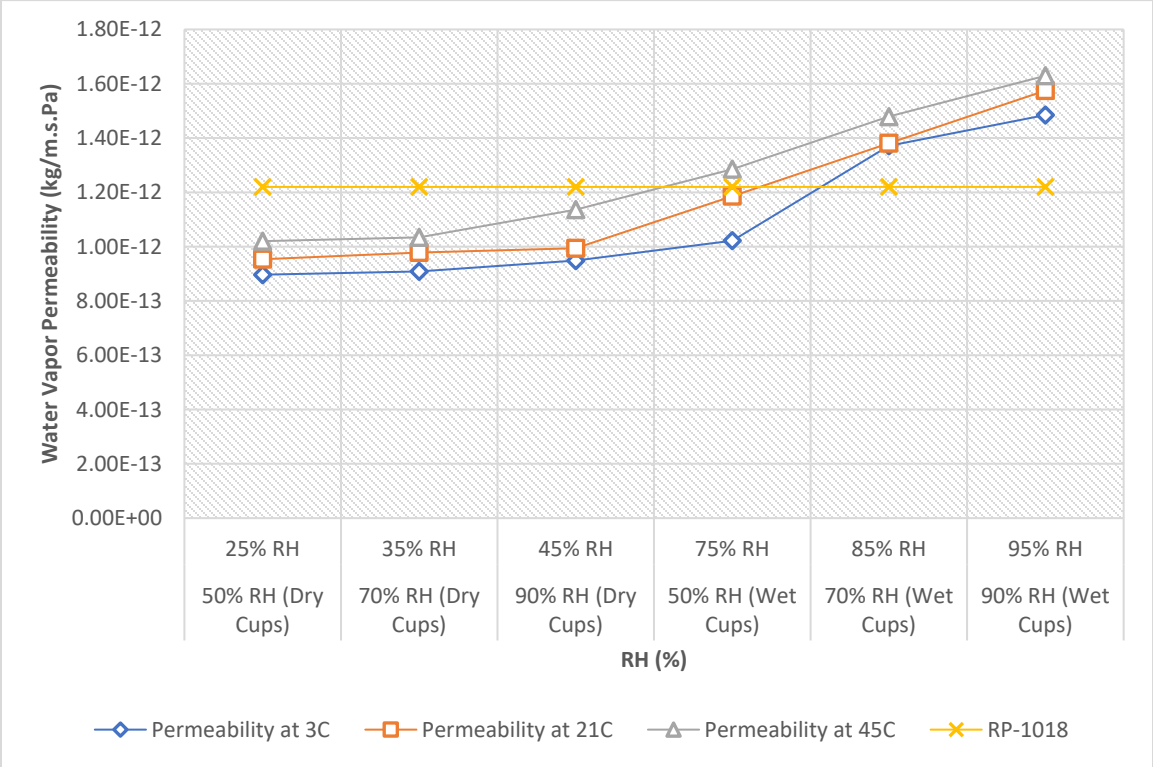

Figure 7-71. XPS-Water Vapor Permeability.

7.3.15 **Open Cell Sprayed Polyurethane Foam**

Due to the rigorous process of preparing open cell sprayed polyurethane insulation samples, highly sensitive permeability test procedure at high temperatures and the project time limit, the permeability test was not carried out at temperature 45°C. Nevertheless, the measured data for water vapor permeability (WVP) and water vapor transmission rate (WVT) of open cell sprayed polyurethane insulation samples at temperatures: 3°C and 21°C determined increase of WVP and WVT with increasing temperature. It was noted that the permeability of tested sprayed polyurethane samples was influenced slightly more by relative humidity than temperature. The vapor permeability of samples increased as 35% and 56% at temperatures 3°C and 21°C, respectively by increasing relative humidity from 25% to 95%. While, the impact of temperature was observed to be between 6% and 28% for relative humidities of 25% and 85% for increasing temperature from 3°C to 45°C.

Comparing our measured permeability for open cell sprayed polyurethane at 21°C with the result from ASHRAE report RP-1018 we found that in contrast with the constant value from ASHRAE report, our results revealed an influence of relative humidity through both dry and wet cup measurements.

Table 7-48. Open Cell Spray Polyurethane-Water Vapor Permeability.

Open Cell Spray Polyurethane-Water Vapor Permeability (kg/m.s.Pa)							
	25% RH	**35% RH**	**45% RH**	**75% RH**	**85% RH**	**95% RH**	Difference between 50% and 90% RH
	Dry Cups			**Wet Cups**			
	50% RH	70% RH	90% RH	50% RH	70% RH	90% RH	
Permeability at 3°C	8.73E-11	9.20E-11	9.51E-11	1.03E-10	1.09E-10	1.18E-10	35%
Permeability at 21°C	9.25E-11	1.05E-10	1.19E-10	1.31E-10	1.40E-10	1.44E-10	56%
Difference between 21°C and 3°C	6%	15%	25%	28%	28%	23%	

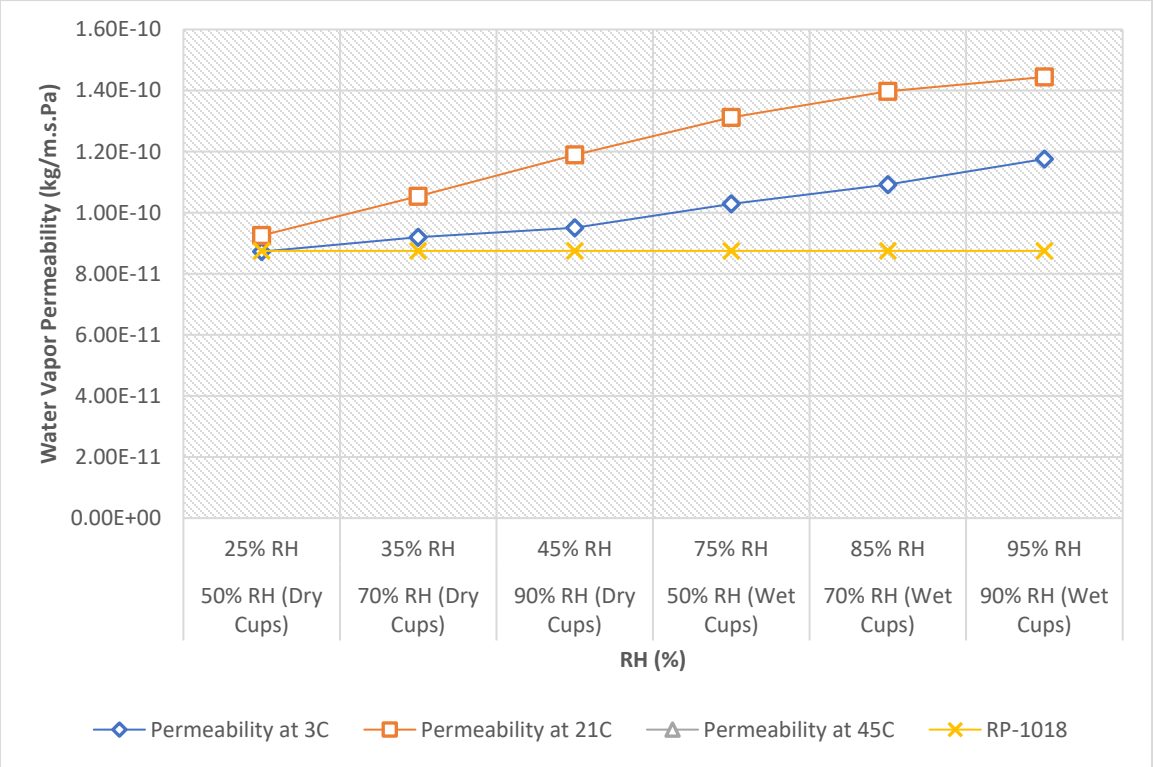

Figure 7-72. Polyurethane Foam-Water Vapor Permeability.

7.3.16 **Polyisocyanurate**

The measured data for water vapor permeability (WVP) and water vapor transmission rate (WVT) of polyisocyanurate samples at different temperatures indicated an increase of WVP and WVT with increasing temperature. According to our results, it was noted that the permeability of tested polyisocyanurate samples was influenced more by relative humidity than temperature. Although the permeability values at 45°C through all relative humidities were higher than the other temperatures, the amplitude of permeability decreased by rising the temperature. For instance, the vapor permeability of samples increased as 191%, 181% and 121% at temperatures 3°C, 21°C and 45°C, respectively by increasing relative humidity from 25% to 95%. Furthermore, the impact of temperature on vapor transmission rate was observed to be more at low relative humidities. The fluctuation of permeability in polyisocyanurate was between 47% and 118% for relative humidities of 95% and 75% for rising temperature from 3°C to 45°C.

Furthermore, our measured permeability appeared to be lower than the associated results from ASHRAE report RP-1018 for polyisocyanurate at 21°C while they both expressed a similar upward trend in permeability graph against the relative humidity.

Table 7-49. Polyisocyanurate-Water Vapor Permeability.

Polyisocyanurate-Water Vapor Permeability (kg/m.s.Pa)							
	25% RH	**35% RH**	**45% RH**	**75% RH**	**85% RH**	**95% RH**	Difference between 50% and 90% RH
	Dry Cups			**Wet Cups**			
	50% RH	70% RH	90% RH	50% RH	70% RH	90% RH	
Permeability at 3°C	1.24E-12	1.34E-12	1.55E-12	2.08E-12	2.94E-12	3.60E-12	191%
Permeability at 21°C	1.50E-12	1.58E-12	2.05E-12	2.72E-12	3.35E-12	4.21E-12	181%
Permeability at 45°C	2.39E-12	2.88E-12	3.32E-12	4.53E-12	4.98E-12	5.28E-12	121%
Difference between 21°C and 3°C	21%	18%	32%	31%	14%	17%	
Difference between 45°C and 21°C	59%	82%	62%	67%	49%	25%	
Difference between 45°C and 3°C	93%	114%	115%	118%	69%	47%	

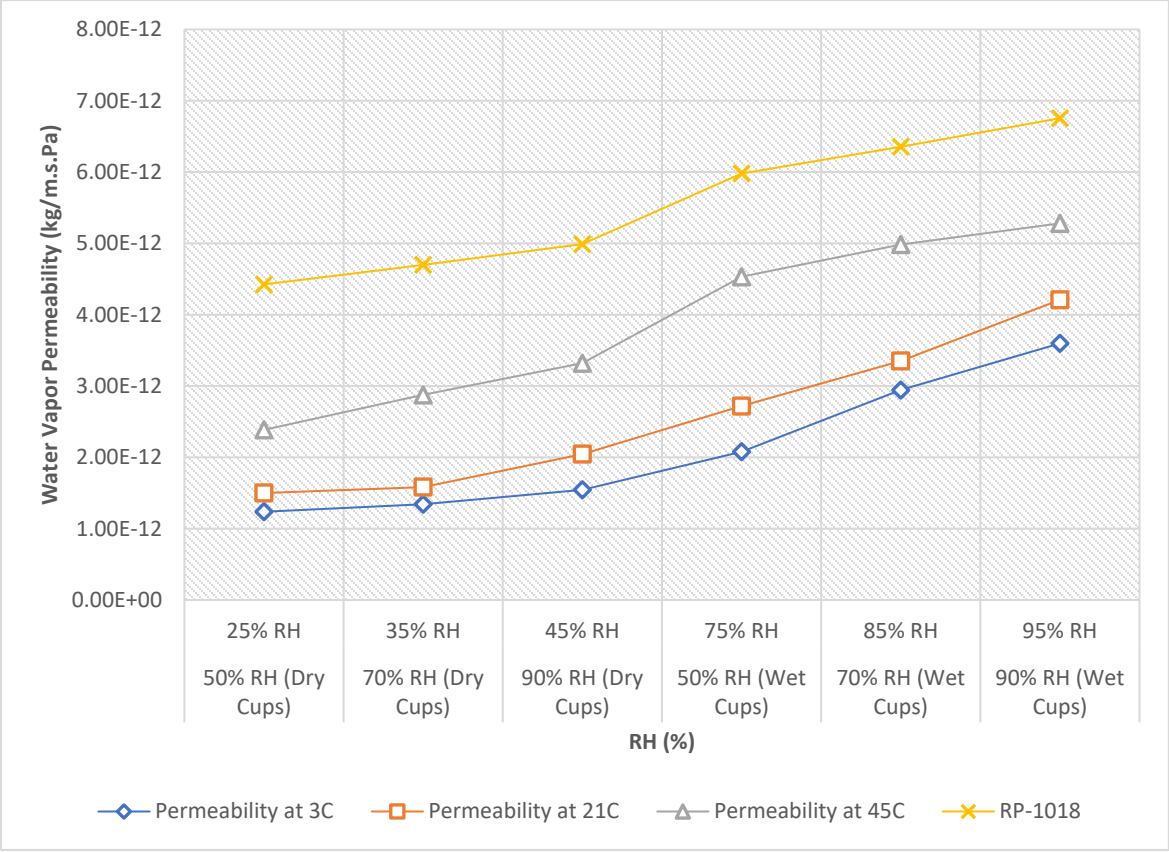

Figure 7-73. Polyiso-Water Vapor Permeability.

7.3.17 **Mineral Fiber (Stone Wool)**

The measured data for water vapor permeability (WVP) and water vapor transmission rate (WVT) of mineral fiber samples at different temperatures indicated an increase of WVP and WVT with increasing temperature. Based on the results, it was noted that the permeability of tested mineral fiber samples was influenced by relative humidity slightly more than temperature. The vapor permeability of samples increased as 40%, 97% and 98% at temperatures 3°C, 21°C and 45°C, respectively by increasing relative humidity from 25% to 95%. However, the impact of temperature was observed to be between 23% and 74% for relative humidities of 25% and 95% for rising temperature from 3°C to 45°C.

Furthermore, the results for permeability of mineral fiber at 21°C from IEA-Annex 24 represented a single value throughout all ranges of relative humidities highlighting no effect of relative humidity on permeability. However, in contrast, our measured values showed a clear impact of relative humidity on permeability of the tested mineral fiber board samples in both dry and wet cup tests.

Table 7-50. Mineral Fiber-Water Vapor Permeability.

Mineral Fiber-Water Vapor Permeability (kg/m.s.Pa)							
	25% RH	**35% RH**	**45% RH**	**75% RH**	**85% RH**	**95% RH**	Difference between 50% and 90% RH
	Dry Cups			**Wet Cups**			
	50% RH	70% RH	90% RH	50% RH	70% RH	90% RH	
Permeability at 3°C	1.03E-10	1.07E-10	1.14E-10	1.19E-10	1.29E-10	1.44E-10	40%
Permeability at 21°C	1.11E-10	1.28E-10	1.45E-10	1.72E-10	1.92E-10	2.19E-10	97%
Permeability at 45°C	1.26E-10	1.37E-10	1.56E-10	1.96E-10	2.19E-10	2.50E-10	98%
Difference between 21°C and 3°C	8%	19%	27%	45%	49%	52%	
Difference between 45°C and 21°C	14%	7%	8%	14%	14%	14%	
Difference between 45°C and 3°C	23%	28%	37%	65%	70%	74%	

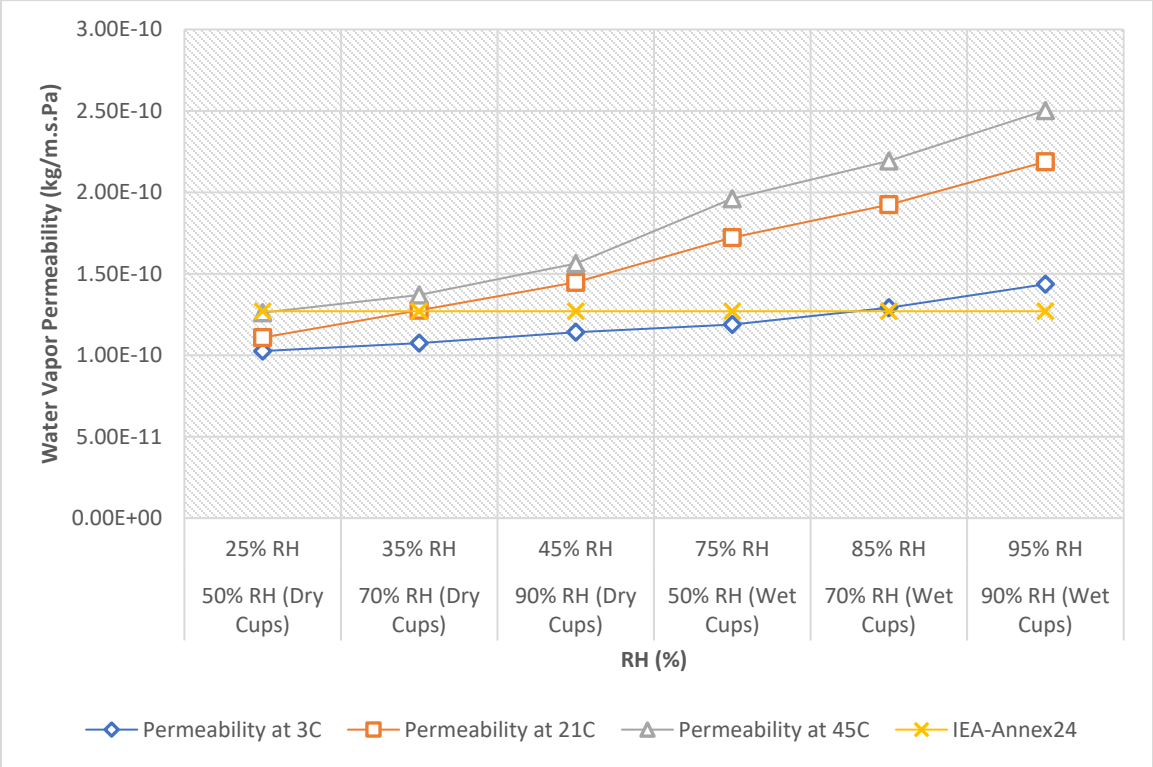

Figure 7-74. Mineral Fiber-Water Vapor Permeability.

7.3.18 **Summary**

The water vapor permeabilities of test materials were determined according to the analysis procedure established by Kumaran (1998a) and standards ASTM-E96/E96M (2013) and EN.ISO.12572 (2001). Through the comparison of water vapor transmission rate for different building products tested in this work, diverse vapor transport abilities were measured. Table 7-51 presents a summary of the impact of increasing temperature on the vapor permeability of tested materials at different relative humidities.

Among those tested products, Cellulose fiber insulation and XPS had the highest and lowest vapor transmission rates at conditions of 45°C and 90% RH in dry cup and 3°C and 90% RH in wet cup, respectively. Furthermore, Tyvek and Douglas Fir samples had the highest and lowest water vapor permeability at conditions of 45°C and 90% RH in wet cup and 3°C and 50% RH in dry cup, respectively. Graphical comparison of measured vapor permeabilities and vapor transmission rates of all tested building materials at different relative humidities are shown in Figure 7-75 and Figure 7-76, respectively.

Spruce at 21°C is more permeable than other wooden products, whereas OSB has the lowest water vapor permeability. The study also found that fiber cement is more permeable than other cladding products at all temperatures. However, stucco had the highest transmission rate at 21°C and 45°C while at 3°C fiber cement presented more vapor transmission rate. Our results presented that the water vapor permeability in all tested materials raised by increasing the temperature, and the influence of temperature was more significant at higher relative humidities. The most influenced vapor transmission rate upon rising temperature is found in cellulose followed by Tyvek, mineral wool and Densglass gold gypsum products. It is notable that the impact of temperature on vapor permeability at lower relative humidities in clay brick and fiber cement board among the cladding materials was observed to be less than the stucco and western red cedar samples. The difference between our measured values for vapor permeability of some tested materials and the results from ASHRAE RP-1018 is assumed to be due to the differences in the material composition, manufactures, workmanship and preparation process.

Table 7-51. Water Vapor Permeability Difference between 45°C and 3°C.

Water Vapor Permeability Difference between 45°C and 3°C (%)								
Material	**Thickness (mm)**	**Density (kg/m^3)**	**Dry Cups**			**Wet Cups**		
			50% RH	**70% RH**	**90% RH**	**50% RH**	**70% RH**	**90% RH**
Claddings								
Clay Brick	14.2	2080.78 ± 27	60%	35%	73%	70%	116%	249%
Fiber Cement	7.7	1358 ± 12	21%	33%	20%	105%	110%	188%
Stucco	17.1	2399 ± 39	522%	482%	468%	387%	414%	490%
Western Red Cedar	12.7	380 ± 4	119%	164%	113%	104%	131%	165%
Weather Resistive Barriers (WRB)								
Tyvek	0.14	65 g/m^2	12%	18%	24%	26%	36%	37%
60 Min Building Paper	0.35	310.5 g/m^2	74%	132%	123%	180%	161%	153%
Wall Sheathing Boards								
OSB	11.4	620 ± 12	38%	47%	101%	82%	90%	155%
Plywood	12.3	461 ± 8	32%	34%	46%	115%	115%	129%
Densglass Gold Gypsum	13.2	755 ± 7	11%	8%	5%	40%	58%	91%
Wood Studs								
Spruce	12.2	469 ± 1.7	81%	127%	49%	194%	311%	302%
Douglas Fir	12.4	572 ± 9	183%	174%	36%	63%	29%	68%
Insulations								
Cellulose Fiber	25.8	79.24	151%	147%	75%	85%	87%	112%
EPS	12.7	21.9 ± 0.1	31%	38%	44%	53%	55%	56%
XPS	15.4	26.6 ± 0.15	14%	14%	20%	26%	8%	10%
Open Cell Sprayed Polyurethane Foam ***(Difference between 21°C and 3°C)***	14.3	14.75 ± 1.2	6%	15%	25%	28%	28%	23%
Polyisocyanurate	24.1	27.5 ± 0.16	93%	114%	115%	118%	69%	47%
Mineral Fiber	38.7	128 ± 4	23%	28%	37%	65%	70%	74%

Figure 7-75. Comparing Water Vapor Permeability of all tested building materials at different temperatures.

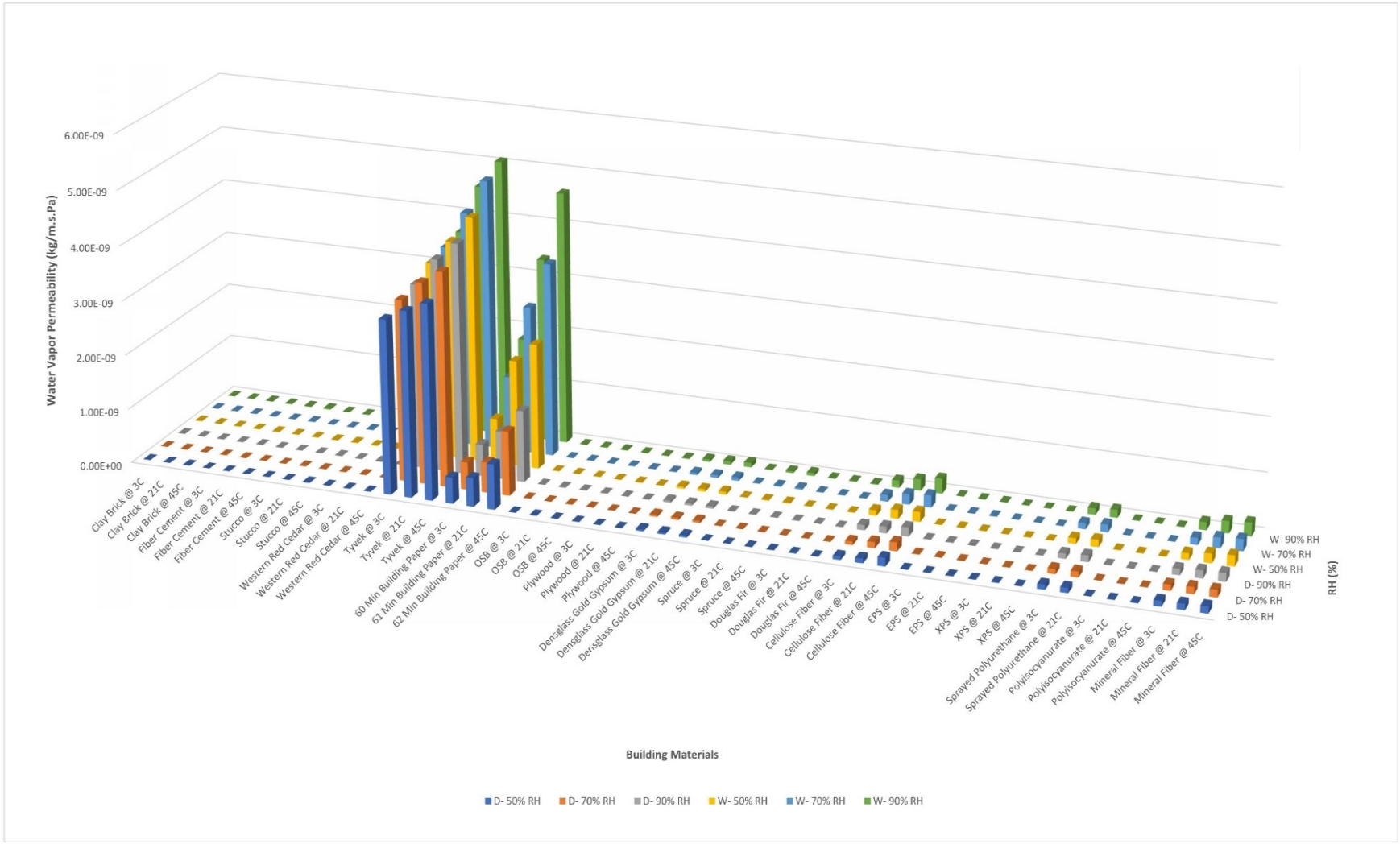

Figure 7-76. Comparing Water Vapor Transmission rate of all tested building materials at different temperatures.

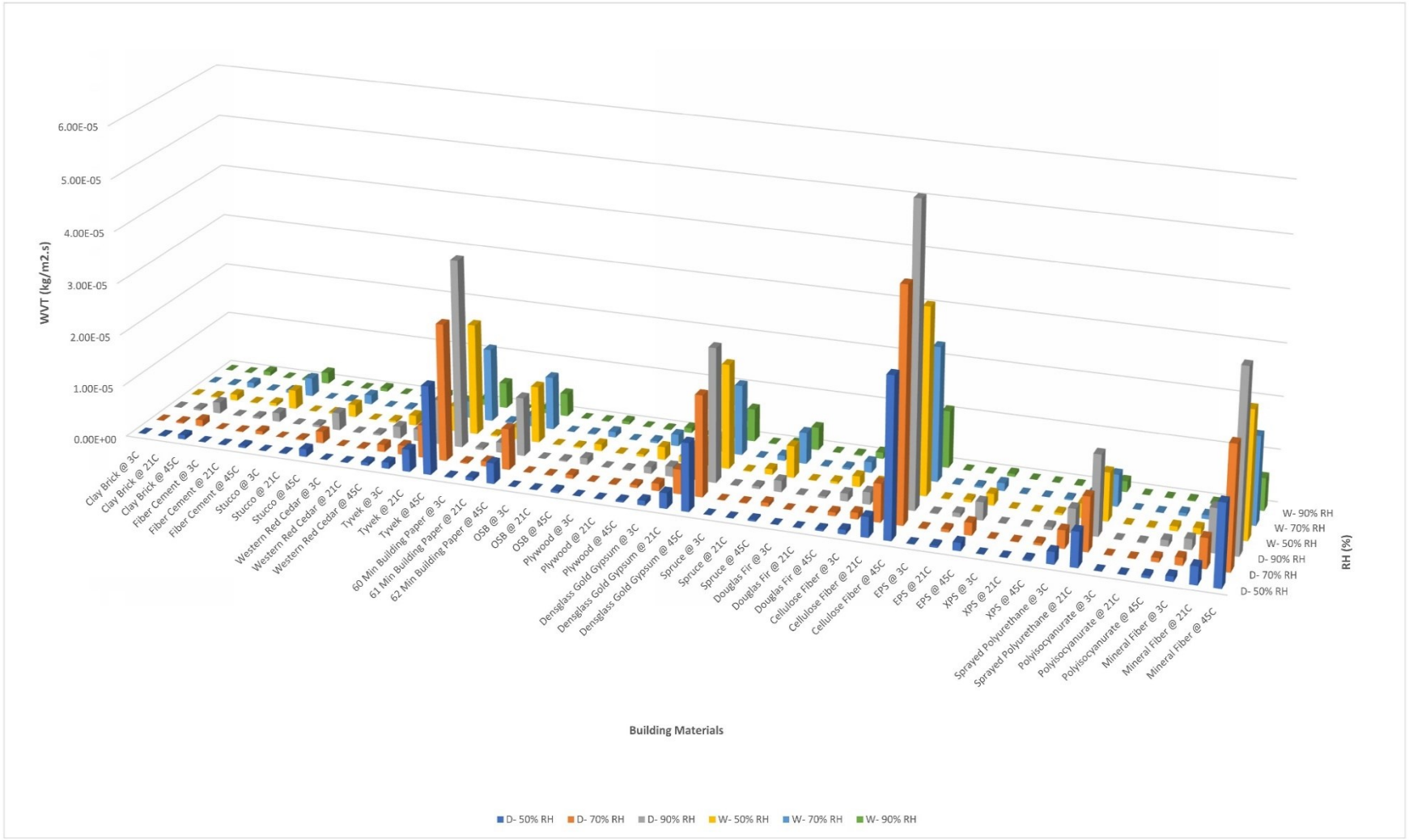

7.4 Water Absorption Coefficients of Building Materials

The water absorption coefficient (WAC) of building materials was initially measured at temperature 21°C exposing to ascending relative humidities of 50%, 70% and 90%. Then, the water absorption coefficient of the materials was measured at lower temperature of 3°C and higher temperature of 45°C while they were exposed to the same increasing steps of relative humidities. Measuring the absorption rate for some building materials including: EPS, XPS and polyisocyanurate through partial immersion might take several days. Accordingly, in this project, those building materials were excluded from absorption test through partial immersion into water.

Unlike the results for absorption coefficient from ASHRAE report RP-1018 which is a single value obtained at temperature of 22°C while exposed to the room relative humidity, we measured three values for the absorption coefficient at each tested temperature. This enables us to attain more detailed characteristic pertinent to moisture movement and capillary transport of the building materials while exposed and maintained in different conditions of temperature and relative humidities. The results of water absorption coefficient of the corresponding building material which is available in the ASHRAE RP-1018 is presented in a graph along with our measured values for the purposes of general comparison.

7.4.1 **Clay Brick**

According to the measured water intake values through partial immersion test for the clay brick samples at different relative humidities and temperatures, the water absorption coefficient for clay brick decreased as relative humidity increase while increased by rising temperature. It was noted that the influence of temperature was significant at 90% relative humidity where the absorption coefficient increased as 1012% by rising temperature from 3°C to 45°C.

Table 7-52. Clay Brick-Effect of Relative Humidity on Water Absorption Coefficient.

Clay Brick-Effect of Relative Humidity on Water Absorption Coefficient				**Difference between RHs**		
	50% RH	**70% RH**	**90% RH**	**70%-50%**	**90%-70%**	**90%-50%**
WAC at 3°C	7.15E-03	5.81E-03	6.96E-04	-19%	-88%	-90%
WAC at 21°C	1.02E-02	8.33E-03	3.36E-03	-18%	-60%	-67%
WAC at 45°C	1.14E-02	8.77E-03	7.74E-03	-23%	-12%	-32%
Difference between 21°C and 3°C	42%	43%	383%			
Difference between 45°C and 21°C	12%	5%	130%			
Difference between 45°C and 3°C	60%	51%	1012%			

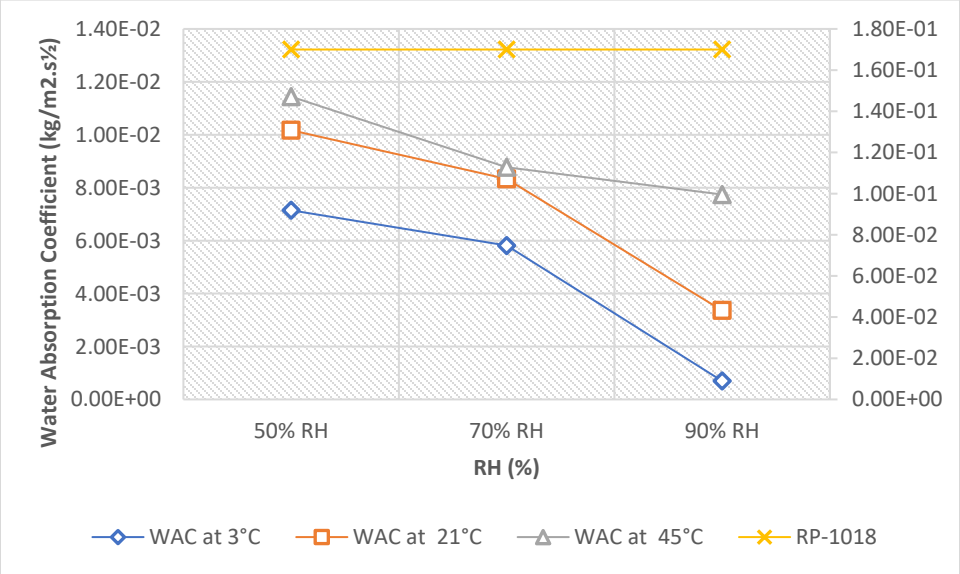

Figure 7-77. Clay Brick-Effect of Relative Humidity on Water Absorption Coefficient.

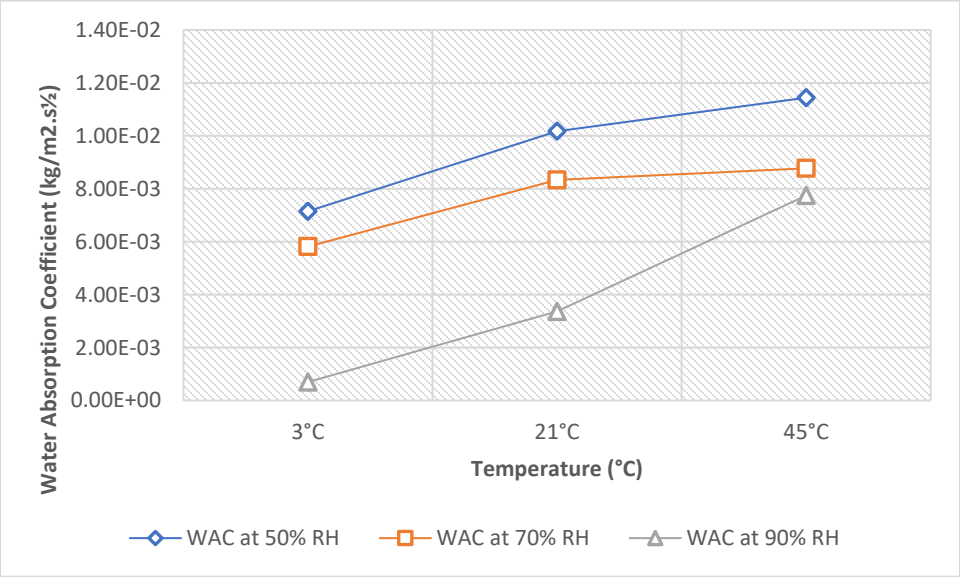

Figure 7-78. Clay Brick-Effect of Relative Humidity on Water Absorption Coefficient.

7.4.2 **Fiber Cement**

According to the measured data of water uptake values test for the fiber cement samples at multiple relative humidities and temperatures, the water absorption coefficient for fiber cement decreased with relative humidity and increased by rising temperature. It was noted that the influence of temperature was significant at 90% relative humidity since the absorption coefficient increased as 340% by rising temperature from 3°C to 45°C.

Table 7-53. Fiber Cement -Effect of Relative Humidity on Water Absorption Coefficient.

Fiber Cement -Effect of Relative Humidity on Water Absorption Coefficient				**Difference between RHs**		
	50% RH	**70% RH**	**90% RH**	**70%-50%**	**90%-70%**	**90%-50%**
WAC at 3°C	6.76E-04	3.11E-04	8.01E-05	-54%	-74%	-88%
WAC at 21°C	7.94E-04	4.20E-04	3.21E-04	-47%	-23%	-60%
WAC at 45°C	8.44E-04	5.18E-04	3.53E-04	-39%	-32%	-58%
Difference between 21°C and 3°C	17%	35%	301%			
Difference between 45°C and 21°C	6%	23%	10%			
Difference between 45°C and 3°C	25%	67%	340%			

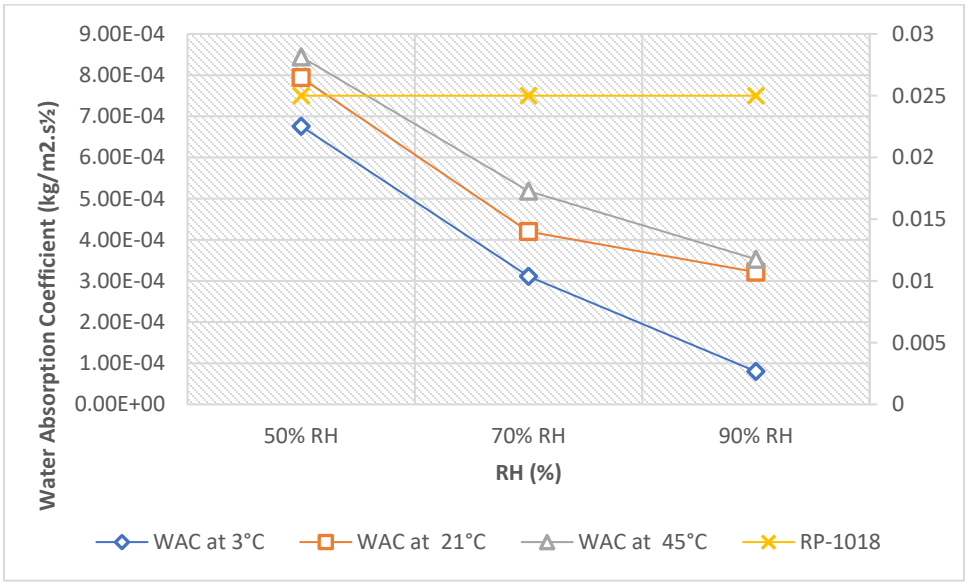

Figure 7-79. Fiber Cement-Effect of Relative Humidity on Water Absorption Coefficient.

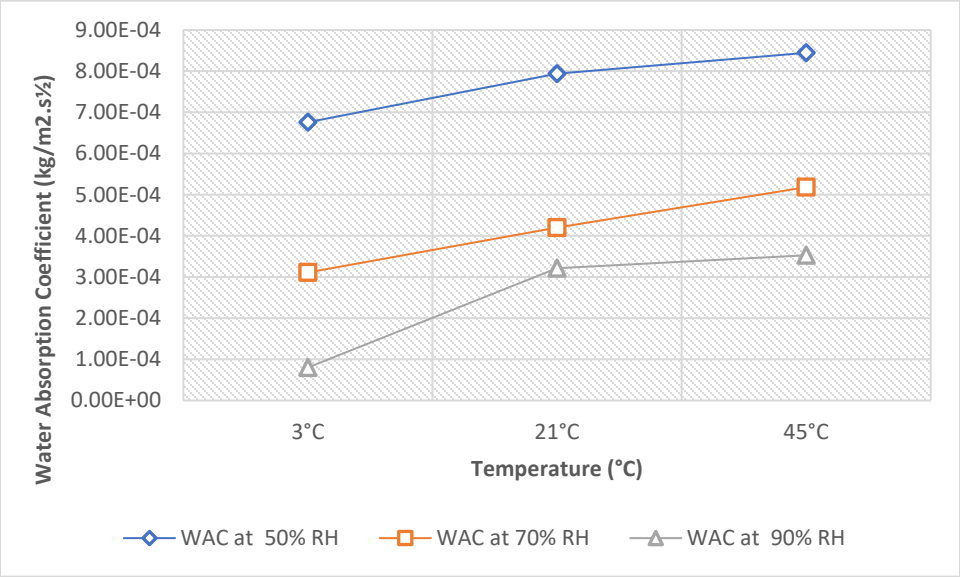

Figure 7-80. Fiber Cement-Effect of Temperature on Water Absorption Coefficient.

7.4.3 **Stucco**

The measured water intake values through partial immersion test for the stucco samples at different relative humidities and temperatures, showed that the water absorption coefficient for stucco decreased with relative humidity while increased by rising temperature. It was noted that the influence of temperature was significant at higher relative humidities. The absorption coefficient increased by 42% and 127% at 50% and 90% RH due to rising temperature from 3°C to 45°C. However, at 45°C, the absorption rate did not present significant drop at higher relative humidities.

Table 7-54. Stucco -Effect of Relative Humidity on Water Absorption Coefficient.

Stucco -Effect of Relative Humidity on Water Absorption Coefficient				**Difference between RHs**		
	50% RH	**70% RH**	**90% RH**	**70%-50%**	**90%-70%**	**90%-50%**
WAC at 3°C	7.98E-03	5.50E-03	4.66E-03	-31%	-15%	-42%
WAC at 21°C	9.54E-03	6.16E-03	5.19E-03	-35%	-16%	-46%
WAC at 45°C	1.13E-02	1.08E-02	1.06E-02	-4%	-2%	-6%
Difference between 21°C and 3°C	20%	12%	11%			
Difference between 45°C and 21°C	18%	75%	104%			
Difference between 45°C and 3°C	42%	96%	127%			

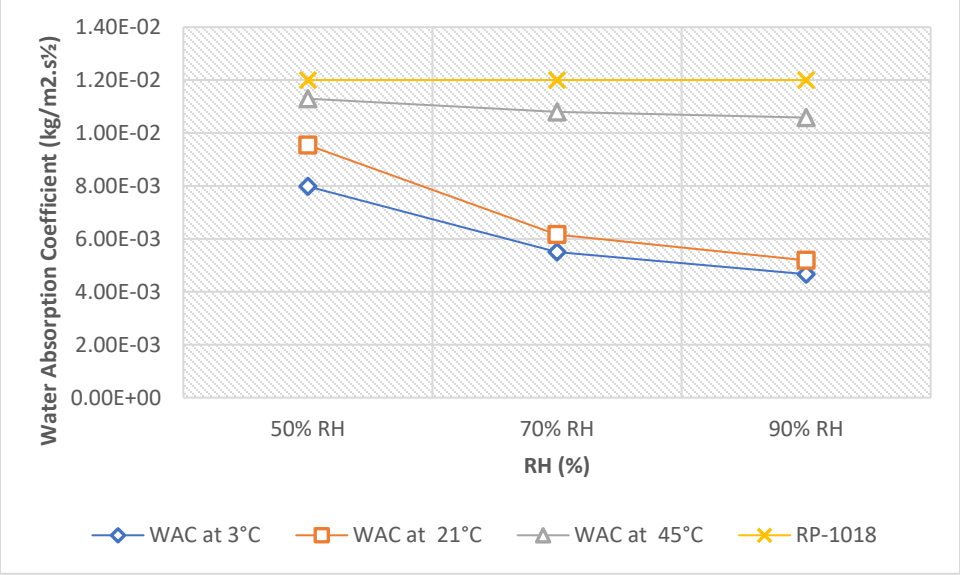

Figure 7-81. Stucco-Effect of Relative Humidity on Water Absorption Coefficient.

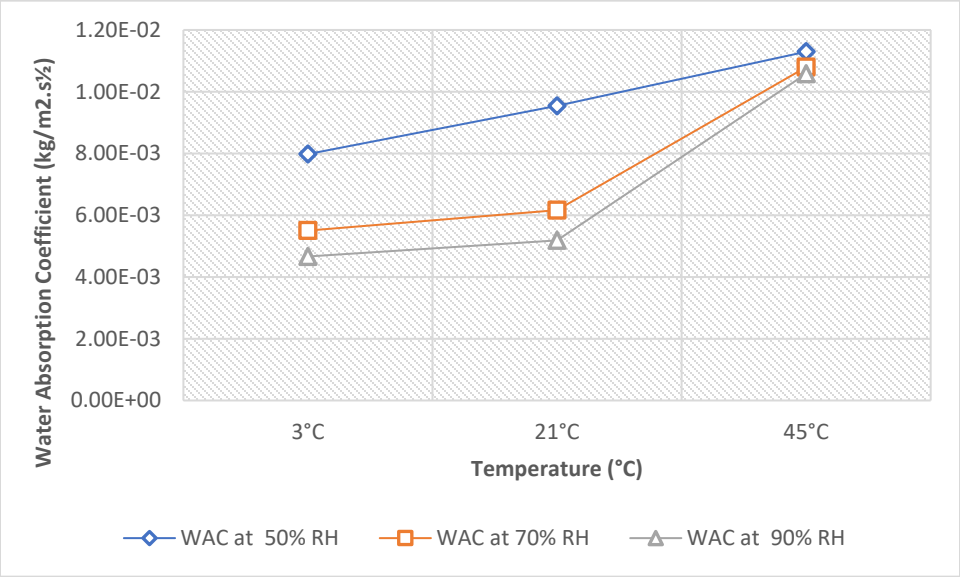

Figure 7-82. Stucco-Effect of Relative Humidity on Water Absorption Coefficient.

7.4.4 **Western Red Cedar**

Based on the measured data of partial immersion test for the western red cedar samples at multiple relative humidities and temperatures, the water absorption coefficient for western red cedar wood decreased with relative humidity and increased by rising temperature. The result presented that reducing temperature from 21°C to 3°C considerably lowered the values for absorbing water by 64% to 114%. While, by increasing temperature from 21°C to 45°C, the rate of water intake increased slightly between 3% and 22%.

Table 7-55. Western Red Cedar -Effect of Relative Humidity on Water Absorption Coefficient.

Western Red Cedar -Effect of Relative Humidity on Water Absorption Coefficient				**Difference between RHs**		
	50% RH	**70% RH**	**90% RH**	**70%-50%**	**90%-70%**	**90%-50%**
WAC at 3°C	2.77E-03	2.05E-03	1.15E-03	-26%	-44%	-58%
WAC at 21°C	4.54E-03	3.35E-03	2.47E-03	-26%	-26%	-46%
WAC at 45°C	5.52E-03	3.45E-03	2.81E-03	-38%	-19%	-49%
Difference between 21°C and 3°C	64%	64%	114%			
Difference between 45°C and 3°C	22%	3%	13%			
Difference between 45°C and 3°C	99%	68%	143%			

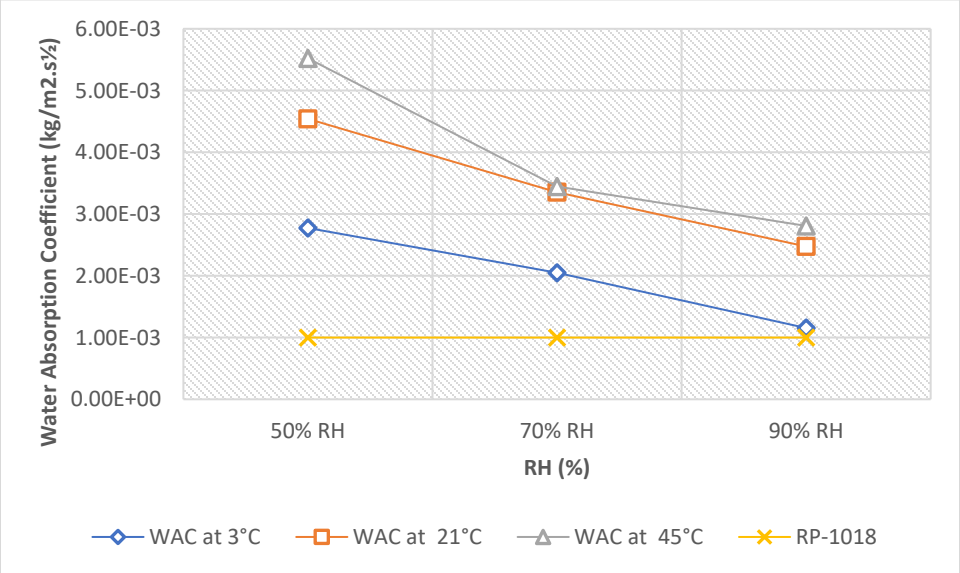

Figure 7-83. Western Red Cedar-Effect of Relative Humidity on Water Absorption Coefficient.

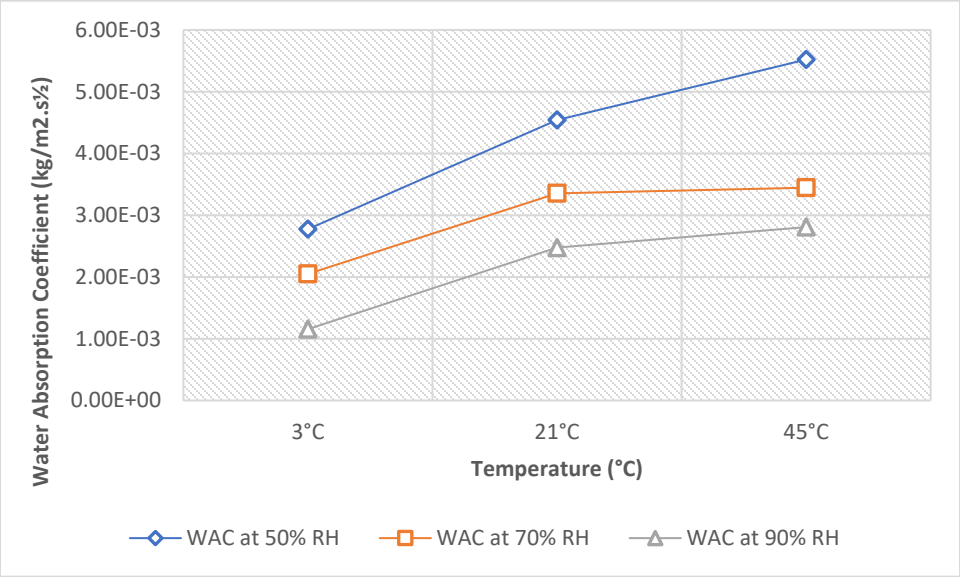

Figure 7-84. Western Red Cedar-Effect of Temperature on Water Absorption Coefficient.

7.4.5 **Tyvek**

Analyzing measured data of partial immersion test for Tyvek samples at different relative humidities and temperatures, indicated that the water absorption coefficient for Tyvek building wrap decreased with relative humidity and increased by rising temperature. However, the result showed that the variation in relative humidity affected the rate of water uptake more than temperature. Additionally, by increasing relative humidity above 50% the changes in absorption coefficient was insignificant as the influence of temperature at 90% relative humidity was noted to be negligible.

Table 7-56. Tyvek -Effect of Relative Humidity on Water Absorption Coefficient.

Tyvek -Effect of Relative Humidity on Water Absorption Coefficient				**Difference between RHs**		
	50% RH	**70% RH**	**90% RH**	**70%-50%**	**90%-70%**	**90%-50%**
WAC at 3°C	1.06E-04	5.91E-05	5.01E-05	-44%	-15%	-53%
WAC at 21°C	1.20E-04	7.80E-05	5.33E-05	-35%	-32%	-56%
WAC at 45°C	1.35E-04	7.72E-05	5.47E-05	-43%	-29%	-59%
Difference between 21°C and 3°C	14%	32%	6%			
Difference between 45°C and 21°C	12%	-1%	3%			
Difference between 45°C and 3°C	27%	31%	9%			

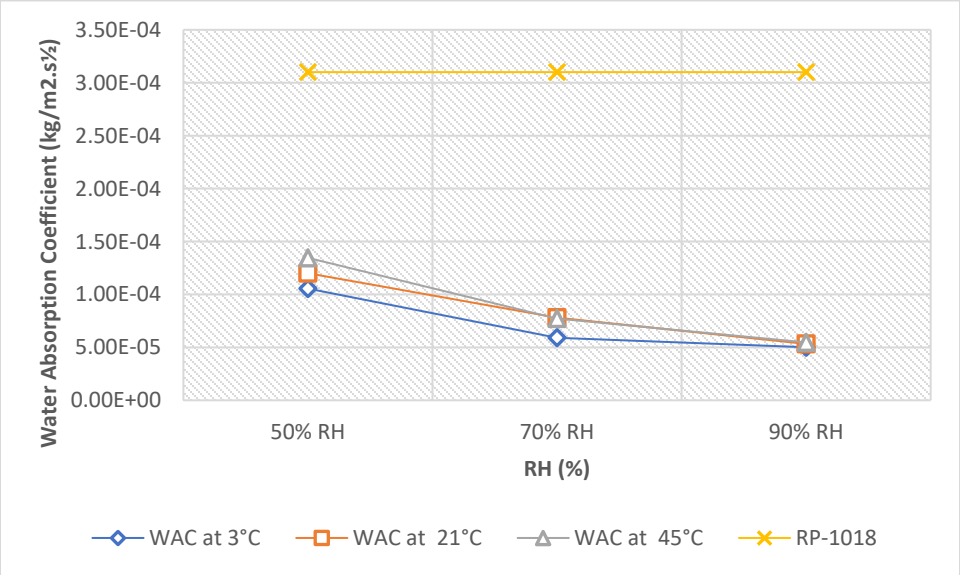

Figure 7-85. Tyvek-Effect of Relative Humidity on Water Absorption Coefficient.

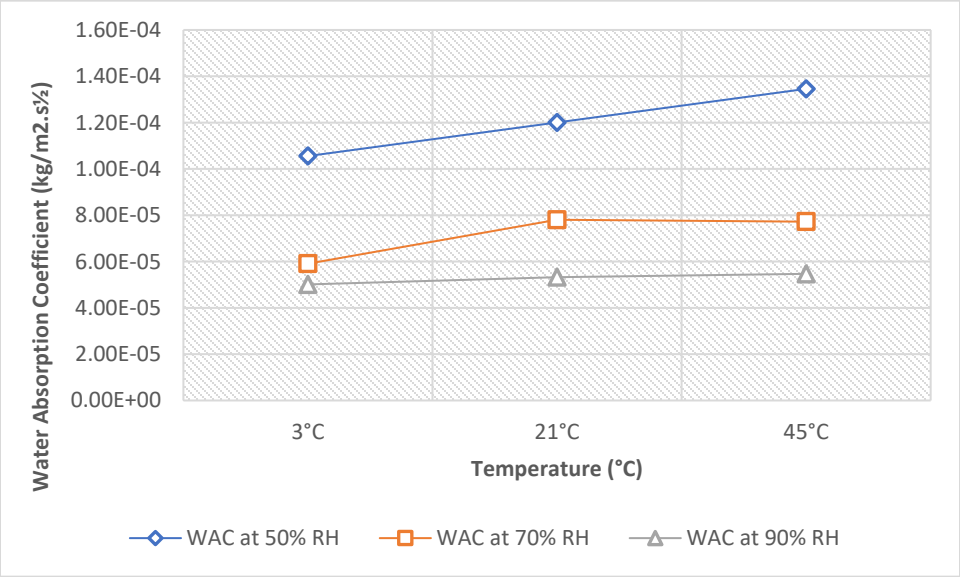

Figure 7-86. Tyvek-Effect of Temperature on Water Absorption Coefficient.

7.4.6 **60 Min Building Paper**

According to the measured data of partial immersion test for the 60-min building paper samples at different relative humidities and temperatures, the water absorption coefficient for tested building paper decreased with relative humidity and increased by rising temperature. The result indicated that the rate of absorbing water was more influenced by temperature than relative humidity. For example, changes in the rate of water absorption through escalating relative humidity was the highest as 33% at 3°C and dropped significantly to -9% and -1% when temperature rose to 21°C and 45°C, respectively.

Table 7-57. Building Paper 60 min -Effect of Relative Humidity on Water Absorption Coefficient.

Building Paper 60 min -Effect of Relative Humidity on Water Absorption Coefficient				**Difference between RHs**		
	50% RH	**70% RH**	**90% RH**	**70%-50%**	**90%-70%**	**90%-50%**
WAC at 3°C	3.77E-04	3.72E-04	2.54E-04	-1%	-32%	-33%
WAC at 21°C	5.66E-04	5.02E-04	3.81E-04	-11%	-24%	-33%
WAC at 45°C	6.77E-04	6.30E-04	6.18E-04	-7%	-2%	-9%
Difference between 21°C and 3°C	50%	35%	50%			
Difference between 45°C and 3°C	19%	26%	62%			
Difference between 45°C and 3°C	79%	69%	143%			

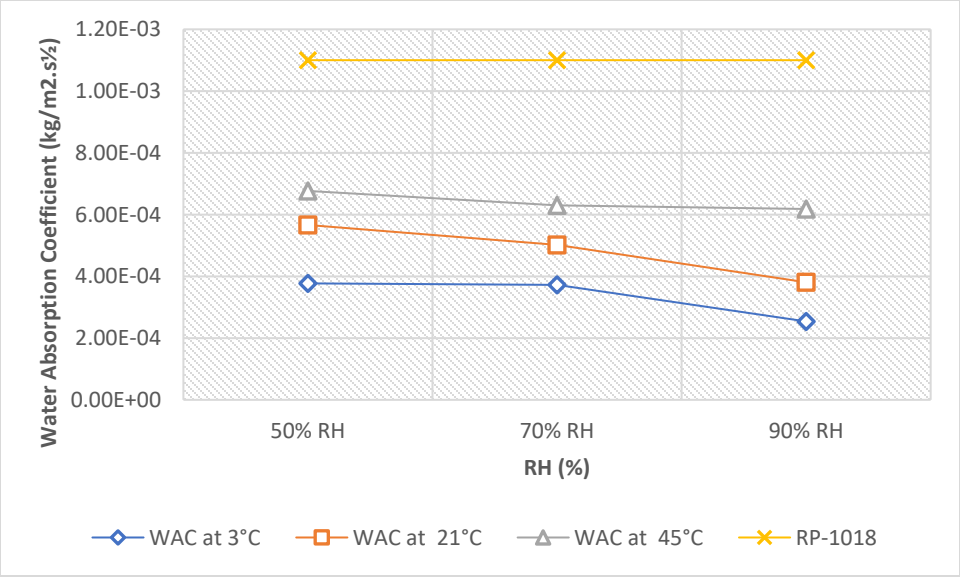

Figure 7-87. Building Paper 60 min-Effect of Relative Humidity on Water Absorption Coefficient.

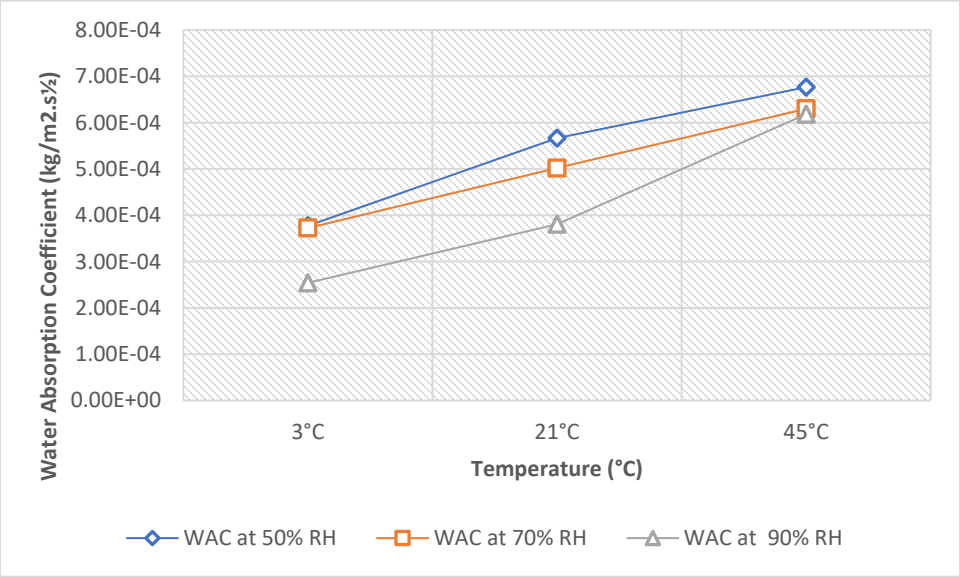

Figure 7-88. Building Paper 60 mins-Effect of Temperature on Water Absorption Coefficient.

7.4.7 **Oriented Strand Board (OSB)**

Analyzing the measured data of partial immersion test for the OSB samples at different relative humidities and temperatures, the water absorption coefficient for tested OSB decreased with relative humidity while increased by rising temperature. The result indicated that the rate of absorbing water was more influenced by temperature than relative humidity. For example, changes in the rate of water absorption through escalating relative humidity were -53%, -24% and -82% at temperatures 3°C, 21°C and 45°C, respectively. However, the absorption rate increased as 1169%, 432% and 378% at 50%, 70% and 90% RH, respectively while temperature increased from 3°C to 45°C.

Table 7-58. OSB -Effect of Relative Humidity on Water Absorption Coefficient.

OSB -Effect of Relative Humidity on Water Absorption Coefficient				**Difference between RHs**		
	50% RH	**70% RH**	**90% RH**	**70%-50%**	**90%-70%**	**90%-50%**
WAC at 3°C	1.36E-03	1.07E-03	6.43E-04	-21%	-40%	-53%
WAC at 21°C	2.34E-03	1.90E-03	1.78E-03	-19%	-6%	-24%
WAC at 45°C	1.73E-02	5.71E-03	3.07E-03	-67%	-46%	-82%
Difference between 21°C and 3°C	72%	77%	177%			
Difference between 45°C and 21°C	636%	201%	73%			
Difference between 45°C and 3°C	1169%	432%	378%			

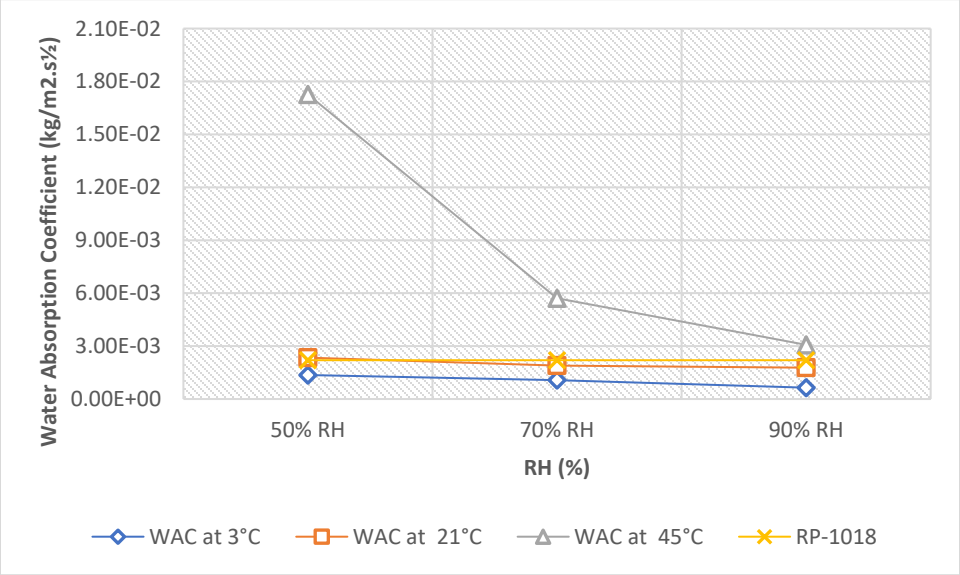

Figure 7-89. OSB-Effect of Relative Humidity on Water Absorption Coefficient.

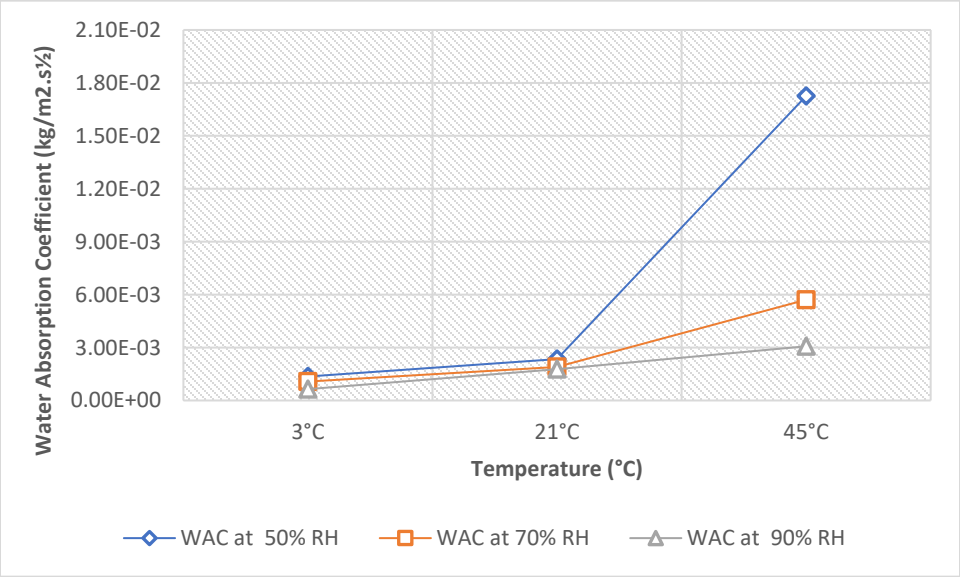

Figure 7-90. OSB-Effect of Temperature on Water Absorption Coefficient.

7.4.8 **Plywood**

Analyzing the measured data of partial immersion test for the plywood samples at different relative humidities and temperatures, the water absorption coefficient for tested plywood decreased with relative humidity while increased by rising temperature. The result indicated that the influence by temperature was more considerable than relative humidity. For example, changes in the rate of water absorption through rising relative humidity were -28%, -41% and -36% at temperatures 3°C, 21°C and 45°C, respectively. However, the absorption rate increased by 169%, 158% and 139% at 50%, 70% and 90% RH, respectively, while temperature increased from 3°C to 45°C.

Table 7-59. Plywood -Effect of Relative Humidity on Water Absorption Coefficient.

Plywood -Effect of Relative Humidity on Water Absorption Coefficient				**Difference between RHs**		
	50% RH	**70% RH**	**90% RH**	**70%-50%**	**90%-70%**	**90%-50%**
WAC at 3°C	1.40E-03	1.21E-03	1.02E-03	-14%	-16%	-28%
WAC at 21°C	2.78E-03	2.06E-03	1.65E-03	-26%	-20%	-41%
WAC at 45°C	3.77E-03	3.11E-03	2.43E-03	-18%	-22%	-36%
Difference between 21°C and 3°C	98%	71%	62%			
Difference between 45°C and 21°C	36%	51%	47%			
Difference between 45°C and 3°C	169%	158%	139%			

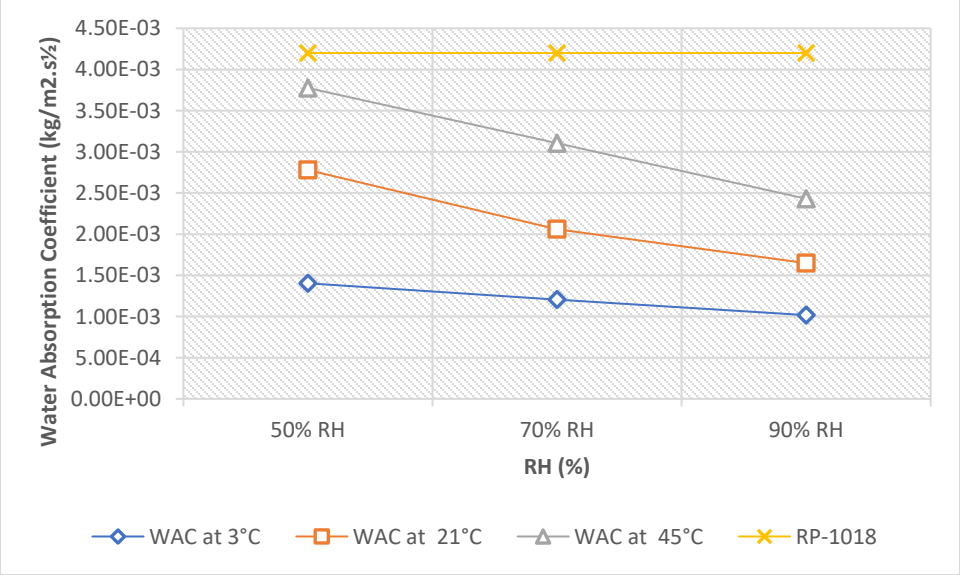

Figure 7-91. Plywood-Effect of Relative Humidity on Water Absorption Coefficient.

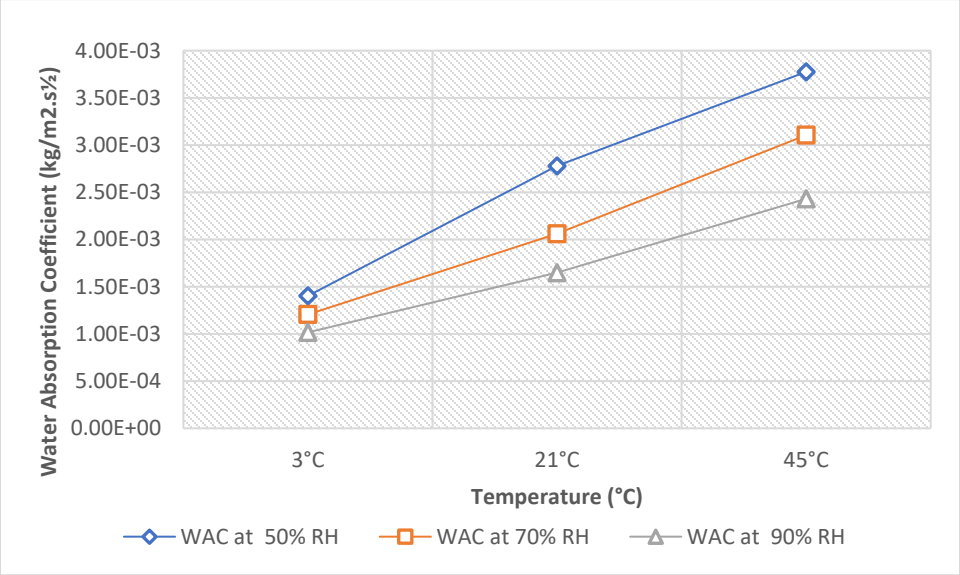

Figure 7-92. Plywood-Effect of Temperature on Water Absorption Coefficient.

7.4.9 **Densglass Gold Gypsum Sheathing Board**

Analyzing the measured data of partial immersion test for the exterior gypsum sheathing samples at different relative humidities and temperatures, the water absorption coefficient for tested exterior gypsum sheathing decreased with relative humidity while increased by rising temperature. The result indicated that the influence by temperature was more considerable than relative humidity. For example, changes in the rate of water absorption through rising relative humidity were -6%, -40% and -38% at temperatures 3°C, 21°C and 45°C, respectively. While, the absorption rate increased dramatically by 1133%, 975% and 717% at 50%, 70% and 90% RH, respectively, while temperature increased from 3°C to 45°C. Additionally, it is worthwhile that a great increase took place between 3°C and 21°C as 803%, 975% and 717% for relative humidities of 50%, 70% and 90%, respectively.

Table 7-60. Densglass Gypsum -Effect of Relative Humidity on Water Absorption Coefficient.

Densglass Gypsum -Effect of Relative Humidity on Water Absorption Coefficient				**Difference between RHs**		
	50% RH	**70% RH**	**90% RH**	**70%-50%**	**90%-70%**	**90%-50%**
WAC at 3°C	1.86E-04	1.85E-04	1.74E-04	-1%	-6%	-6%
WAC at 21°C	1.68E-03	1.16E-03	1.01E-03	-31%	-13%	-40%
WAC at 45°C	2.30E-03	1.99E-03	1.43E-03	-13%	-28%	-38%
Difference between 21°C and 3°C	803%	525%	481%			
Difference between 45°C and 21°C	37%	72%	41%			
Difference between 45°C and 3°C	1133%	975%	717%			

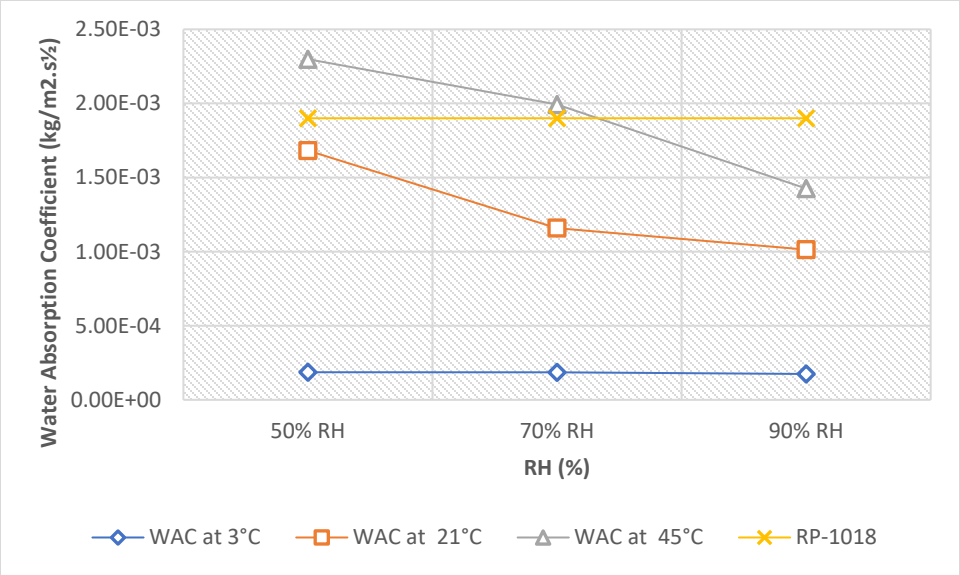

Figure 7-93. Densglass Gypsum Sheathing-Effect of Relative Humidity on Water Absorption Coefficient.

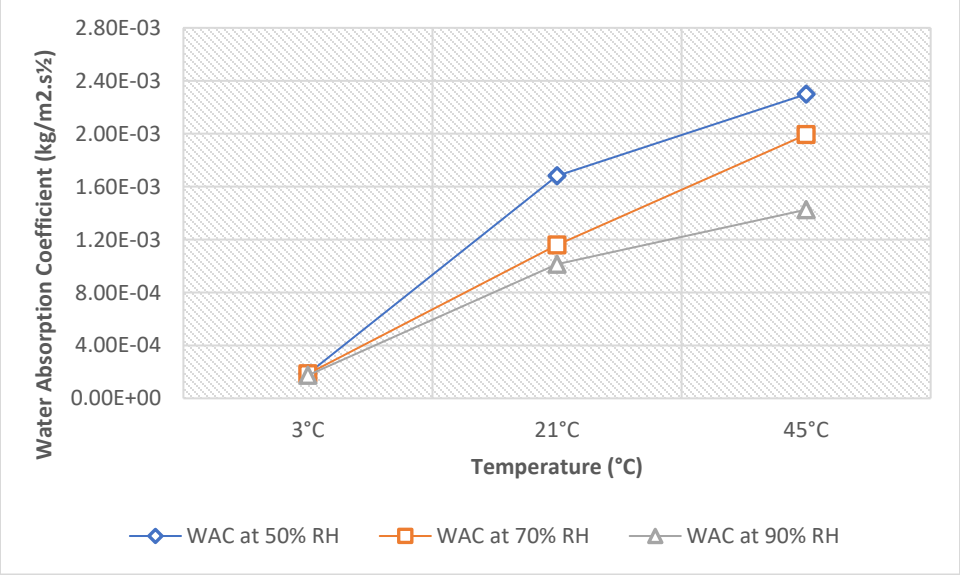

Figure 7-94. Densglass Gypsum Sheathing-Effect of Temperature on Water Absorption Coefficient.

7.4.10 **Spruce**

Analyzing the measured data of partial immersion test for the spruce samples at different relative humidities and temperatures, the water absorption coefficient for spruce decreased with relative humidity while increased by rising temperature. The result indicated that the influence by temperature was more than relative humidity. For example, changes in the rate of water absorption through rising relative humidity were -51%, -46% and -31% at temperatures 3°C, 21°C and 45°C, respectively. However, the absorption rate increased dramatically by 101%, 116% and 185% at 50%, 70% and 90% RH, respectively, while temperature increased from 3°C to 45°C.

Table 7-61. Spruce -Effect of Relative Humidity on Water Absorption Coefficient.

Spruce -Effect of Relative Humidity on Water Absorption Coefficient				**Difference between RHs**		
	50% RH	**70% RH**	**90% RH**	**70%-50%**	**90%-70%**	**90%-50%**
WAC at 3°C	9.21E-04	8.41E-04	4.50E-04	-9%	-46%	-51%
WAC at 21°C	1.54E-03	9.85E-04	8.33E-04	-36%	-15%	-46%
WAC at 45°C	1.86E-03	1.81E-03	1.28E-03	-2%	-29%	-31%
Difference between 21°C and 3°C	68%	17%	85%			
Difference between 45°C and 21°C	20%	84%	54%			
Difference between 45°C and 3°C	101%	116%	185%			

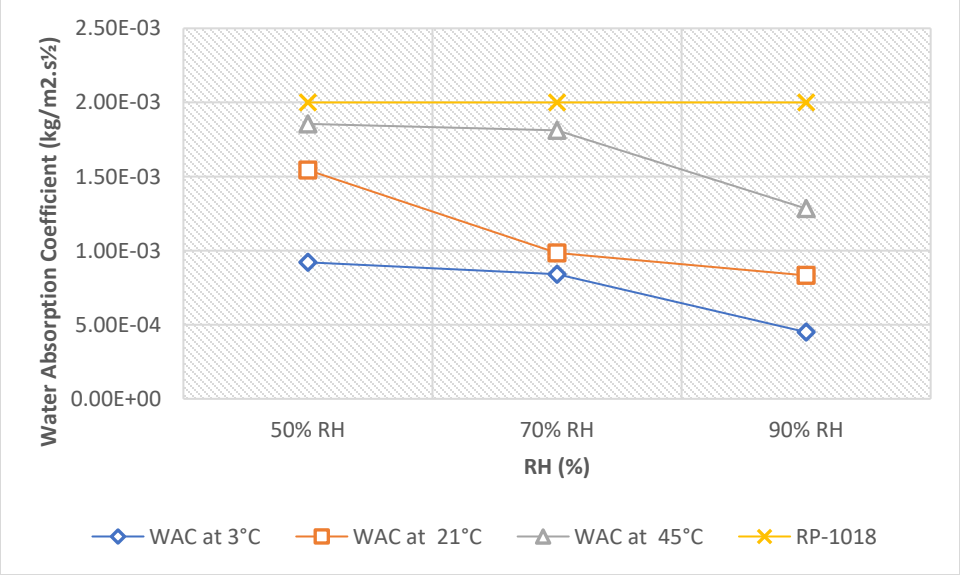

Figure 7-95. Spruce-Effect of Relative Humidity on Water Absorption Coefficient.

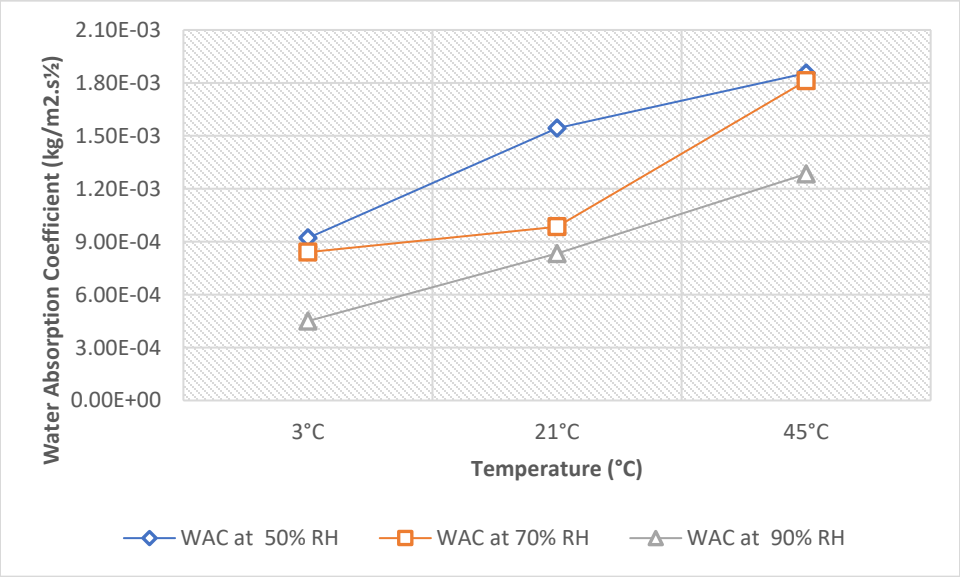

Figure 7-96. Spruce-Effect of Temperature on Water Absorption Coefficient.

7.4.11 **Douglas Fir**

Analyzing the measured data of partial immersion test for the douglas fir samples at different relative humidities and temperatures, the water absorption coefficient for douglas fir decreased with relative humidity while increased by rising temperature. The result indicated that the influence by temperature was more than relative humidity. For example, changes in the rate of water absorption through rising relative humidity were -53%, -44% and -26% at temperatures 3°C, 21°C and 45°C, respectively. However, the absorption rate increased dramatically by 86%, 114% and 191% at 50%, 70% and 90% RH, respectively, while temperature increased from 3°C to 45°C.

Table 7-62. Douglas Fir -Effect of Relative Humidity on Water Absorption Coefficient.

Douglas Fir -Effect of Relative Humidity on Water Absorption Coefficient				**Difference between RHs**		
	50% RH	**70% RH**	**90% RH**	**70%-50%**	**90%-70%**	**90%-50%**
WAC at 3°C	8.81E-04	7.05E-04	4.16E-04	-20%	-41%	-53%
WAC at 21°C	1.42E-03	1.23E-03	7.96E-04	-13%	-35%	-44%
WAC at 45°C	1.64E-03	1.51E-03	1.21E-03	-8%	-20%	-26%
Difference between 21°C and 3°C	61%	75%	91%			
Difference between 45°C and 21°C	16%	23%	52%			
Difference between 45°C and 3°C	86%	114%	191%			

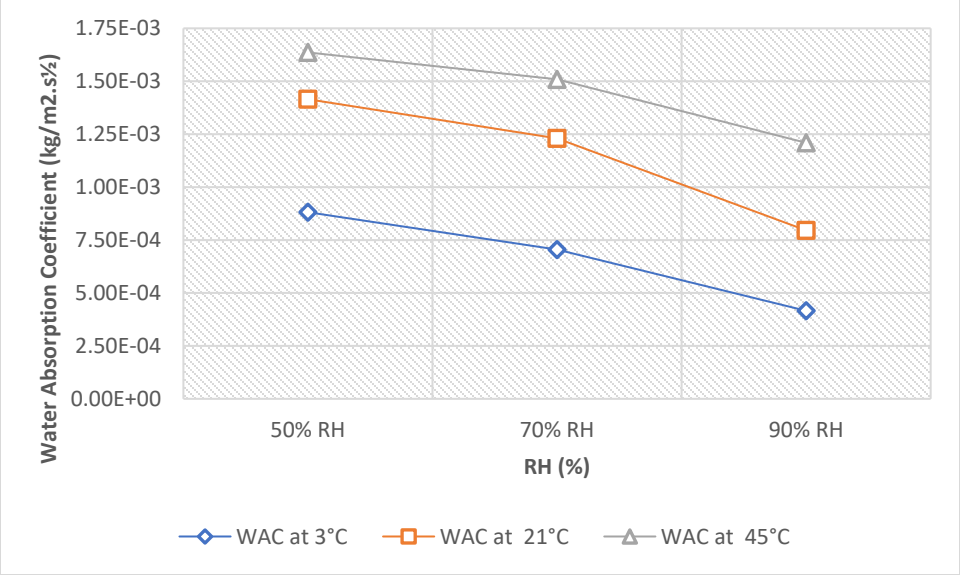

Figure 7-97. Douglas Fir-Effect of Relative Humidity on Water Absorption Coefficient.

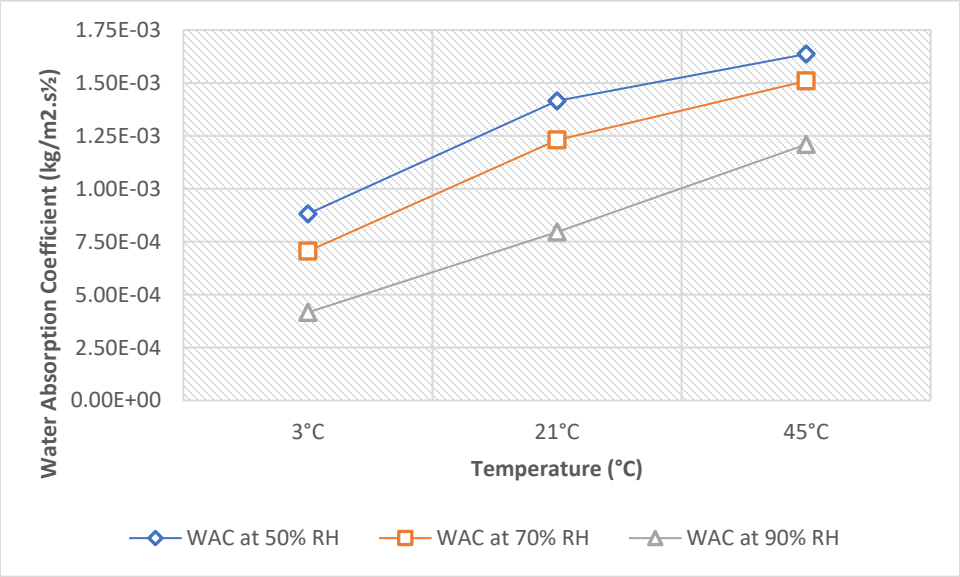

Figure 7-98. Douglas Fir-Effect of Temperature on Water Absorption Coefficient.

7.4.12 **Cellulose Fiber**

The measured data of partial immersion test for the cellulose fiber samples at different relative humidities and temperatures, showed that the water absorption coefficient for cellulose fiber decreased with relative humidity while increased by rising temperature. The result indicated that the influence by temperature was more than relative humidity. For example, changes in the rate of water absorption through rising relative humidity were -15%, -70% and -61% at temperatures 3°C, 21°C and 45°C, respectively. However, the absorption rate increased dramatically by 523%, 275% and 188% at 50%, 70% and 90% RH, respectively, while temperature increased from 3°C to 45°C.

Table 7-63. Cellulose Fiber -Effect of Relative Humidity on Water Absorption Coefficient.

Cellulose Fiber -Effect of Relative Humidity on Water Absorption Coefficient				**Difference between RHs**		
	50% RH	**70% RH**	**90% RH**	**70%-50%**	**90%-70%**	**90%-50%**
WAC at 3°C	8.04E-02	7.73E-02	6.84E-02	-4%	-12%	-15%
WAC at 21°C	3.18E-01	1.33E-01	9.46E-02	-58%	-29%	-70%
WAC at 45°C	5.01E-01	2.90E-01	1.97E-01	-42%	-32%	-61%
Difference between 21°C and 3°C	296%	72%	38%			
Difference between 45°C and 3°C	523%	275%	188%			

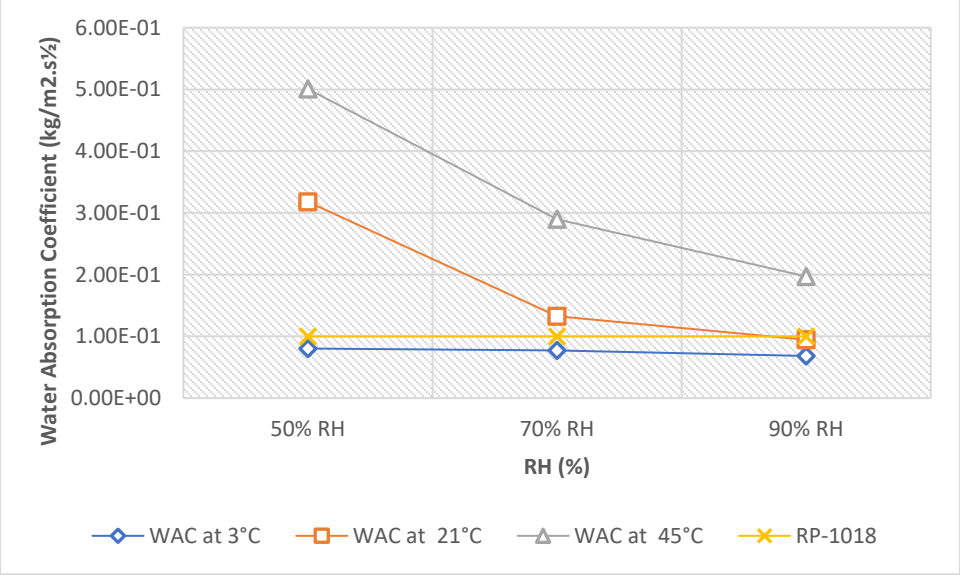

Figure 7-99. Cellulos Fiber-Effect of Relative Humidity on Water Absorption Coefficient.

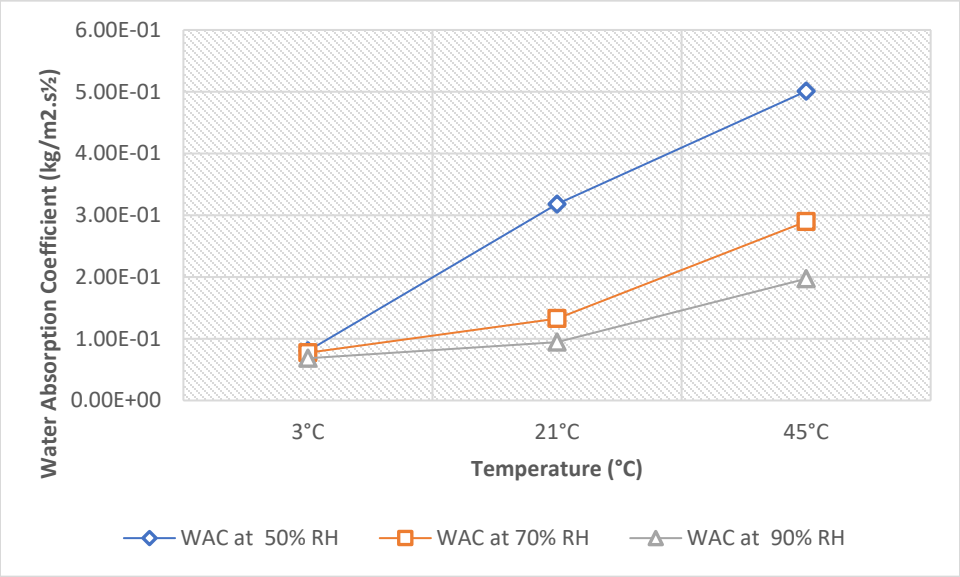

Figure 7-100. Cellulose Fiber-Effect of Temperature on Water Absorption Coefficient.

7.4.13 **Open Cell Spray Polyurethane**

Analyzing the measured data of partial immersion test for the open-cell sprayed polyurethane samples at different relative humidities and temperatures, the water absorption coefficient for open-cell sprayed foam decreased with relative humidity while increased by rising temperature. The result indicated that the influence by temperature was more than relative humidity. For example, changes in the rate of water absorption through rising relative humidity were -73%, -42% and -8% at temperatures 3°C, 21°C and 45°C, respectively. However, the absorption rate increased dramatically by 99%, 372% and 585% at 50%, 70% and 90% RH, respectively, while temperature increased from 3°C to 45°C.

Table 7-64. Open Cell Spray Polyurethane -Effect of Relative Humidity on Water Absorption Coefficient.

Open Cell Spray Polyurethane -Effect of Relative Humidity on Water Absorption Coefficient				**Difference between RHs**		
	50% RH	**70% RH**	**90% RH**	**70%-50%**	**90%-70%**	**90%-50%**
WAC at 3°C	1.07E-02	4.42E-03	2.87E-03	-59%	-35%	-73%
WAC at 21°C	2.00E-02	1.35E-02	1.16E-02	-32%	-14%	-42%
WAC at 45°C	2.13E-02	2.09E-02	1.97E-02	-2%	-6%	-8%
Difference between 21°C and 3°C	87%	206%	305%			
Difference between 45°C and 21°C	7%	54%	69%			
Difference between 45°C and 3°C	99%	372%	585%			

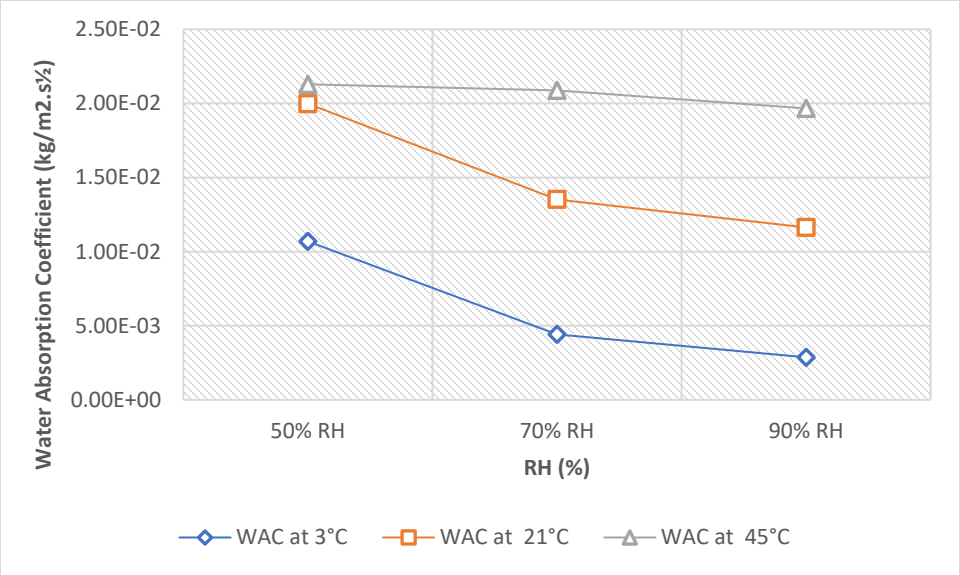

Figure 7-101. Open Cell Spray Polyurethane-Effect of Relative Humidity on Water Absorption Coefficient.

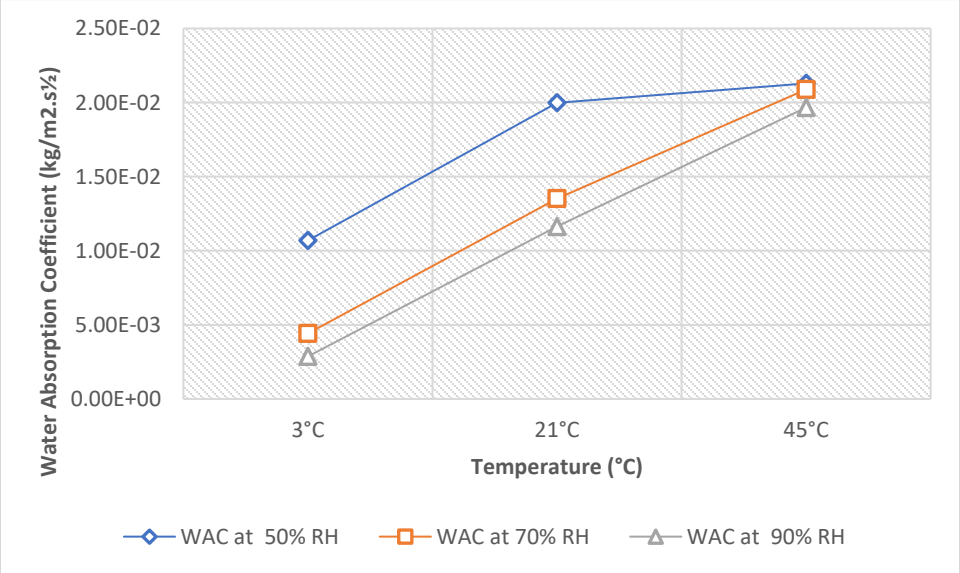

Figure 7-102. Open Cell Spray Polyurethane-Effect of Temperature on Water Absorption Coefficient.

7.4.14 **Mineral Fiber (Stone Wool)**

The measured data from partial immersion test for the mineral fiber samples at different relative humidities and temperatures, showed that the water absorption coefficient for mineral fiber decreased with relative humidity and increased by escalating temperature. The result indicated that the impact of temperature was significantly higher than relative humidity. For example, changes in the rate of water absorption through rising relative humidity were -67%, -36% and -88% at temperatures 3°C, 21°C and 45°C, respectively. While, the absorption rate elevated dramatically by 2278%, 599% and 782% at 50%, 70% and 90% RH, respectively, while temperature increased from 3°C to 45°C. Furthermore, the water uptake rate was influenced drastically when temperature increased above 21°C and was more significant at relative humidity of 50%. For instance, the water absorption coefficient of mineral fiber samples rose by 19% and 1903% when temperature increased from 3°C to 21°C and 21°C to 45°C, respectively.

Table 7-65. Mineral Fiber -Effect of Relative Humidity on Water Absorption Coefficient.

Mineral Fiber -Effect of Relative Humidity on Water Absorption Coefficient				**Difference between RHs**		
	50% RH	**70% RH**	**90% RH**	**70%-50%**	**90%-70%**	**90%-50%**
WAC at 3°C	3.62E-03	2.54E-03	1.18E-03	-30%	-53%	-67%
WAC at 21°C	4.30E-03	3.71E-03	2.75E-03	-14%	-26%	-36%
WAC at 45°C	8.61E-02	1.77E-02	1.04E-02	-79%	-41%	-88%
Difference between 21°C and 3°C	19%	46%	133%			
Difference between 45°C and 21°C	1903%	378%	279%			
Difference between 45°C and 3°C	2278%	599%	782%			

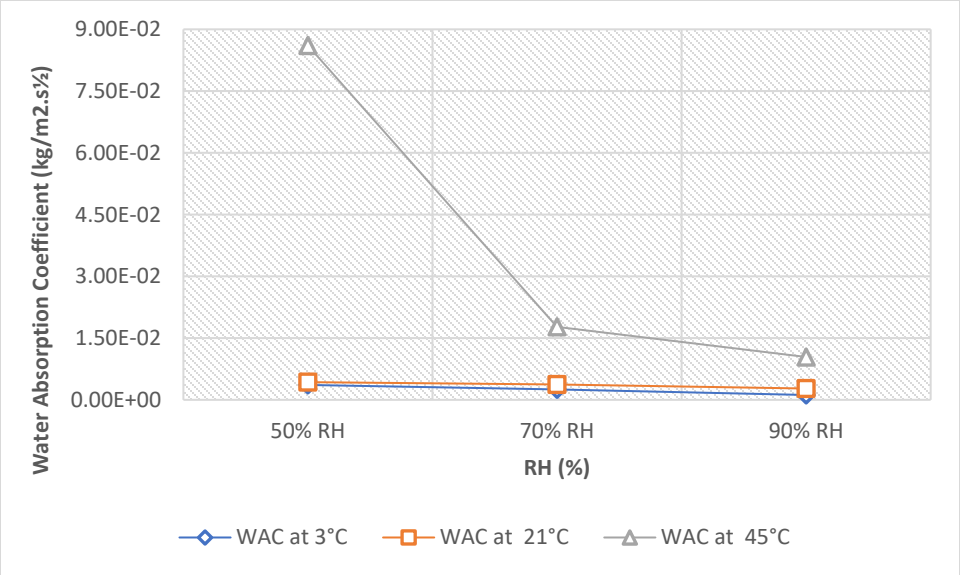

Figure 7-103. Mineral Fiber-Effect of Relative Humidity on Water Absorption Coefficient.

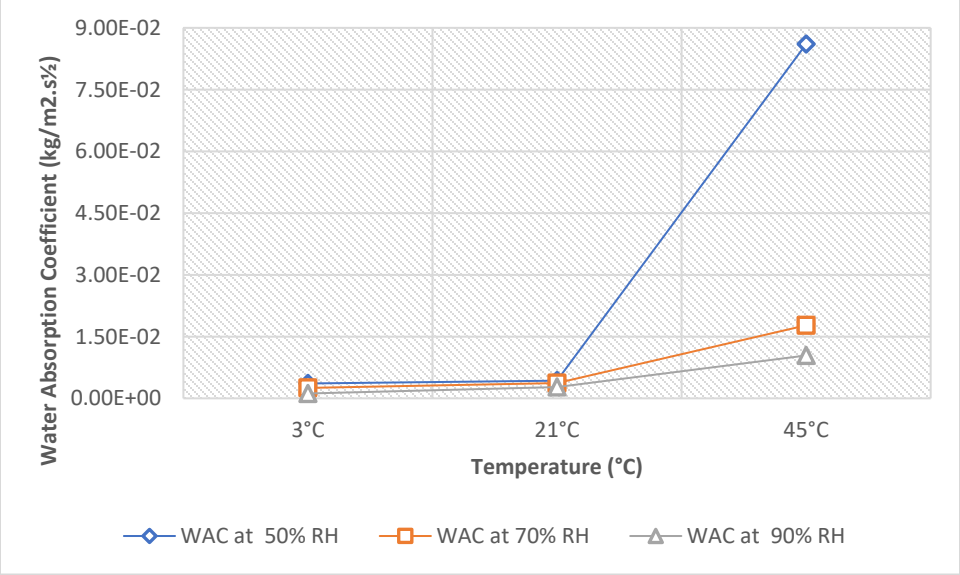

Figure 7-104. Mineral Fiber-Effect of Temperature on Water Absorption Coefficient.

7.4.15 **Summary**

The calculated absorption coefficients from the partial immersion test for tested building products are listed in Table 7-66 and plotted in Figure 7-105. The measured results in all materials exhibited a decrease in water vapor coefficient with the relative humidity at all three temperatures. However, the water intake rate in all tested materials at each relative humidity expressed an increase with rising temperature. The lowest fluctuation in water absorption coefficient at different relative humidities was observed in cellulose fiber insulation material and OSB at 3°C. According to the measured data, the rate of water intake in cellulose is the highest through all temperatures. At 21°C the next highest absorption rates were noticed for open-cell sprayed polyurethane, brick, stucco and mineral fiber. Upon increasing temperature from 21°C to 45°C, the absorption rate changed dramatically in cellulose fiber followed by mineral fiber, open-cell sprayed polyurethane, stucco, brick. Between tested cladding materials, clay brick appeared to possess the highest water absorption coefficient while the absorption coefficient in stucco samples found to be the most affected by temperature variation. Building paper and Tyvek was found to have the lowest water absorption coefficient among all other tested materials. Among the sheathing boards, OSB presented the highest impact upon rising temperature to 45°C while at lower temperature of 3°C, Densglass gold gypsum sheathing had the lowest water absorption value.

From the comparison, it was noticed that between wood-based products western red cedar and Douglas fir had the highest and lowest water absorption coefficients, respectively. However, the differences of those wood-based products are small.

We found that when the influence of temperature was dominant, the impact of relative humidity on the water absorption coefficient was negligible as it was notable in few building materials such as stucco, Densglass gypsum sheathing board and open-cell sprayed polyurethane.

Table 7-66. The impact of variations in relative humidity and temperature on Water Absorption Coefficient of all tested building materials.

Material	Thickness (mm)	Density (kg/m^3)	Relative Humidity Dependency of WAC (@90% - @50%)			Temperature Dependency of WAC (@45°C - @3°C)		
			30°C	21°C	45°C	50%	70%	90%
Claddings								
Clay Brick	14.5	2080.78 ± 27	-90%	-67%	-32%	60%	51%	1012%
Fiber Cement Board	7.7	1358 ± 12	-88%	-60%	-58%	25%	67%	340%
Stucco	27.8	2399 ± 39	-42%	-46%	-6%	42%	96%	127%
Western Red Cedar	42.9	380 ± 4	-58%	-46%	-49%	99%	68%	143%
Weather Resistive Barriers (WRB)								
Tyvek	0.14+0.02mm plaster	65 g/m^2	-53%	-56%	-59%	27%	31%	9%
60 min Building Paper	0.35+0.02mm plaster	310.5 g/m^2	-33%	-33%	-9%	79%	69%	143%
Wall Sheathing Boards								
OSB	12.3	620 ± 12	-53%	-24%	-82%	1169%	432%	378%
Plywood	12.9	461 ± 8	-28%	-41%	-36%	169%	158%	139%
Densglass Gold Gypsum Sheathing	13.3	755 ± 7	-6%	-40%	-38%	1133%	975%	717%
Wood Studs								
Spruce	37.3	469 ± 1.7	-51%	-46%	-31%	101%	116%	185%
Douglas Fir	36.2	572 ± 9	-53%	-44%	-26%	86%	114%	191%
Insulations								
Cellulose Fiber	25.9	79.24	-15%	-70%	-61%	523%	275%	188%
Open Cell Spray polyurethane	26.5	14.75 ± 1.2	-73%	-42%	-8%	99%	372%	585%
Mineral Fiber (Stone Wool)	39.5	128 ± 4	-67%	-36%	-88%	2278%	599%	782%

Figure 7-105. Comparing the Water Absorption Coefficients of building materials at different temperatures and relative humidities.

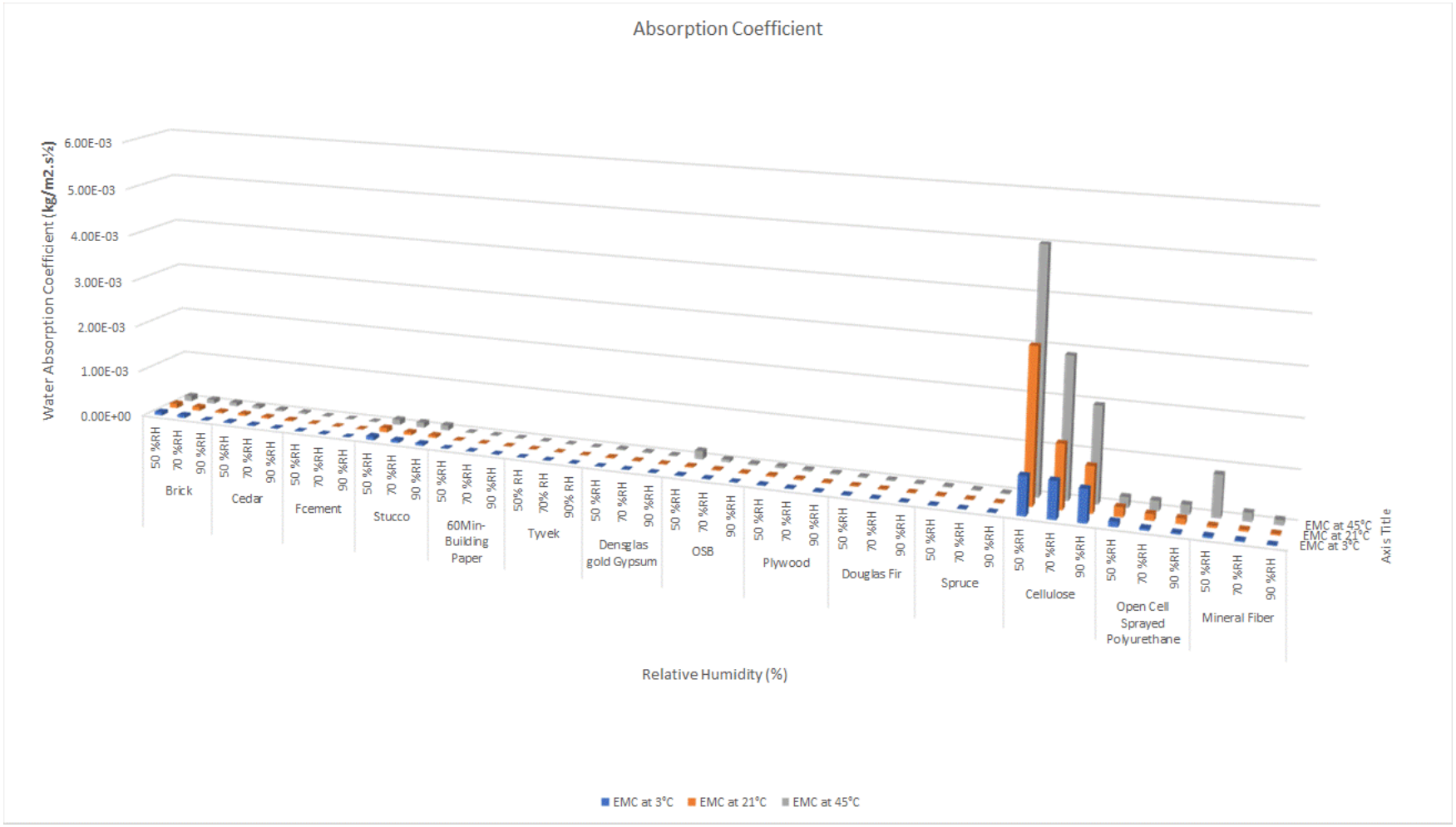

8 Conclusion

This study starts with a rigorous literature review in building physics and provides a profound knowledge in thermal and moisture performance of building materials with the focus on temperature dependency of hygrothermal properties. In this research project, the hygrothermal characteristics including thermal performance, moisture storage and moisture transport of 17 building materials under different climate conditions were measured according to the instructions provided by the designated standards from International Standards Organization ISO and American Society for Testing and Materials (ASTM) for each specific property and material. In order to obtain a complete set of data of the aforementioned material characteristics, 536 measurement tests were carried out in total.

The current available standards methods for measuring material properties provide instructions for tests at normal room conditions as temperature range of 20°C to 23°C and relative humidity range between 40%-50%, however, in real world, materials in the building envelopes are exposed to a wide range of temperatures from -50°C to +50°C. Therefore, new proposed conditions in this study included 9 combinations of three temperatures including 3°C, 21°C and 45°C and 3 relative humidities including 50%, 70% and 90%.

The available standard methods are not applicable or feasible at higher or lower temperatures. Thus, one of our objectives in this study was to develop various extensions to the current methods and procedures to make them applicable at higher and lower designated temperature conditions. Additionally, extra actions on material preparation and measuring processes had to be taken carefully to achieve meaningful measurements since a small variation in the procedures particularly at lower and higher temperature can yield to calculating invalid results. Through iteration, we achieved an effective approach for each test method. For example, proper cups sealing at different test temperatures was one of the challenges in vapor permeability test, since the normal wax mixture proposed by the standard did not seal the cups properly at high and low temperatures. The sealing became brittle and melted at low and high operating temperatures, respectively. In order to address this issue, we had to offer and make different wax mixtures accordingly. Furthermore, different steps were taken for measuring processes particularly at the lower temperature where the risk of condensation was high enough to interfere the obtained values for moisture content and vapor permeability test measurements. To mitigate the risk of condensation,

all measurements at low temperature were performed quickly and closed to the climatic chambers while the temperature inside the chamber room was lowered to 8-10°C with RH of 40%. One series of all measurements at the standard condition (temperature 21°C and relative humidity 50%) was carried out following the standard test methods and the results were compared with different resources in order to confirm the validity of the tests method and results. Consequently, the obtained results showed good alignments with the published literature including ASHRAE report 1018 and IEA-Annex 24.

Through analysis of the measurements and calculations, following results were derived. The thermal conductivity in all materials increased with rising the mean temperature. Similar to the thermal conductivity, the specific heat capacity of the materials increased with the mean temperature. The results showed that regardless of the operating mean temperature, among all materials, stucco possessed the highest thermal conductivity as 0.39 (W/m.K), and polyisocyanurate had the lowest conductivity as 0.273 (W/m.K).

Furthermore, according to the obtained results, there was a direct relationship between moisture content and relative humidity i.e. increasing relative humidity lead to higher moisture content, while there was an inverse relationship between moisture content and temperature i.e. increasing temperature lead to lower moisture content. Additionally, it was found that wood-based materials along with cellulose fiber had higher moisture storage capacity than others. For instance, the moisture content of Douglas fir and cellulose fiber reached to 20% and 22%, respectively. On the other hand, Brick, Densglass gold gypsum and EPS products had lowest moisture content under different relative humidity conditions as 0.13%, 0.41% and 0.73%, respectively.

Our results presented that the water vapor permeability in all tested materials raised by increasing the temperature, and the influence of temperature was more significant at higher relative humidities. Among those tested products, Cellulose fiber insulation and XPS had the highest and lowest vapor transmission rates, respectively and Tyvek and Douglas Fir samples had the highest and lowest water vapor permeability, respectively.

The measured results in all materials exhibited a decrease in water vapor coefficient with escalating the relative humidity at all three temperatures. However, the water intake rate in all tested materials at each relative humidity expressed an increase with rising temperature. According to the measured

data, the rate of water intake in cellulose was the highest through all temperatures. Between tested cladding materials, clay brick appeared to possess the highest water absorption coefficient while the absorption coefficient in stucco samples found to be the most affected by temperature variation.

9 limitations and Future works

This study presented some challenges towards expanding the test conditions beyond the ranges which are suggested by current ASTM and ISO standards for measuring properties of thermal conductivity, sorption isotherm, water vapor permeability and water absorption coefficient. Accordingly, some developments on current standard test methods and measuring processes have been accomplished which allowed us to perform tests at 3°C and 45°C under different relative humidities. Yet, conducting any experiment to measure the hygrothermal properties beyond the conditions studied here, requires further research and probably investigating different approaches. For example, hygrothermal characteristics of building materials can be studied and measured at temperatures as high as +70°C and as low as -30°C as representatives of the exposure of materials within building envelopes to real harsh conditions. Since all properties in this study was measured under isothermal condition, therefore, further studies can be carried out to investigate the building materials' behaviors under non-isothermal conditions with the presence of temperature gradient. Considering the nature of some materials, measuring their properties can take long time from three to six months in only one condition. As a result, we were limited in selecting particular materials (e.g. membranes). Given the volume of the measured properties of tested building materials in this project, further theoretical investigation can be accomplished through analyzing the results. Furthermore, the influence of the obtained data base on the final energy and moisture performance of buildings can be more explored within the energy simulation tools and HAM models.

10 References

Abdou, A. and I. Budaiwi, (2013). The variation of thermal conductivity of fibrous insulation materials under different levels of moisture content. *Construction and Building Materials* 43(0): 533-544.

Abdou, A. A. and I. M. Budaiwi, (2005). Comparison of thermal conductivity measurements of building insulation materials under various operating temperatures. *Journal of Building Physics* 29(2): 171-184.

Adan, O. C. G., (1994). On the fungal defacement of interior finishes.

Al-Ajlan, S. A., (2006). Measurements of thermal properties of insulation materials by using transient plane source technique. *Applied Thermal Engineering* 26(17–18): 2184-2191.

Aldrich, D. and R. Bond, (1985). Thermal performance of rigid cellular foam insulation at subfreezing temperatures. Thermal Performance of the Exterior Envelopes of Buildings III. ASHRAE/DOE/BTECC Conference.

Anderberg, A. and L. Wadsö, (2008). Method for simultaneous determination of sorption isotherms and diffusivity of cement-based materials. *Cement and Concrete Research* 38(1): 89-94.

Anderson, B., L. Kosmina, E. Panzhauser, J. Lechleitner, J. Achtziger, P. Sandberg, B. Johnsson, C. Pompeo, T. Frank and H. Mühlebach, (1999). Analysis, selection and statistical treatment of thermal properties of building materials for the preparation of harmonised design values. Contract SMT4-CT96-2050.

Arai, C., S. Hosaka, K. Murase and Y. Sano, (1976). Measurements of the relative humidity of saturated aqueous salt solutions. *Journal of Chemical Engineering of Japan* 9(4): 328-330.

Asdrubali, F., G. Baldinelli, F. Bianchi, A. Libbra and A. Muscio, (2010). Comparative analysis of different methods to evaluate the thermal conductivity of homogenous materials. *Proceedings of ASME–ATI–UIT Thermal and Environmental Issues in Energy System. Sorrento, Italy*.

ASHRAE, (1985). ASHRAE Handbook-1985 Fundamentals, American Society of Heating. Refrigerating, and Air-Conditioning Engineering, Inc., Atlanta,DOI:

ASHRAE, I., (2017). Heat, Air, and Moisture Control in Building Assemblies - Fundamentals. American Society of Heating, Refrigerating and Air-Conditioning Engineers, Inc. 1-1.

ASTM-C20-00, (2015). Standard Test Methods for Apparent Porosity, Water Absorption, Apparent Specific Gravity, and Bulk Density of Burned Refractory Brick and Shapes by Boiling Water, ASTM International, West Conshohocken, PA,DOI: 10.1520/C0020-00R15, http://www.astm.org

ASTM-C177, (2013). Standard Test Method for Steady-State Heat Flux Measurements and Thermal Transmission Properties by Means of the Guarded-Hot-Plate Apparatus, ASTM International, West Conshohocken, PA,DOI: 10.1520/C0177-13, www.astm.org

ASTM-C518, (2010). Standard Test Method for Steady-State Thermal Transmission Properties by Means of the Heat Flow Meter Apparatus, ASTM International, West Conshohocken, PA,DOI: 10.1520/C0518-10, www.astm.org

ASTM-C1104/C1104M-13a, (2013). Standard Test Method for Determining the Water Vapor Sorption of Unfaced Mineral Fiber Insulation, ASTM International, West Conshohocken, PA,DOI: 0.1520/C1104_C1104M-13A, www.astm.org

ASTM-C1498−04a, (2011). Standard Test Method for Hygroscopic Sorption Isotherms of Building Materials, ASTM International, West Conshohocken, PA,DOI: 10.1520/C1498-04AR10E01, www.astm.org
ASTM-C1699, (2009). Standard Test Method for Moisture Retention Curves of Porous Building Materials Using Pressure Plates, ASTM International, West Conshohocken, PA,DOI: 10.1520/C1699-09, www.astm.org
ASTM-C1784-14, (2014). Standard Test Method for Using a Heat Flow Meter Apparatus for Measuring Thermal Storage Properties of Phase Change Materials and Products, ASTM International, West Conshohocken, PA,DOI: 10.1520/C1784-14, www.astm.org
ASTM-C1794, (2015). Standard Test Method for Determination of the Water Absorption Coefficient by Partial Immersion, ASTM International, West Conshohocken, PA,DOI: 10.1520/ C1794–15, www.astm.org
ASTM-E96/E96M, (2013). Standard Test Methods for Water Vapor Transmission of Materials, ASTM International, West Conshohocken, PA,DOI: 10.1520/E0096_E0096M-13, www.astm.org
Avramidis, S., (1989). Evaluation of "three-variable" models for the prediction of equilibrium moisture content in wood. *Wood Science and Technology* 23(3): 251-257.
Babbitt, J., (1940). Observations On The Permeability Of Hygroscopic Materials To Water Vapour: I. Observations At Relative Humidities Less Than 75%. *Canadian Journal of Research* 18(6): 105-121.
Bachmann, J., R. Horton, S. A. Grant and R. R. van der Ploeg, (2002). Temperature Dependence of Water Retention Curves for Wettable and Water-Repellent Soils. *Soil Science Society of America Journal* 66(1): 44.
Backstrom, G., (1982). Determination of thermal properties using a shielded thermocouple. *Journal of Physics E: Scientific Instruments* 15: 1049.
Baker, P. H., G. H. Galbraith and R. C. McLean, (2009). Temperature gradient effects on moisture transport in porous building materials. *Building Services Engineering Research and Technology* 30(1): 37-48.
Bažant, Z. P. and L. J. Najjar, (1972). Nonlinear water diffusion in nonsaturated concrete. *Matériaux et Constructions* 5(1): 3-20.
Berardi, U. and M. Naldi, (2017). The impact of the temperature dependent thermal conductivity of insulating materials on the effective building envelope performance. *Energy & Buildings* 144: 262-275.
Berardi, U., L. Tronchin, M. Manfren and B. Nastasi, (2018). On the Effects of Variation of Thermal Conductivity in Buildings in the Italian Construction Sector. *Energies* 11(4): 872.
Bird, R. B., W. E. Stewart and E. N. Lightfoot, (2002). *Transport phenomena*, New York, J. Wiley.
Bomberg, M. and S. Klarsfeld, (1983). Semi-empirical model of heat transfer in dry mineral fiber insulations. *Journal of Building Physics* 6(3): 156-173.
Bomberg, M., M. Pazera and R. Plagge, (2005). Analysis of selected water absorption coefficient measurements. *Journal of Thermal Envelope and Building Science* 28(3): 227-243.
Bomberg, M. and K. R. Solvason, (1983). Comments on Calibration and Design of a Heat Flow Meter. 277-292.
Bomberg, M. T., C. M. Pelanne and W. S. Newton, (1985). Analysis of uncertainties in calibration of a heat flow meter apparatus**:** 259-272.

Bouguerra, A., A. Aït-Mokhtar, O. Amiri and M. B. Diop, (2001). Measurement of thermal conductivity, thermal diffusivity and heat capacity of highly porous building materials using transient plane source technique. *International Communications in Heat and Mass Transfer* 28(8): 1065-1078.

Brocken, H. J. P., (1998). Moisture transport in brick masonry: the grey area between bricks. PhD, Technische Universiteit Eindhoven.

Brue, F., C. A. Davy, F. Skoczylas, N. Burlion and X. Bourbon, (2012). Effect of temperature on the water retention properties of two high performance concretes. *Cement and Concrete Research* 42(2): 384-396.

Brunauer, S., (1943). *The adsorption of gases and vapors*, Princeton, London, Princeton university press; London, H. Milford, Oxford university press.

Brunauer, S., L. S. Deming, W. E. Deming and E. Teller, (1940). On a theory of the van der Waals adsorption of gases. *Journal of the American Chemical society* 62(7): 1723-1732.

Brunauer, S. and P. H. Emmett, (1937). The use of low temperature van der Waals adsorption isotherms in determining the surface areas of various adsorbents. *Journal of the American Chemical Society* 59(12): 2682-2689.

Brunauer, S., P. H. Emmett and E. Teller, (1938). Adsorption of gases in multimolecular layers. *Journal of the American chemical society* 60(2): 309-319.

Brunauer, S., J. Skalny and E. E. Bodor, (1969). Adsorption on nonporous solids. *Journal of Colloid And Interface Science* 30(4): 546-552.

Budaiwi, I., A. Abdou and M. Al-Homoud, (2002). Variations of Thermal Conductivity of Insulation Materials Under Different Operating Temperatures: Impact on Envelope-Induced Cooling Load. *Journal of Architectural Engineering* 8(4): 125-132.

Burch, D., W. Thomas and A. Fanney, (1993). Water vapor permeability measurements of common building materials. *Transactions-American Society Of Heating Refrigerating And Air Conditioning Engineers* 98: 486-486.

Burch, D. M. and A. O. Desjarlais, (1995). *Water-vapor measurements of low-slope roofing materials*, National Institute of Standards and Technology.

Cagnon, H., J. E. Aubert, M. Coutand and C. Magniont, (2014). Hygrothermal properties of earth bricks. *Energy and Buildings* 80: 208-217.

Candanedo, L. and D. Derome, (2005). Numerical simulation of water absorption in softwoods. Proceedings of the 9th International IBPSA Conference, Canada.

Černý, R. and Z. Pavlík, (2007). Homogenization techniques for determination of thermal conductivity of porous materials. Meeting of the Thermophysical Society, Proceedings of the THERMOPHYSICS.

Chahal, R., (1964). Effect of Temperature and Trapped Air on the Energy Status of Water in Porous Media. *Soil Science* 98(2): 107-112.

Chahal, R. S., (1965). Effect of Temperature And Trapped Air on Matric Suction. *Soil Science* 100(4): 262-266.

Chang, S. C. and N. B. Hutcheon, (1956). Dependence of water vapor permeability on temperature and humidity. *Heating*.

Chevrier, V. F. o., (1996). Moisture transfer in porous materials exposed to combined humidity and temperature gradients. MSc, Virginia Polytechnic Institute and State University.

Chung, D. S. and H. Pfost, (1967). Adsorption and desorption of water vapour by cereal grains and their products. *Transactions of the ASAE* 4: 549-551.

Collet, F., F. Achchaq, K. Djellab, L. Marmoret and H. Beji, (2011). Water vapor properties of two hemp wools manufactured with different treatments. *Construction and Building Materials* 25(2): 1079-1085.
Cull, J. P., (1974). Thermal conductivity probes for rapid measurements in rock. *Journal of Physics E: Scientific Instruments* 7: 771.
Czichos, H., T. Saito and L. Smith, (2006). *Springer handbook of materials measurement methods*, Springer.
Daryabeigi, K., G. R. Cunnington and J. R. Knutson, (2011). Combined heat transfer in high-porosity high-temperature fibrous insulation: Theory and experimental validation. *Journal of thermophysics and heat transfer* 25(4): 536-546.
Day, D. and G. Nelson, (1965). Desorption isotherms for wheat. *Transactions of the ASAE* 8(2): 293-297.
de Burgh, J. M. and S. J. Foster, (2017). Influence of temperature on water vapour sorption isotherms and kinetics of hardened cement paste and concrete. *Cement and Concrete Research* 92: 37-55.
De Saussure, N. T., (1814). No Title. *Gilbert's Annual der Physik* 47: 113-118.
de Wit, M. and J. van Schindel, (1993). The Estimation of the Moisture Diffusivity. IEA Annex XXIV, Report T1-NL-93/04.
Delgado, J., N. M. M. Ramos and V. P. de Freitas, (2012). Application of different transient sorption methods to evaluate moisture diffusion coefficients of building materials on the hygroscopic range. *Journal of Building Physics* 35(3): 251-266.
Delgado, J. M. P. Q., E. Barreira, N. M. M. Ramos and V. P. d. Freitas, (2013). *Hygrothermal numerical simulation tools applied to building physics*, Heidelberg;New York;, Springer.
Della Vecchia, G., C. Jommi and E. Romero, (2011). An insight into the water retention properties of compacted clayey soils. *Géotechnique* 61(4): 313-328.
Descamps, F., (1997). Continuum and discrete modelling of isothermal water and air transfer in porous media. PhD, University in Leuven.
Domínguez-Muñoz, F., B. Anderson, J. M. Cejudo-López and A. Carrillo-Andrés, (2010). Uncertainty in the thermal conductivity of insulation materials. *Energy & Buildings* 42(11): 2159-2168.
Donohue, M. D. and G. L. Aranovich, (1999). A new classification of isotherms for Gibbs adsorption of gases on solids. *Fluid Phase Equilibria* 158: 557-563.
Dorthe Wildenschild, Jeffery J. Roberts, Ernest Hardin and W. Lin, (1998). Experimental tests of enhancement of thermal vapor diffusion in Topopah Spring Tuff. International High-Level Radioactive Waste Management Conference. Las Vegas, NV, *United States. Dept. of Energy. Office of Civilian Radioactive Waste Management*.
Doty, P. M., W. H. Aiken and H. Mark, (1946). Temperature Dependence of Water Vapor Permeability. *Industrial & Engineering Chemistry* 38(8): 788-791.
Douglas, J. S., T. H. Kuehn and J. W. Ramsey, (1992). A New Moisture Permeability Measurement Method and Representative Test Data. *ASHRAE Transactions* 98(2): 513-519.
Eitelberger, J. and K. Hofstetter, (2011). A comprehensive model for transient moisture transport in wood below the fiber saturation point: Physical background, implementation and experimental validation. *International Journal of Thermal Sciences* 50(10): 1861-1866.

Eitelberger, J., S. Svensson and K. Hofstetter, (2011). Theory of transport processes in wood below the fiber saturation point. Physical background on the microscale and its macroscopic description. *Holzforschung* 65(3): 337-342.
EN.ISO.8301:1991, (2014). Thermal insulation - Determination of steady-state thermal resistance and related properties - Heat flow meter apparatus, the International Organization for Standardization, Geneve, Switzerland,DOI: http://www.iso.org
EN.ISO.12571, (2013). Hygrothermal performance of building materials and products - Determination of hygroscopic sorption properties, the International Organization for Standardization, Geneve, Switzerland,DOI: http://www.iso.org
EN.ISO.12572, (2001). Hygrothermal performance of building materials and products - Determination of water vapour transmission properties, the International Organization for Standardization, Geneve, Switzerland,DOI: http://www.iso.org
EN.ISO.15148, (2002). Hygrothermal performance of building materials and products - Determination of water absorption coefficient by partial immersion, the International Organization for Standardization, Geneve, Switzerland,DOI: http://www.iso.org
Environment-Canada, (2015). Canadian Climate Normals.
Feng, C. and H. Janssen, (2016). Hygric properties of porous building materials (II): Analysis of temperature influence. *Building Environment* 99: 107-118.
Feng, C., H. J. B. Janssen and Environment, (2017). The influence of temperature on the capillary absorption coefficient-a confrontation of two recent papers in building and environment. 116: 257-258.
Ferrand, L. A. and J. A. Sulayman, (1996). A Computational Investigation of Some Effects of Temperature on Soil Moisture. *Water Resources Research* 32(12): 3429.
Fick, A., (1855). Ueber Diffusion. *Annalen der Physik* 170(1): 59-86.
Fořt, J., Z. Pavlík, J. Žumár, M. Pavlíková and R. Černý, (2014). Effect of temperature on water vapor transport properties. *Journal of Building Physics* 38(2): 156-169.
Galbraith, G., J. Guo and R. McLean, (2000a). The effect of temperature on the moisture permeability of building materials. *Building Research & Information* 28(4): 245-259.
Galbraith, G., J. Guo, R. McLean, C. Lee and D. Kelly, (2000b). The temperature dependence of moisture permeability. CIB REPORT. 105-110.
Galbraith, G. and R. McLean, (1986). Realistic vapour permeability values: The concept of 'differential'permeability. *Building research and practice* 14(2): 98-103.
Galbraith, G. and R. McLean, (1990). Interstitial condensation and the vapour permeability of building materials. *Energy and Buildings* 14(3): 193-196.
Galbraith, G., R. McLean, I. Gillespie, J. Guo and D. Kelly, (1998). Nonisothermal moisture diffusion in porous building materials. *Building Research & Information* 26(6): 330-339.
Gibson, P. W., (2000). Effect of temperature on water vapor transport through polymer membrane laminates. *Polymer Testing* 19(6): 673-691.
Glatzmaier, G. C. and W. F. Ramirez, (1985). Simultaneous measurement of the thermal conductivity and thermal diffusivity of unconsolidated materials by the transient hot wire method. *Review of Scientific Instruments* 79(7): 1394-1398.
Gnip, I. Y., S. A. Veyalis and V. I. Kershulis, (2006). Isotherms of water vapor sorption by light inorganic and polymer heat-insulating materials. *Journal of Engineering Physics and Thermophysics* 79(1): 40-47.

Goula, A. M., T. D. Karapantsios, D. S. Achilias and K. G. Adamopoulos, (2008). Water sorption isotherms and glass transition temperature of spray dried tomato pulp. *Journal of Food Engineering* 85(1): 73-83.
Guizzardi, M., D. Derome and J. Carmeliet, (2016). Water uptake in clay brick at different temperatures: Experiments and numerical simulations. *Journal of Building Physics* 39(4): 373-389.
Gummerson, R. J., C. Hall and W. D. Hoff, (1980). Water movement in porous building materials—II. Hydraulic suction and sorptivity of brick and other masonry materials. *Building and Environment* 15(2): 101-108.
Gustafsson, S. E., (1991). Transient plane source techniques for thermal conductivity and thermal diffusivity measurements of solid materials. *Review of Scientific Instruments* 79(3): 797-804.
Gustafsson, S. E., E. Karawacki and M. N. Khan, (1979). Transient hot-strip method for simultaneously measuring thermal conductivity and thermal diffusivity of solids and fluids. *Journal of Physics D: Applied Physics* 12: 1411.
Hailwood, A. and S. Horrobin, (1946). Absorption of water by polymers: analysis in terms of a simple model. *Transactions of the Faraday Society* 42: B084-B092.
Hall, C., (1977). Water movement in porous building materials—I. Unsaturated flow theory and its applications. *Building and Environment* 12(2): 117-125.
Hall, C., (1989). Water sorptivity of mortars and concretes: a review. *Magazine of concrete research* 41(147): 51-61.
Halsey, G., (1948). Physical Adsorption on Non-Uniform Surfaces. *The Journal of Chemical Physics* 16(10): 931.
Hansen, K. K., (1986). Sorption isotherms: a catalogue. Technical Report 162/86. Technical University of DenmarkDanmarks Tekniske Universitet, Department of Structural Engineering and MaterialsInstitut for Bærende Konstruktioner og Materialer.
Hansen, K. K. and H. Lund, (1990). Cup method for determination of water vapour transmission properties of building materials. Sources of uncertainty in the method. Proceedings of the 2nd Symposium, Trondheim, Building Physics in the Nordic Countries.
Hansen, K. K., C. Rode, E. Hansen, T. Padfield and F. H. Kristiansen, (2001). Experimental investigation of the hygrothermal performance of insulation materials. *Proceedings of performance of exterior envelopes of whole buildings VIII (CD-Rom)*.
Hay, B., R. Zarr, C. Stacey, L. Lira-Cortes, U. Hammerschmidt, N. Sokolov, J. Zhang, J. R. Filtz and N. Fleurence, (2013). Analysis of Thermal-Conductivity Measurement Data from International Comparison of National Laboratories. *International Journal of Thermophysics* 34(5): 737-762.
He, Y., (2005). Rapid thermal conductivity measurement with a hot disk sensor: Part 1. Theoretical considerations. *Thermochimica acta* 436(1): 122-129.
Hedlin, C. P., (1977). Moisture Gains by Foam Plastic Roof Insulations Under Controlled Temperature Gradients. *Journal of Cellular Plastics* 13(5): 313-319.
Hens, H., (1996). Final report Task 1. Modeling Common Exercises. Summary reports. International Energy Agency. Energy Conservation in Buildings and Community Systems, Annex 24 Heat, Air and Moisture Transport in New and Retrofitted Building Envelope Parts (HAMTIE).
Hens, H., (2017). *Building Physics - Heat, Air and Moisture: Fundamentals and Engineering Methods with Examples and Exercises*, DE, Ernst & Sohn.

Hill, C. A., A. J. Norton and G. Newman, (2010). The water vapour sorption properties of Sitka spruce determined using a dynamic vapour sorption apparatus. *Wood Science and Technology* 44(3): 497-514.
Hill, C. A. S., A. Norton and G. Newman, (2009). The water vapor sorption behavior of natural fibers. *Journal of Applied Polymer Science* 112(3): 1524-1537.
Hill, T. L., (1951). Thermodynamics of adsorption. *Transactions of the Faraday Society* 47(0): 376-380.
Hoff, W. D., M. A. Wilson, D. M. Benton, M. R. Hawkesworth, D. J. Parker and P. Flowles, (1996). The use of positron emission tomography to monitor unsaturated water flow within porous construction materials. *Journal of Materials Science Letters* 15(13): 1101-1104.
Hokoi, S. and M. K. Kumaran, (1993). Experimental and Analytical Investigations of Simultaneous Heat and Moisture Transport through Glass Fiber Insulation. *Journal of Building Physics* 16(3): 263-292.
Hust, J., (1985). Status of thermal conductivity standard reference materials at the National Bureau of Standards. *Thermal Conductivity 18*. Springer. 327-338.
Jerman, M. and R. Černý, (2012). Effect of moisture content on heat and moisture transport and storage properties of thermal insulation materials. *Energy and Buildings* 53: 39-46.
Johannesson, B. and M. Janz, (2002). Test of four different experimental methods to determine sorption isotherms. *Journal of materials in civil engineering* 14(6): 471-477.
Jooss, M. and H. W. Reinhardt, (2002). Permeability and diffusivity of concrete as function of temperature. *Cement and Concrete Research* 32(9): 1497-1504.
Joy, F. A. and A. G. Wilson, (1966). Standardization of the dish method for measuring water vapor transmission. International Symposium on Humanity and Moisture., Washington, DC.
Karagiannis, N., M. Karoglou, A. Bakolas, M. Krokida and A. Moropoulou, (2019). The influence of dynamic environmental conditions on capillary water uptake of building materials. 42(4): 506-526.
Karagiannis, N., M. Karoglou, A. Bakolas and A. Moropoulou, (2016). Effect of temperature on water capillary rise coefficient of building materials. *Building and Environment* 106: 402-408.
Karagiozis, A., H. Künzel and A. Holm, (2001). WUFI ORNL/IBP–A North American Hygrothermal Model. Proceedings of the Thermal Performance of the Exterior Envelopes of Whole Buildings VIII (Buildings VIII), Clearwater Beach, Florida, USA.
Karamanos, A., S. Hadiarakou and A. M. Papadopoulos, (2008). The impact of temperature and moisture on the thermal performance of stone wool. *Energy and Buildings* 40(8): 1402-1411.
Kelly, M. W. and C. A. Hart, (1970). Water vapor sorption rates by wood cell walls. *Wood and Fiber Science* 1(4): 270-282.
King, G., (1960). Theories of multi-layer adsorption. *Moisture in textiles. Textile Book Publ. Inst., Inc., New York*.
Klute, A., (1986). Water retention: laboratory methods. *Methods of Soil Analysis: Part 1—Physical and Mineralogical Methods*(methodsofsoilan1): 635-662.
Koru, M., (2016). Determination of Thermal Conductivity of Closed-Cell Insulation Materials That Depend on Temperature and Density. *Arabian Journal for Science and Engineering* 41(11): 4337-4346.

Krus, M., (1996). Moisture transport and storage coefficients of porous mineral building materials: Theoretical principles and new test methods. Fraunhofer IRB Verlag.
Krus, M. and H. Künzel, (1993). Determination of Dw from A-value. IEA Annex XXIV Report T3-D-93/02.
Kumaran, M., (1987). Moisture transport through glass-fibre insulation in the presence of a thermal gradient. *Journal of Building Physics* 10(4): 243-255.
Kumaran, M., (1998a). An alternative procedure for the analysis of data from the cup method measurements for determination of water vapor transmission properties. *Journal of testing and evaluation* 26(6): 575-581.
Kumaran, M., (2001a). Hygrothermal properties of building materials.
Kumaran, M. and M. Bomberg, (1985). *A gamma-spectrometer for determination of density distribution and moisture distribution in building materials*.
Kumaran, M., J. Lackey, N. Normandin, F. Tariku and D. Van Reenen, (2003). Variations in the hygrothermal properties of several wood-based building products.
Kumaran, M. and G. Mitalas, (1987). Analysis of simultaneous heat and moisture transport through glass fibre insulation. Heat Transfer in Building and Structures-HTD, ASME/AICHE.
Kumaran, M. K., (1989). Vapor transport characteristics of mineral fiber insulation from heat flow meter measurements. H. R. Trechsel and M. T. Bomberg.(Eds), *Water Vapor Transmission Through Building Materials and Systems, ASTM STP*. 1039**,** Philadelphia. American Society for Testing and Materials. 19-27.
Kumaran, M. K., (1996a). *Final report, Volume 3: Task 3: Material properties*, International Energy Agency Annex 24 on Heat, Air and Moisture Transport in New and Retrofitted Building Envelope Parts (HAMTIE).
Kumaran, M. K., (1996b). *IEA Annex 24, Heat Air and Moisture Transfer Through New and Retrofitted Insulated Envelope Parts (Hamtie): Task 3, Material Properties, Final Report*, Katholieke Universiteit Leuven.
Kumaran, M. K., (1998b). Interlaboratory comparison of the ASTM standard test methods for water vapor transmission of materials (E96-95). *Journal of Testing and Evaluation* 26(2).
Kumaran, M. K., (1999). Moisture Diffusivity of Building Materials from Water Absorption Measurements. *Journal of Thermal Envelope and Building Science* 22(4): 349-355.
Kumaran, M. K., (2001b). Hygrothermal properties of building materials. H. R. Trechsel.(Eds), *Moisture Analysis and Condensation Control in Building Envelopes*. W. Conshohocken, PA. American Society for Testing and Materials. 29-65.
Kumaran, M. K., (2002). A Thermal and Moisture Transport Property Database for Common Building and Insulating Materials. Final Report from ASHRAE Research Project RP-1018. NRC.
Kumaran, M. K., (2006). A thermal and moisture property database for common building and insulation materials. *ASHRAE transactions*: 485-497.
Kumaran, M. K., J. C. Lackey, N. Normandin, F. Tariku and D. van Reenen, (2004). Heat, air, and moisture transport properties of several North American bricks and mortar mixes. *Journal of Testing and Evaluation* 32(5): 383-389.
Kumaran, M. K., G. P. Mitalas and M. T. Bomberg, (1994). Fundamentals of transport and storage of moisture in building materials and components. *Moisture Control in Buildings* 18: 3-17.

Kumaran, M. K., P. Mukhopadhyaya and N. Normandin, (2006). Determination of equilibrium moisture contents of building materials: some practical difficulties. *Journal of ASTM International U6*

Künzel, H. M., (1995). Simultaneous heat and moisture transport in building components, One- and two-dimensional calculation using simple parameters. PhD, Fraunhofer IRB Verlag Suttgart.

Lackey, J., R. Marchand and M. Kumaran, (1997). A Logical extension of the ASTM standard E96 to determine the dependence of water vapour transmission on relative humidity. *ASTM special technical publication* 1320: 456-470.

Lakatos, Á. and F. Kalmár, (2012). Analysis of water sorption and thermal conductivity of expanded polystyrene insulation materials. *Building Services Engineering Research and Technology*: 0143624412462043.

Lakatos, Á. and F. Kalmár, (2013a). Analysis of water sorption and thermal conductivity of expanded polystyrene insulation materials. *Building Services Engineering Research & Technology* 34(4): 407-416.

Lakatos, Á. and F. Kalmár, (2013b). Investigation of thickness and density dependence of thermal conductivity of expanded polystyrene insulation materials. *Materials and Structures* 46(7): 1101-1105.

LaserComp, I., (2007). *Measurements of the Volumetric Specific Heat Cρ and Enthalpy of the Phase-Change Materials (PCM) Using the FOX Heat Flow Meter Instruments, AN-PCM LaserComp, Inc*. 5.

Latif, E., S. Tucker, M. A. Ciupala, D. C. Wijeyesekera and D. Newport, (2014). Hygric properties of hemp bio-insulations with differing compositions. *Construction and Building Materials* 66: 702.

Luikov, A. V., (1966). *Heat and mass transfer in capillary-porous bodies*, New York;Oxford, Pergamon Press.

Maroulis, Z. B., M. K. Krokida, A. Moropoulou and M. Karoglou, (2005). Water Sorption Isotherms of Some Building Materials. *Drying Technology* 23(1): 289-303.

Maroulis, Z. B., E. Tsami, D. Marinos-Kouris and G. D. Saravacos, (1988). Application of the GAB model to the moisture sorption isotherms for dried fruits. *Journal of Food Engineering* 7(1): 63-78.

McElroy, D. L. and R. P. Tye, (1980). *Thermal Insulation Performance, Special Technical Publication 718*, Tampa, Fla, ASTM International. P. 560.

Mills, R. H., (1985). Mass transfer of water vapour through concrete. *Cement and Concrete Research* 15(1): 74-82.

Milly, P. C. D., (1980). The coupled transport of water and heat in a vertical soil column under atmospheric excitation. PhD, Massachusetts Institute of Technology-Dissertation.

Moore, R., (1940). The relation of soil temperature to soil moisture: pressure potential, retention, and infiltration rate. Soil Sci. Soc. Amer. Proc. 5.

Mukhopadhyaya, P., P. Goudreau, M. K. Kumaran and D. van Reenen, (2002a). Influence of material properties on the moisture response of an ideal stucco wall : results from hygrothermal simulation. 6th Symposium on Building Physics in the Nordic Countries, Trondheim, Norway.

Mukhopadhyaya, P., K. Kumaran, N. Normandin and P. Goudreau, (2002b). Effect of surface temperature on water absorption coefficient of building materials. *Journal of Building Physics* 26(2): 179-195.

Mukhopadhyaya, P., M. K. Kumaran and J. Lackey, (2005). Use of the modified cup method to determine temperature dependency of water vapor transmission properties of building materials. *Journal of Testing and Evaluation* 33(5): 316.
2018. *Lambda 436*. from https://www.netzsch.com/en/.
Newton, W. S., C. M. Pelanne and M. T. Bomberg, (1985). Calibration of heat flow meter apparatus used for quality control of low-density mineral fiber insulations. Proceedings of the Eighteenth International Conference on Thermal Conductivity, Rapid City,SD, Thermal Conductivity 18.
NRC, N. R. C. o. C., (2015). National Building Code of Canada NBC, National Research Council of Canada, Ottawa, Canada,DOI:
Ochs, F., W. Heidemann and H. Müller-Steinhagen, (2008). Effective thermal conductivity of moistened insulation materials as a function of temperature. *International Journal of Heat and Mass Transfer* 51(3): 539-552.
Papadopoulos, A. M., (2005). State of the art in thermal insulation materials and aims for future developments. *Energy and Buildings* 37(1): 77-86.
Pavlík, Z. and R. Černý, (2012). Determination of Moisture Diffusivity as a Function of Both Moisture and Temperature. *International Journal of Thermophysics* 33(8): 1704-1714.
Pavlík, Z., J. Fořt, J. Žumár, M. Pavlíková and R. Černý, (2013). Secondary effects on water vapor transport properties measured by cup method. *International Science Index* 7(1): 746-751.
Pavlík, Z., J. Žumár, I. Medved and R. Černý, (2012). Water Vapor Adsorption in Porous Building Materials: Experimental Measurement and Theoretical Analysis. *Transport in Porous Media* 91(3): 939-954.
Peavy, B. A., (1996). A Heat Transfer Note on Temperature Dependent Thermal Conductivity. *Journal of Thermal Insulation and Building Envelopes* 20(1): 76-90.
Pedersen, C. R., (1990). Combined heat and moisture transfer in building constructions. PhD Thesis, Thermal Insulation Laboratory, Technical University of Denmark.
Pel, L., A. A. J. Ketelaars, O. C. G. Adan and A. A. Van Well, (1993). Determination of moisture diffusivity in porous media using scanning neutron radiography. *International Journal of Heat and Mass Transfer* 36(5): 1261-1267.
Pel, L., K. Kopinga and H. Brocken, (1995). Moisture transport in porous building materials. *HERON* 41(2).
Peuhkuri, R., (2003a). Moisture dynamics in building envelopes, Report R-071. PhD Thesis, Technical University of Denmark.
Peuhkuri, R., C. Rode and K. K. Hansen, (2005). Effect of method, step size and drying temperature on sorption isotherms. 7th Nordic Symposium on Building Physics, Reykjavík.
Peuhkuri, R., C. Rode and K. K. Hansen, (2008). Non-isothermal moisture transport through insulation materials. *Building and Environment* 43(5): 811-822.
Peuhkuri, R. H., (2003b). Moisture dynamics in building envelopes. PhD, Technical University of Denmark.
Philip, J. and D. De Vries, (1957). Moisture movement in porous materials under temperature gradients. *Transactions, American Geophysical Union* 38: 222-232.
Plagge, R., C. H. Roth and M. Renger, (1996). Dielectric Soil Water Content Determination Using Time-Domain Reflectometry (TDR). Workshop on Electromagnetic Wave Interaction with Water and Moist Substances at the 1996 IEEE Microwave Theory and

Techniques Society International Microwave Symposium. A. e. Kraszewski. San Francisco, CA, *International Microwave Symposium***:** 59-62.
Plagge, R., G. Scheffler and J. Grunewald, (Unpublished). Automatic Measurement Of Water Uptake Coefficient Of Building Materials.
Plagge, R., G. Scheffler and A. Nicolai, (2007). Experimental methods to derive hygrothermal material functions for numerical simulation tools. *Thermal Performance of Exterior Envelopes of Buildings X*.
Poyet, S. and S. Charles, (2009). Temperature dependence of the sorption isotherms of cement-based materials: Heat of sorption and Clausius–Clapeyron formula. *Cement and Concrete Research* 39(11): 1060-1067.
Pražák, J., J. Tywoniak, F. Peterka and T. Šlonc, (1990). Description of transport of liquid in porous media—a study based on neutron radiography data. *International Journal of Heat and Mass Transfer* 33(6): 1105-1120.
Promis, G., L. F. Dutra, O. Douzane, A. T. Le and T. Langlet, (2019). Temperature-dependent sorption models for mass transfer throughout bio-based building materials. *Construction and Building Materials* 197: 513-525.
Reinhardt, H.-W. and M. Jooss, (1998). Permeability, diffusion, and capillary absorption of concrete at elevated temperature in the service range. *Otto-Graf-Journal* 9: 34.
Richards, L. A., (1948). Porous Plate Apparatus For Measuring Moisture Retention And Transmission By Soil. *Soil Science* 66(2): 105-110.
Roels, S., (2000). Modelling unsaturated moisture transport in heterogeneous limestone. PhD, Katholieke Universiteit Leuven.
Roels, S., J. Carmeliet and H. Hens, (2003a). HAMSTAD WP1: Final report–moisture transport properties and material characterisation. Technical report, Laboratory of Building Physics, KU Leuven.
Roels, S., J. Carmeliet, H. Hens, O. Adan, H. Brocken, R. Cerny, Z. Pavlik, C. Hall, K. Kumaran and L. Pel, (2004a). Interlaboratory comparison of hygric properties of porous building materials. *Journal of thermal envelope and building science* 27(4): 307-325.
Roels, S., J. E. J. Carmeliet, H. Hens, O. C. G. O. Adan, H. J. P. H. Brocken, R. Cerny, Z. Pavlik, A. T. Ellis, C. Hall, K. Kumaran, L. L. Pel and R. Plagge, (2004b). A comparison of different techniques to quantify moisture content profiles in porous building materials. *Journal of Thermal Envelope and Building Science* 27(4): 261-276.
Roels, S., K. Vandersteen and J. Carmeliet, (2003b). Measuring and simulating moisture uptake in a fractured porous medium. *Advances in Water Resources* 26(3): 237-246.
Romero, E., A. Gens and A. Lloret, (2001). Temperature effects on the hydraulic behaviour of an unsaturated clay. *Geotechnical and Geological Engineering* 19(3): 311-332.
Rose, D. A., (1963). Water movement in porous materials: Part 2 - The separation of the components of water movement. *British Journal of Applied Physics* 14(8): 491-496.
Salmon, D. R. and R. P. Tye, (2010). An inter-comparison of a steady-state and transient methods for measuring the thermal conductivity of thin specimens of masonry materials. *Journal of Building Physics*: 1744259109360060.
Scheffler, G., (2007). Validation of hygrothermal material modelling under consideration of the hysteresis of moisture storage. *PhD Dissertation*.
Schneider, M. and K. U. Goss, (2011). Temperature dependence of the water retention curve for dry soils. *Water Resources Research* 47(3).

Schwartz, N. V., (1988). Water vapor transmission and moisture accumulation in cellular plastics. Proceedings of The SPI 31st Annual Technical/Marketing Conference, Philadelphia, Society of The Plastics Industry, Polyurethane Division.
Schwartz, N. V., M. T. Bomberg and M. K. Kumaran, (1989). Water vapor transmission and moisture accumulation in polyurethane and polyisocyanurate foams. H. R. Trechsel and M. Bomberg.(Eds), *Water Vapor Transmission Through Building Materials and Systems: Mechanisms and Measurement, ASTM STP*. 1039**,** Philadelphia. American Society for Testing and Materials. 63-72.
Scott, J. and R. Bell, (1994). Discussion of Heat Flow Meter Apparatus Calibration and Traceability Issues for Thermal Conductivity Measurements. *Journal of Building Physics* 18(2): 146-162.
Siau, J. F., (1984). *Transport processes in wood*, New York; Berlin, Springer-Verlag.
Simpson, W. T., (1971). Equilibrium moisture content prediction for wood. *Forest Prod J*.
Simpson, W. T., (1973). Predicting equilibrium moisture content of wood by mathematical models. *Wood and fiber science* 5(1): 41-49.
Sing, K. S. W., (1985). Reporting physisorption data for gas/solid systems with special reference to the determination of surface area and porosity (Recommendations 1984). *Pure and Applied Chemistry* 57(4): 603-619.
Skaar, C., (1988). *Wood-Water Relations*, Berlin/Heidelberg, Springer Berlin Heidelberg.
Smith, D. R., (1997). Thermal conductivity of fibrous glass board by guarded hot plates and heat flow meters: An international round-robin. *International Journal of Thermophysics* 18(6): 1557-1573.
Sonderegger, W., M. Vecellio, P. Zwicker and P. Niemz, (2011). Combined bound water and water vapour diffusion of Norway spruce and European beech in and between the principal anatomical directions. *Holzforschung* 65(6): 819-828.
Spinnler, M., E. R. F. Winter and R. Viskanta, (2004). Studies on high-temperature multilayer thermal insulations. *International Journal of Heat and Mass Transfer* 47(6): 1305-1312.
Staudt, P., I. Tessaro, L. Marczak, R. d. P. Soares and N. Cardozo, (2013a). A new method for predicting sorption isotherms at different temperatures: Extension to the GAB model. *Journal of Food Engineering* 118(3): 247-255.
Staudt, P. B., C. P. Kechinski, I. C. Tessaro, L. D. F. Marczak, R. de P. Soares and N. S. M. Cardozo, (2013b). A new method for predicting sorption isotherms at different temperatures using the BET model. *Journal of Food Engineering* 114(1): 139-145.
Tada, S. and K. Watanabe, (2005). Dynamic determination of sorption isotherm of cement based materials. *Cement and Concrete Research* 35(12): 2271-2277.
Tariku, F., (2008). Whole building heat and moisture analysis. PhD Thesis, Concordia University.
TenWolde, A., (1989). Moisture transfer through materials and systems in buildings. *Water Vapor Transmission Through Building Materials and Systems: Mechanisms and Measurement*. ASTM International.
Thygesen, L. G., E. Tang Engelund and P. Hoffmeyer, (2010). Water sorption in wood and modified wood at high values of relative humidity. Part I: Results for untreated, acetylated, and furfurylated Norway spruce. *Holzforschung* 64(3): 315-323.
Timmermann, E. O., (2003). Multilayer sorption parameters: BET or GAB values? *Colloids and Surfaces A: Physicochemical and Engineering Aspects* 220(1-3): 235-260.

Tleoubaev, A. and A. Brzezinski, (2007). Thermal Diffusivity and Volumetric Specific Heat Measurements Using Heat Flow Meter Instruments Proceedings of the 29th International Thermal Conductivity Conference and the 17th International Thermal Expansion Symposium, Birmingham, Alabama, USA.

Tleoubaev, A., A. Brzezinski and L. C. Braga, (2008). Accurate simultaneous measurements of thermal conductivity and specific heat of rubber, elastomers, and other materials. Proceedings of 12th Brazilian Rubber Technology Congress, Sao Paulo, Brazil, April.

Toas, M., (1989). Results of the 1985 round-robin test series using ASTM E 96–80. H. R. Trechsel and M. Bomberg.(Eds), *Water vapor transmission through building materials and systems: mechanisms and measurement. ASTM STP*. 1039**,** Philadelphia. American Society for Testing and Materials. 73-90.

Tobiasson, W., A. Greatorex and D. Van Pelt, (1987). Wetting of Polystyrene and Urethane Roof Insulations in the Laboratory and on a Protected Membrane Roof. *Journal of Thermal Insulation* 11(Oct): 108-119.

Trabelsi, A., R. Belarbi, K. Abahri and M. Qin, (2012). Assessment of temperature gradient effects on moisture transfer through thermogradient coefficient. *Building Simulation* 5(2): 107-115.

Tsami, E., M. K. Krokida and A. E. Drouzas, (1998). Effect of drying method on the sorption characteristics of model fruit powders. *Journal of Food Engineering* 38(4): 381-392.

Tveit, A., (1966). *Measurements of moisture sorption and moisture permeability of porous materials*, Norwegian Building Research Inst.

Tye, R. P. and S. Spinney, (1979). A study of the effects of moisture vapour on the thermal transmittance characteristics of cellulose fibre thermal insulation. *Journal of Building Physics* 2(4): 175-196.

USDA, F. P. L., (1955). *Wood Handbook- Basic information on wood as a material of construction with Datafor Its Use in Design and Specification No. 72*, Washington, D.C., U.S. Dept. of Agriculture, Forest Products Laboratory, Forest Service.

Valovirta, I. and J. Vinha, (2004). Water vapor permeability and thermal conductivity as a function of temperature and relative humidity. *ASHRAE Journal*.

Vejmelková, E., M. Pavlíková, M. Jerman and R. Černý, (2009). Free Water Intake as Means of Material Characterization. *Journal of Building Physics* 33(1): 29-44.

Vishwakarma, R. K., U. S. Shivhare and S. K. Nanda, (2011). Moisture adsorption isotherms of guar (Cyamposis tetragonoloba) grain and guar gum splits. *LWT - Food Science and Technology* 44(4): 969-975.

Vololonirina, O., M. Coutand and B. Perrin, (2014). Characterization of hygrothermal properties of wood-based products – Impact of moisture content and temperature. *Construction and Building Materials* 63: 223-233.

Voutilainen, J., (2005). Methods and instrumentation for measuring moisture in building structures. PhD, Helsinki University of Technology.

Vrána, T. and F. Björk, (2008). A laboratory equipment for the study of moisture processes in thermal insulation materials when placed in a temperature field. *Construction and Building Materials* 22(12): 2335-2344.

Wadsö, I. and L. Wadsö, (1996). A new method for determination of vapour sorption isotherms using a twin double microcalorimeter. *Thermochimica Acta* 271: 179-187.

Wadsö, I. and L. Wadsö, (1997). A second generation twin double microcalorimeter: Measurements of sorption isotherms, heats of sorption and sorption kinetics. *Journal of Thermal Analysis* 49(2): 1045-1052.
Wadsö, L., (1993a). Measurements of water vapour sorption in Wood Part 1. Instrumentation. *Wood Science and Technology* 27(5): 396-400.
Wadsö, L., (1993b). Measurements of Water Vapour Sorption in Wood Part 2. Results. *Wood Science and Technology* 28(1): 59-65.
Wang, J., P. Mukhopadhyaya and P. I. Morris, (2014). Sorption and capillary condensation in wood and the moisture content of red pine. *Journal of Building Physics* 37(4): 327-347.
Wexler, A. and S. Hasegawa, (1954). Relative humidity-temperature relationships of some saturated salt solutions in the temperature range 0 to 50 C. *Journal of Research of the National Bureau of Standards* 53(1): 19-26.
Wijeysundera, N. E., M. N. A. Hawlader and Y. T. Tan, (1989). Water vapour diffusion and condensation in fibrous insulations. *International Journal of Heat and Mass Transfer* 32(10): 1865-1878.
Wilkes, K. E. and A. N. Karagiozis, (2004). The Importance of Measuring Method for Gypsum Sorption Isotherm. L. UT-Battelle. USA, *Oak Ridge National Laboratory*.
Wilkinson, G. E. and A. Klute, (1962). The temperature effect on the equilibrium energy status of water held by porous media. *Soil Science Society of America Journal* 26(4): 326-329.
Wu, M., B. Johannesson and M. Geiker, (2014). A study of the water vapor sorption isotherms of hardened cement pastes: Possible pore structure changes at low relative humidity and the impact of temperature on isotherms. *Cement and Concrete Research* 56: 97-105.
Wu, Y., (2007). Experimental study of hygrothermal properties for building materials.
Xi, Y., Z. P. Bažant and H. M. Jennings, (1994). Moisture diffusion in cementitious materials Adsorption isotherms. *Advanced Cement Based Materials* 1(6): 248-257.
Yener, Y., C. P. Naveira-Cotta and S. Kakac, (2018). *Heat Conduction, Fifth Edition*, Milton, CRC Press.
Yüksel, N., A. Avcı and M. Kılıç, (2010). The temperature dependence of effective thermal conductivity of the samples of glass wool reinforced with aluminium foil. *International Communications in Heat and Mass Transfer* 37(6): 675-680.
Yüksel, N., A. Avcı and M. Kılıç, (2012). The effective thermal conductivity of insulation materials reinforced with aluminium foil at low temperatures. *Heat and Mass Transfer* 48(9): 1569-1574.
Zarr, R., (1997). Standard Reference Materials: Glass Fiberboard, SRM 1450c, for Thermal Resistance from 280 K to 340 K. . NIST Special Publication 260-130.
Zarr, R., (2008). Status of NIST thermal insulation reference materials. *Thermal Conductivity* 29: 120-128.
Zarr, R. R. and J. J. Filliben, (2002). An International Study of Guarded Hot Plate Laboratories Using Fibrous Glass and Expanded Polystyrene Reference Materials. *ASTM SPECIAL TECHNICAL PUBLICATION* 1426: 3-16.
Zarr, R. R., N. A. Heckert and S. D. Leigh, (2014). Retrospective Analysis of NIST Standard Reference Material 1450, Fibrous Glass Board, for Thermal Insulation Measurements. *Journal of research of the National Institute of Standards and Technology* 119(1): 296.
Zhang, B.-M., S.-Y. Zhao and X.-D. He, (2008). Experimental and theoretical studies on high-temperature thermal properties of fibrous insulation. *Journal of Quantitative Spectroscopy and Radiative Transfer* 109(7): 1309-1324.

Zhang, X., X. Zhang, W. Zillig, H. M. Künzel and C. Mitterer, (2015). Evaluation of moisture sorption models and modified Mualem model for prediction of desorption isotherm for wood materials. *Building and Environment* 92: 387-395.

Zhao, C. Y., T. J. Lu, H. P. Hodson and J. D. Jackson, (2004). The temperature dependence of effective thermal conductivity of open-celled steel alloy foams. *Materials Science and Engineering: A* 367(1–2): 123-131.

Zuritz, C., R. P. Singh, S. Moini and S. Henderson, (1979). Desorption isotherms of rough rice from 10 to 40 degrees Celsius [Equilibrium moisture contents]. *Transactions of the ASAE [American Society of Agricultural Engineers]*.

11 Appendix A

11.1 Measured Equilibrium Moisture Content for each sample of building materials

The equilibrium moisture content (EMC) of each tested building material in three temperatures: 3°C, 21°C and 45°C are tabulated in three tables. The SD in the tables indicates standard deviations for moisture content, obtained from statistical analyses of the measured data at each operating temperature.

11.1.1 **Clay Brick**

Table 11-1. Clay Brick-Adsorption Isotherm at 3°C (kg/kg).

EMC at	50 %RH	70 %RH	90 %RH
Specimen 1	9.93E-04	1.13E-03	1.39E-03
Specimen 2	7.69E-04	8.79E-04	1.26E-03
Specimen 3	1.07E-03	1.14E-03	1.25E-03
Mean	**9.42E-04**	**1.05E-03**	**1.30E-03**
SD	1.55E-04	1.49E-04	7.87E-05

Table 11-2. Clay Brick-Adsorption Isotherm at 21°C (kg/kg).

EMC at	50 %RH	70 %RH	90 %RH
Specimen 1	7.43E-04	9.68E-04	1.12E-03
Specimen 2	8.10E-04	1.08E-03	1.33E-03
Specimen 3	8.37E-04	9.94E-04	1.25E-03
Mean	**7.97E-04**	**1.02E-03**	**1.23E-03**
SD	4.80E-05	6.14E-05	1.04E-04

Table 11-3. Clay Brick-Adsorption Isotherm at 45°C (kg/kg).

EMC at	50 %RH	70 %RH	90 %RH
Specimen 1	3.22E-04	3.99E-04	6.91E-04
Specimen 2	3.80E-04	4.59E-04	6.96E-04
Specimen 3	5.33E-04	6.30E-04	1.03E-03
Mean	**4.12E-04**	**4.96E-04**	**8.07E-04**
SD	1.09E-04	1.20E-04	1.96E-04

11.1.2 **Fiber Cement**

Table 11-4. Fiber Cement- Adsorption Isotherm at 3 °C (kg/kg).

EMC at	50 %RH	70 %RH	90 %RH
Specimen 1	4.89E-02	6.12E-02	1.18E-01
Specimen 2	5.78E-02	7.08E-02	1.26E-01
Specimen 3	4.46E-02	5.63E-02	1.11E-01
Mean	**5.05E-02**	**6.28E-02**	**1.18E-01**
SD	6.73E-03	7.34E-03	7.37E-03

Table 11-5. Fiber Cement- Adsorption Isotherm at 21°C (kg/kg).

EMC at	50 %RH	70 %RH	90 %RH
Specimen 1	4.32E-02	5.85E-02	1.07E-01
Specimen 2	4.27E-02	5.73E-02	1.09E-01
Specimen 3	4.30E-02	5.74E-02	1.10E-01
Mean	**4.30E-02**	**5.78E-02**	**1.09E-01**
SD	2.42E-04	6.76E-04	1.47E-03

Table 11-6. Fiber Cement- Adsorption Isotherm at 45 °C (kg/kg).

EMC at	50 %RH	70 %RH	90 %RH
Specimen 1	3.25E-02	5.08E-02	1.02E-01
Specimen 2	3.08E-02	4.78E-02	9.81E-02
Specimen 3	5.48E-02	7.37E-02	1.27E-01
Mean	**3.94E-02**	**5.74E-02**	**1.09E-01**
SD	1.34E-02	1.42E-02	1.58E-02

11.1.3 **Stucco**

Table 11-7. Stucco-Adsorption Isotherm at 3°C (kg/kg).

EMC at	50 %RH	70 %RH	90 %RH
Specimen 1	4.48E-02	6.31E-02	7.50E-02
Specimen 2	3.13E-02	4.91E-02	6.13E-02
Specimen 3	3.13E-02	4.86E-02	6.17E-02
Mean	**3.58E-02**	**5.36E-02**	**6.60E-02**
SD	7.80E-03	8.26E-03	7.83E-03

Table 11-8. Stucco-Adsorption Isotherm at 21°C (kg/kg).

EMC at	50 %RH	70 %RH	90 %RH
Specimen 1	2.68E-02	3.96E-02	5.89E-02
Specimen 2	2.56E-02	3.77E-02	5.69E-02
Specimen 3	2.64E-02	3.61E-02	5.47E-02
Mean	**2.63E-02**	**3.78E-02**	**5.69E-02**
SD	6.27E-04	1.78E-03	2.13E-03

Table 11-9. Stucco-Adsorption Isotherm at 45°C (kg/kg).

EMC at	50 %RH	70 %RH	90 %RH
Specimen 1	2.50E-02	3.24E-02	5.07E-02
Specimen 2	2.56E-02	3.24E-02	5.14E-02
Specimen 3	2.68E-02	3.34E-02	5.32E-02
Mean	**2.58E-02**	**3.27E-02**	**5.18E-02**
SD	9.34E-04	5.68E-04	1.28E-03

11.1.4 **Western Red Cedar**

Table 11-10. Western Red Cedar-Adsorption Isotherm at 3°C (kg/kg).

EMC at	50 %RH	70 %RH	90 %RH
Specimen 1	6.28E-02	9.31E-02	1.44E-01
Specimen 2	6.87E-02	9.96E-02	1.53E-01
Specimen 3	6.79E-02	9.84E-02	1.51E-01
Mean	**6.65E-02**	**9.70E-02**	**1.49E-01**
SD	3.17E-03	3.47E-03	4.38E-03

Table 11-11. Western Red Cedar-Adsorption Isotherm at 21°C (kg/kg).

EMC at	50 %RH	70 %RH	90 %RH
Specimen 1	6.17E-02	9.31E-02	1.48E-01
Specimen 2	6.13E-02	9.29E-02	1.49E-01
Specimen 3	6.14E-02	9.27E-02	1.48E-01
Mean	**6.15E-02**	**9.29E-02**	**1.48E-01**
SD	1.95E-04	2.01E-04	5.99E-04

Table 11-12. Western Red Cedar-Adsorption Isotherm at 45°C (kg/kg).

EMC at	50 %RH	70 %RH	90 %RH
Specimen 1	5.72E-02	8.85E-02	1.40E-01
Specimen 2	5.62E-02	8.71E-02	1.39E-01
Specimen 3	5.71E-02	8.86E-02	1.41E-01
Mean	**5.68E-02**	**8.81E-02**	**1.40E-01**
SD	5.78E-04	8.36E-04	8.52E-04

11.1.5 **60 Min Building Paper**

Table 11-13. 60 Min Building Paper-Adsorption Isotherm at 3°C (kg/kg).

EMC at	50 %RH	70 %RH	90 %RH
Specimen 1	9.42E-02	1.06E-01	1.45E-01
Specimen 2	6.79E-02	9.13E-02	1.20E-01
Specimen 3	1.22E-01	1.63E-01	1.77E-01
Mean	**9.48E-02**	**1.20E-01**	**1.47E-01**
SD	2.72E-02	3.78E-02	2.88E-02

Table 11-14. 60 Min Building Paper-Adsorption Isotherm at 21°C (kg/kg).

EMC at	50 %RH	70 %RH	90 %RH
Specimen 1	8.37E-02	1.01E-01	1.40E-01
Specimen 2	6.27E-02	8.05E-02	1.20E-01
Specimen 3	5.96E-02	7.54E-02	1.14E-01
Mean	**6.87E-02**	**8.57E-02**	**1.25E-01**
SD	1.31E-02	1.35E-02	1.35E-02

Table 11-15. 60 Min Building Paper-Adsorption Isotherm at 45°C (kg/kg).

EMC at	50 %RH	70 %RH	90 %RH
Specimen 1	4.09E-02	4.45E-02	1.17E-01
Specimen 2	4.72E-02	5.64E-02	1.18E-01
Specimen 3	5.98E-02	6.90E-02	1.38E-01
Mean	**4.93E-02**	**5.66E-02**	**1.24E-01**
SD	9.66E-03	1.22E-02	1.20E-02

11.1.6 **Oriented Strand Board (OSB)**

Table 11-16. OSB-Adsorption Isotherm at 3°C (kg/kg).

EMC at	50 %RH	70 %RH	90 %RH
Specimen 1	6.61E-02	7.92E-02	1.73E-01
Specimen 2	6.43E-02	1.43E-01	1.72E-01
Specimen 3	6.21E-02	1.51E-01	1.69E-01
Mean	**6.42E-02**	**1.24E-01**	**1.72E-01**
SD	1.99E-03	3.92E-02	2.10E-03

Table 11-17. OSB-Adsorption Isotherm at 21°C (kg/kg).

EMC at	50 %RH	70 %RH	90 %RH
Specimen 1	5.37E-02	8.55E-02	1.58E-01
Specimen 2	5.32E-02	8.61E-02	1.58E-01
Specimen 3	5.44E-02	8.67E-02	1.59E-01
Mean	**5.38E-02**	**8.61E-02**	**1.59E-01**
SD	5.95E-04	6.18E-04	4.25E-04

Table 11-18. OSB-Adsorption Isotherm at 45°C (kg/kg).

EMC at	50 %RH	70 %RH	90 %RH
Specimen 1	5.29E-02	7.67E-02	1.56E-01
Specimen 2	5.37E-02	7.80E-02	1.59E-01
Specimen 3	5.48E-02	7.93E-02	1.59E-01
Mean	**5.38E-02**	**7.80E-02**	**1.58E-01**
SD	9.72E-04	1.32E-03	1.86E-03

11.1.7 **Plywood**

Table 11-19. Plywood-Adsorption Isotherm at 3°C (kg/kg).

EMC at	50 %RH	70 %RH	90 %RH
Specimen 1	7.47E-02	9.11E-02	1.65E-01
Specimen 2	7.69E-02	9.43E-02	1.68E-01
Specimen 3	7.63E-02	9.54E-02	1.66E-01
Mean	**7.60E-02**	**9.36E-02**	**1.66E-01**
SD	1.13E-03	2.22E-03	1.71E-03

Table 11-20. Plywood-Adsorption Isotherm at 21°C (kg/kg).

EMC at	50 %RH	70 %RH	90 %RH
Specimen 1	6.75E-02	9.26E-02	1.61E-01
Specimen 2	6.77E-02	9.27E-02	1.62E-01
Specimen 3	6.80E-02	9.31E-02	1.62E-01
Mean	**6.77E-02**	**9.28E-02**	**1.62E-01**
SD	2.23E-04	2.33E-04	4.09E-04

Table 11-21. Plywood-Adsorption Isotherm at 45°C (kg/kg).

EMC at	50 %RH	70 %RH	90 %RH
Specimen 1	5.86E-02	8.05E-02	1.57E-01
Specimen 2	6.12E-02	8.43E-02	1.63E-01
Specimen 3	6.10E-02	8.42E-02	1.64E-01
Mean	**6.02E-02**	**8.30E-02**	**1.62E-01**
SD	1.45E-03	2.18E-03	3.95E-03

11.1.8 **Densglass Gold Gypsum Sheathing Board**

Table 11-22. Densglass Gold Gypsum-Adsorption Isotherm at 3°C (kg/kg).

EMC at	50 %RH	70 %RH	90 %RH
Specimen 1	2.04E-03	2.41E-03	3.95E-03
Specimen 2	2.08E-03	2.62E-03	4.23E-03
Specimen 3	2.23E-03	2.73E-03	4.26E-03
Mean	**2.12E-03**	**2.59E-03**	**4.15E-03**
SD	1.03E-04	1.60E-04	1.70E-04

Table 11-23. Densglass Gold Gypsum-Adsorption Isotherm at 21°C (kg/kg).

EMC at	50 %RH	70 %RH	90 %RH
Specimen 1	1.14E-03	2.04E-03	3.65E-03
Specimen 2	1.15E-03	2.22E-03	3.98E-03
Specimen 3	1.23E-03	2.05E-03	3.94E-03
Mean	**1.17E-03**	**2.10E-03**	**3.86E-03**
SD	5.07E-05	9.67E-05	1.78E-04

Table 11-24. Densglass Gold Gypsum-Adsorption Isotherm at 45°C (kg/kg).

EMC at	50 %RH	70 %RH	90 %RH
Specimen 1	2.48E-04	1.03E-03	3.47E-03
Specimen 2	2.05E-04	1.27E-03	3.37E-03
Specimen 3	1.21E-03	1.25E-03	3.03E-03
Mean	**5.55E-04**	**1.19E-03**	**3.29E-03**
SD	5.70E-04	1.34E-04	2.26E-04

11.1.9 **Spruce**

Table 11-25. Spruce-Adsorption Isotherm at 3°C (kg/kg).

EMC at	50 %RH	70 %RH	90 %RH
Specimen 1	8.85E-02	1.27E-01	1.91E-01
Specimen 2	8.91E-02	1.27E-01	1.92E-01
Specimen 3	8.96E-02	1.28E-01	1.93E-01
Mean	**8.91E-02**	**1.27E-01**	**1.92E-01**
SD	5.38E-04	3.49E-04	1.42E-03

Table 11-26. Spruce-Adsorption Isotherm at 21°C (kg/kg).

EMC at	50 %RH	70 %RH	90 %RH
Specimen 1	7.89E-02	1.18E-01	1.89E-01
Specimen 2	7.90E-02	1.18E-01	1.89E-01
Specimen 3	7.85E-02	1.17E-01	1.87E-01
Mean	**7.88E-02**	**1.17E-01**	**1.88E-01**
SD	2.57E-04	3.21E-04	7.99E-04

Table 11-27. Spruce-Adsorption Isotherm at 45°C (kg/kg).

EMC at	50 %RH	70 %RH	90 %RH
Specimen 1	7.12E-02	1.10E-01	1.78E-01
Specimen 2	7.12E-02	1.10E-01	1.77E-01
Specimen 3	7.16E-02	1.10E-01	1.76E-01
Mean	**7.13E-02**	**1.10E-01**	**1.77E-01**
SD	2.57E-04	1.54E-04	9.71E-04

11.1.10 **Douglas Fir**

Table 11-28. Douglas Fir-Adsorption Isotherm at 3°C (kg/kg).

EMC at	50 %RH	70 %RH	90 %RH
Specimen 1	8.53E-02	1.22E-01	1.85E-01
Specimen 2	8.51E-02	1.22E-01	1.82E-01
Specimen 3	1.40E-01	1.80E-01	2.46E-01
Mean	**1.04E-01**	**1.41E-01**	**2.04E-01**
SD	3.18E-02	3.37E-02	3.62E-02

Table 11-29. Douglas Fir-Adsorption Isotherm at 21°C (kg/kg).

EMC at	50 %RH	70 %RH	90 %RH
Specimen 1	7.85E-02	1.17E-01	1.82E-01
Specimen 2	7.86E-02	1.18E-01	1.82E-01
Specimen 3	7.83E-02	1.17E-01	1.83E-01
Mean	**7.85E-02**	**1.17E-01**	**1.82E-01**
SD	1.64E-04	3.33E-04	7.80E-04

Table 11-30. Douglas Fir-Adsorption Isotherm at 45°C (kg/kg).

EMC at	50 %RH	70 %RH	90 %RH
Specimen 1	7.00E-02	1.03E-01	1.73E-01
Specimen 2	7.01E-02	1.04E-01	1.72E-01
Specimen 3	7.64E-02	1.04E-01	1.71E-01
Mean	**7.22E-02**	**1.04E-01**	**1.72E-01**
SD	3.68E-03	2.31E-04	6.79E-04

11.1.11 **Cellulose Fiber**

Table 11-31. Cellulose Fiber-Adsorption Isotherm at 3°C (kg/kg).

EMC at	50 %RH	70 %RH	90 %RH
Specimen 1	1.78E-01	1.85E-01	2.33E-01
Specimen 2	1.93E-01	2.02E-01	2.57E-01
Specimen 3	1.11E-01	1.21E-01	1.69E-01
Mean	**1.61E-01**	**1.70E-01**	**2.20E-01**
SD	4.37E-02	4.26E-02	4.53E-02

Table 11-32. Cellulose Fiber-Adsorption Isotherm at 21°C (kg/kg).

EMC at	50 %RH	70 %RH	90 %RH
Specimen 1	7.97E-02	1.31E-01	1.94E-01
Specimen 2	6.51E-02	9.76E-02	1.71E-01
Specimen 3	1.22E-01	1.47E-01	2.38E-01
Mean	**8.89E-02**	**1.25E-01**	**2.01E-01**
SD	2.95E-02	2.53E-02	3.36E-02

11.1.12 **Expanded Polystyrene (EPS)**

Table 11-33. EPS-Adsorption Isotherm at 3°C (kg/kg).

EMC at	50 %RH	70 %RH	90 %RH
Specimen 1	6.20E-03	6.47E-03	7.36E-03
Specimen 2	6.10E-03	6.54E-03	7.51E-03
Specimen 3	5.94E-03	6.21E-03	7.25E-03
Mean	**6.08E-03**	**6.40E-03**	**7.37E-03**
SD	1.31E-04	1.76E-04	1.29E-04

Table 11-34. EPS-Adsorption Isotherm at 21°C (kg/kg).

EMC at	50 %RH	70 %RH	90 %RH
Specimen 1	1.58E-03	1.14E-03	9.66E-04
Specimen 2	1.75E-03	7.89E-04	7.89E-04
Specimen 3	7.64E-03	7.12E-03	6.87E-03
Mean	**3.66E-03**	**3.02E-03**	**2.87E-03**
SD	3.45E-03	3.56E-03	3.46E-03

Table 11-35. EPS-Adsorption Isotherm at 45°C (kg/kg).

EMC at	50 %RH	70 %RH	90 %RH
Specimen 1	4.42E-04	1.41E-03	2.30E-03
Specimen 2	2.64E-04	6.17E-04	9.69E-04
Specimen 3	3.43E-04	9.44E-04	1.80E-03
Mean	**3.50E-04**	**9.91E-04**	**1.69E-03**
SD	8.89E-05	4.01E-04	6.71E-04

11.1.13 **Extruded Polystyrene (XPS)**

Table 11-36. XPS-Adsorption Isotherm at 3°C (kg/kg).

EMC at	50 %RH	70 %RH	90 %RH
Specimen 1	1.00E-02	1.13E-02	1.45E-02
Specimen 2	9.15E-03	1.03E-02	1.25E-02
Specimen 3	9.92E-03	1.09E-02	1.32E-02
Mean	**9.70E-03**	**1.08E-02**	**1.34E-02**
SD	4.75E-04	4.76E-04	9.88E-04

Table 11-37. XPS-Adsorption Isotherm at 21°C (kg/kg).

EMC at	50 %RH	70 %RH	90 %RH
Specimen 1	1.14E-02	1.22E-02	1.40E-02
Specimen 2	7.26E-03	8.25E-03	9.79E-03
Specimen 3	9.21E-03	9.75E-03	1.16E-02
Mean	**9.29E-03**	**1.01E-02**	**1.18E-02**
SD	2.07E-03	1.97E-03	2.11E-03

Table 11-38. XPS-Adsorption Isotherm at 45°C (kg/kg).

EMC at	50 %RH	70 %RH	90 %RH
Specimen 1	6.26E-03	8.10E-03	8.86E-03
Specimen 2	7.15E-03	1.10E-02	1.32E-02
Specimen 3	7.49E-03	8.46E-03	9.74E-03
Mean	**6.97E-03**	**9.19E-03**	**1.06E-02**
SD	6.34E-04	1.58E-03	2.30E-03

11.1.14 **Open Cell Spray Polyurethane**

Table 11-39. Open Cell Sprayed Foam-Adsorption Isotherm at 3°C (kg/kg).

EMC at	50 %RH	70 %RH	90 %RH
Specimen 1	6.82E-02	8.31E-02	1.17E-01
Specimen 2	2.80E-02	4.66E-02	7.00E-02
Specimen 3	1.06E-02	3.07E-02	5.50E-02
Mean	**3.56E-02**	**5.35E-02**	**8.07E-02**
SD	2.95E-02	2.68E-02	3.25E-02

Table 11-40. Open Cell Sprayed Foam-Adsorption Isotherm at 21°C (kg/kg).

EMC at	50 %RH	70 %RH	90 %RH
Specimen 1	6.66E-02	6.98E-02	7.00E-02
Specimen 2	2.76E-02	2.97E-02	3.05E-02
Specimen 3	2.87E-03	9.59E-03	1.05E-02
Mean	**3.23E-02**	**3.64E-02**	**3.70E-02**
SD	3.21E-02	3.07E-02	3.03E-02

Table 11-41. Open Cell Sprayed Foam-Adsorption Isotherm at 45°C (kg/kg).

EMC at	50 %RH	70 %RH	90 %RH
Specimen 1	5.09E-02	5.14E-02	5.20E-02
Specimen 2	9.98E-03	1.06E-02	1.13E-02
Specimen 3	2.11E-03	2.57E-03	3.25E-03
Mean	**2.10E-02**	**2.15E-02**	**2.22E-02**
SD	2.62E-02	2.62E-02	2.61E-02

11.1.15 **Polyisocyanurate**

Table 11-42. Polyisocyanurate-Adsorption Isotherm at 3°C (kg/kg).

EMC at	50 %RH	70 %RH	90 %RH
Specimen 1	8.96E-03	1.08E-02	2.19E-02
Specimen 2	9.02E-03	1.13E-02	2.27E-02
Specimen 3	9.21E-03	1.11E-02	2.23E-02
Mean	**9.06E-03**	**1.10E-02**	**2.23E-02**
SD	1.32E-04	2.37E-04	4.10E-04

Table 11-43. Polyisocyanurate-Adsorption Isotherm at 21°C (kg/kg).

EMC at	50 %RH	70 %RH	90 %RH
Specimen 1	2.77E-03	7.98E-03	1.79E-02
Specimen 2	1.42E-02	1.77E-02	2.83E-02
Specimen 3	4.09E-03	7.05E-03	1.74E-02
Mean	**7.01E-03**	**1.09E-02**	**2.12E-02**
SD	6.24E-03	5.92E-03	6.16E-03

Table 11-44. Polyisocyanurate-Adsorption Isotherm at 45°C (kg/kg).

EMC at	50 %RH	70 %RH	90 %RH
Specimen 1	4.77E-03	8.59E-03	1.47E-02
Specimen 2	5.64E-03	9.61E-03	1.53E-02
Specimen 3	5.91E-03	8.74E-03	1.43E-02
Mean	**5.44E-03**	**8.98E-03**	**1.48E-02**
SD	5.98E-04	5.49E-04	5.17E-04

11.1.16 **Mineral Fiber (Stone Wool)**

Table 11-45. Mineral Fiber-Adsorption Isotherm at 3°C (kg/kg).

EMC at	50 %RH	70 %RH	90 %RH
Specimen 1	1.23E-02	1.36E-02	1.66E-02
Specimen 2	1.08E-02	1.18E-02	1.47E-02
Specimen 3	1.43E-02	1.47E-02	1.70E-02
Mean	**1.25E-02**	**1.34E-02**	**1.61E-02**
SD	1.72E-03	1.46E-03	1.21E-03

Table 11-46. Mineral Fiber-Adsorption Isotherm at 21°C (kg/kg).

EMC at	50 %RH	70 %RH	90 %RH
Specimen 1	3.74E-03	4.19E-03	6.84E-03
Specimen 2	6.47E-03	7.60E-03	9.45E-03
Specimen 3	7.17E-03	9.43E-03	1.12E-02
Mean	**5.79E-03**	**7.07E-03**	**9.16E-03**
SD	1.81E-03	2.66E-03	2.19E-03

Table 11-47. Mineral Fiber-Adsorption Isotherm at 45°C (kg/kg).

EMC at	50 %RH	70 %RH	90 %RH
Specimen 1	1.15E-03	2.51E-03	7.64E-03
Specimen 2	1.26E-03	2.64E-03	7.75E-03
Specimen 3	2.45E-03	3.58E-03	9.55E-03
Mean	**1.62E-03**	**2.91E-03**	**8.31E-03**
SD	7.25E-04	5.87E-04	1.07E-03

12 Appendix B

12.1 Measured Water Vapor Transmission (WVT) rate for each building materials

The permeability test includes three samples for dry cup test and three samples for wet cup test. The separate measurement for each sample is presented here.

12.1.1 **Clay Brick**

Table 12-1. Clay Brick-Water Vapor Permeability at 3°C.

Clay Brick-Water Vapor Permeability at 3°C					
	Cup Method	**Sample No.**	**50% RH**	**70% RH**	**90% RH**
WVT (kg/s.m2)	Dry	1	3.724E-08	2.333E-08	5.379E-08
		2	6.286E-08	8.443E-08	1.220E-07
		3	2.362E-08	1.062E-07	1.165E-07
	Wet	4	7.337E-08	1.327E-08	8.247E-09
		5	3.134E-09	9.485E-08	3.841E-08
		6	9.937E-08	5.703E-09	5.673E-09
Permeance (kg/m2.s.Pa)	Dry	1	9.580E-11	4.399E-11	7.908E-11
		2	1.617E-10	1.592E-10	1.794E-10
		3	6.078E-11	2.003E-10	1.713E-10
	Wet	4	1.994E-10	5.840E-11	1.061E-10
		5	8.516E-12	4.175E-10	4.939E-10
		6	2.700E-10	2.510E-11	7.296E-11
Water Vapor Permeability (kg/m.s.Pa)	Dry	1	1.293E-12	5.938E-13	1.068E-12
		2	2.393E-12	2.356E-12	2.656E-12
		3	9.117E-13	3.005E-12	2.570E-12
	Wet	4	2.482E-12	7.271E-13	1.320E-12
		5	1.307E-13	6.409E-12	7.582E-12
		6	3.861E-12	3.590E-13	1.043E-12

Table 12-2. Clay Brick-Water Vapor Permeability at 21°C.

Clay Brick-Water Vapor Permeability at 21°C					
	Cup Method	**Sample No.**	**50% RH**	**70% RH**	**90% RH**
WVT (kg/s.m2)	Dry	1	2.673E-07	4.763E-07	5.078E-07
		2	2.058E-07	1.845E-07	2.487E-07
		3	7.908E-08	2.182E-07	4.153E-07
	Wet	4	2.542E-07	2.009E-07	7.063E-08
		5	1.885E-07	1.888E-07	8.181E-08
		6	2.864E-07	8.254E-08	5.790E-08
Permeance (kg/m2.s.Pa)	Dry	1	2.169E-10	2.735E-10	2.267E-10
		2	1.670E-10	1.060E-10	1.110E-10
		3	6.418E-11	1.253E-10	1.854E-10
	Wet	4	2.025E-10	2.693E-10	2.858E-10
		5	1.502E-10	2.531E-10	3.311E-10
		6	2.282E-10	1.107E-10	2.343E-10
Water Vapor Permeability (kg/m.s.Pa)	Dry	1	3.363E-12	4.240E-12	3.514E-12
		2	2.421E-12	1.536E-12	1.610E-12
		3	9.306E-13	1.817E-12	2.689E-12
	Wet	4	2.834E-12	3.771E-12	4.002E-12
		5	2.328E-12	3.923E-12	5.132E-12
		6	3.491E-12	1.693E-12	3.585E-12

Table 12-3. Clay Brick-Water Vapor Permeability at 45°C.

Clay Brick-Water Vapor Permeability at 45°C					
	Cup Method	**Sample No.**	**50% RH**	**70% RH**	**90% RH**
WVT (kg/s.m2)	Dry	1	1.041E-06	6.169E-07	1.910E-06
		2	7.557E-07	1.569E-06	3.051E-06
		3	6.346E-07	1.525E-06	1.506E-06
	Wet	4	1.349E-06	7.207E-07	1.785E-06
		5	8.075E-07	1.744E-06	1.699E-07
		6	1.396E-06	6.289E-07	3.707E-07
Permeance (kg/m2.s.Pa)	Dry	1	2.171E-10	9.208E-11	2.214E-10
		2	1.577E-10	2.342E-10	3.537E-10
		3	1.324E-10	2.275E-10	1.746E-10
	Wet	4	2.814E-10	2.497E-10	1.858E-09
		5	1.685E-10	6.044E-10	1.769E-10
		6	2.912E-10	2.179E-10	3.860E-10
Water Vapor Permeability (kg/m.s.Pa)	Dry	1	3.148E-12	1.335E-12	3.211E-12
		2	2.286E-12	3.396E-12	5.129E-12
		3	1.920E-12	3.299E-12	2.532E-12
	Wet	4	3.939E-12	3.496E-12	2.602E-11
		5	2.611E-12	9.368E-12	2.742E-12
		6	4.456E-12	3.334E-12	5.906E-12

Table 12-4. Clay Brick-Water Vapor Transmission Rate.

Clay Brick-Water Vapor Transmission Rate (kg/s.m^2)						
	ΔRH:50%	**ΔRH:70%**	**ΔRH:90%**	**ΔRH:50%**	**ΔRH:30%**	**ΔRH:10%**
	Dry Cups			**Wet Cups**		
	50% RH	70% RH	90% RH	50% RH	70% RH	90% RH
WVT at 3°C	4.12E-08	7.13E-08	9.75E-08	5.86E-08	3.79E-08	1.74E-08
WVT at 21°C	1.84E-07	2.93E-07	3.91E-07	2.43E-07	1.57E-07	7.01E-08
WVT at 45°C	8.10E-07	1.24E-06	2.16E-06	1.18E-06	1.03E-06	7.75E-07
Difference between 21°C and 3°C	346%	311%	301%	315%	315%	302%
Difference between 45°C and 21°C	340%	322%	452%	387%	555%	1005%
Difference between 45°C and 3°C	1865%	1634%	2112%	1920%	2618%	4344%

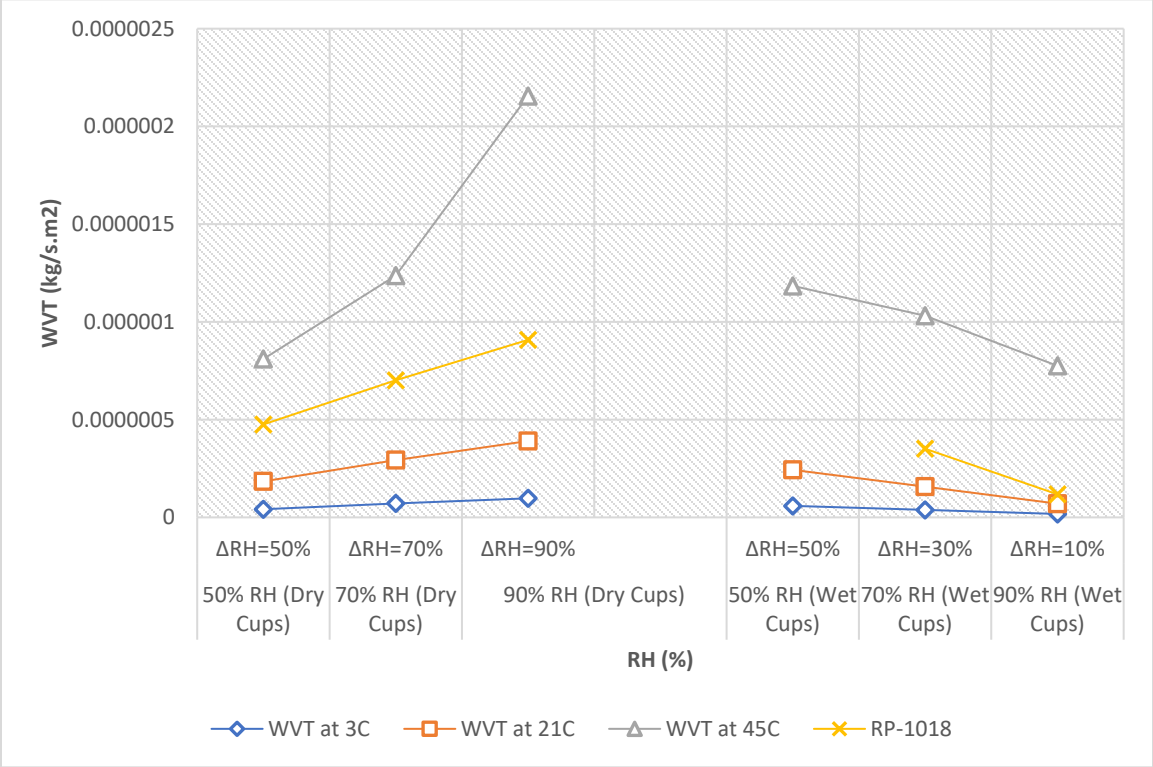

Figure 12-1. Clay Brick-Water Vapor Transmission Rate.

12.1.2 **Fiber Cement**

Table 12-5. Fiber Cement-Water Vapor Permeability at 3°C.

Fiber Cement-Water Vapor Permeability at 3°C					
	Cup Method	**Sample No.**	**50% RH**	**70% RH**	**90% RH**
WVT (kg/s.m2)	Dry	1	2.518E-08	3.929E-08	1.166E-07
		2	2.752E-08	4.076E-08	9.826E-08
		3	3.131E-08	4.451E-08	1.215E-07
	Wet	4	1.476E-07	1.142E-07	4.897E-08
		5	1.214E-07	3.998E-08	3.694E-08
		6	1.556E-07	2.513E-07	9.814E-08
Permeance (kg/m2.s.Pa)	Dry	1	6.646E-11	7.407E-11	1.711E-10
		2	7.263E-11	7.685E-11	1.442E-10
		3	8.263E-11	8.391E-11	1.783E-10
	Wet	4	3.900E-10	5.007E-10	6.359E-10
		5	3.207E-10	1.752E-10	4.797E-10
		6	4.110E-10	1.101E-09	1.274E-09
Water Vapor Permeability (kg/m.s.Pa)	Dry	1	5.151E-13	5.740E-13	1.326E-12
		2	5.665E-13	5.995E-13	1.125E-12
		3	6.404E-13	6.503E-13	1.382E-12
	Wet	4	3.023E-12	3.881E-12	4.928E-12
		5	2.502E-12	1.367E-12	3.742E-12
		6	3.144E-12	8.425E-12	9.748E-12

Table 12-6. Fiber Cement-Water Vapor Permeability at 21°C.

Fiber Cement-Water Vapor Permeability at 21°C					
	Cup Method	**Sample No.**	**50% RH**	**70% RH**	**90% RH**
WVT (kg/s.m2)	Dry	1	1.026E-07	1.516E-07	3.911E-07
		2	1.063E-07	1.566E-07	3.991E-07
		3	1.065E-07	1.586E-07	4.314E-07
	Wet	4	5.810E-07	6.502E-07	3.288E-07
		5	5.069E-07	6.243E-07	3.721E-07
		6	6.241E-07	2.993E-07	2.524E-07
Permeance (kg/m2.s.Pa)	Dry	1	8.286E-11	8.708E-11	1.748E-10
		2	8.582E-11	8.990E-11	1.784E-10
		3	8.602E-11	9.107E-11	1.928E-10
	Wet	4	4.636E-10	8.733E-10	1.324E-09
		5	4.045E-10	8.384E-10	1.499E-09
		6	4.979E-10	4.020E-10	1.016E-09
Water Vapor Permeability (kg/m.s.Pa)	Dry	1	6.339E-13	6.662E-13	1.337E-12
		2	6.651E-13	6.968E-13	1.382E-12
		3	6.581E-13	6.967E-13	1.475E-12
	Wet	4	3.593E-12	6.768E-12	1.026E-11
		5	3.135E-12	6.498E-12	1.161E-11
		6	3.784E-12	3.056E-12	7.724E-12

Table 12-7. Fiber Cement-Water Vapor Permeability at 45°C.

Fiber Cement-Water Vapor Permeability at 45°C					
	Cup Method	**Sample No.**	**50% RH**	**70% RH**	**90% RH**
WVT (kg/s.m2)	Dry	1	3.243E-07	4.591E-07	2.025E-06
		2	5.085E-07	7.638E-07	1.809E-06
		3	4.611E-07	8.823E-07	1.298E-06
	Wet	4	5.797E-06	4.786E-06	4.353E-06
		5	2.455E-06	3.917E-06	1.009E-06
		6	2.705E-06	1.969E-06	1.172E-06
Permeance (kg/m2.s.Pa)	Dry	1	6.772E-11	6.853E-11	2.346E-10
		2	1.062E-10	1.140E-10	2.096E-10
		3	9.627E-11	1.317E-10	1.504E-10
	Wet	4	1.209E-09	1.658E-09	4.545E-09
		5	5.119E-10	1.357E-09	1.053E-09
		6	5.640E-10	6.821E-10	1.224E-09
Water Vapor Permeability (kg/m.s.Pa)	Dry	1	5.214E-13	5.277E-13	1.807E-12
		2	8.176E-13	8.779E-13	1.614E-12
		3	7.509E-13	1.027E-12	1.173E-12
	Wet	4	9.367E-12	1.285E-11	3.522E-11
		5	3.993E-12	1.058E-11	8.216E-12
		6	4.399E-12	5.320E-12	9.547E-12

Table 12-8. Fiber Cement-Water Vapor Transmission Rate.

Fiber Cement-Water Vapor Transmission Rate (kg/s.m^2)						
	ΔRH:50%	**ΔRH:70%**	**ΔRH:90%**	**ΔRH:50%**	**ΔRH:30%**	**ΔRH:10%**
	Dry Cups			**Wet Cups**		
	50% RH	70% RH	90% RH	50% RH	70% RH	90% RH
WVT at 3°C	2.80E-08	4.15E-08	1.12E-07	1.41E-07	1.35E-07	6.14E-08
WVT at 21°C	1.05E-07	1.56E-07	4.07E-07	5.70E-07	5.25E-07	3.18E-07
WVT at 45°C	4.31E-07	7.02E-07	1.71E-06	3.65E-06	3.56E-06	2.18E-06
Difference between 21°C and 3°C	276%	275%	263%	303%	288%	418%
Difference between 45°C and 21°C	310%	351%	320%	540%	578%	585%
Difference between 45°C and 3°C	1440%	1590%	1426%	2481%	2532%	3450%

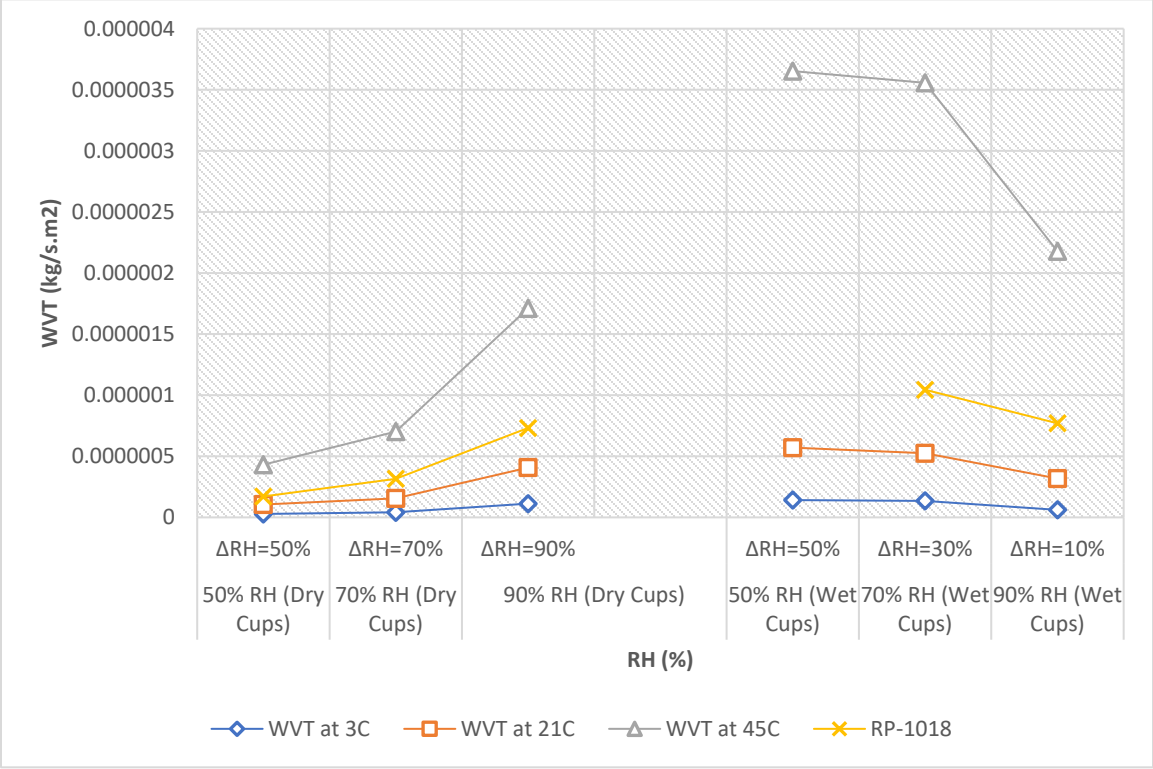

Figure 12-2. Fiber Cement-Water Vapor Transmission Rate.

12.1.3 **Stucco**

Table 12-9. Stucco-Water Vapor Permeability at 3°C.

Stucco-Water Vapor Permeability at 3°C					
	Cup Method	**Sample No.**	**50% RH**	**70% RH**	**90% RH**
WVT (kg/s.m2)	Dry	1	2.110E-08	8.541E-09	5.161E-08
		2	2.862E-08	5.183E-08	4.144E-08
		3	6.983E-09	3.228E-08	4.675E-08
	Wet	4	1.016E-07	6.579E-09	2.815E-09
		5	1.540E-08	5.404E-08	3.716E-09
		6	2.232E-09	2.142E-08	3.329E-08
Permeance (kg/m2.s.Pa)	Dry	1	5.578E-11	1.606E-11	7.602E-11
		2	7.566E-11	9.749E-11	6.104E-11
		3	1.846E-11	6.071E-11	6.886E-11
	Wet	4	2.678E-10	2.877E-11	3.539E-11
		5	4.060E-11	2.363E-10	4.672E-11
		6	5.884E-12	9.366E-11	4.185E-10
Water Vapor Permeability (kg/m.s.Pa)	Dry	1	9.677E-13	2.787E-13	1.319E-12
		2	1.362E-12	1.755E-12	1.099E-12
		3	3.249E-13	1.069E-12	1.212E-12
	Wet	4	4.527E-12	4.861E-13	5.981E-13
		5	6.902E-13	4.017E-12	7.943E-13
		6	1.012E-13	1.611E-12	7.199E-12

Table 12-10. Stucco-Water Vapor Permeability at 21°C.

Stucco-Water Vapor Permeability at 21°C					
	Cup Method	**Sample No.**	**50% RH**	**70% RH**	**90% RH**
WVT (kg/s.m2)	Dry	1	1.211E-07	1.995E-07	3.090E-07
		2	1.737E-07	5.683E-07	4.111E-07
		3	2.707E-07	9.792E-08	6.277E-07
	Wet	4	2.419E-07	1.602E-07	8.543E-08
		5	2.239E-07	1.888E-07	5.558E-08
		6	3.870E-07	2.907E-07	1.238E-07
Permeance (kg/m2.s.Pa)	Dry	1	9.740E-11	1.146E-10	1.382E-10
		2	1.397E-10	3.265E-10	1.838E-10
		3	2.177E-10	5.626E-11	2.807E-10
	Wet	4	1.941E-10	2.149E-10	3.440E-10
		5	1.797E-10	2.534E-10	2.238E-10
		6	3.106E-10	3.901E-10	4.985E-10
Water Vapor Permeability (kg/m.s.Pa)	Dry	1	1.690E-12	1.988E-12	2.397E-12
		2	2.514E-12	5.877E-12	3.309E-12
		3	3.831E-12	9.902E-13	4.940E-12
	Wet	4	3.281E-12	3.632E-12	5.814E-12
		5	3.055E-12	4.308E-12	3.805E-12
		6	5.343E-12	6.709E-12	8.574E-12

Table 12-11. Stucco-Water Vapor Permeability at 45°C.

Stucco-Water Vapor Permeability at 45°C					
	Cup Method	**Sample No.**	**50% RH**	**70% RH**	**90% RH**
WVT (kg/s.m2)	Dry	1	1.430E-06	2.626E-06	3.761E-06
		2	2.174E-06	1.932E-06	2.560E-06
		3	8.611E-07	2.318E-06	3.786E-06
	Wet	4	2.290E-06	1.944E-06	5.914E-07
		5	2.090E-06	2.377E-06	4.890E-07
		6	2.899E-06	1.007E-06	8.113E-07
Permeance (kg/m2.s.Pa)	Dry	1	2.984E-10	3.916E-10	4.357E-10
		2	4.537E-10	2.881E-10	2.966E-10
		3	1.797E-10	3.456E-10	4.387E-10
	Wet	4	4.779E-10	6.751E-10	6.171E-10
		5	4.361E-10	8.253E-10	5.103E-10
		6	6.050E-10	3.497E-10	8.466E-10
Water Vapor Permeability (kg/m.s.Pa)	Dry	1	5.177E-12	6.794E-12	7.560E-12
		2	8.166E-12	5.187E-12	5.339E-12
		3	3.163E-12	6.082E-12	7.720E-12
	Wet	4	8.076E-12	1.141E-11	1.043E-11
		5	7.414E-12	1.403E-11	8.675E-12
		6	1.041E-11	6.015E-12	1.456E-11

Table 12-12. Stucco-Water Vapor Transmission Rate.

Stucco-Water Vapor Transmission Rate (kg/s.m^2)						
	ΔRH:50%	**ΔRH:70%**	**ΔRH:90%**	**ΔRH:50%**	**ΔRH:30%**	**ΔRH:10%**
	Dry Cups			**Wet Cups**		
	50% RH	70% RH	90% RH	50% RH	70% RH	90% RH
WVT at 3°C	1.88E-08	3.088E-08	4.66E-08	3.97E-08	2.73E-08	1.33E-08
WVT at 21°C	1.885E-07	2.885E-07	4.49262E-07	2.843E-07	2.13E-07	8.83E-08
WVT at 45°C	1.48E-06	2.292E-06	3.368E-06	2.42E-06	1.78E-06	6.31E-07
Difference between 21°C and 3°C	897%	834%	864%	615%	680%	565%
Difference between 45°C and 21°C	690%	694%	650%	754%	733%	978%
Difference between 45°C and 3°C	7775%	7321%	7129%	6005%	6394%	7072%

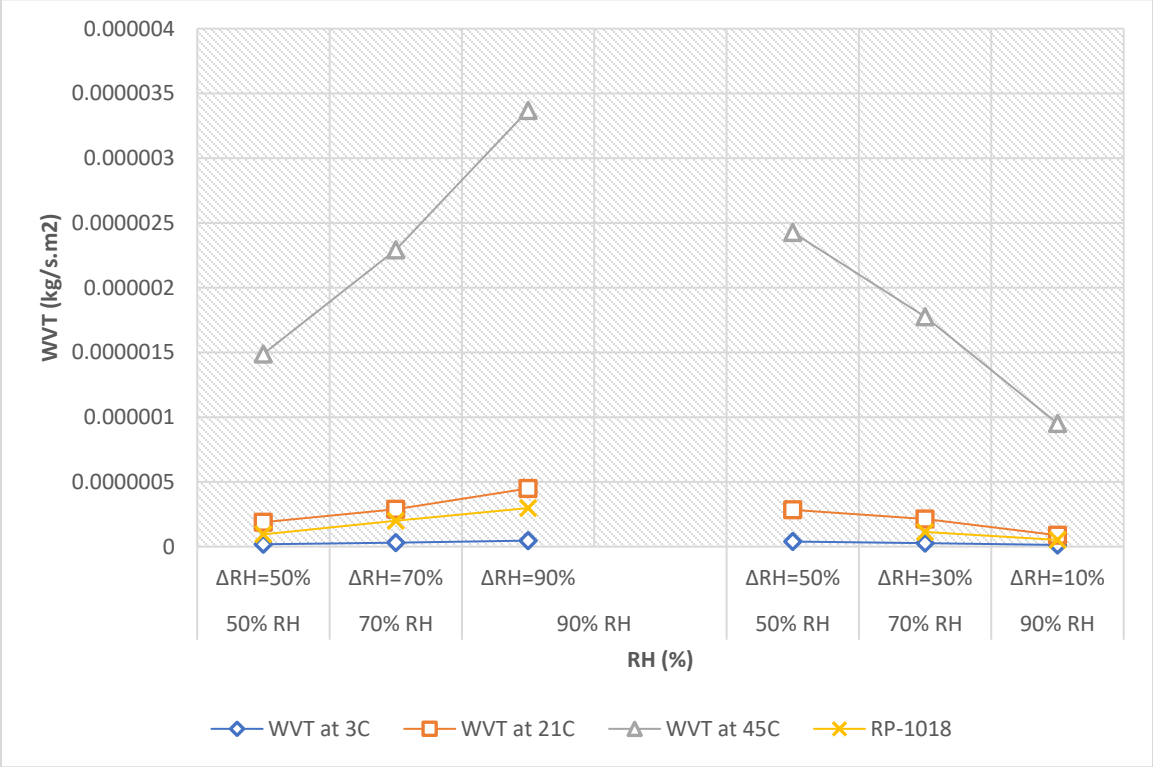

Figure 12-3. Stucco-Water Vapor Transmission Rate.

12.1.4 **Western Red Cedar**

Table 12-13. Western Red Cedar-Water Vapor Permeability at 3°C.

Western Red Cedar-Water Vapor Permeability at 3°C					
	Cup Method	**Sample No.**	**50% RH**	**70% RH**	**90% RH**
WVT (kg/s.m2)	Dry	1	5.613E-09	2.859E-08	6.417E-08
		2	8.171E-09	5.946E-08	1.016E-07
		3	5.405E-08	3.181E-08	8.927E-08
	Wet	4	1.519E-07	6.004E-08	7.717E-09
		5	1.352E-09	6.605E-08	1.148E-08
		6	5.777E-08	4.973E-08	6.410E-08
Permeance (kg/m2.s.Pa)	Dry	1	1.482E-11	5.388E-11	9.413E-11
		2	2.158E-11	1.120E-10	1.490E-10
		3	1.428E-10	5.994E-11	1.309E-10
	Wet	4	4.007E-10	2.628E-10	1.004E-10
		5	3.566E-12	2.891E-10	1.493E-10
		6	1.523E-10	2.177E-10	8.342E-10
Water Vapor Permeability (kg/m.s.Pa)	Dry	1	2.038E-13	7.408E-13	1.294E-12
		2	2.719E-13	1.412E-12	1.877E-12
		3	1.734E-12	7.282E-13	1.591E-12
	Wet	4	5.309E-12	3.482E-12	1.331E-12
		5	4.832E-14	3.917E-12	2.024E-12
		6	1.813E-12	2.590E-12	9.927E-12

Table 12-14. Western Red Cedar-Water Vapor Permeability at 21°C.

Western Red Cedar-Water Vapor Permeability at 21°C					
	Cup Method	**Sample No.**	**50% RH**	**70% RH**	**90% RH**
WVT (kg/s.m2)	Dry	1	6.388E-08	1.385E-07	2.257E-07
		2	1.896E-07	3.225E-07	6.653E-07
		3	5.561E-08	1.140E-07	3.233E-07
	Wet	4	1.638E-07	1.064E-07	7.792E-08
		5	3.789E-07	4.272E-07	3.263E-07
		6	5.951E-07	3.216E-07	1.406E-08
Permeance (kg/m2.s.Pa)	Dry	1	5.190E-11	7.956E-11	1.009E-10
		2	1.540E-10	1.852E-10	2.974E-10
		3	4.518E-11	6.548E-11	1.445E-10
	Wet	4	1.300E-10	1.428E-10	3.137E-10
		5	3.008E-10	5.737E-10	1.314E-09
		6	4.725E-10	4.319E-10	5.660E-11
Water Vapor Permeability (kg/m.s.Pa)	Dry	1	6.228E-13	9.547E-13	1.211E-12
		2	1.972E-12	2.371E-12	3.806E-12
		3	5.693E-13	8.250E-13	1.821E-12
	Wet	4	1.729E-12	1.900E-12	4.173E-12
		5	3.761E-12	7.172E-12	1.642E-11
		6	5.670E-12	5.183E-12	6.791E-13

Table 12-15. Western Red Cedar-Water Vapor Permeability at 45°C.

Western Red Cedar-Water Vapor Permeability at 45°C					
	Cup Method	**Sample No.**	**50% RH**	**70% RH**	**90% RH**
WVT (kg/s.m2)	Dry	1	5.975E-07	1.099E-06	1.508E-06
		2	5.143E-07	8.455E-07	2.962E-06
		3	7.709E-07	2.191E-06	2.616E-06
	Wet	4	2.270E-06	2.353E-06	1.180E-06
		5	1.268E-06	1.080E-06	7.999E-07
		6	2.241E-06	2.050E-06	8.003E-07
Permeance (kg/m2.s.Pa)	Dry	1	1.247E-10	1.640E-10	1.748E-10
		2	1.073E-10	1.262E-10	3.432E-10
		3	1.608E-10	3.270E-10	3.032E-10
	Wet	4	4.736E-10	8.150E-10	1.232E-09
		5	2.646E-10	3.740E-10	8.350E-10
		6	4.675E-10	7.102E-10	8.353E-10
Water Vapor Permeability (kg/m.s.Pa)	Dry	1	1.533E-12	2.017E-12	2.150E-12
		2	1.341E-12	1.578E-12	4.290E-12
		3	1.970E-12	4.006E-12	3.714E-12
	Wet	4	5.801E-12	9.983E-12	1.509E-11
		5	3.175E-12	4.488E-12	1.002E-11
		6	5.681E-12	8.629E-12	1.015E-11

Table 12-16. Western Red Cedar-Water Vapor Transmission Rate.

Western Red Cedar-Water Vapor Transmission Rate (kg/s.m^2)						
	ΔRH:50%	**ΔRH:70%**	**ΔRH:90%**	**ΔRH:50%**	**ΔRH:30%**	**ΔRH:10%**
	Dry Cups			**Wet Cups**		
	50% RH	70% RH	90% RH	50% RH	70% RH	90% RH
WVT at 3°C	2.26E-08	4E-08	8.5E-08	7.03E-08	5.86E-08	2.78E-08
WVT at 21°C	1.03E-07	1.92E-07	4.05E-07	3.79E-07	2.85E-07	1.39E-07
WVT at 45°C	6.27E-07	1.38E-06	2.36E-06	1.92E-06	1.83E-06	9.27E-07
Difference between 21°C and 3°C	356%	380%	376%	439%	386%	402%
Difference between 45°C and 21°C	509%	619%	484%	408%	541%	565%
Difference between 45°C and 3°C	2675%	3350%	2679%	2638%	3018%	3238%

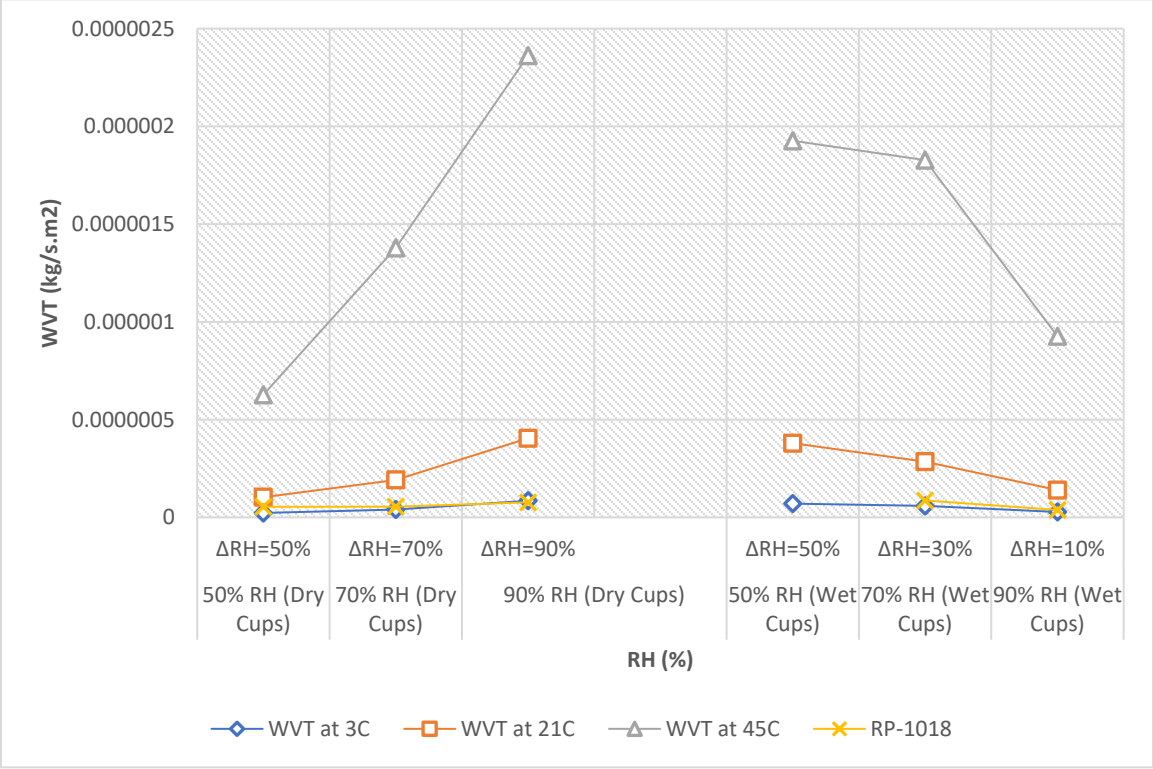

Figure 12-4. Western Red Cedar-Water Vapor Transmission Rate.

12.1.5 **Tyvek**

Table 12-17. Tyvek-Water Vapor Permeability at 3°C.

Tyvek-Water Vapor Permeability at 3°C					
	Cup Method	**Sample No.**	**50% RH**	**70% RH**	**90% RH**
WVT (kg/s.m2)	Dry	1	1.033E-06	1.677E-06	1.397E-06
		2	1.357E-06	1.912E-06	3.403E-06
		3	1.235E-06	1.693E-06	2.211E-06
	Wet	4	8.878E-07	1.588E-06	1.657E-07
		5	1.629E-06	1.669E-07	2.252E-07
		6	1.522E-06	7.270E-07	3.760E-07
Permeance (kg/m2.s.Pa)	Dry	1	2.727E-09	3.170E-09	2.023E-09
		2	3.585E-09	3.616E-09	4.928E-09
		3	3.262E-09	3.202E-09	3.201E-09
	Wet	4	2.347E-09	6.979E-09	2.398E-09
		5	4.307E-09	7.336E-10	3.259E-09
		6	4.023E-09	3.195E-09	5.442E-09
Water Vapor Permeability (kg/m.s.Pa)	Dry	1	4.091E-13	4.756E-13	3.034E-13
		2	5.378E-13	5.424E-13	7.392E-13
		3	4.892E-13	4.803E-13	4.802E-13
	Wet	4	3.521E-13	1.047E-12	3.597E-13
		5	6.461E-13	1.100E-13	4.888E-13
		6	6.034E-13	4.792E-13	8.163E-13

Table 12-18. Tyvek-Water Vapor Permeability at 21°C.

Tyvek-Water Vapor Permeability at 21°C					
	Cup Method	**Sample No.**	**50% RH**	**70% RH**	**90% RH**
WVT (kg/s.m2)	Dry	1	4.877E-06	8.173E-06	1.247E-05
		2	4.320E-06	5.074E-06	8.510E-06
		3	3.644E-06	5.780E-06	5.098E-06
	Wet	4	4.294E-06	3.999E-06	1.263E-06
		5	2.548E-06	1.201E-06	7.265E-07
		6	7.862E-06	4.570E-06	1.429E-06
Permeance (kg/m2.s.Pa)	Dry	1	3.872E-09	4.746E-09	5.578E-09
		2	3.429E-09	2.946E-09	3.808E-09
		3	2.893E-09	3.357E-09	2.281E-09
	Wet	4	3.501E-09	5.290E-09	5.082E-09
		5	2.077E-09	1.588E-09	2.924E-09
		6	6.409E-09	6.046E-09	5.753E-09
Water Vapor Permeability (kg/m.s.Pa)	Dry	1	5.807E-13	7.119E-13	8.367E-13
		2	5.144E-13	4.420E-13	5.711E-13
		3	4.339E-13	5.035E-13	3.421E-13
	Wet	4	5.251E-13	7.935E-13	7.623E-13
		5	3.116E-13	2.382E-13	4.386E-13
		6	9.614E-13	9.068E-13	8.630E-13

Table 12-19. Tyvek-Water Vapor Permeability at 45°C.

Tyvek-Water Vapor Permeability at 45°C					
	Cup Method	**Sample No.**	**50% RH**	**70% RH**	**90% RH**
WVT (kg/s.m2)	Dry	1	2.379E-05	4.382E-05	3.840E-05
		2	1.402E-05	1.826E-05	3.612E-05
		3	1.348E-05	1.722E-05	3.444E-05
	Wet	4	1.844E-05	1.578E-05	3.784E-06
		5	1.797E-05	1.208E-05	4.755E-06
		6	2.798E-05	1.432E-05	6.149E-06
Permeance (kg/m2.s.Pa)	Dry	1	4.968E-09	6.506E-09	4.454E-09
		2	2.927E-09	2.711E-09	4.189E-09
		3	2.815E-09	2.557E-09	3.994E-09
	Wet	4	3.847E-09	5.534E-09	3.931E-09
		5	3.748E-09	4.239E-09	4.940E-09
		6	5.836E-09	5.023E-09	6.389E-09
Water Vapor Permeability (kg/m.s.Pa)	Dry	1	7.452E-13	9.760E-13	6.681E-13
		2	4.391E-13	4.066E-13	6.284E-13
		3	4.223E-13	3.836E-13	5.991E-13
	Wet	4	5.770E-13	8.301E-13	5.896E-13
		5	5.622E-13	6.358E-13	7.410E-13
		6	8.754E-13	7.534E-13	9.583E-13

Table 12-20. Tyvek-Water Vapor Transmission Rate.

Tyvek-Water Vapor Transmission Rate (kg/s.m^2)						
	ΔRH:50%	**ΔRH:70%**	**ΔRH:90%**	**ΔRH:50%**	**ΔRH:30%**	**ΔRH:10%**
	Dry Cups			**Wet Cups**		
	50% RH	70% RH	90% RH	50% RH	70% RH	90% RH
WVT at 3°C	1.20E-06	1.76E-06	2.34E-06	1.34E-06	8.27E-07	2.56E-07
WVT at 21°C	4.28E-06	6.34E-06	8.69E-06	4.90E-06	3.26E-06	1.14E-06
WVT at 45°C	1.71E-05	2.64E-05	3.63E-05	2.14E-05	1.41E-05	4.9E-06
Difference between 21°C and 3°C	254%	260%	272%	264%	294%	346%
Difference between 45°C and 21°C	299%	317%	318%	338%	332%	330%
Difference between 45°C and 3°C	1315%	1401%	1454%	1494%	1599%	1815%

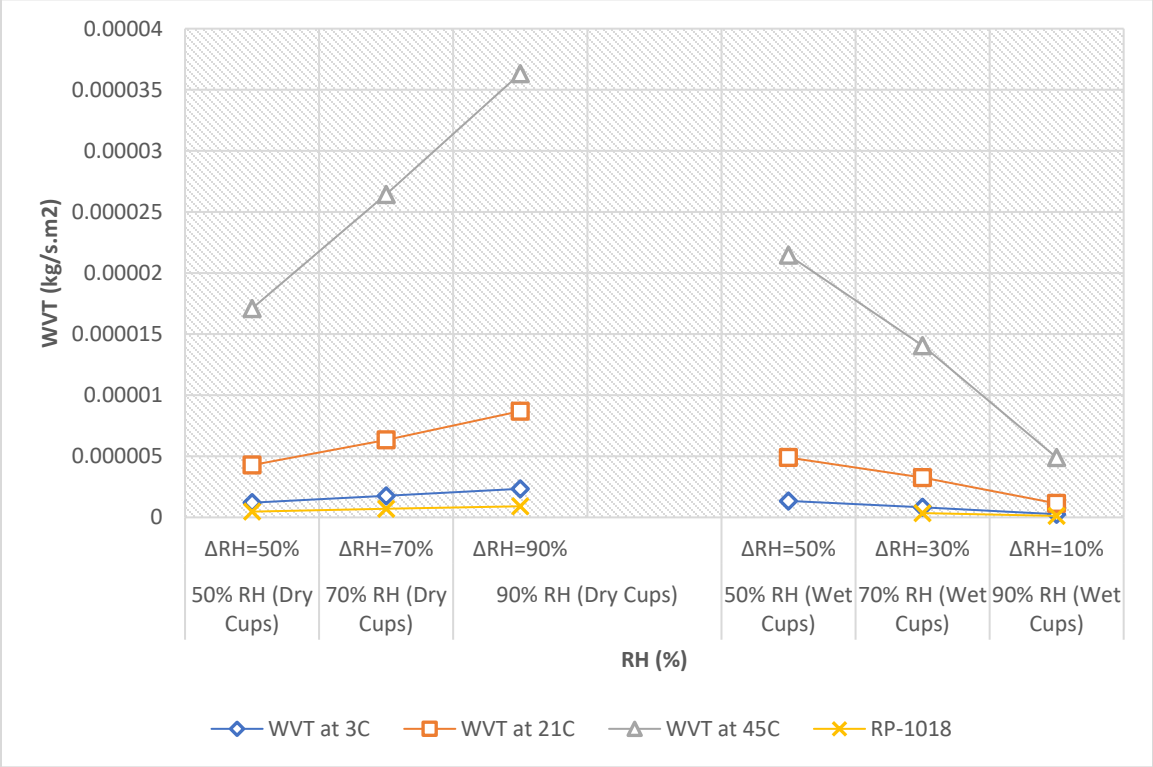

Figure 12-5. Tyvek-Water Vapor Transmission Rate.

12.1.6 **60 Min Building Paper**

Table 12-21. Building Paper 60min. -Water Vapor Permeability at 3°C.

Building Paper 60min. -Water Vapor Permeability at 3°C					
	Cup Method	**Sample No.**	**50% RH**	**70% RH**	**90% RH**
WVT (kg/s.m2)	Dry	1	1.688E-07	2.549E-07	3.825E-07
		2	1.457E-07	2.182E-07	3.392E-07
		3	2.279E-07	3.342E-07	4.830E-07
	Wet	4	3.955E-07	5.309E-07	1.346E-07
		5	2.854E-07	1.962E-07	1.048E-07
		6	2.511E-07	2.051E-07	1.680E-07
Permeance (kg/m2.s.Pa)	Dry	1	4.453E-10	4.808E-10	5.570E-10
		2	3.843E-10	4.115E-10	4.939E-10
		3	6.011E-10	6.302E-10	7.033E-10
	Wet	4	1.040E-09	2.330E-09	1.815E-09
		5	7.504E-10	8.611E-10	1.413E-09
		6	6.602E-10	9.002E-10	2.265E-09
Water Vapor Permeability (kg/m.s.Pa)	Dry	1	1.514E-13	1.635E-13	1.894E-13
		2	1.306E-13	1.399E-13	1.679E-13
		3	2.044E-13	2.143E-13	2.391E-13
	Wet	4	3.535E-13	7.922E-13	6.172E-13
		5	2.551E-13	2.928E-13	4.804E-13
		6	2.245E-13	3.061E-13	7.701E-13

Table 12-22. Building Paper 60min. -Water Vapor Permeability at 21°C.

Building Paper 60min. -Water Vapor Permeability at 21°C					
	Cup Method	**Sample No.**	**50% RH**	**70% RH**	**90% RH**
WVT (kg/s.m2)	Dry	1	5.965E-07	9.028E-07	2.768E-06
		2	5.261E-07	8.090E-07	1.309E-06
		3	8.186E-07	1.221E-06	1.824E-06
	Wet	4	3.282E-06	1.310E-06	9.157E-07
		5	3.347E-06	3.373E-06	9.442E-07
		6	5.840E-07	1.340E-06	6.496E-07
Permeance (kg/m2.s.Pa)	Dry	1	4.810E-10	5.184E-10	1.237E-09
		2	4.242E-10	4.645E-10	5.853E-10
		3	6.601E-10	7.014E-10	8.155E-10
	Wet	4	2.645E-09	1.760E-09	3.692E-09
		5	2.697E-09	4.530E-09	3.807E-09
		6	4.706E-10	1.800E-09	2.619E-09
Water Vapor Permeability (kg/m.s.Pa)	Dry	1	1.635E-13	1.763E-13	4.207E-13
		2	1.442E-13	1.579E-13	1.990E-13
		3	2.244E-13	2.385E-13	2.773E-13
	Wet	4	8.992E-13	5.985E-13	1.255E-12
		5	9.170E-13	1.540E-12	1.295E-12
		6	1.600E-13	6.119E-13	8.906E-13

Table 12-23. Building Paper 60min. -Water Vapor Permeability at 45°C.

Building Paper 60min. -Water Vapor Permeability at 45°C					
	Cup Method	**Sample No.**	**50% RH**	**70% RH**	**90% RH**
WVT (kg/s.m2)	Dry	1	5.441E-06	7.587E-06	9.932E-06
		2	3.631E-06	6.988E-06	1.207E-05
		3	2.846E-06	9.186E-06	1.183E-05
	Wet	4	1.042E-05	1.152E-05	3.514E-06
		5	1.187E-05	9.175E-06	3.226E-06
		6	1.056E-05	9.777E-06	6.512E-06
Permeance (kg/m2.s.Pa)	Dry	1	1.135E-09	1.128E-09	1.150E-09
		2	7.574E-10	1.039E-09	1.397E-09
		3	5.937E-10	1.365E-09	1.369E-09
	Wet	4	2.175E-09	4.032E-09	3.685E-09
		5	2.477E-09	3.211E-09	3.383E-09
		6	2.204E-09	3.421E-09	6.829E-09
Water Vapor Permeability (kg/m.s.Pa)	Dry	1	3.859E-13	3.835E-13	3.909E-13
		2	2.575E-13	3.532E-13	4.749E-13
		3	2.019E-13	4.642E-13	4.655E-13
	Wet	4	7.395E-13	1.371E-12	1.253E-12
		5	8.423E-13	1.092E-12	1.150E-12
		6	7.493E-13	1.163E-12	2.322E-12

Table 12-24. Building Paper 60 min-Water Vapor Transmission Rate.

Building Paper 60 min-Water Vapor Transmission Rate (kg/s.m^2)						
	ΔRH:50%	**ΔRH:70%**	**ΔRH:90%**	**ΔRH:50%**	**ΔRH:30%**	**ΔRH:10%**
	Dry Cups			**Wet Cups**		
	50% RH	70% RH	90% RH	50% RH	70% RH	90% RH
WVT at 3°C	1.80E-07	2.69E-07	4.02E-07	3.10E-07	3.11E-07	1.36E-07
WVT at 21°C	6.47E-07	9.78E-07	1.97E-06	2.40E-06	2.01E-06	8.37E-07
WVT at 45°C	3.97E-06	7.92E-06	1.13E-05	1.09E-05	1.02E-05	4.42E-06
Difference between 21°C and 3°C	258%	263%	390%	674%	546%	516%
Difference between 45°C and 21°C	514%	710%	473%	355%	406%	428%
Difference between 45°C and 3°C	2097%	2843%	2708%	3425%	3169%	3153%

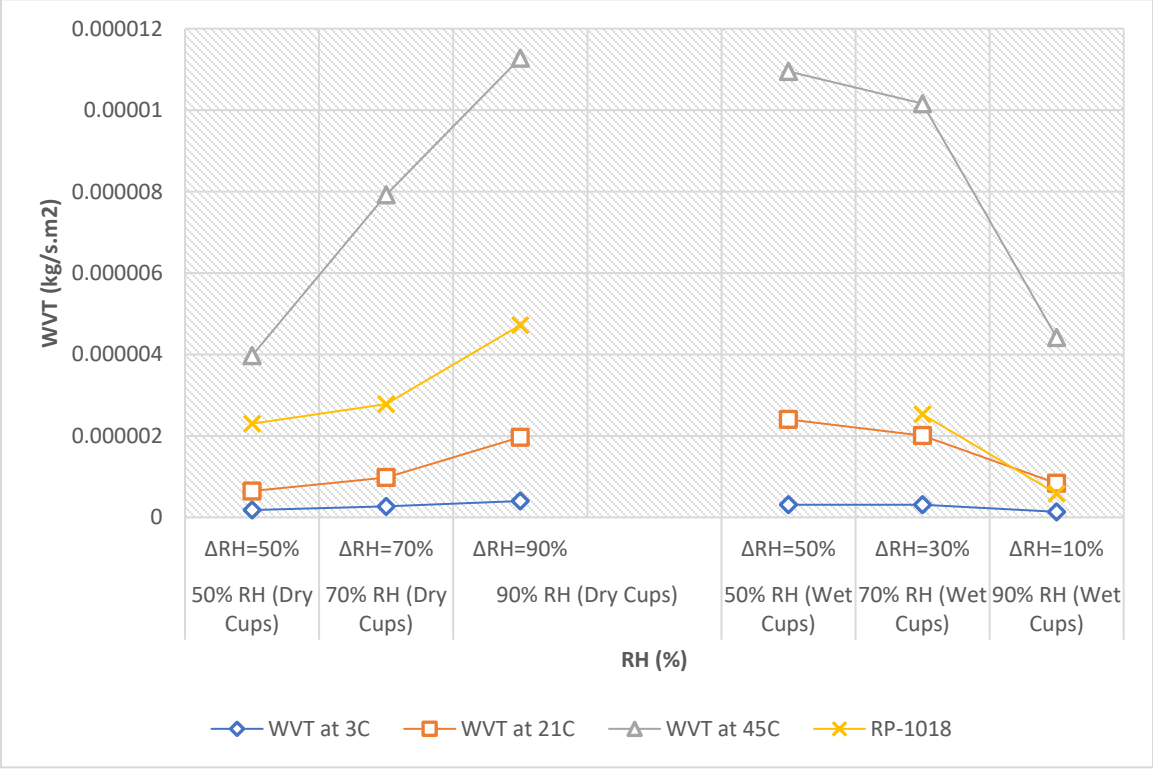

Figure 12-6. Building Paper 60 min-Water Vapor Transmission Rate.

12.1.7 **Oriented Strand Board (OSB)**

Table 12-25. OSB-Water Vapor Permeability at 3°C.

OSB-Water Vapor Permeability at 3°C					
	Cup Method	**No. of Samples**	**50% RH**	**70% RH**	**90% RH**
WVT (kg/s.m2)	Dry	3	2.411E-08	4.0214E-08	4.99425E-08
	Wet	3	5.629E-08	4.5333E-08	1.83894E-08
Permeance (kg/m2.s.Pa)	Dry	3	6.453E-11	7.56728E-11	7.31444E-11
	Wet	3	1.463E-10	2.00132E-10	2.43175E-10
Water Vapor Permeability (kg/m.s.Pa)	Dry	3	7.329E-13	8.59427E-13	8.30711E-13
	Wet	3	1.662E-12	2.27292E-12	2.76178E-12

Table 12-26. OSB-Water Vapor Permeability at 21°C.

OSB-Water Vapor Permeability at 21°C					
	Cup Method	**No. of Samples**	**50% RH**	**70% RH**	**90% RH**
WVT (kg/s.m2)	Dry	3	8.201E-08	1.38201E-07	2.83077E-07
	Wet	3	2.774E-07	2.68841E-07	1.2322E-07
Permeance (kg/m2.s.Pa)	Dry	3	6.602E-11	7.9488E-11	1.26487E-10
	Wet	3	2.233E-10	3.59489E-10	4.95732E-10
Water Vapor Permeability (kg/m.s.Pa)	Dry	3	7.454E-13	8.97533E-13	1.42822E-12
	Wet	3	2.521E-12	4.05914E-12	5.59753E-12

Table 12-27. OSB-Water Vapor Permeability at 45°C.

OSB-Water Vapor Permeability at 45°C					
	Cup Method	**No. of Samples**	**50% RH**	**70% RH**	**90% RH**
WVT (kg/s.m2)	Dry	3	4.289E-07	7.43004E-07	1.27054E-06
	Wet	3	1.280E-06	1.10532E-06	5.94089E-07
Permeance (kg/m2.s.Pa)	Dry	3	8.950E-11	1.1106E-10	1.47258E-10
	Wet	3	2.671E-10	3.81686E-10	6.19938E-10
Water Vapor Permeability (kg/m.s.Pa)	Dry	3	1.015E-12	1.25942E-12	1.66991E-12
	Wet	3	3.029E-12	4.32832E-12	7.03009E-12

Table 12-28. OSB-Water Vapor Transmission Rate.

OSB-Water Vapor Transmission Rate (kg/s.m^2)						
	ΔRH:50%	**ΔRH:70%**	**ΔRH:90%**	**ΔRH:50%**	**ΔRH:30%**	**ΔRH:10%**
	Dry Cups			**Wet Cups**		
	50% RH	70% RH	90% RH	50% RH	70% RH	90% RH
WVT at 3°C	2.41E-08	4.02E-08	4.99E-08	5.62E-08	4.53E-08	1.84E-08
WVT at 21°C	8.20E-08	1.38E-07	2.83E-07	2.77E-07	2.69E-07	1.23E-07
WVT at 45°C	4.28E-07	7.43E-07	1.27E-06	1.28E-06	1.11E-06	5.94E-07
Difference between 21°C and 3°C	240%	244%	467%	393%	493%	570%
Difference between 45°C and 21°C	423%	438%	349%	362%	311%	382%
Difference between 45°C and 3°C	1679%	1748%	2444%	2174%	2338%	3131%

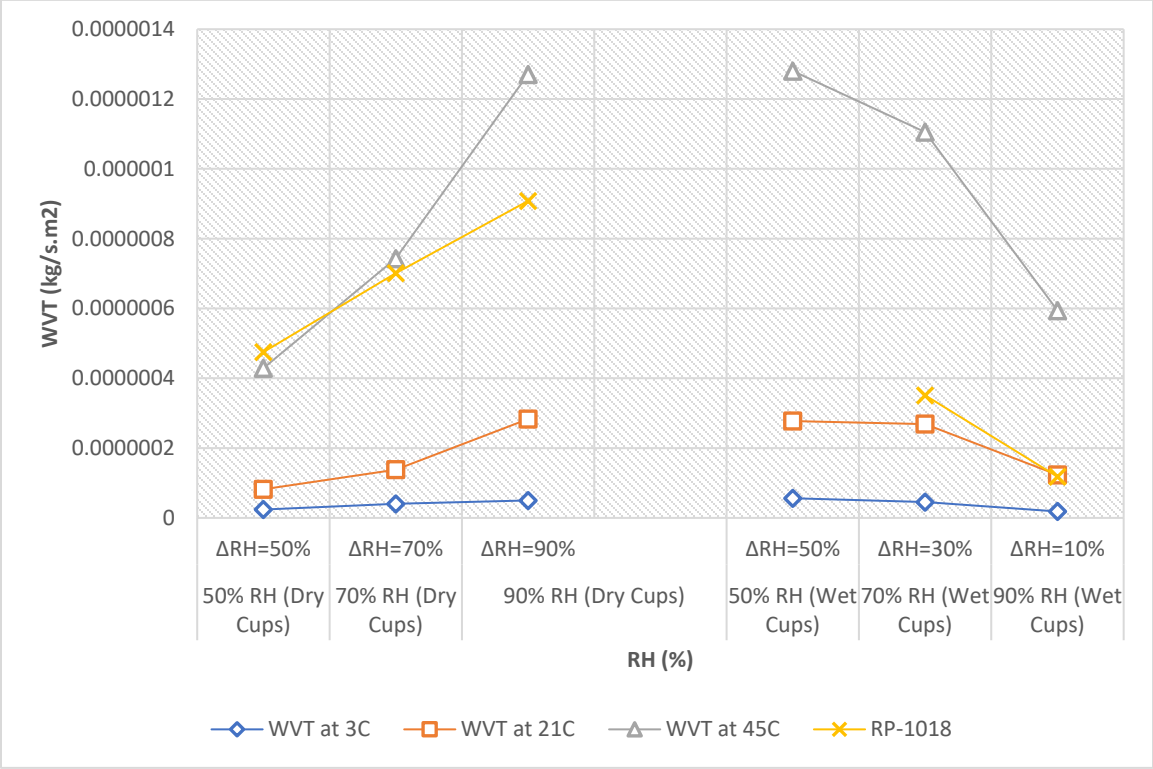

Figure 12-7. OSB-Water Vapor Transmission Rate.

12.1.8 **Plywood**

Table 12-29. Plywood-Water Vapor Permeability at 3°C.

Plywood-Water Vapor Permeability at 3°C					
	Cup Method	**No. of Samples**	**50% RH**	**70% RH**	**90% RH**
WVT (kg/s.m2)	Dry	3	1.777E-08	3.23919E-08	6.95704E-08
	Wet	3	8.994E-08	8.13023E-08	3.13828E-08
Permeance (kg/m2.s.Pa)	Dry	3	4.758E-11	6.09472E-11	1.019E-10
	Wet	3	2.337E-10	3.5922E-10	4.14876E-10
Water Vapor Permeability (kg/m.s.Pa)	Dry	3	5.898E-13	7.55397E-13	1.26297E-12
	Wet	3	2.897E-12	4.45227E-12	5.14209E-12

Table 12-30. Plywood-Water Vapor Permeability at 21°C.

Plywood-Water Vapor Permeability at 21°C					
	Cup Method	**No. of Samples**	**50% RH**	**70% RH**	**90% RH**
WVT (kg/s.m2)	Dry	3	6.587E-08	1.15232E-07	2.83738E-07
	Wet	3	4.839E-07	4.13371E-07	1.81691E-07
Permeance (kg/m2.s.Pa)	Dry	3	5.389E-11	6.62773E-11	1.26779E-10
	Wet	3	3.832E-10	5.52753E-10	7.30994E-10
Water Vapor Permeability (kg/m.s.Pa)	Dry	3	6.681E-13	8.2165E-13	1.5717E-12
	Wet	3	4.750E-12	6.85255E-12	9.06224E-12

Table 12-31. Plywood-Water Vapor Permeability at 45°C.

Plywood-Water Vapor Permeability at 45°C					
	Cup Method	**No. of Samples**	**50% RH**	**70% RH**	**90% RH**
WVT (kg/s.m2)	Dry	3	3.017E-07	5.48639E-07	1.28518E-06
	Wet	3	2.406E-06	2.22902E-06	9.121E-07
Permeance (kg/m2.s.Pa)	Dry	3	6.294E-11	8.19378E-11	1.48967E-10
	Wet	3	5.019E-10	7.71201E-10	9.5112E-10
Water Vapor Permeability (kg/m.s.Pa)	Dry	3	7.803E-13	1.01579E-12	1.84677E-12
	Wet	3	6.222E-12	9.56069E-12	1.17912E-11

Table 12-32. Plywood-Water Vapor Transmission Rate.

Plywood-Water Vapor Transmission Rate (kg/s.m^2)						
	ΔRH:50%	**ΔRH:70%**	**ΔRH:90%**	**ΔRH:50%**	**ΔRH:30%**	**ΔRH:10%**
	Dry Cups			**Wet Cups**		
	50% RH	70% RH	90% RH	50% RH	70% RH	90% RH
WVT at 3°C	1.77E-08	3.24E-08	6.96E-08	8.99E-08	8.13E-08	3.14E-08
WVT at 21°C	6.58E-08	1.15E-07	2.84E-07	4.83E-07	4.13E-07	1.82E-07
WVT at 45°C	3.01E-07	5.49E-07	1.29E-06	2.46E-06	2.23E-06	9.12E-07
Difference between 21°C and 3°C	271%	256%	308%	438%	408%	479%
Difference between 45°C and 21°C	358%	376%	353%	397%	439%	402%
Difference between 45°C and 3°C	1598%	1594%	1747%	2575%	2642%	2806%

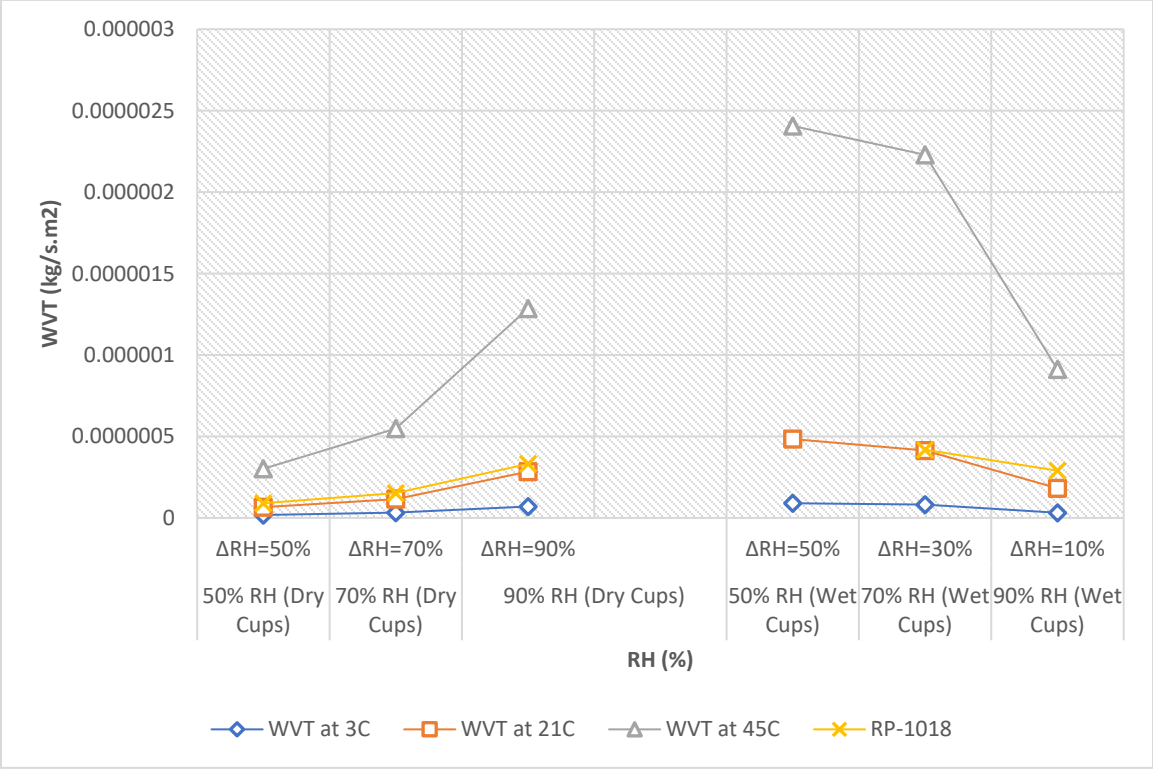

Figure 12-8. Plywood-Water Vapor Transmission Rate.

12.1.9 **Densglass Gold Gypsum Sheathing Board**

Table 12-33. Densglass Gold Gypsum Sheathing Board -Water Vapor Permeability at 3°C.

Densglass Gold Gypsum Sheathing Board -Water Vapor Permeability at 3°C					
	Cup Method	**No. of Samples**	**50% RH**	**70% RH**	**90% RH**
WVT (kg/s.m2)	Dry	3	9.401E-07	1.41979E-06	1.94629E-06
	Wet	3	1.128E-06	6.82249E-07	2.62471E-07
Permeance (kg/m2.s.Pa)	Dry	3	2.476E-09	2.6842E-09	2.84439E-09
	Wet	3	2.980E-09	2.98369E-09	3.47454E-09
Water Vapor Permeability (kg/m.s.Pa)	Dry	3	3.274E-11	3.54928E-11	3.7611E-11
	Wet	3	3.941E-11	3.94529E-11	4.59434E-11

Table 12-34. Densglass Gold Gypsum Sheathing Board -Water Vapor Permeability at 21°C.

Densglass Gold Gypsum Sheathing Board -Water Vapor Permeability at 21°C					
	Cup Method	**No. of Samples**	**50% RH**	**70% RH**	**90% RH**
WVT (kg/s.m2)	Dry	3	2.979E-06	4.68358E-06	6.43234E-06
	Wet	3	4.614E-06	2.90455E-06	1.21086E-06
Permeance (kg/m2.s.Pa)	Dry	3	2.495E-09	2.68069E-09	2.86881E-09
	Wet	3	3.564E-09	3.92029E-09	4.88117E-09
Water Vapor Permeability (kg/m.s.Pa)	Dry	3	3.310E-11	3.55651E-11	3.8061E-11
	Wet	3	4.729E-11	5.20111E-11	6.47592E-11

Table 12-35. Densglass Gold Gypsum Sheathing Board -Water Vapor Permeability at 45°C.

Densglass Gold Gypsum Sheathing Board -Water Vapor Permeability at 45°C					
	Cup Method	**No. of Samples**	**50% RH**	**70% RH**	**90% RH**
WVT (kg/s.m2)	Dry	3	1.299E-05	1.93957E-05	2.57563E-05
	Wet	3	2.013E-05	1.35122E-05	6.33285E-06
Permeance (kg/m2.s.Pa)	Dry	3	2.738E-09	2.89322E-09	2.98424E-09
	Wet	3	4.155E-09	4.68919E-09	6.62064E-09
Water Vapor Permeability (kg/m.s.Pa)	Dry	3	3.633E-11	3.83848E-11	3.95923E-11
	Wet	3	5.512E-11	6.22121E-11	8.7837E-11

Table 12-36. Densglass Gold Gypsum Sheathing-Water Vapor Transmission Rate.

Densglass Gold Gypsum Sheathing-Water Vapor Transmission Rate (kg/s.m²)						
	ΔRH:50%	ΔRH:70%	ΔRH:90%	ΔRH:50%	ΔRH:30%	ΔRH:10%
	Dry Cups			Wet Cups		
	50% RH	70% RH	90% RH	50% RH	70% RH	90% RH
WVT at 3°C	9.40E-07	1.42E-06	1.95E-06	1.13E-06	6.82E-07	2.62E-07
WVT at 21°C	2.98E-06	4.68E-06	6.43E-06	4.61E-06	2.90E-06	1.21E-06
WVT at 45°C	1.30E-05	1.94E-05	2.58E-05	2.01E-05	1.35E-05	6.33E-06
Difference between 21°C and 3°C	217%	230%	230%	309%	326%	361%
Difference between 45°C and 21°C	336%	314%	300%	336%	365%	423%
Difference between 45°C and 3°C	1282%	1266%	1223%	1684%	1881%	2313%

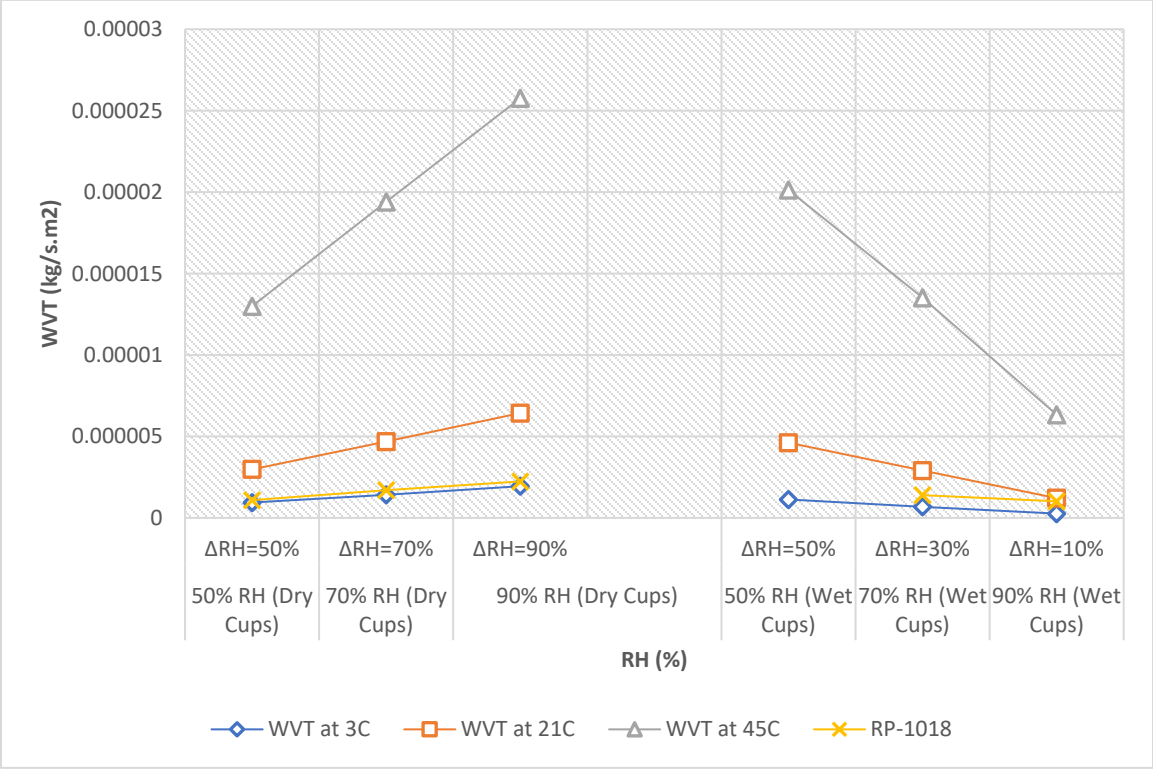

Figure 12-9. Densglass Gold Gypsum Sheathing-Water Vapor Transmission Rate.

12.1.10 **Spruce**

Table 12-37. Spruce-Water Vapor Permeability at 3°C.

Spruce-Water Vapor Permeability at 3°C					
	Cup Method	**Sample No.**	**50% RH**	**70% RH**	**90% RH**
WVT (kg/s.m2)	Dry	1	1.141E-08	3.071E-08	1.125E-07
		2	1.803E-08	2.271E-08	1.203E-07
		3	1.206E-08	2.165E-08	1.074E-07
	Wet	4	3.314E-08	1.232E-07	1.007E-07
		5	3.599E-07	1.438E-07	9.584E-08
		6	9.677E-08	8.439E-08	7.421E-08
Permeance (kg/m2.s.Pa)	Dry	1	3.006E-11	5.777E-11	1.650E-10
		2	4.752E-11	4.274E-11	1.764E-10
		3	3.178E-11	4.073E-11	1.574E-10
	Wet	4	8.770E-11	5.389E-10	1.288E-09
		5	9.524E-10	6.292E-10	1.226E-09
		6	2.561E-10	3.692E-10	9.491E-10
Water Vapor Permeability (kg/m.s.Pa)	Dry	1	3.698E-13	7.106E-13	2.029E-12
		2	5.750E-13	5.171E-13	2.135E-12
		3	3.909E-13	5.010E-13	1.936E-12
	Wet	4	1.048E-12	6.440E-12	1.539E-11
		5	1.186E-11	7.834E-12	1.526E-11
		6	3.098E-12	4.467E-12	1.148E-11

Table 12-38. Spruce-Water Vapor Permeability at 21°C.

Spruce-Water Vapor Permeability at 21°C					
	Cup Method	**Sample No.**	**50% RH**	**70% RH**	**90% RH**
WVT (kg/s.m2)	Dry	1	5.421E-08	1.412E-07	4.052E-07
		2	8.305E-08	2.076E-07	6.417E-07
		3	4.789E-08	1.451E-07	4.386E-07
	Wet	4	1.118E-06	1.019E-06	7.152E-07
		5	8.461E-07	7.807E-07	4.726E-07
		6	1.239E-06	1.121E-06	8.228E-07
Permeance (kg/m2.s.Pa)	Dry	1	4.380E-11	8.101E-11	1.808E-10
		2	6.710E-11	1.191E-10	2.864E-10
		3	3.870E-11	8.324E-11	1.958E-10
	Wet	4	8.965E-10	1.368E-09	2.880E-09
		5	6.782E-10	1.048E-09	1.903E-09
		6	9.933E-10	1.505E-09	3.313E-09
Water Vapor Permeability (kg/m.s.Pa)	Dry	1	5.387E-13	9.965E-13	2.224E-12
		2	8.086E-13	1.435E-12	3.452E-12
		3	5.205E-13	1.120E-12	2.633E-12
	Wet	4	1.080E-11	1.648E-11	3.471E-11
		5	9.019E-12	1.394E-11	2.531E-11
		6	1.237E-11	1.874E-11	4.125E-11

Table 12-39. Spruce-Water Vapor Permeability at 45°C.

Spruce-Water Vapor Permeability at 45°C					
	Cup Method	**Sample No.**	**50% RH**	**70% RH**	**90% RH**
WVT (kg/s.m2)	Dry	1	3.250E-07	7.284E-07	2.109E-06
		2	2.872E-07	6.584E-07	2.227E-06
		3	3.432E-07	7.904E-07	2.165E-06
	Wet	4	4.981E-06	7.566E-06	4.449E-06
		5	6.318E-06	6.140E-06	4.760E-06
		6	6.924E-06	4.392E-06	4.003E-06
Permeance (kg/m2.s.Pa)	Dry	1	6.781E-11	1.085E-10	2.443E-10
		2	5.992E-11	9.809E-11	2.580E-10
		3	7.160E-11	1.178E-10	2.509E-10
	Wet	4	1.039E-09	2.632E-09	4.643E-09
		5	1.318E-09	2.136E-09	4.967E-09
		6	1.445E-09	1.528E-09	4.178E-09
Water Vapor Permeability (kg/m.s.Pa)	Dry	1	8.138E-13	1.302E-12	2.932E-12
		2	7.040E-13	1.153E-12	3.031E-12
		3	8.950E-13	1.472E-12	3.136E-12
	Wet	4	1.237E-11	3.133E-11	5.525E-11
		5	1.615E-11	2.617E-11	6.085E-11
		6	1.849E-11	1.956E-11	5.347E-11

Table 12-40. Spruce-Water Vapor Transmission Rate.

Spruce-Water Vapor Transmission Rate (kg/s.m^2)						
	ΔRH:50%	**ΔRH:70%**	**ΔRH:90%**	**ΔRH:50%**	**ΔRH:30%**	**ΔRH:10%**
	Dry Cups			**Wet Cups**		
	50% RH	70% RH	90% RH	50% RH	70% RH	90% RH
WVT at 3°C	1.38E-08	2.50E-08	1.13E-07	1.63E-07	1.17E-07	9.03E-08
WVT at 21°C	6.17E-08	1.65E-07	4.95E-07	1.07E-06	9.74E-07	6.70E-07
WVT at 45°C	3.18E-07	7.26E-07	2.17E-06	6.07E-06	6.03E-06	4.40E-06
Difference between 21°C and 3°C	346%	558%	337%	554%	731%	643%
Difference between 45°C and 21°C	416%	341%	338%	469%	520%	557%
Difference between 45°C and 3°C	2203%	2800%	1811%	3620%	5050%	4779%

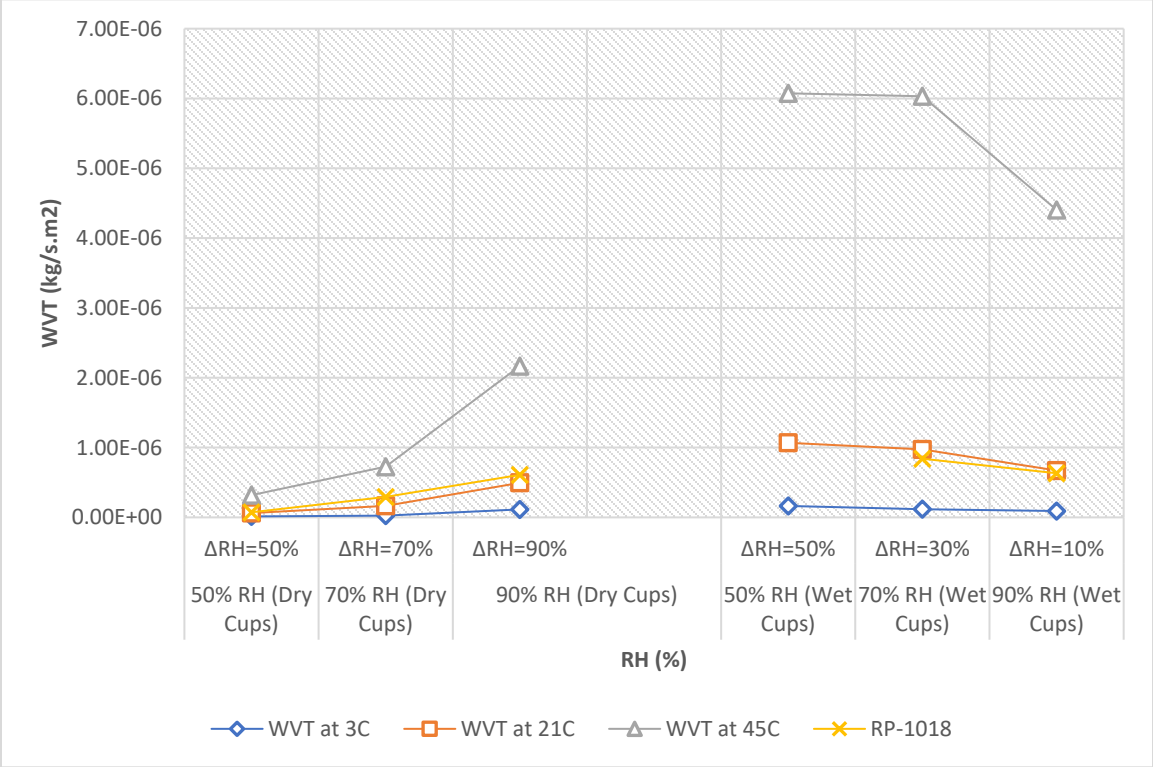

Figure 12-10. Spruce-Water Vapor Transmission Rate.

12.1.11 **Douglas Fir**

Table 12-41. Douglas Fir-Water Vapor Permeability at 3°C.

Douglas Fir-Water Vapor Permeability at 3°C					
	Cup Method	**Sample No.**	**50% RH**	**70% RH**	**90% RH**
WVT (kg/s.m2)	Dry	1	9.762E-09	2.405E-08	9.723E-08
		2	9.180E-09	2.713E-08	1.058E-07
		3	7.651E-09	1.179E-08	6.198E-08
	Wet	4	1.064E-07	2.196E-07	6.291E-08
		5	9.592E-08	9.963E-08	6.217E-08
		6	8.514E-08	5.043E-08	4.756E-08
Permeance (kg/m2.s.Pa)	Dry	1	2.572E-11	4.532E-11	1.429E-10
		2	2.419E-11	5.113E-11	1.555E-10
		3	2.016E-11	2.223E-11	9.109E-11
	Wet	4	2.823E-10	9.590E-10	7.902E-10
		5	2.545E-10	4.351E-10	7.809E-10
		6	2.259E-10	2.203E-10	5.973E-10
Water Vapor Permeability (kg/m.s.Pa)	Dry	1	3.138E-13	5.529E-13	1.743E-12
		2	2.975E-13	6.289E-13	1.912E-12
		3	2.480E-13	2.734E-13	1.120E-12
	Wet	4	3.557E-12	1.208E-11	9.957E-12
		5	3.155E-12	5.395E-12	9.683E-12
		6	2.823E-12	2.753E-12	7.467E-12

Table 12-42. Douglas Fir-Water Vapor Permeability at 21°C.

Douglas Fir-Water Vapor Permeability at 21°C					
	Cup Method	**Sample No.**	**50% RH**	**70% RH**	**90% RH**
WVT (kg/s.m2)	Dry	1	3.568E-08	1.102E-07	3.467E-07
		2	3.647E-08	1.114E-07	3.324E-07
		3	5.172E-08	1.417E-07	4.606E-07
	Wet	4	6.706E-07	7.902E-07	3.327E-07
		5	4.212E-07	2.121E-07	1.286E-07
		6	1.953E-07	2.107E-07	2.213E-07
Permeance (kg/m2.s.Pa)	Dry	1	2.859E-11	6.329E-11	1.547E-10
		2	2.922E-11	6.399E-11	1.483E-10
		3	4.143E-11	8.136E-11	2.055E-10
	Wet	4	5.419E-10	1.061E-09	1.337E-09
		5	3.404E-10	2.849E-10	5.168E-10
		6	1.578E-10	2.830E-10	8.890E-10
Water Vapor Permeability (kg/m.s.Pa)	Dry	1	3.602E-13	7.975E-13	1.949E-12
		2	3.536E-13	7.743E-13	1.795E-12
		3	5.096E-13	1.001E-12	2.528E-12
	Wet	4	6.773E-12	1.327E-11	1.671E-11
		5	4.289E-12	3.590E-12	6.511E-12
		6	1.910E-12	3.425E-12	1.076E-11

Table 12-43. Douglas Fir-Water Vapor Permeability at 45°C.

Douglas Fir-Water Vapor Permeability at 45°C					
	Cup Method	**Sample No.**	**50% RH**	**70% RH**	**90% RH**
WVT (kg/s.m2)	Dry	1	2.936E-07	6.675E-07	1.470E-06
		2	3.466E-07	9.124E-07	1.519E-06
		3	3.017E-07	5.715E-07	1.510E-06
	Wet	4	2.158E-06	2.281E-06	1.237E-06
		5	1.879E-06	2.121E-06	1.167E-06
		6	1.988E-06	1.686E-06	1.134E-06
Permeance (kg/m2.s.Pa)	Dry	1	6.106E-11	9.949E-11	1.704E-10
		2	7.210E-11	1.360E-10	1.761E-10
		3	6.275E-11	8.519E-11	1.750E-10
	Wet	4	4.540E-10	7.929E-10	1.290E-09
		5	3.952E-10	7.373E-10	1.217E-09
		6	4.181E-10	5.862E-10	1.183E-09
Water Vapor Permeability (kg/m.s.Pa)	Dry	1	7.633E-13	1.244E-12	2.130E-12
		2	8.868E-13	1.673E-12	2.166E-12
		3	7.843E-13	1.065E-12	2.188E-12
	Wet	4	5.629E-12	9.833E-12	1.599E-11
		5	4.941E-12	9.216E-12	1.522E-11
		6	5.017E-12	7.034E-12	1.419E-11

Table 12-44. Douglas Fir-Water Vapor Transmission Rate.

Douglas Fir-Water Vapor Transmission Rate (kg/s.m^2)						
	ΔRH:50%	**ΔRH:70%**	**ΔRH:90%**	**ΔRH:50%**	**ΔRH:30%**	**ΔRH:10%**
	Dry Cups			**Wet Cups**		
	50% RH	70% RH	90% RH	50% RH	70% RH	90% RH
WVT at 3°C	8.86E-09	2.10E-08	8.83E-08	9.58E-08	1.23E-07	5.75E-08
WVT at 21°C	4.13E-08	1.21E-07	3.80E-07	4.29E-07	4.04E-07	2.28E-07
WVT at 45°C	3.14E-07	7.17E-07	1.50E-06	2.01E-06	2.03E-06	1.18E-06
Difference between 21°C and 3°C	366%	477%	330%	348%	228%	295%
Difference between 45°C and 21°C	660%	492%	295%	368%	402%	418%
Difference between 45°C and 3°C	3442%	3317%	1598%	1996%	1547%	1949%

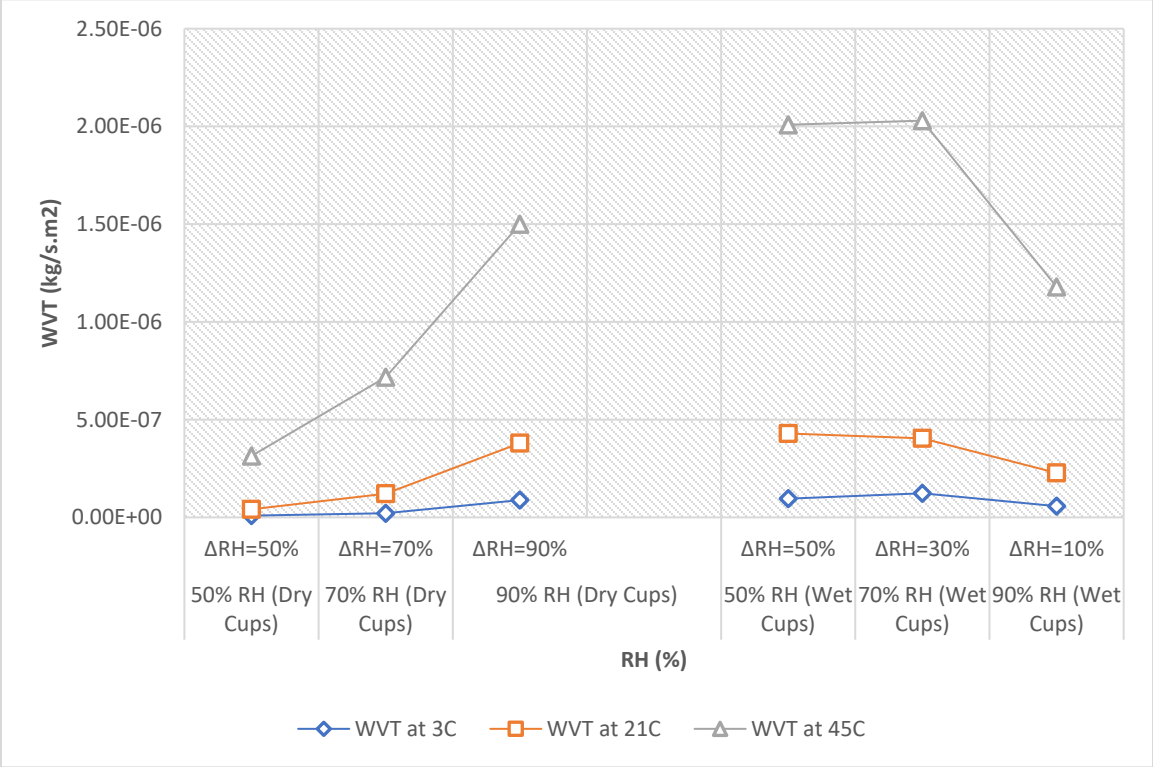

Figure 12-11. Douglas Fir-Water Vapor Transmission Rate.

12.1.12 **Cellulose Fiber**

Table 12-45. Cellulose Fiber-Water Vapor Permeability at 3°C.

Cellulose Fiber-Water Vapor Permeability at 3°C					
	Cup Method	**Sample No.**	**50% RH**	**70% RH**	**90% RH**
WVT (kg/s.m2)	Dry	1	8.410E-07	1.262E-06	2.185E-06
		2	8.745E-07	1.246E-06	2.173E-06
		3	8.723E-07	1.276E-06	2.672E-06
	Wet	4	1.317E-06	1.660E-06	2.374E-06
		5	1.639E-06	2.481E-07	3.163E-06
		6	1.611E-06	1.378E-06	-4.316E-06
Permeance (kg/m2.s.Pa)	Dry	1	2.220E-09	2.384E-09	3.223E-09
		2	2.309E-09	2.353E-09	3.205E-09
		3	2.303E-09	2.410E-09	3.942E-09
	Wet	4	3.470E-09	7.232E-09	2.971E-08
		5	4.319E-09	1.081E-09	3.958E-08
		6	4.246E-09	6.003E-09	-5.402E-08
Water Vapor Permeability (kg/m.s.Pa)	Dry	1	6.129E-11	6.580E-11	8.896E-11
		2	5.966E-11	6.079E-11	8.282E-11
		3	6.437E-11	6.735E-11	1.102E-10
	Wet	4	9.182E-11	1.914E-10	7.862E-10
		5	9.989E-11	2.501E-11	9.156E-10
		6	1.030E-10	1.456E-10	-1.310E-09

Table 12-46. Cellulose Fiber-Water Vapor Permeability at 21°C.

Cellulose Fiber-Water Vapor Permeability at 21°C					
	Cup Method	**Sample No.**	**50% RH**	**70% RH**	**90% RH**
WVT (kg/s.m2)	Dry	1	3.860E-06	7.206E-06	1.040E-05
		2	3.828E-06	7.069E-06	1.016E-05
		3	4.007E-06	7.652E-06	1.037E-05
	Wet	4	6.650E-06	4.870E-06	2.083E-06
		5	8.390E-06	6.355E-06	2.418E-06
		6	9.619E-06	6.185E-06	1.715E-06
Permeance (kg/m2.s.Pa)	Dry	1	3.110E-09	4.118E-09	4.661E-09
		2	3.084E-09	4.040E-09	4.553E-09
		3	3.228E-09	4.373E-09	4.650E-09
	Wet	4	5.368E-09	6.603E-09	8.554E-09
		5	6.773E-09	8.616E-09	9.929E-09
		6	7.765E-09	8.387E-09	7.044E-09
Water Vapor Permeability (kg/m.s.Pa)	Dry	1	8.303E-11	1.100E-10	1.245E-10
		2	7.660E-11	1.004E-10	1.131E-10
		3	9.021E-11	1.222E-10	1.300E-10
	Wet	4	1.420E-10	1.747E-10	2.263E-10
		5	1.567E-10	1.993E-10	2.297E-10
		6	1.883E-10	2.034E-10	1.708E-10

Table 12-47. Cellulose Fiber-Water Vapor Permeability at 45°C.

Cellulose Fiber-Water Vapor Permeability at 45°C					
	Cup Method	**Sample No.**	**50% RH**	**70% RH**	**90% RH**
WVT (kg/s.m2)	Dry	1	2.870E-05	4.439E-05	5.141E-05
		2	3.177E-05	4.031E-05	7.592E-05
		3	3.130E-05	4.903E-05	4.598E-05
	Wet	4	4.115E-05	3.783E-05	1.210E-05
		5	3.309E-05	2.761E-05	9.421E-06
		6	3.321E-05	1.207E-05	1.135E-05
Permeance (kg/m2.s.Pa)	Dry	1	5.988E-09	6.572E-09	5.956E-09
		2	6.627E-09	5.967E-09	8.795E-09
		3	6.529E-09	7.258E-09	5.327E-09
	Wet	4	8.583E-09	1.336E-08	1.262E-08
		5	6.903E-09	9.752E-09	9.826E-09
		6	6.928E-09	4.262E-09	1.184E-08
Water Vapor Permeability (kg/m.s.Pa)	Dry	1	1.547E-10	1.698E-10	1.538E-10
		2	1.671E-10	1.505E-10	2.218E-10
		3	1.436E-10	1.596E-10	1.171E-10
	Wet	4	2.192E-10	3.413E-10	3.224E-10
		5	1.709E-10	2.414E-10	2.432E-10
		6	1.558E-10	9.582E-11	2.662E-10

Table 12-48. Cellulose Fiber-Water Vapor Transmission Rate.

Cellulose Fiber-Water Vapor Transmission Rate (kg/s.m^2)						
	ΔRH:50%	**ΔRH:70%**	**ΔRH:90%**	**ΔRH:50%**	**ΔRH:30%**	**ΔRH:10%**
	Dry Cups			**Wet Cups**		
	50% RH	70% RH	90% RH	50% RH	70% RH	90% RH
WVT at 3°C	8.63E-07	1.26E-06	2.34E-06	1.52E-06	1.10E-06	4.07E-07
WVT at 21°C	3.90E-06	7.31E-06	1.03E-05	8.22E-06	5.80E-06	2.07E-06
WVT at 45°C	3.06E-05	4.46E-05	5.78E-05	3.58E-05	2.58E-05	1.10E-05
Difference between 21°C and 3°C	352%	479%	340%	440%	430%	409%
Difference between 45°C and 21°C	685%	510%	460%	336%	345%	429%
Difference between 45°C and 3°C	3446%	3434%	2365%	2252%	2259%	2593%

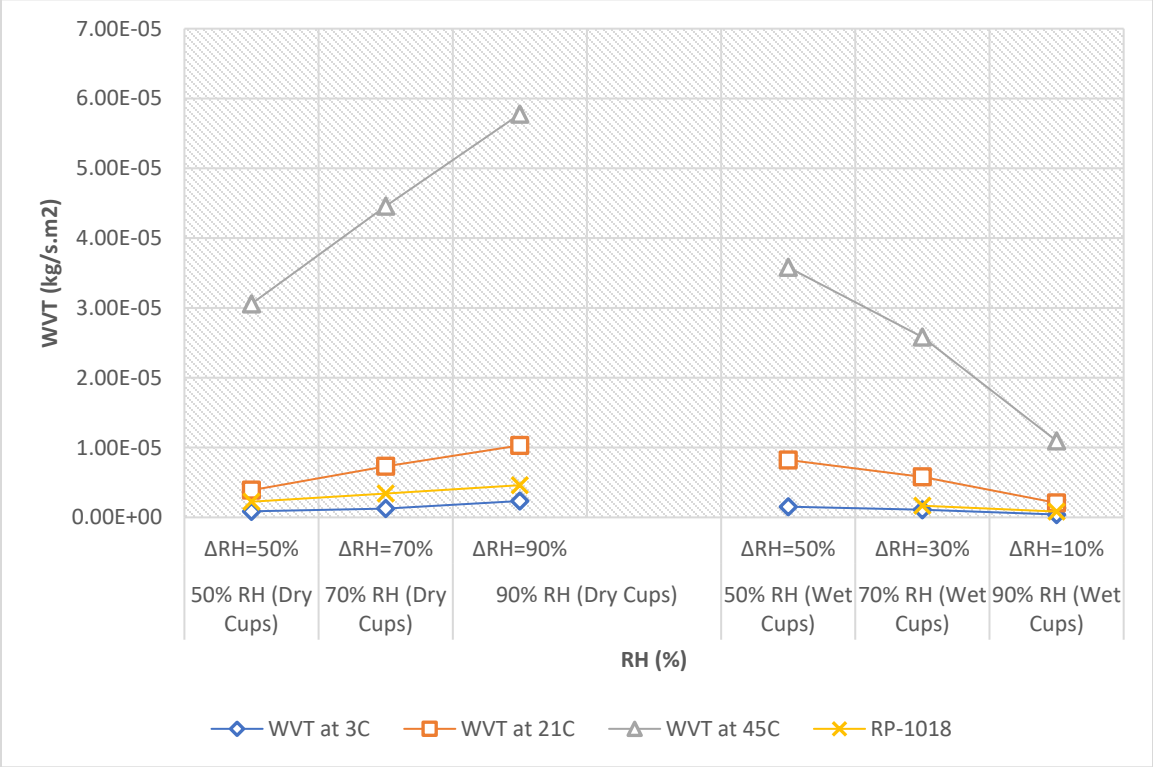

Figure 12-12. Cellulose Fiber-Water Vapor Transmission Rate.

12.1.13 **Expanded Polystyrene (EPS)**

Table 12-49. Expanded Polystyrene (EPS)-Water Vapor Permeability at 3°C.

Expanded Polystyrene (EPS)-Water Vapor Permeability at 3°C					
	Cup Method	**Sample No.**	**50% RH**	**70% RH**	**90% RH**
WVT (kg/s.m2)	Dry	1	6.715E-08	1.310E-07	1.829E-07
		2	9.542E-08	1.199E-07	1.906E-07
		3	1.108E-07	1.529E-07	1.809E-07
	Wet	4	1.472E-07	8.753E-08	2.483E-08
		5	8.717E-08	1.014E-07	2.433E-08
		6	1.045E-07	3.477E-08	3.423E-08
Permeance (kg/m2.s.Pa)	Dry	1	1.773E-10	2.469E-10	2.687E-10
		2	2.519E-10	2.259E-10	2.801E-10
		3	2.924E-10	2.882E-10	2.658E-10
	Wet	4	3.889E-10	3.840E-10	3.193E-10
		5	2.302E-10	4.449E-10	3.129E-10
		6	2.759E-10	1.525E-10	4.402E-10
Water Vapor Permeability (kg/m.s.Pa)	Dry	1	2.251E-12	3.136E-12	3.413E-12
		2	3.199E-12	2.870E-12	3.557E-12
		3	3.714E-12	3.660E-12	3.375E-12
	Wet	4	4.938E-12	4.876E-12	4.055E-12
		5	2.924E-12	5.650E-12	3.973E-12
		6	3.505E-12	1.937E-12	5.590E-12

Table 12-50. Expanded Polystyrene (EPS)-Water Vapor Permeability at 21°C.

Expanded Polystyrene (EPS)-Water Vapor Permeability at 21°C					
	Cup Method	**Sample No.**	**50% RH**	**70% RH**	**90% RH**
WVT (kg/s.m2)	Dry	1	3.323E-07	5.157E-07	8.069E-07
		2	3.765E-07	6.008E-07	8.055E-07
		3	3.827E-07	5.772E-07	7.723E-07
	Wet	4	5.187E-07	3.220E-07	1.173E-07
		5	5.347E-07	3.206E-07	1.109E-07
		6	4.445E-07	3.156E-07	1.087E-07
Permeance (kg/m2.s.Pa)	Dry	1	2.670E-10	2.961E-10	3.608E-10
		2	3.025E-10	3.450E-10	3.602E-10
		3	3.074E-10	3.314E-10	3.453E-10
	Wet	4	4.164E-10	4.312E-10	4.731E-10
		5	4.292E-10	4.293E-10	4.472E-10
		6	3.568E-10	4.226E-10	4.384E-10
Water Vapor Permeability (kg/m.s.Pa)	Dry	1	3.390E-12	3.761E-12	4.582E-12
		2	3.842E-12	4.381E-12	4.574E-12
		3	3.905E-12	4.209E-12	4.386E-12
	Wet	4	5.288E-12	5.476E-12	6.009E-12
		5	5.451E-12	5.452E-12	5.680E-12
		6	4.532E-12	5.367E-12	5.567E-12

Table 12-51. Expanded Polystyrene (EPS)-Water Vapor Permeability at 45°C.

Expanded Polystyrene (EPS)-Water Vapor Permeability at 45°C					
	Cup Method	**Sample No.**	**50% RH**	**70% RH**	**90% RH**
WVT (kg/s.m2)	Dry	1	1.713E-06	2.103E-06	3.436E-06
		2	1.340E-06	2.631E-06	3.435E-06
		3	1.573E-06	2.458E-06	3.436E-06
	Wet	4	2.021E-06	1.120E-06	5.092E-07
		5	2.893E-06	1.869E-06	5.682E-07
		6	1.739E-06	1.484E-06	5.479E-07
Permeance (kg/m2.s.Pa)	Dry	1	3.573E-10	3.139E-10	3.981E-10
		2	2.796E-10	3.926E-10	3.980E-10
		3	3.283E-10	3.668E-10	3.981E-10
	Wet	4	4.217E-10	3.880E-10	5.316E-10
		5	6.035E-10	6.477E-10	5.931E-10
		6	3.628E-10	5.143E-10	5.720E-10
Water Vapor Permeability (kg/m.s.Pa)	Dry	1	4.395E-12	3.861E-12	4.897E-12
		2	3.509E-12	4.927E-12	4.995E-12
		3	4.103E-12	4.584E-12	4.977E-12
	Wet	4	5.271E-12	4.850E-12	6.644E-12
		5	7.543E-12	8.096E-12	7.414E-12
		6	4.535E-12	6.429E-12	7.150E-12

Table 12-52. EPS-Water Vapor Transmission Rate.

EPS-Water Vapor Transmission Rate (kg/s.m^2)						
	ΔRH:50%	**ΔRH:70%**	**ΔRH:90%**	**ΔRH:50%**	**ΔRH:30%**	**ΔRH:10%**
	Dry Cups			**Wet Cups**		
	50% RH	70% RH	90% RH	50% RH	70% RH	90% RH
WVT at 3°C	9.11E-08	1.35E-07	1.85E-07	1.13E-07	7.46E-08	2.78E-08
WVT at 21°C	3.64E-07	5.65E-07	7.95E-07	4.99E-07	3.19E-07	1.12E-07
WVT at 45°C	1.54E-06	2.40E-06	3.44E-06	2.22E-06	1.49E-06	5.42E-07
Difference between 21°C and 3°C	299%	320%	330%	342%	328%	304%
Difference between 45°C and 21°C	324%	325%	332%	344%	367%	382%
Difference between 45°C and 3°C	1592%	1681%	1760%	1863%	1899%	1849%

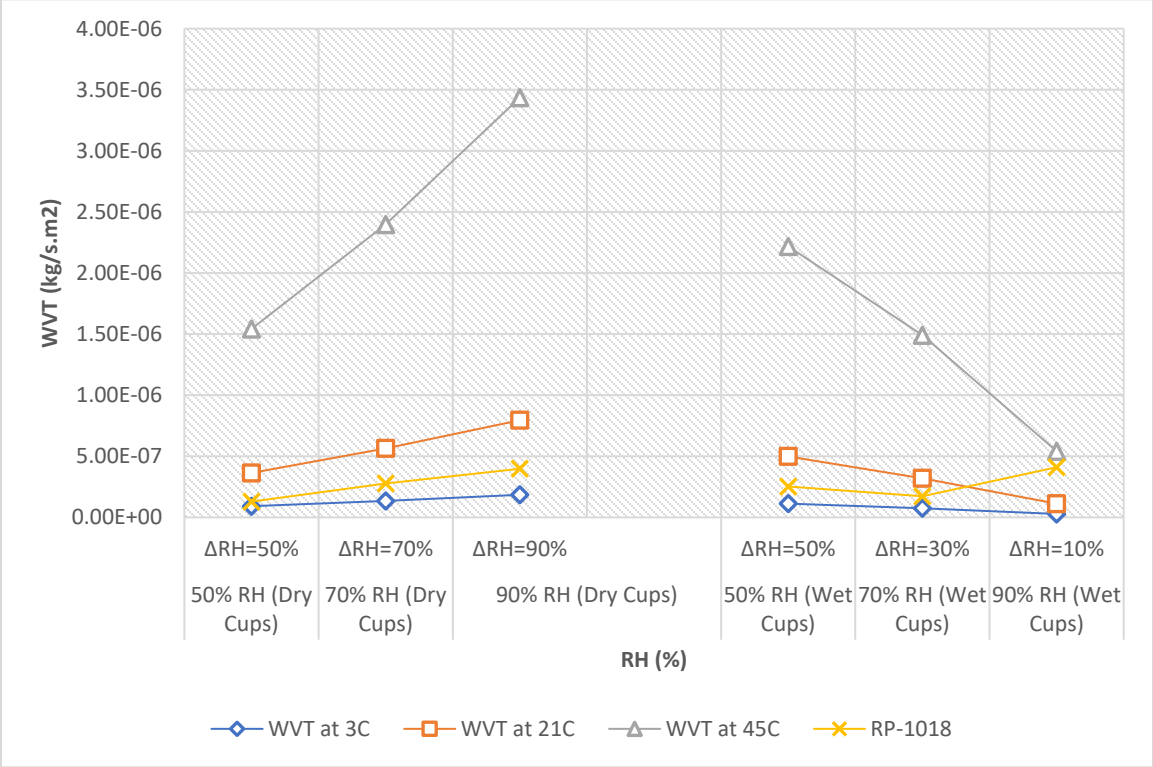

Figure 12-13. EPS-Water Vapor Transmission Rate.

12.1.14 **Extruded Polystyrene (XPS)**

Table 12-53. Extruded Polystyrene (XPS)-Water Vapor Permeability at 3°C.

Extruded Polystyrene (XPS)-Water Vapor Permeability at 3°C					
	Cup Method	**Sample No.**	**50% RH**	**70% RH**	**90% RH**
WVT (kg/s.m2)	Dry	1	2.039E-08	3.773E-08	4.389E-08
		2	2.198E-08	2.893E-08	3.789E-08
		3	2.378E-08	2.711E-08	4.421E-08
	Wet	4	2.590E-08	2.631E-08	6.712E-09
		5	2.512E-08	1.209E-08	9.003E-09
		6	2.444E-08	2.290E-08	6.549E-09
Permeance (kg/m2.s.Pa)	Dry	1	5.384E-11	7.123E-11	6.436E-11
		2	5.805E-11	5.462E-11	5.557E-11
		3	6.280E-11	5.118E-11	6.484E-11
	Wet	4	6.832E-11	1.147E-10	8.720E-11
		5	6.627E-11	5.269E-11	1.170E-10
		6	6.448E-11	9.981E-11	8.508E-11
Water Vapor Permeability (kg/m.s.Pa)	Dry	1	8.292E-13	1.097E-12	9.912E-13
		2	8.939E-13	8.411E-13	8.557E-13
		3	9.671E-13	7.882E-13	9.985E-13
	Wet	4	1.052E-12	1.766E-12	1.343E-12
		5	1.021E-12	8.114E-13	1.801E-12
		6	9.930E-13	1.537E-12	1.310E-12

Table 12-54. Extruded Polystyrene (XPS)-Water Vapor Permeability at 21°C.

Extruded Polystyrene (XPS)-Water Vapor Permeability at 21°C					
	Cup Method	**Sample No.**	**50% RH**	**70% RH**	**90% RH**
WVT (kg/s.m2)	Dry	1	7.733E-08	9.765E-08	1.450E-07
		2	7.620E-08	1.160E-07	1.419E-07
		3	7.768E-08	1.182E-07	1.461E-07
	Wet	4	9.219E-08	7.441E-08	2.558E-08
		5	9.673E-08	6.726E-08	2.526E-08
		6	9.884E-08	5.922E-08	2.524E-08
Permeance (kg/m2.s.Pa)	Dry	1	6.213E-11	5.607E-11	6.485E-11
		2	6.122E-11	6.663E-11	6.344E-11
		3	6.241E-11	6.789E-11	6.535E-11
	Wet	4	7.400E-11	9.964E-11	1.031E-10
		5	7.765E-11	9.006E-11	1.019E-10
		6	7.934E-11	7.930E-11	1.018E-10
Water Vapor Permeability (kg/m.s.Pa)	Dry	1	9.568E-13	8.636E-13	9.987E-13
		2	9.428E-13	1.026E-12	9.769E-13
		3	9.611E-13	1.045E-12	1.006E-12
	Wet	4	1.140E-12	1.534E-12	1.588E-12
		5	1.196E-12	1.387E-12	1.569E-12
		6	1.222E-12	1.221E-12	1.567E-12

Table 12-55. Extruded Polystyrene (XPS)-Water Vapor Permeability at 45°C.

Extruded Polystyrene (XPS)-Water Vapor Permeability at 45°C					
	Cup Method	**Sample No.**	**50% RH**	**70% RH**	**90% RH**
WVT (kg/s.m2)	Dry	1	2.746E-07	4.558E-07	6.050E-07
		2	3.548E-07	4.117E-07	7.262E-07
		3	3.304E-07	4.899E-07	5.942E-07
	Wet	4	4.293E-07	3.128E-07	9.719E-08
		5	3.989E-07	3.086E-07	1.081E-07
		6	3.851E-07	2.181E-07	1.020E-07
Permeance (kg/m2.s.Pa)	Dry	1	5.731E-11	6.804E-11	7.011E-11
		2	7.402E-11	6.147E-11	8.415E-11
		3	6.895E-11	7.313E-11	6.885E-11
	Wet	4	8.956E-11	1.084E-10	1.014E-10
		5	8.321E-11	1.069E-10	1.128E-10
		6	8.034E-11	7.554E-11	1.065E-10
Water Vapor Permeability (kg/m.s.Pa)	Dry	1	8.883E-13	1.055E-12	1.087E-12
		2	1.110E-12	9.220E-13	1.262E-12
		3	1.062E-12	1.126E-12	1.060E-12
	Wet	4	1.361E-12	1.647E-12	1.542E-12
		5	1.290E-12	1.657E-12	1.749E-12
		6	1.205E-12	1.133E-12	1.598E-12

Table 12-56. XPS-Water Vapor Transmission Rate.

XPS-Water Vapor Transmission Rate (kg/s.m^2)						
	ΔRH:50%	**ΔRH:70%**	**ΔRH:90%**	**ΔRH:50%**	**ΔRH:30%**	**ΔRH:10%**
	Dry Cups			**Wet Cups**		
	50% RH	70% RH	90% RH	50% RH	70% RH	90% RH
WVT at 3°C	2.20E-08	3.13E-08	4.20E-08	2.52E-08	2.04E-08	7.42E-09
WVT at 21°C	7.71E-08	1.11E-07	1.44E-07	9.59E-08	6.70E-08	2.54E-08
WVT at 45°C	3.20E-07	4.52E-07	6.42E-07	4.04E-07	2.80E-07	1.02E-07
Difference between 21°C and 3°C	250%	254%	244%	281%	228%	242%
Difference between 45°C and 21°C	315%	309%	345%	322%	318%	304%
Difference between 45°C and 3°C	1351%	1348%	1428%	1508%	1269%	1280%

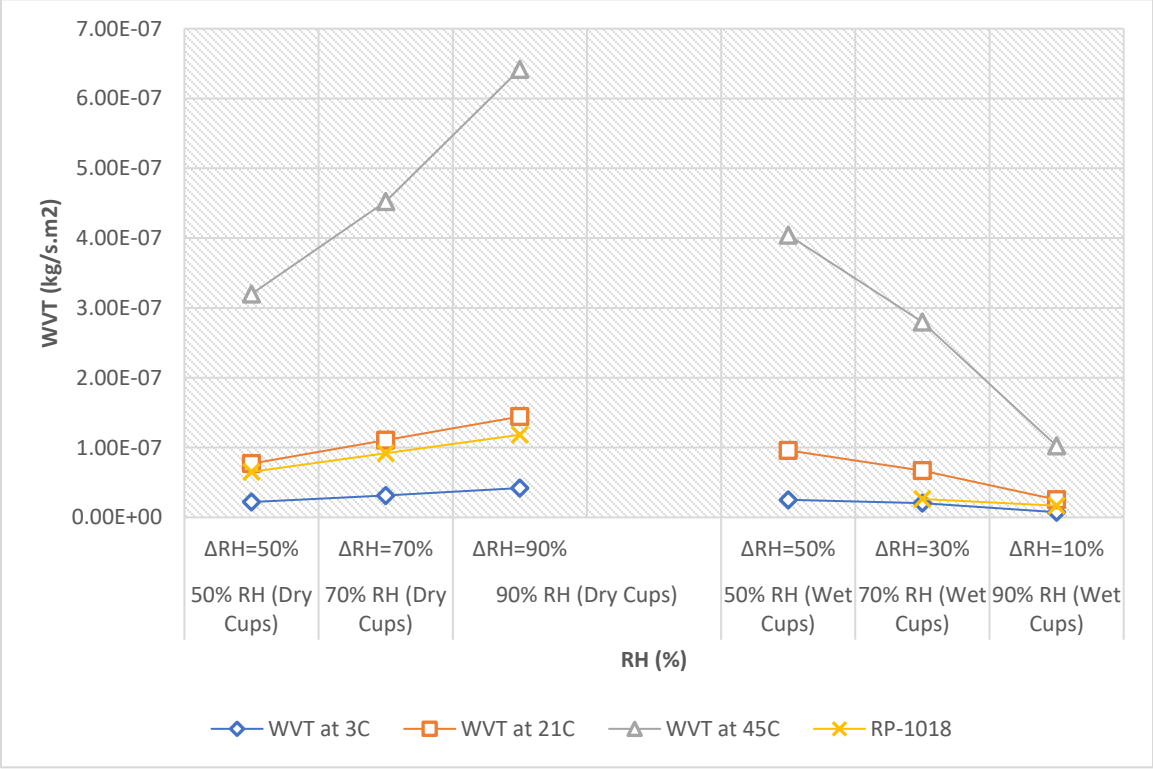

Figure 12-14. XPS-Water Vapor Transmission Rate.

12.1.15 **Open Cell Sprayed Polyurethane Foam**

Table 12-57. Open Cell Spray Polyurethane -Water Vapor Permeability at 3°C.

Open Cell Spray Polyurethane -Water Vapor Permeability at 3°C					
	Cup Method	**Sample No.**	**50% RH**	**70% RH**	**90% RH**
WVT (kg/s.m2)	Dry	1	2.954E-06	2.817E-06	4.696E-06
		2	2.065E-06	3.948E-06	5.285E-06
		3	1.995E-06	3.549E-06	3.872E-06
	Wet	4	2.618E-06	3.054E-06	7.415E-07
		5	3.085E-06	1.873E-07	4.015E-07
		6	2.548E-06	2.177E-06	7.272E-07
Permeance (kg/m2.s.Pa)	Dry	1	7.756E-09	5.293E-09	6.845E-09
		2	5.421E-09	7.418E-09	7.704E-09
		3	5.237E-09	6.668E-09	5.645E-09
	Wet	4	6.968E-09	1.351E-08	1.003E-08
		5	8.213E-09	8.287E-10	5.431E-09
		6	6.783E-09	9.635E-09	9.838E-09
Water Vapor Permeability (kg/m.s.Pa)	Dry	1	1.086E-10	7.410E-11	9.583E-11
		2	7.048E-11	9.644E-11	1.002E-10
		3	8.275E-11	1.054E-10	8.919E-11
	Wet	4	8.920E-11	1.730E-10	1.284E-10
		5	1.191E-10	1.202E-11	7.876E-11
		6	1.004E-10	1.426E-10	1.456E-10

Table 12-58. Open Cell Spray Polyurethane -Water Vapor Permeability at 21°C.

Open Cell Spray Polyurethane -Water Vapor Permeability at 21°C					
	Cup Method	**Sample No.**	**50% RH**	**70% RH**	**90% RH**
WVT (kg/s.m2)	Dry	1	6.207E-06	7.178E-06	1.282E-05
		2	6.085E-06	9.411E-06	1.187E-05
		3	7.756E-06	1.426E-05	2.117E-05
	Wet	4	7.585E-06	6.633E-06	1.676E-06
		5	8.178E-06	5.842E-06	1.630E-06
		6	1.189E-05	5.744E-06	2.881E-06
Permeance (kg/m2.s.Pa)	Dry	1	4.880E-09	4.114E-09	5.613E-09
		2	4.784E-09	5.394E-09	5.200E-09
		3	6.098E-09	8.172E-09	9.272E-09
	Wet	4	6.257E-09	8.884E-09	6.817E-09
		5	6.746E-09	7.824E-09	6.629E-09
		6	9.809E-09	7.693E-09	1.172E-08
Water Vapor Permeability (kg/m.s.Pa)	Dry	1	7.564E-11	6.377E-11	8.701E-11
		2	8.612E-11	9.709E-11	9.360E-11
		3	1.159E-10	1.553E-10	1.762E-10
	Wet	4	1.001E-10	1.421E-10	1.091E-10
		5	1.248E-10	1.448E-10	1.226E-10
		6	1.687E-10	1.323E-10	2.016E-10

Table 12-59. Open Cell Spray Polyurethane-Water Vapor Transmission Rate.

Open Cell Spray Polyurethane-Water Vapor Transmission Rate (kg/s.m^2)						
	ΔRH:50%	**ΔRH:70%**	**ΔRH:90%**	**ΔRH:50%**	**ΔRH:30%**	**ΔRH:10%**
	Dry Cups			**Wet Cups**		
	50% RH	70% RH	90% RH	50% RH	70% RH	90% RH
WVT at 3°C	2.34E-06	3.44E-06	4.62E-06	2.75E-06	1.81E-06	6.23E-07
WVT at 21°C	6.68E-06	1.03E-05	1.53E-05	9.22E-06	6.07E-06	2.06E-06
Difference between 21°C and 3°C	186%	199%	231%	235%	236%	231%

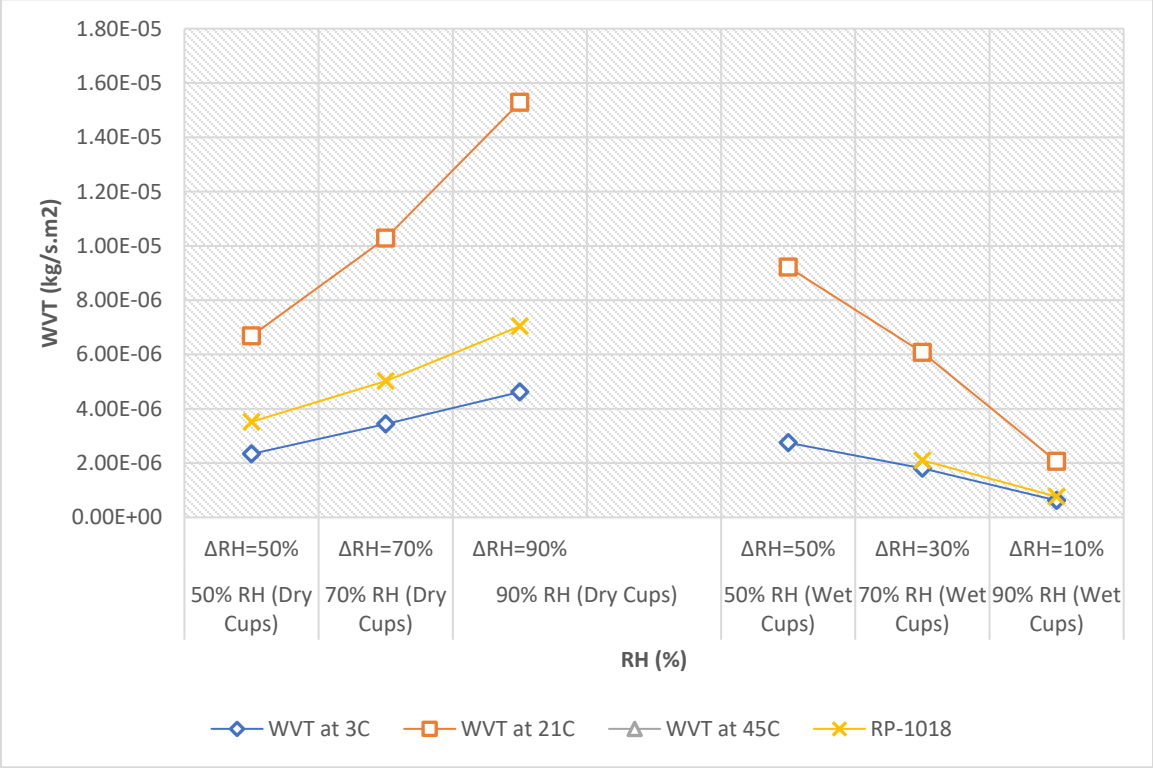

Figure 12-15. Open Cell Spray Polyurethane-Water Vapor Transmission Rate.

12.1.16 **Polyisocyanurate**

Table 12-60. Polyisocyanurate-Water Vapor Permeability at 3°C.

Polyisocyanurate-Water Vapor Permeability at 3°C					
	Cup Method	**Sample No.**	**50% RH**	**70% RH**	**90% RH**
WVT (kg/s.m2)	Dry	1	1.957E-08	2.878E-08	4.260E-08
		2	1.538E-08	3.057E-08	4.483E-08
		3	2.341E-08	2.935E-08	4.372E-08
	Wet	4	3.119E-08	2.022E-08	1.145E-08
		5	3.448E-08	5.263E-08	1.023E-08
		6	3.231E-08	1.078E-08	1.279E-08
Permeance (kg/m2.s.Pa)	Dry	1	5.164E-11	5.424E-11	6.247E-11
		2	4.059E-11	5.762E-11	6.575E-11
		3	6.180E-11	5.531E-11	6.412E-11
	Wet	4	8.241E-11	8.862E-11	1.488E-10
		5	9.111E-11	2.306E-10	1.329E-10
		6	8.536E-11	4.723E-11	1.662E-10
Water Vapor Permeability (kg/m.s.Pa)	Dry	1	1.244E-12	1.307E-12	1.506E-12
		2	9.782E-13	1.389E-12	1.584E-12
		3	1.489E-12	1.333E-12	1.545E-12
	Wet	4	1.986E-12	2.136E-12	3.586E-12
		5	2.196E-12	5.558E-12	3.203E-12
		6	2.057E-12	1.138E-12	4.005E-12

Table 12-61. Polyisocyanurate-Water Vapor Permeability at 21°C.

Polyisocyanurate-Water Vapor Permeability at 21°C					
	Cup Method	**Sample No.**	**50% RH**	**70% RH**	**90% RH**
WVT (kg/s.m2)	Dry	1	6.986E-08	1.125E-07	1.872E-07
		2	7.305E-08	1.156E-07	1.915E-07
		3	8.953E-08	1.152E-07	1.909E-07
	Wet	4	1.361E-07	1.004E-07	4.634E-08
		5	1.473E-07	9.098E-08	3.655E-08
		6	1.384E-07	1.201E-07	4.703E-08
Permeance (kg/m2.s.Pa)	Dry	1	5.613E-11	6.463E-11	8.369E-11
		2	5.869E-11	6.638E-11	8.561E-11
		3	7.193E-11	6.612E-11	8.538E-11
	Wet	4	1.092E-10	1.345E-10	1.869E-10
		5	1.183E-10	1.218E-10	1.474E-10
		6	1.111E-10	1.608E-10	1.897E-10
Water Vapor Permeability (kg/m.s.Pa)	Dry	1	1.353E-12	1.557E-12	2.017E-12
		2	1.414E-12	1.600E-12	2.063E-12
		3	1.734E-12	1.594E-12	2.058E-12
	Wet	4	2.632E-12	3.242E-12	4.504E-12
		5	2.850E-12	2.936E-12	3.552E-12
		6	2.677E-12	3.875E-12	4.571E-12

Table 12-62. Polyisocyanurate-Water Vapor Permeability at 45°C.

Polyisocyanurate-Water Vapor Permeability at 45°C					
	Cup Method	**Sample No.**	**50% RH**	**70% RH**	**90% RH**
WVT (kg/s.m2)	Dry	1	4.646E-07	7.829E-07	1.155E-06
		2	5.275E-07	8.845E-07	1.327E-06
		3	4.360E-07	7.431E-07	1.098E-06
	Wet	4	9.160E-07	5.639E-07	2.161E-07
		5	8.889E-07	5.848E-07	2.004E-07
		6	9.105E-07	6.373E-07	2.132E-07
Permeance (kg/m2.s.Pa)	Dry	1	9.695E-11	1.167E-10	1.338E-10
		2	1.101E-10	1.318E-10	1.537E-10
		3	9.097E-11	1.108E-10	1.271E-10
	Wet	4	1.911E-10	1.967E-10	2.266E-10
		5	1.854E-10	2.040E-10	2.101E-10
		6	1.899E-10	2.223E-10	2.235E-10
Water Vapor Permeability (kg/m.s.Pa)	Dry	1	2.278E-12	2.742E-12	3.145E-12
		2	2.697E-12	3.230E-12	3.766E-12
		3	2.183E-12	2.658E-12	3.051E-12
	Wet	4	4.586E-12	4.721E-12	5.437E-12
		5	4.451E-12	4.895E-12	5.042E-12
		6	4.559E-12	5.335E-12	5.364E-12

Table 12-63. Polyisocyanurate-Water Vapor Transmission Rate.

Polyisocyanurate-Water Vapor Transmission Rate (kg/s.m^2)						
	ΔRH:50%	**ΔRH:70%**	**ΔRH:90%**	**ΔRH:50%**	**ΔRH:30%**	**ΔRH:10%**
	Dry Cups			**Wet Cups**		
	50% RH	70% RH	90% RH	50% RH	70% RH	90% RH
WVT at 3°C	1.95E-08	2.96E-08	4.37E-08	3.27E-08	2.79E-08	1.15E-08
WVT at 21°C	7.75E-08	1.14E-07	1.90E-07	1.41E-07	1.04E-07	4.33E-08
WVT at 45°C	4.76E-07	8.03E-07	1.19E-06	9.05E-07	5.95E-07	2.10E-07
Difference between 21°C and 3°C	298%	287%	334%	330%	272%	277%
Difference between 45°C and 21°C	514%	602%	529%	544%	473%	385%
Difference between 45°C and 3°C	2347%	2618%	2630%	2671%	2036%	1727%

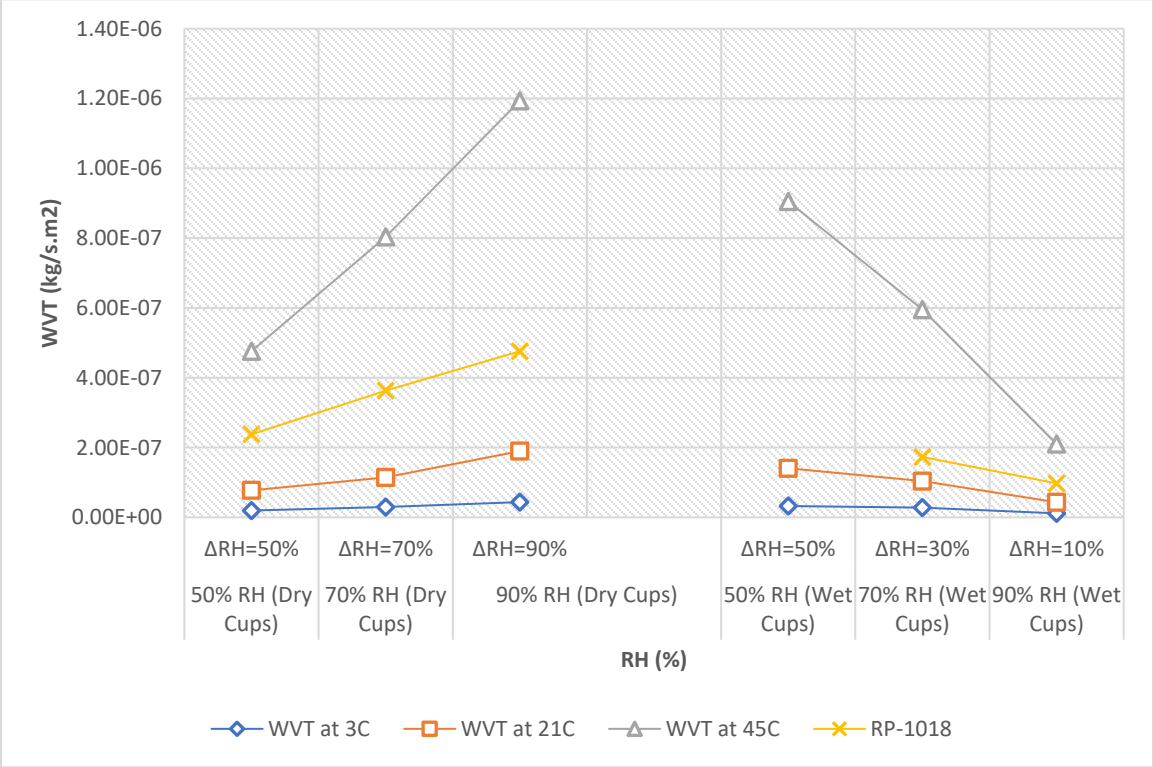

Figure 12-16. Polyisocyanurate-Water Vapor Transmission Rate.

12.1.17 **Mineral Fiber (Stone Wool)**

Table 12-64. Mineral Fiber-Water Vapor Permeability at 3°C.

Mineral Fiber-Water Vapor Permeability at 3°C					
	Cup Method	**Sample No.**	**50% RH**	**70% RH**	**90% RH**
WVT (kg/s.m2)	Dry	1	8.608E-07	1.366E-06	1.815E-06
		2	9.246E-07	1.419E-06	2.004E-06
		3	1.202E-06	1.651E-06	2.257E-06
	Wet	4	1.779E-06	8.743E-07	2.963E-07
		5	7.763E-07	2.139E-07	2.658E-07
		6	9.687E-07	1.131E-06	2.417E-07
Permeance (kg/m2.s.Pa)	Dry	1	2.288E-09	2.561E-09	2.639E-09
		2	2.457E-09	2.661E-09	2.914E-09
		3	3.195E-09	3.095E-09	3.281E-09
	Wet	4	4.657E-09	3.949E-09	4.107E-09
		5	2.032E-09	9.662E-10	3.686E-09
		6	2.536E-09	5.107E-09	3.350E-09
Water Vapor Permeability (kg/m.s.Pa)	Dry	1	8.876E-11	9.936E-11	1.024E-10
		2	9.534E-11	1.032E-10	1.131E-10
		3	1.236E-10	1.198E-10	1.270E-10
	Wet	4	1.798E-10	1.524E-10	1.585E-10
		5	7.865E-11	3.739E-11	1.426E-10
		6	9.814E-11	1.976E-10	1.297E-10

Table 12-65. Mineral Fiber-Water Vapor Permeability at 21°C.

Mineral Fiber-Water Vapor Permeability at 21°C					
	Cup Method	**Sample No.**	**50% RH**	**70% RH**	**90% RH**
WVT (kg/s.m2)	Dry	1	3.573E-06	5.788E-06	8.797E-06
		2	3.294E-06	5.445E-06	7.984E-06
		3	3.511E-06	5.931E-06	8.333E-06
	Wet	4	5.581E-06	3.984E-06	1.737E-06
		5	5.874E-06	4.343E-06	1.172E-06
		6	5.620E-06	2.702E-06	1.265E-06
Permeance (kg/m2.s.Pa)	Dry	1	2.954E-09	3.330E-09	3.923E-09
		2	2.723E-09	3.132E-09	3.561E-09
		3	2.902E-09	3.413E-09	3.716E-09
	Wet	4	4.369E-09	5.394E-09	7.065E-09
		5	4.598E-09	5.879E-09	4.767E-09
		6	4.399E-09	3.658E-09	5.144E-09
Water Vapor Permeability (kg/m.s.Pa)	Dry	1	1.146E-10	1.292E-10	1.522E-10
		2	1.057E-10	1.215E-10	1.381E-10
		3	1.123E-10	1.321E-10	1.438E-10
	Wet	4	1.686E-10	2.082E-10	2.727E-10
		5	1.779E-10	2.275E-10	1.845E-10
		6	1.702E-10	1.416E-10	1.991E-10

Table 12-66. Mineral Fiber-Water Vapor Permeability at 45°C.

Mineral Fiber-Water Vapor Permeability at 45°C					
	Cup Method	**Sample No.**	**50% RH**	**70% RH**	**90% RH**
WVT (kg/s.m2)	Dry	1	1.911E-05	2.401E-05	3.852E-05
		2	1.395E-05	2.311E-05	3.458E-05
		3	1.365E-05	2.314E-05	3.135E-05
	Wet	4	2.452E-05	1.662E-05	5.728E-06
		5	2.671E-05	1.491E-05	6.914E-06
		6	2.184E-05	1.882E-05	5.921E-06
Permeance (kg/m2.s.Pa)	Dry	1	3.993E-09	3.624E-09	4.460E-09
		2	2.915E-09	3.487E-09	4.004E-09
		3	2.852E-09	3.493E-09	3.630E-09
	Wet	4	5.107E-09	5.616E-09	5.991E-09
		5	5.562E-09	5.041E-09	7.232E-09
		6	4.548E-09	6.359E-09	6.193E-09
Water Vapor Permeability (kg/m.s.Pa)	Dry	1	1.549E-10	1.406E-10	1.730E-10
		2	1.131E-10	1.353E-10	1.553E-10
		3	1.104E-10	1.352E-10	1.405E-10
	Wet	4	1.971E-10	2.168E-10	2.312E-10
		5	2.152E-10	1.951E-10	2.799E-10
		6	1.760E-10	2.461E-10	2.397E-10

Table 12-67. Mineral Fiber-Water Vapor Transmission Rate.

Mineral Fiber-Water Vapor Transmission Rate (kg/s.m^2)						
	ΔRH:50%	**ΔRH:70%**	**ΔRH:90%**	**ΔRH:50%**	**ΔRH:30%**	**ΔRH:10%**
	Dry Cups			**Wet Cups**		
	50% RH	70% RH	90% RH	50% RH	70% RH	90% RH
WVT at 3°C	9.96E-07	1.48E-06	2.03E-06	1.17E-06	7.40E-07	2.68E-07
WVT at 21°C	3.46E-06	5.72E-06	8.37E-06	5.69E-06	3.68E-06	1.39E-06
WVT at 45°C	1.56E-05	2.34E-05	3.48E-05	2.44E-05	1.68E-05	6.19E-06
Difference between 21°C and 3°C	247%	287%	313%	385%	397%	419%
Difference between 45°C and 21°C	350%	309%	316%	328%	356%	345%
Difference between 45°C and 3°C	1464%	1484%	1619%	1973%	2169%	2209%

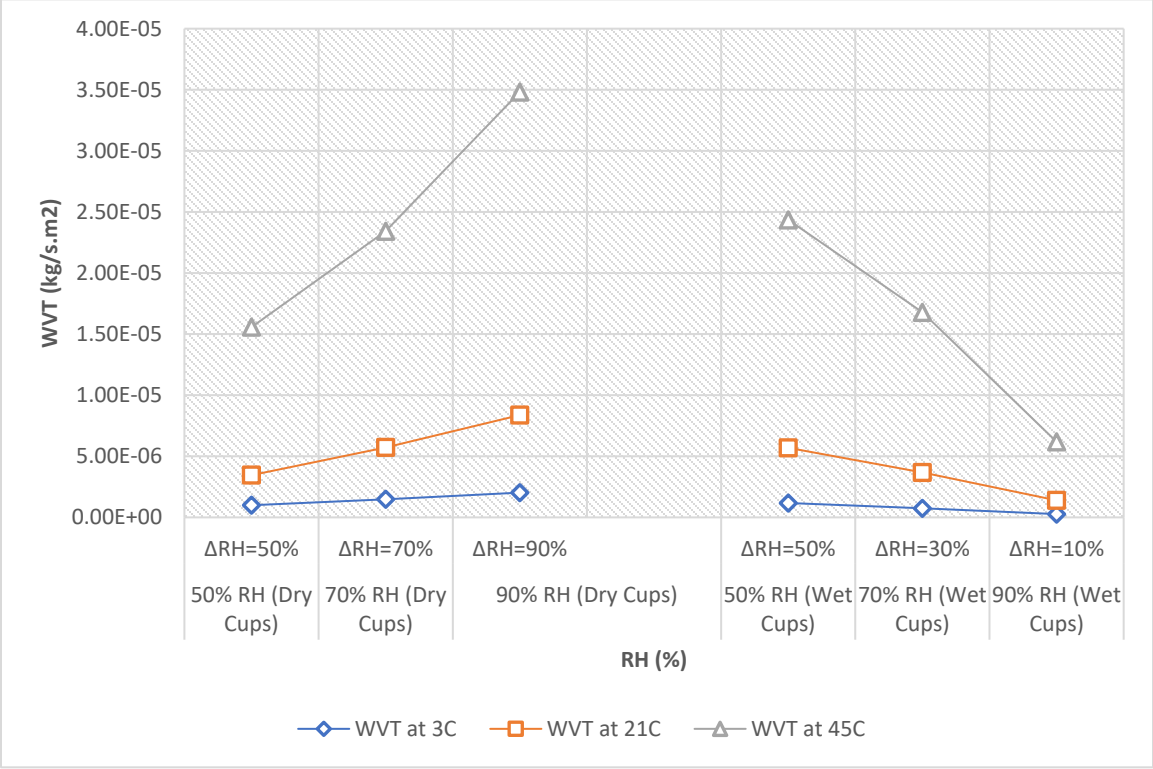

Figure 12-17. Mineral Fiber-Water Vapor Transmission Rate.